Light-Matter Interaction Models in Relativistic Quantum Information

by

Richard Lopp

A thesis
presented to the University of Waterloo
in fulfillment of the
thesis requirement for the degree of
Doctor of Philosophy
in
Applied Mathematics - Quantum Information

Waterloo, Ontario, Canada, 2021

Examining Committee Membership

The following served on the Examining Committee for this thesis. The decision of the Examining Committee is by majority vote.

External Examiner:	Martin Wilkens Professor Dept. of Physics, University of Potsdam
Supervisor:	Eduardo Martín-Martínez Associate Professor Dept. of Applied Mathematics, University of Waterloo
Internal Member:	Achim Kempf Professor Dept. of Applied Mathematics, University of Waterloo
Internal-External Member:	Robert Mann Professor Dept. of Physics, University of Waterloo
Other Member:	Adrian Lupascu Associate Professor Dept. of Physics, University of Waterloo

Author's Declaration

This thesis consists of material all of which I authored or co-authored: see Statement of Contributions included in the thesis. This is a true copy of the thesis, including any required final revisions, as accepted by my examiners.

I understand that my thesis may be made electronically available to the public.

Statement of Contributions

Chapters 2, 6, 7 are adapted for this thesis from the accepted version of "Quantum delocalization, gauge, and quantum optics: Light-matter interaction in relativistic quantum information" [1] (©2021 American Physical Society). Chapter 3, and part of Sec. 2.1 and Sec. 2.4 are based on the submitted version of "Light, matter, and quantum randomness generation: A relativistic quantum information perspective" [2]. Both [1] and [2] were written under supervision of Prof. Eduardo Martín-Martínez. The calculations were performed by myself, the conceptual structures and physical reasonings were done in collaboration with Eduardo Martín-Martínez. The manuscripts for publication were subsequently jointly crafted.

Chapter 4, Sec. 5.4.1 as well as part of Sec. 2.4 are based on the submitted version of "Relativity and quantum optics: accelerated atoms in optical cavities" [3] which was co-authored with Prof. Eduardo Martín-Martínez and Prof. Don N. Page. While I performed the calculations, the ideas and structure of the publication were a collaborative effort. The manuscript was collaboratively written.

Chapter 5 is adapted from the submitted version of "Dimensional reduction of cavities with axial symmetry: Are optical fibers really one-dimensional?"[4] (under review at Phys. Rev. A) which was in co-authored with Dr. Daniel Grimmer and Prof. Eduardo Martín-Martínez. Daniel Grimmer and Eduardo Martín-Martínez provided the original idea based on [3]. While I performed the calculations for the example geometry of Sec. 5.4, Daniel Grimmer did the remaining calculations; the plots were jointly obtained by Daniel Grimmer and myself. The manuscript has been collaboratively written.

Abstract

In this thesis, we study the interaction of a first-quantized atomic system with the quantum electromagnetic field within the context of relativistic quantum information (RQI). To that end, we examine common classes of Hamiltonians – in particular, the dipolar coupling model as well as scalar field analogues (Unruh-DeWitt models) – for their applicability in RQI setups. Firstly, we investigate how quantum randomness generation based on unbiased measurements on an atom can get compromised by an adversary that has access to the electromagnetic field. We show that preparing the atom in the ground state in the presence of no field excitations is, in general, not the best choice to generate randomness. Secondly, at the study of light-matter interactions inside optical cavities, we show that frequently employed approximations, such as the single-mode approximation and dimensional reduction, fail for relativistic regimes but can be already ill-behaved for non-relativistic scenarios. In particular, we show how approximating a very long and thin cavity by a one-dimensional system can be understood by recasting the $D+1$ dimensional quantum field inside the cavity as an infinite sum of massive $1+1$ dimensional fields. The dimensional reduction approximation can subsequently be identified with ignoring all but *one* of these subfields or, equivalently, with a change of the atomic localization.

Up to this point, we have treated the atomic center of mass classically – a feature that is shared by usual Hamiltonians in RQI and quantum optics. We therefore revisit the interaction of atoms and light by considering all atomic degrees of freedom to be quantum. Further, we discuss subtleties with respect to the gauge nature of light and the effect that multipole approximations have. This allows us to connect the multipolar Hamiltonian with the common effective models of quantum optics and relativistic quantum information. In particular, we discuss the influence of atomic center-of-mass delocalization and the presence of the so-called Röntgen term. Significantly, Unruh-DeWitt models fail to account for the entangling interaction between all atomic and field degrees of freedom, and we present then a scalar analogue of the Röntgen term. Finally, we demonstrate how the usual dipole model preserves covariance when considering atoms on relativistic trajectories and how this model can be used as a qualitative means to study RQI scenarios.

Acknowledgements

I would like to thank my Supervisor Eduardo Martín-Martínez for his support and dedication. In particular, I would also like to thank Achim Kempf and Robert Mann for their insights and feedback.

Further, I want to thank my collaborators, colleagues and friends that helped me grow professionally and personally during my time in Waterloo. Amongst those are Don N. Page, José de Ramón Rivera, Juan Cayuso, Aida Ahmadzadegan, Nicholas Funai, Daniel Grimmer, Robert Jonsson, Maria Papageorgiou, Rick Perche, Jason Pye, Nayeli Rodríguez-Briones, Petar Simidzija, Nadine Stritzelberger, and Erickson Tjoa.

Lastly, I am indebted to my family and friends back home in Europe, and to my partner who supported me all the way.

Im Nebel ruhet noch die Welt,
Noch träumen Wald und Wiesen:
Bald siehst du, wenn der Schleier fällt,
Den blauen Himmel unverstellt,
Herbstkräftig die gedämpfte Welt
In warmem Golde fließen.

Eduard Mörike (1804–1875)

Table of Contents

List of Figures

List of Tables

Chapter 1

Introduction

A whole plethora of fields and methods has been established around the goal to model light-matter interactions: from phenomenological approaches to the pure quantum field theoretic perspective, from the single electron response to the collective behavior of macroscopic matter. One of the simplest, yet abundant in its phenomenology and experimental relevance, is the interaction of light with a single bound system – an atom, and in particular hydrogen. From a physical point of view, the importance of atomic optics is explained by the richness of dynamics due to the internal atomic degrees of freedom.

Historically, atoms allowed for many insights into quantum mechanics and the development of quantum technologies. In 1913, the Bohr-Sommerfeld model as a first-order approximation enabled the computation of the energy levels of hydrogen by quantizing the electron's orbital angular momentum [5, 6]. These results have long been refined through the inclusion of relativity. First due to Dirac in 1928 [7], and then later, after noting the presence of the Lamb shift [8] in 1947, through quantum electrodynamics. Resonance fluorescence [9, 10, 11], i.e. the emission of photons from an atom driven by light close to its transition frequency, led to witness the non-classical effect of photon antibunching in 1977 [12]. With the development of high finesse cavities, one-atom masers [13, 14] and one-atom lasers [15, 16], radiation sources in the microwave and optical regime could be constructed which in turn led to the study of quantum features such as entanglement and decoherence [17, 18]. Generally, high control can be exerted on atoms through the method of laser cooling and traps, such as the Paul trap [19]. Moreover, through atom interferometers, similar to a Stern-Gerlach setup, one can for instance measure the fine-structure constant [20] and the gravitational constant [21].

On the other hand, extracting local information from a quantum field theoretic (QFT)

setup led to the idea of detector models [22, 23, 24, 25, 26] – bound systems with (non-relativistic) internal degrees of freedom. Atoms seem then a natural choice for real-life detectors. For example, they can be used to describe the Unruh effect [27, 28, 22] which predicts that an accelerated detector registers a thermal bath of a temperature proportional to the acceleration – a purely QFT result. On top of that, experimental accuracy is reaching extraordinary scales. For instance, the delay in a molecule between photon absorption and electron emission has been resolved via means of electron interferometry to $2.5 \cdot 10^{-19}$ seconds [29]. This implies the necessity to consider relativistic aspects – within simple atomic models at leading order. Namely, what is the role of causality, and how and when do approximations break down?

Taking together the long historical development and the physical complexity, it is thus not surprising that even within the realm of a single atom interacting with light there exists a multitude of different interaction models. Ultimately, this is not only due to gauge degrees of freedom, e.g. departing from the minimal coupling Hamiltonian using a semi-classical Goeppert-Mayer [30] or a quantum Power-Zienau-Woolley transformation [31], but also due to the level of approximation, e.g. using the dipole model [30] versus Jaynes-Cummings models [32, 33]. In particular, when one is interested in relativistic regimes, as for instance in Relativistic Quantum Information (RQI), stronger simplifications are often employed to allow for tractable models, i.e. the scalar simplification of electromagnetism via Unruh-DeWitt (UDW) models [22, 23]. The purpose of this thesis is to analyze the different common effective Hamiltonian models for their applicability and limitations in RQI. 'Effective' refers to models that neglect the dynamical nature of a quantum center of mass (COM) of an atom that interacts with a quantum field. Instead, the COM is here being treated classically. These effective models will then be compared to a more realistic interaction model – the multipolar Hamiltonian with a quantized atomic COM – yet with the limitation of being non-relativistic. The insights learned from both approaches, effective and fully quantized theory, will then be used to motivate two perspectives on the former method. Effective models may be modified to account for new phenomenology, or their limitations may be accepted in a qualitative fashion so as to gain order of magnitude insights into physical scenarios.

In Chapter 2 we will examine effective models of the light-matter interaction. We will begin by discussing the UDW Hamiltonian, which is the most common model in studies of RQI. Here, the electric field is replaced by a scalar field to emulate a simplified dipole coupling. As this reduces the complexity of electromagnetism to a scalar theory, aspects connected to angular momentum exchange cannot be accounted for by it [24, 25, 26]. Naturally then, we will also analyze the dipolar coupling interaction itself. It is the leading order approximation to the light-matter interaction derived from the minimal

coupling Hamiltonian via a canonical transformation [34]. Ultimately, it is the centerpiece of many quantum optical models, and we will revisit its connection to those. The Jaynes-Cummings model, for instance, is one of the most ubiquitously used ones in quantum optics due to its simplifying approximations, amongst others the single-mode and rotating-wave approximation [35, Ch. 5], that render it an easily analytically-solvable problem.

In the following three chapters, we will see applications of effective light-matter models and the validity of typical approximations within those. We will focus on both free space and cavity scenarios. In Chapter 3, we will, within the dipole model, analyze quantum random number generation based on measurements on a hydrogenic atom when an adversary has access to the electromagnetic field. Through atom-field correlations the adversary can compromise the randomness generation, and it will become apparent that the usual notion of the atomic ground state, being the most secure state, cannot hold in general. Further, we will compare predictions of the dipole model to the predictions of different UDW interaction prescriptions. Indeed, in the scalarization of the dipole coupling some degree of arbitrariness is inherent. We therefore examine the standard UDW model and a derivative version, where the electric field is replaced by the time derivative of a scalar field. For an example scenario it will be shown that both UDW models coincide with the dipolar model for long times. For short time scales, however, the derivative coupling model deviates significantly from the dipolar one.

Secondly, in Chapter 4, we will study the physics of moving atoms crossing an optical cavity. Here, we will work within the UDW model and examine the aptitude of common approximations, in particular a single-mode and a non-relativistic approximation. To that end, we will focus on both the response of the atom as well as the number of excitations in the field after the atom crossed the cavity. We will consider accelerated and constant-velocity atoms in different relativistic regimes. We will show that the single-mode approximation not only fails generally for relativistic atomic trajectories, mainly due to the Doppler effect, but also in non-relativistic regimes for vacuum excitations processes. A non-relativistic approximation, as we will see, will only hold for a limited number of field modes (for *any* fixed atomic acceleration) that are either close to resonance with the atom or have sufficiently low quantum numbers.

In Chapter 5 we will continue working with atoms in optical cavities. Here, however, the focus will lie on the dimensional reduction approximation. Our objective will be to determine if we can treat, for instance, a three dimensional cavity as a one dimensional system in the case of separation of length scales, i.e. if one cavity length is much smaller than the remaining ones. We will investigate this for cavities that observe an axial symmetry and show that the (usually massless) higher-dimensional quantum field inside the cavity can be recast as an infinite sum of effectively massive fields in one dimension (which we call

subfields). The dimensional reduction approximation, as we will show, can be understood then as dropping the coupling of the atom to all but *one* subfield, which in turn alters the atom's spatial profile. We will argue for the generality of the approach for a broad variety of cavity geometries and boundary conditions. Thus, any dimensional reduction approximation will have to take into account these effective masses. Finally, as a concrete example by connecting back to Chapter 4, we will evaluate for moving and stationary atoms how many of these lower-dimensional subfields will be needed to accurately reconstruct the full physical process. We will find a strong dependence on the spatio-temporal coupling between atom and field, on the relativistic nature of the atomic trajectory as well as on the atom's resonance to individual subfields.

The effective models that we will have studied until then only consider externally prescribed atomic trajectories but evidently neglect phenomenology connected to quantum delocalization of the COM as well as leading order interaction terms [36, 37, 38]. This will be studied in Chapter 6 when we will re-derive the (non-relativistic) multipolar Hamiltonian from the two-particle minimal coupling Hamiltonian using a canonical Power-Zienau-Woolley transformation [36]. All degrees of freedom of the atom and light will be treated as quantum, which results in, to leading order, the usual dipole term as well as what is known as a Röntgen term. This term arises due to the COM-induced currents coupling to the magnetic field and entangles all (internal and external) atomic and field degrees of freedom. From the phenomenological example of atomic transition rates, we shall study the implication of COM delocalization and the Röntgen term. In particular, the standard expressions are corrected by a term quadratic in the initial uncertainty of the COM momentum as well as by a term proportional to the energy difference between the initial and final state. Lastly, the influence of higher order relativistic corrections to the multipolar Hamiltonian will be discussed. Specifically, as the multipolar Hamiltonian is the lowest order non-relativistic approximation, it does not account for a dynamical mass-energy relationship and instead allows for spurious friction forces [39].

With the results of the previous chapter, we will then have the means to evaluate the effective models from a new perspective in Chapter 7, and we will address the issue in what sense they can retain their validity. Even though effective models ignore dynamics associated with the COM, they can be regarded as qualitative models in relativistic regimes. In particular, we will show that, at the example of the dipole model, covariant predictions for changes of reference frames are maintained. This is made explicit by studying the transformation properties of the effective dipole Hamiltonian and for the example of transition probabilities, first calculated in the atomic rest frame, and then compared to a boosted observer. To that end we will also provide analytic expressions for all electromagnetic Wightman tensors. The covariance of the effective dipole model is contrasted

by the multipolar Hamiltonian and other non-relativistic atomic models that at most observe a Galilean invariance. Thus, we have the means to qualitatively study RQI setups. As an alternative approach to effective models, now at the example of the UDW model, we will show that the models may be modified to account for the dynamics induced by COM degrees of freedom. In particular, we will introduce a scalar analogue of the Röntgen interaction.

Chapter 2

Effective Light-Matter Interaction Models

We will examine in this chapter some of the most commonly applied models in RQI and quantum optics to represent the interaction between an atom and light. Importantly, they share the common feature of a classical atomic COM, and we shall refer to them as *effective models*. We will see that these most common effective models are all connected in some form to the dipole model, either through approximations (like the single-mode or rotating-wave approximation) or analogue identifications (like replacing the electric vector field operator with a scalar one). Understanding the assumptions and simplifications that lead to these models will be crucial before we can work with them, and before we extend them beyond the assumption of a classical COM, in the following chapters.

The structure of this chapter is as follows: In Sec. 2.1 we will present the Unruh-DeWitt model as a representative of scalar-field analogues to the light-matter interaction. In Sec. 2.2 we will discuss the dipolar coupling Hamiltonian and show how it relates to the UDW model. We will, further, see in Sec. 2.3 how the dipolar model can be reduced to common models in quantum optics, such as the Jaynes-Cummings or Dicke Hamiltonians. In Sec. 2.4 we will provide the background for studying the dynamics of the interaction models that we will use throughout this thesis. Lastly, in Sec. 2.5 we will provide a summary of this chapter.

2.1 The Unruh-DeWitt Model

In the context of RQI, or generally if the objective is to obtain information in a QFT setting, the notion of a *particle detector* that can extract this information locally from a quantum field is crucial. A particle detector is an internally non-relativistic[1] quantum system that couples in a covariant way to a second-quantized field. It circumvents the problems of projective measurements in QFT [40, 41], and may give rise to a phenomenological interpretation for the elusive notion of particles in QFT [42]. Particle detectors have been crucially used in a plethora of scenarios in quantum field theory in flat and curved spacetimes (e.g., the Unruh and Hawking effects [22, 43], cosmological particle creation [44], entanglement harvesting [45, 46], etc). The most common model of a particle detector is the UDW model, e.g. [22, 23]. This model typically considers a two-level non-relativistic quantum system rigidly localized in space and time that covariantly couples to a quantum scalar field amplitude $\hat{\phi}(t, \boldsymbol{x})$ along its (possibly relativistic) trajectory. The UDW interaction-picture interaction Hamiltonian in the most general case is given by [47]:

$$\hat{H}_{\text{UDW}} = \hbar c \lambda \chi(\tau) \hat{\mu}(\tau) \otimes \int_{\Sigma_\tau} \mathrm{d}^3\boldsymbol{\xi} \sqrt{-g}\, F(\boldsymbol{\xi}) \hat{\phi}(t(\tau, \boldsymbol{\xi}), \boldsymbol{x}(\tau, \boldsymbol{\xi})), \tag{2.1}$$

where $[t, \boldsymbol{x}]$ is the field quantization frame, $[\tau, \boldsymbol{\xi}]$ is the Fermi-Walker frame comoving with the center-of-mass of the detector, Σ_τ are the spatial sections associated with the coordinates $[\tau, \boldsymbol{\xi}]$, g is the determinant of the metric, $\hat{\mu}(\tau)$ is the monopole moment representing the internal degree of freedom of the detector, $\chi(\tau)$ encodes the time-dependence of the coupling in the detectors COM frame, $F(\boldsymbol{\xi})$ is the spatial profile of the detector, and, finally, λ is the (in 3+1D dimensionless) coupling strength.

From a practical perspective, the so-called switching function $\chi(t)$ enables us to let the boundaries of the integration of the time evolution go to $\pm\infty$. We will also assume in most calculations that in the asymptotic past and future, atom (or detector) and field are uncoupled, i.e. the switching function falls off rapidly enough or has compact support. From a physical side it can be thought of as a way to account for the finite time between preparation and measurement: a compactly supported switching function sets a clear time stamp of the preparation time (the initial interaction time after preparation) and the measurement time (the amount of time from preparation to measurement). In addition, a switching function allows us to model more accurately experimental setups. For instance, we could initially place an atom inside a small enough cavity such that the lowest energy

[1] This assumption is motivated by the fact that in hydrogenic atoms the electron is usually well within the non-relativistic regime.

mode of the cavity determined by the IR cut-off is already off-resonant to the energy gap of the atom. In that case, the atom being placed inside a Faraday cage effectively does not interact with the cavity field nor with the field outside. When we subsequently remove the cavity, we create a coupling between atom and field. The interaction time is finite if we bring back the cavity. This could correspond to a sudden top-hat switching function if the cavity is removed and brought back quick enough [48]. More generally, even when we study the behavior of atom-field interaction in free space in the following, one can model the evolution in a highly controlled light-matter interaction setup. It is possible to temporally vary the coupling strength between a superconducting qubit and the electromagnetic field inside a microwave cavity. In that way one can design a range of switching functions [49, 48].

In flat spacetime, the Hamiltonian (2.1) simply becomes

$$\hat{H}_{\text{UDW}} = \hbar c\lambda\, \chi(\tau)\hat{\mu}(\tau) \otimes \int_{\mathbb{R}^3} \mathrm{d}^3\boldsymbol{x}\; F(\boldsymbol{\xi})\, \hat{\phi}\left(t(\tau,\boldsymbol{\xi}), \boldsymbol{x}(\tau,\boldsymbol{\xi})\right). \tag{2.2}$$

Accordingly, we can expand the scalar field in terms of plane wave modes of momentum $\boldsymbol{k}$ with respective creation ($\hat{a}^\dagger_{\boldsymbol{k}}$) and annihilation ($\hat{a}_{\boldsymbol{k}}$) operators, satisfying equal-time canonical commutation relations:

$$\hat{\phi}(t,\boldsymbol{x}) = \int \frac{\mathrm{d}^3\boldsymbol{k}}{(2\pi)^{3/2}} \sqrt{\frac{c}{2\omega}} \left(e^{-\mathrm{i}\omega t + \mathrm{i}\boldsymbol{k}\cdot\boldsymbol{x}} \hat{a}_{\boldsymbol{k}} + \text{H.c.}\right), \tag{2.3}$$

where $\omega = c|\boldsymbol{k}|$. Although simple, the Hamiltonian (2.2) already captures a large amount of the phenomenology of the light-matter interaction. Indeed, the popular Dicke [50] and Jaynes-Cummings models [32] are but further simplifications of the UDW model (typically assuming point-like detectors, single-mode approximation and some form of rotating-wave approximation). We will show an explicit comparison in Sec. 2.3.

The power of the UDW model lies in its computational applicability: while it certainly gives a reasonable effective model for carrying out measurements on quantum fields, computable results can be obtained even in complicated curved spacetime scenarios or involved relativistic detector trajectories.

There are, however, shortcomings of the model when it comes to describing the light-matter interaction. First, the scalar nature of the coupling makes it impossible for the model to capture phenomenology associated with the exchange of angular momentum between the detector and the field [24, 25, 26]. Also, the spatial smearing has to be prescribed 'by hand' since we do not have a first-principle-inspired reason to choose the exact shape of the detector's localization [24]. Finally, this model considers that the COM

of the detector is a classical degree of freedom whose dynamics are decoupled from the detector's internal levels. This does not mean that the model is not useful, but rather that refinements are needed if we want to go beyond rough order of magnitude estimates in realistic atomic systems, or in regimes where the neglected aspects of the interaction play a key role.

2.2 The Dipole Coupling

One step forward in adding complications to the effective light-matter interaction models is obtained by assuming that the atom is modelled by a classical infinite mass proton (as compared to the electron of mass m_e) that generates a classical Couloumb potential in the atomic COM frame (which, in turn, gives rise to the internal energy levels for the atomic system). Therefore, the (effective one-particle) minimal coupling Hamiltonian reads [51]:

$$\hat{H}^{\text{eff}} = \frac{1}{2m_e}(\hat{\boldsymbol{p}}_e + e\hat{\boldsymbol{A}}(t, \hat{\boldsymbol{r}}_e))^2 - e\hat{U}(t, \hat{\boldsymbol{r}}_e) - \frac{e^2}{4\pi\epsilon_0|\hat{\boldsymbol{r}}_e|}, \tag{2.4}$$

where $(\hat{U}, \hat{\boldsymbol{A}})$ are the quantized scalar and vector potentials, $(\hat{\boldsymbol{r}}_e, \hat{\boldsymbol{p}}_e)$ are the electron position operator and its canonical momentum, and e is the elementary electric charge. Here, we assumed that the field degrees of freedom are in the interaction picture with respect to time t. Let us consider the transformation [34]

$$\hat{\mathcal{U}}_1 = \exp\left(\frac{\mathrm{i}}{\hbar}e\hat{\Lambda}_1\right), \tag{2.5}$$

generated by

$$\hat{\Lambda}_1(t, \hat{\boldsymbol{r}}_e) = \hat{\boldsymbol{r}}_e \cdot \int_0^1 \mathrm{d}u\, \hat{\boldsymbol{A}}\left(t, u\hat{\boldsymbol{r}}_e\right), \tag{2.6}$$

and apply it to the minimal coupling Hamiltonian (2.4). Note that (2.6) corresponds to a line integral over the vector potential from the proton to the electron position where, for simplicity, we assumed that the atom is comoving with the field quantization frame (something that we will relax in Sec. 7.1). In contrast to the case where there is COM dynamics, (2.6) is a gauge transformation where the transformed potentials can be expressed in terms

of the electric and magnetic field [34]:

$$\hat{\mathcal{U}}_1 \hat{\boldsymbol{A}}(t, \hat{\boldsymbol{r}}_e)\hat{\mathcal{U}}_1^\dagger + \frac{1}{e}\hat{\mathcal{U}}_1 \hat{\boldsymbol{p}}_e \hat{\mathcal{U}}_1 = -\hat{\boldsymbol{r}}_e \times \int_0^1 \mathrm{d}u\ u\hat{\boldsymbol{B}}(t, u\hat{\boldsymbol{r}}_e), \tag{2.7}$$

$$\hat{\mathcal{U}}_1 \hat{U}(t, \hat{\boldsymbol{r}}_e)\hat{\mathcal{U}}_1^\dagger + \frac{\mathrm{i}\hbar}{e}\hat{\mathcal{U}}_1 \partial_t \hat{\mathcal{U}}_1 = -\hat{\boldsymbol{r}}_e \cdot \int_0^1 \mathrm{d}u\ \hat{\boldsymbol{E}}(t, u\hat{\boldsymbol{r}}_e) - e\hat{\delta}, \tag{2.8}$$

with $\hat{\delta}$ being a self-energy that needs to be regularized. If we insert the transformed potentials Eq. (2.7) and (2.8) into the minimal coupling Hamiltonian (2.4), this yields [34]

$$\hat{H}^{\text{eff}} = \frac{1}{2m_e}\left(\hat{\boldsymbol{p}}_e - e\hat{\boldsymbol{r}}_e \times \int_0^1 \mathrm{d}u\ u\hat{\boldsymbol{B}}(t, u\hat{\boldsymbol{r}}_e)\right)^2 + e\hat{\boldsymbol{r}}_e \cdot \int_0^1 \mathrm{d}u\ \hat{\boldsymbol{E}}(t, u\hat{\boldsymbol{r}}_e) + e^2\hat{\delta} - \frac{e^2}{4\pi\epsilon_0|\hat{\boldsymbol{r}}_e|}. \tag{2.9}$$

We will consider now those interaction terms that are leading order in the coupling e and Bohr radius a_0. Note that, as we shall see later in more detail, the factors of the Bohr radius appear in position representation through the hydrogenic wavefunctions. Therefore, the only leading order interaction contribution is the electric field term. Since, again, we are interested in the lowest order electric multipole, i.e. the dipole, we approximate the non-local integral form to

$$\hat{\boldsymbol{r}}_e \cdot \int_0^1 \mathrm{d}u\ \hat{\boldsymbol{E}}(t, u\hat{\boldsymbol{r}}_e) \approx \hat{\boldsymbol{r}}_e \cdot \hat{\boldsymbol{E}}(t, \hat{\boldsymbol{r}}_e). \tag{2.10}$$

In the next section we will discuss another prescription that evaluates the field at the origin. However, as we are considering the full field operator without any further approximations such a prescription would result in divergences unless we introduce a UV cutoff. Of course, this cutoff is ultimately necessary in a non-relativistic description of the atom [52, Ch. 3]. Nonetheless, it can be avoided by localizing the interaction with the electronic wavefunctions from the beginning in a natural way.

Hence, after gauge transformation and to leading order, the atom couples dipolarly to a time dependent second-quantized electric field as seen from the COM frame of the atom [24]:

$$\hat{H}^{\text{eff}} = \hat{H}_0^{\text{eff}} + \hat{H}_I^{\text{eff}}, \tag{2.11}$$

$$\hat{H}_0^{\text{eff}} = \frac{\hat{\boldsymbol{p}}_e^2}{2m_e} - \frac{1}{4\pi\epsilon_0}\frac{e^2}{|\hat{\boldsymbol{r}}_e|}, \tag{2.12}$$

$$\hat{H}_I^{\text{eff}} = e\hat{\boldsymbol{r}}_e \cdot \hat{\boldsymbol{E}}(t, \hat{\boldsymbol{r}}_e). \tag{2.13}$$

To effectively compare this model with the UDW model (2.2), let us introduce a position representation in terms of the hydrogenic wavefunctions that are solutions of the Schrödinger equation for $\hat{H}_0^{\text{eff}}$. That is, $\Psi_{\boldsymbol{a}}(\boldsymbol{r}_e) = \langle \boldsymbol{r}_e | \boldsymbol{a} \rangle$, where $\{|\boldsymbol{a}\rangle = |(n, \ell, m)\rangle\}$ such that [24, 26]

$$\begin{aligned}
\hat{H}_I^{\text{eff}} =& e \sum_{\boldsymbol{a},\boldsymbol{b}} \int_{\mathbb{R}^3} \mathrm{d}^3 \boldsymbol{r}_e \, \langle \boldsymbol{a} | \boldsymbol{r}_e \rangle \, \langle \boldsymbol{r}_e | \boldsymbol{b} \rangle \, \boldsymbol{r_e} \cdot \hat{\boldsymbol{E}}(t, \boldsymbol{r}_e) \, |\boldsymbol{a}\rangle\langle\boldsymbol{b}| \\
=& e \sum_{\boldsymbol{a},\boldsymbol{b}} \int_{\mathbb{R}^3} \mathrm{d}^3 \boldsymbol{r}_e \, \Psi_{\boldsymbol{a}}(\boldsymbol{r}_e)^* \Psi_{\boldsymbol{b}}(\boldsymbol{r}_e) \boldsymbol{r_e} \cdot \hat{\boldsymbol{E}}(t, \boldsymbol{r}_e) \, |\boldsymbol{a}\rangle\langle\boldsymbol{b}| \\
=:& \sum_{\boldsymbol{a}>\boldsymbol{b}} \int_{\mathbb{R}^3} \mathrm{d}^3 \boldsymbol{r}_e \, \hat{\boldsymbol{d}}_{\boldsymbol{ab}}(\boldsymbol{r}_e) \cdot \hat{\boldsymbol{E}}(t, \boldsymbol{r}_e),
\end{aligned} \tag{2.14}$$

where in the last step we defined the dipole operator $\hat{\boldsymbol{d}}_{\boldsymbol{ab}}(\boldsymbol{r}_e)$, and the ordering $\boldsymbol{a} > \boldsymbol{b}$ is first with respect to n, then ℓ and lastly m – so as to follow the energy hierarchy approximately, (although in this approximate model only the quantum number n gives the internal energy of the atom). Notice that the diagonal terms of the dipole operator can be directly removed since there is a change of parity selection rule for electric dipole transitions [53, Ch. 27]. If we express the internal atomic degrees of freedom in the interaction picture with respect to time t as well, the dipole operator between two levels $|\boldsymbol{a}\rangle$ and $|\boldsymbol{b}\rangle$ is of the form

$$\hat{\boldsymbol{d}}_{\boldsymbol{ab}}(t, \boldsymbol{r}_e) = e \boldsymbol{F}_{\boldsymbol{ab}}(\boldsymbol{r}_e) e^{\mathrm{i}\Omega_{\boldsymbol{ab}} t} \, |\boldsymbol{a}\rangle\langle\boldsymbol{b}| + \text{H.c.} \tag{2.15}$$

The spatial *smearing vector* is given by the hydrogen wavefunctions of the two levels connected by each matrix element: $\boldsymbol{F}_{\boldsymbol{ab}}(\boldsymbol{r}_e) = \boldsymbol{r}_e \Psi_{\boldsymbol{a}}^*(\boldsymbol{r}_e) \Psi_{\boldsymbol{b}}(\boldsymbol{r}_e)$, and $\hbar\Omega_{\boldsymbol{ab}} = E_a - E_b$ is the energy difference between the states $|\boldsymbol{a}\rangle$ and $|\boldsymbol{b}\rangle$.

In the same fashion as for the UDW model, we will encode the time dependent coupling between atom and field in the switching function $\chi(t)$ in order to study finite-time processes. The interaction Hamiltonian (in the joint interaction picture) reads then [24]

$$\hat{H}_I^{\text{eff}} = \chi(t) \sum_{\boldsymbol{a}>\boldsymbol{b}} \int_{\mathbb{R}^3} \mathrm{d}^3 \boldsymbol{r}_e \, \hat{\boldsymbol{d}}_{\boldsymbol{ab}}(t, \boldsymbol{r}_e) \cdot \hat{\boldsymbol{E}}(t, \boldsymbol{r}_e). \tag{2.16}$$

In contrast to the UDW model where the spatial localization of the coupling was introduced by hand, from (2.15) we see that the localization of the dipolar interaction is governed by the electronic wavefunctions. In this light, when we add a switching function modelling the beginning and the end of a finite-time process, a comparison of equations (2.16) and (2.2) shows in what sense this model is a refinement of the UDW model for the light-matter

interaction: we could think of the UDW coupling as the scalar version of this effective dipole coupling, and we have a way to prescribe the localization of the coupling out of the physical assumptions of the dipolar model without having to introduce it *ad hoc* [24].

In the regimes commonly analyzed in RQI finite-time couplings can excite the atom out of its interaction with the vacuum (see, among many others, [54, 55, 56]). This is important because even though the dipole approximation is a rather common one, it is usually obtained claiming the existence of some characteristic wavelength that dominates the process. The reasoning is then that if the atom is small enough as compared to the dominant wavelength, we can approximate it by a point-like object and take only the first term on a multipole expansion, something that is not possible to justify when studying vacuum fluctuations. In those contexts, it was argued in [57] that a multipole (and in particular a dipole) approximation can indeed be justified if the duration of the interaction is much larger than the light-crossing time of the atom. In a few words, the frequencies that take part in a vacuum excitation process are suppressed with the tails of the Fourier transforms of the functions encoding the time-dependence of the coupling, as well as the spatial smearing of the atom. It was then shown in [57] that if the interaction times are much longer than the characteristic length of the atom's wavefunction, the suppression of the shorter frequencies is strong enough for a dipole expansion to be a good approximation.

The advantages of the effective dipole coupling are that it is still a simple model, as the only quantum degree of freedom of the atom is the position of the electron. Furthermore, it still allows for arbitrary relativistic trajectories for the COM frame, whose position is treated classically (as we will see in Sec. 7.1). Additionally it accounts for the exchange of orbital angular momentum between the atomic internal degrees of freedom and the electromagnetic field. Lastly, the dipole coupling is a) gauge unambiguous, and b) it is inspired by typical light-matter interaction assumptions where higher multipoles are neglected.

However, this is still an effective model. We emphasize again that the assumptions that went into the derivation of Eq. (2.13) neglect the dynamics of any atomic degrees of freedom other than the ones associated with the electron. In that sense, the dipole term is introduced somewhat *ad hoc*, instead of rigorously obtained from the two-particle minimal-coupling light-matter interaction after careful gauge and multipole considerations are taken into account. Same as the UDW model, this does not mean that the model is not useful. In fact, as we will discuss in Sec. 7.1 this model can also be made fully covariant same as it was shown for the UDW model in [47, 58]. Rather, we argue that one has to refine this model if one wants to go beyond qualitative results and rough order of magnitude estimations and, instead, wants to predict outcomes of experiments in more involved regimes where the assumptions of the model are not fulfilled.

For later purposes, we give here the expression for the different electromagnetic field operators. We will expand the field operators into plane-wave modes of momentum $\boldsymbol{k}$ and polarization s, with their respective creation and annihilation operators $\hat{a}^\dagger_{\boldsymbol{k},s}$ and $\hat{a}_{\boldsymbol{k},s}$, satisfying the canonical equal-time commutation relations. In this form, the field operators can be written as

$$\hat{\boldsymbol{A}}(t,\boldsymbol{x}) = \sum_{s=1}^{2} \int_{\mathbb{R}^3} \frac{\mathrm{d}^3\boldsymbol{k}}{(2\pi)^{\frac{3}{2}}} \sqrt{\frac{\hbar}{2\epsilon_0 c|\boldsymbol{k}|}} \left(\hat{a}_{\boldsymbol{k},s}\boldsymbol{\epsilon}_{\boldsymbol{k},s} e^{-\mathrm{i}\omega t} e^{\mathrm{i}\boldsymbol{k}\cdot\boldsymbol{x}} + \text{H.c.}\right), \tag{2.17}$$

$$\hat{\boldsymbol{E}}(t,\boldsymbol{x}) = \sum_{s=1}^{2} \int_{\mathbb{R}^3} \frac{\mathrm{d}^3\boldsymbol{k}}{(2\pi)^{\frac{3}{2}}} \sqrt{\frac{\hbar c|\boldsymbol{k}|}{2\epsilon_0}} \left(\mathrm{i}\hat{a}_{\boldsymbol{k},s}\boldsymbol{\epsilon}_{\boldsymbol{k},s} e^{-\mathrm{i}\omega t} e^{\mathrm{i}\boldsymbol{k}\cdot\boldsymbol{x}} + \text{H.c.}\right), \tag{2.18}$$

$$\hat{\boldsymbol{B}}(t,\boldsymbol{x}) = \sum_{s=1}^{2} \int_{\mathbb{R}^3} \frac{\mathrm{d}^3\boldsymbol{k}}{(2\pi)^{\frac{3}{2}}} \sqrt{\frac{\hbar|\boldsymbol{k}|}{2c\epsilon_0}} \left(\mathrm{i}\hat{a}_{\boldsymbol{k},s}(\boldsymbol{e}_{\boldsymbol{k}} \times \boldsymbol{\epsilon}_{\boldsymbol{k},s}) e^{-\mathrm{i}\omega t} e^{\mathrm{i}\boldsymbol{k}\cdot\boldsymbol{x}} + \text{H.c.}\right), \tag{2.19}$$

where $\omega = c|\boldsymbol{k}|$ and we denoted as $\{\boldsymbol{\epsilon}(\boldsymbol{k},s)\}_{s=1}^2$ an arbitrary set of two independent transverse polarization vectors ($\boldsymbol{k}\cdot\boldsymbol{\epsilon}(\boldsymbol{k},s) = 0$). Together with the normalized wave vector $\boldsymbol{e}_{\boldsymbol{k}} = \boldsymbol{k}/|\boldsymbol{k}|$ they form an orthonormal basis of $\mathbb{R}^3$.

2.3 Relation to Common Quantum Optical Models

The dipolar coupling model is indeed of central importance in quantum optics. It generates an important class of quantum optical models simplifying the interaction of a single atom to the electromagnetic field, commonly applied in cavities. Most wide-spread is the Jaynes-Cummings model [32, 33]. In order to derive it, we assume that the electron position is approximately at the origin, or equivalently the COM position. The reasoning behind it is that in the dipole approximation $|\boldsymbol{k}\cdot\boldsymbol{r}_e| \ll 1$, i.e. all wave vector components of the quantum field vary very little over the spatial extent of the atom. The one-particle minimal coupling Hamiltonian (2.4) simplifies then to [52, Ch. 4]

$$\hat{H}^{\text{eff}} \approx \frac{1}{2m_e}(\hat{\boldsymbol{p}}_e + e\hat{\boldsymbol{A}}(t,0))^2 - e\hat{U}(t,0) - \frac{e^2}{4\pi\epsilon_0|\hat{\boldsymbol{r}}_e|}. \tag{2.20}$$

Similarly, the gauge transformation (2.6) reduces to

$$\hat{\Lambda}_1(t,\hat{\boldsymbol{r}}_e) \approx \hat{\boldsymbol{r}}_e \cdot \hat{\boldsymbol{A}}\,(t,0)\,. \tag{2.21}$$

This implies that the interaction Hamiltonian after the transformation is of the form [52, Ch. 4]

$$\hat{\tilde{H}}_I^{\text{eff}} = e\hat{\boldsymbol{r}}_e \cdot \hat{\boldsymbol{E}}(t,0), \tag{2.22}$$

where we, again, go to leading order in the Bohr radius a_0 and coupling e. Importantly, the field operator in Eq. (2.22) is no longer a function of the electron position, cf. (2.13). The difference between both interaction Hamiltonians is to leading order

$$\hat{H}_I^{\text{eff}} - \hat{\tilde{H}}_I^{\text{eff}} = e\hat{\boldsymbol{r}}_e(\hat{\boldsymbol{r}}_e \cdot \boldsymbol{\nabla}_{\boldsymbol{r}})\, \hat{\boldsymbol{E}}(t,\boldsymbol{r})\Big|_{\boldsymbol{r}=0} + \mathcal{O}(a_0^3) \tag{2.23}$$

which is suppressed by an additional factor of the Bohr radius. Note that (2.22), and (2.23) for that matter, is finite as there is the necessity for a UV cutoff in the field in order to stay in the non-relativistic quantum description of the atom. This is ultimately upper bounded by the Compton wavelength [52, Ch. 3].

Second, instead of considering all of the states of the internal atomic Hamiltonian (2.12), we assume now that the atom is a two-level system with eigenstates $\{|g\rangle, |e\rangle\}$ of energy $E_g < E_e$, respectively. Therefore, the full hydrogenic solution to the atomic free dynamics is reduced to a qubit system. Thus, the free atomic (now qubit) Hamiltonian reads [51]

$$\begin{aligned}\hat{H}_0^{\text{JC}} &= E_g\,|g\rangle\langle g| + E_e\,|e\rangle\langle e| \\ &= \frac{E-\hbar\Omega}{2}\mathbb{1} + \hbar\Omega\hat{\sigma}^+\hat{\sigma}^-,\end{aligned} \tag{2.24}$$

where $E = E_g + E_e$, $\hbar\Omega := E_e - E_g$, and $\hat{\sigma}^+ = |e\rangle\langle g| = (\hat{\sigma}^-)^\dagger$ are the qubit ladder operators. Note that Eq. (2.24) is also the common form for the internal dynamics of the particle detector in the UDW model of Sec. 2.1.

The next simplification we will take is the single-mode approximation of the field [51]. The field operator becomes, cf. Eq. (2.18), by considering only one $\{\boldsymbol{k}, s\}$ for wave vector and polarization, respectively,

$$\hat{\boldsymbol{E}}(t,\boldsymbol{x}) = \sum_{s=1}^{2}\int_{\mathbb{R}^3} \mathrm{d}^3\boldsymbol{k}\left(\mathrm{i}\hat{a}_{\boldsymbol{k},s}\boldsymbol{u}_{\boldsymbol{k},s}(\boldsymbol{x})e^{-\mathrm{i}\omega t} + \text{H.c.}\right) \longrightarrow \hat{\boldsymbol{E}}^{\text{SMA}}(t,\boldsymbol{x}) = \mathrm{i}\boldsymbol{u}_{\boldsymbol{k},s}(\boldsymbol{x})\hat{a}_{\boldsymbol{k},s}e^{-\mathrm{i}\omega t} + \text{H.c.}, \tag{2.25}$$

where $\boldsymbol{u}_{\boldsymbol{k},s}(\boldsymbol{x})$ are the mode functions. For instance, the free-space plane wave mode functions read

$$\boldsymbol{u}_{\boldsymbol{k},s}(\boldsymbol{x}) = \frac{\boldsymbol{\epsilon}_{\boldsymbol{k},s}}{(2\pi)^{\frac{3}{2}}}\sqrt{\frac{\hbar c|\boldsymbol{k}|}{2\epsilon_0}}e^{\mathrm{i}\boldsymbol{k}\cdot\boldsymbol{x}}. \tag{2.26}$$

We will evaluate the field operator only at one point in space (the origin), and may choose $\boldsymbol{u}_{\boldsymbol{k},s}$ to be real-valued. Thus, the interaction Hamiltonian (2.22) in the interaction picture reduces to [51]

$$\begin{aligned} e\hat{\boldsymbol{r}}_e(t)\cdot\hat{\boldsymbol{E}}^{\mathrm{SMA}}(t,0) &= \mathrm{i}e\boldsymbol{u}_{\boldsymbol{k},s}(0)\cdot(\,\langle e|\hat{\boldsymbol{r}}_e|g\rangle\,\sigma^+e^{\mathrm{i}\Omega t}+\mathrm{H.c.})(\hat{a}_{\boldsymbol{k},s}e^{-\mathrm{i}\omega t}-\mathrm{H.c.}) \\ &= \hbar g(e^{\mathrm{i}\Omega t}\sigma^+-\mathrm{H.c.})(\hat{a}_{\boldsymbol{k},s}e^{-\mathrm{i}\omega t}-\mathrm{H.c.}), \end{aligned} \tag{2.27}$$

where

$$g=\frac{\mathrm{i}e}{\hbar}\boldsymbol{u}_{\boldsymbol{k},s}(0)\cdot\,\langle e|\hat{\boldsymbol{r}}_e|g\rangle \tag{2.28}$$

is the vacuum Rabi frequency. It is assumed that $u_{\boldsymbol{k},s}(0)\cdot\,\langle e|\hat{\boldsymbol{r}}_e|g\rangle=-\mathrm{i}|u_{\boldsymbol{k},s}(0)\cdot\,\langle e|\hat{\boldsymbol{r}}_e|g\rangle\,|$ to render g real-valued. To arrive at the final expression for the Jaynes-Cummings model, one performs a rotating-wave approximation which removes the terms that have $\pm\mathrm{i}(\Omega+\omega)$ as arguments in the exponentials. As has been noted in [59, 60, 61, 62], the rotating-wave approximation allows for superluminal signalling due to the introduction of nonlocalities in the Hamiltonian. The resulting Jaynes-Cummings Hamiltonian is then of the form

$$\hat{H}_I^{\mathrm{JC}}=\hbar g(e^{\mathrm{i}(\Omega-\omega)t}\sigma^+\hat{a}_{\boldsymbol{k},s}+\mathrm{H.c.}). \tag{2.29}$$

By inspection, it is now possible to relate the UDW model of (2.2) to the Jaynes-Cummings Hamiltonian if we assume that the UDW detector is stationary in the field quantization frame ($\tau=t,\boldsymbol{\xi}=\boldsymbol{x}$), $\chi(t)=\mathrm{const.}$, $F(\boldsymbol{x})=\delta^{(3)}(\boldsymbol{x})$ and

$$\hat{\mu}(t)=e^{\mathrm{i}\Omega t}\hat{\sigma}^++e^{-\mathrm{i}\Omega t}\hat{\sigma}^-, \tag{2.30}$$

i.e. $\hat{\mu}=\hat{\sigma}_x$ in the Schrödinger picture. Further, a single-mode and rotating-wave approximation are required. On the other hand, one can extend (2.29) to include N number of two-level systems interacting with a single cavity mode which results in the Dicke model [63, 64]. Due to the collective behavior of the atoms there exists a superradiant phase of high-intensity emission.

2.4 Time Evolution

As we will be interested in the dynamics of light-matter systems, we will end this chapter by briefly addressing unitary time evolution. This section will be general enough to apply to all the Hamiltonian models we discussed so far. The time evolution of a coupled system

of atom/detector and quantum field is captured by the unitary operator $\hat{\mathcal{U}}$ acting on the initial joint state of the system $\hat{\rho}_0$ such that after the interaction the system is in the state

$$\hat{\rho}_{\mathrm{AF}} = \hat{\mathcal{U}}\hat{\rho}_0\hat{\mathcal{U}}^\dagger, \tag{2.31}$$

where

$$\hat{\mathcal{U}} = \mathcal{T}\exp\left(-\mathrm{i}\int_{-\infty}^{\infty}\mathrm{d}t\hat{H}_I(t)\right), \tag{2.32}$$

$\mathcal{T}$ denotes the time-ordering operation, and $\hat{H}_I$ is the appropriate interaction Hamiltonian. The time-evolved state will be calculated by a perturbative Dyson expansion of (2.32), granted the relevant parameters are small enough [65, Ch. 4]:

$$\hat{\mathcal{U}} = \mathbb{1} \underbrace{-\frac{\mathrm{i}}{\hbar}\int_{-\infty}^{\infty}\mathrm{d}t\,\hat{H}_I(t)}_{\hat{\mathcal{U}}^{(1)}} \underbrace{-\frac{1}{\hbar^2}\int_{-\infty}^{\infty}\mathrm{d}t\int_{-\infty}^{t}\mathrm{d}t'\,\hat{H}_I(t)\hat{H}_I\left(t'\right)}_{\hat{\mathcal{U}}^{(2)}} + \ldots \tag{2.33}$$

Thus, to second order in the appropriate coupling constant g the evolved state takes the form

$$\begin{aligned}\hat{\rho}_{\mathrm{AF}} &= \hat{\rho}_0 + \hat{\mathcal{U}}^{(1)}\hat{\rho}_0 + \hat{\rho}_0\hat{\mathcal{U}}^{(1)\dagger} + \hat{\mathcal{U}}^{(2)}\hat{\rho}_0 + \hat{\rho}_0\hat{\mathcal{U}}^{(2)\dagger} + \hat{\mathcal{U}}^{(1)}\hat{\rho}_0\hat{\mathcal{U}}^{(1)\dagger} + \mathcal{O}(g^3)\\ &=: \hat{\rho}_0 + \Delta\hat{\rho}_{\mathrm{AF}} + \mathcal{O}(g^3).\end{aligned} \tag{2.34}$$

Generally, we will be interested in either the response of the atom or the field after interaction. To that end, we trace over the corresponding complementary degrees of freedom. We shall in the subsequent chapters assume that the initial joint state is uncorrelated and usually of the form

$$\hat{\rho}_0 = \hat{\rho}_{\mathrm{A}} \otimes |0\rangle_{\mathrm{F}}\langle 0|\,, \tag{2.35}$$

where $|0\rangle_{\mathrm{F}}$ is the vacuum state of the field. If we are interested in the final atomic state, e.g. in Chapter 3, we have to trace over the field degrees of freedom. Then after interaction between atom and field, and before subsequent measurement on the atom, the final atomic state reads to second order

$$\hat{\rho}_{\mathrm{A}} = \hat{\rho}_{\mathrm{A}_i} + \mathrm{tr}_{\mathrm{F}}\left(\hat{\mathcal{U}}^{(1)}\hat{\rho}_0\hat{\mathcal{U}}^{(1)\dagger}\right) + \left(\mathrm{tr}_{\mathrm{F}}\left(\hat{\mathcal{U}}^{(2)}\hat{\rho}_0\right) + \mathrm{H.c.}\right) + \mathcal{O}(g^3), \tag{2.36}$$

where $\hat{\rho}_{\mathrm{A}_i}$ is the initial state of the atom. Note that in (2.36) there are no first order terms. This is because for the vacuum state $\mathrm{tr}_{\mathrm{F}}\left(\hat{\mathcal{U}}^{(1)}\hat{\rho}_0\right) = 0$. If, on the other hand, we

are interested in the field state, e.g. in Chapter 4, we will usually assume that the atom is initially in an energy eigenstate of its free Hamiltonian. Likewise, then, after interaction between atom and field, the final state of the field reads to second order

$$\hat{\rho}_{\mathrm{F}} = |0\rangle_{\mathrm{F}}\langle 0| + \mathrm{tr}_{\mathrm{A}}\left(\hat{\mathcal{U}}^{(1)}\hat{\rho}_0\hat{\mathcal{U}}^{(1)\dagger}\right) + \left(\mathrm{tr}_{\mathrm{A}}\left(\hat{\mathcal{U}}^{(2)}\hat{\rho}_0\right) + \mathrm{H.c.}\right) + \mathcal{O}(g^3). \tag{2.37}$$

Note that, as in (2.36), there are no first order terms since the atom starts in an energy eigenstate and therefore $\mathrm{tr}_{\mathrm{A}}\left(\hat{\mathcal{U}}^{(1)}\hat{\rho}_0\right) = 0$.

2.5 Summary

In this chapter, we studied different branches of effective light-matter models that are often applied in RQI and quantum optics. It became clear that all of the represented Hamiltonians can be related to the dipolar coupling Hamiltonian through several routes of simplifications. The UDW model of RQI is the scalar analogue of the dipole interaction introducing a degree of arbitrariness in the correspondence of the coupling and its spatial profile. Quantum optical models, most notably the Jaynes-Cummings model, typically employ approximations like the single-mode and rotating-wave approximation on the dipole model directly and those can become problematic in relativistic regimes. Naturally then, in the following three chapters we want to investigate in detail the usefulness of the here discussed models and approximations within the context of several topics that can be encountered in the literature. First, in the next chapter, we will focus on predictions of the dipole model and deviations from different scalar models in the context of quantum randomness generation.

Chapter 3

Quantum Randomness Generation

In our first study of effective light-matter models we will concentrate on the dipole model in a free space setting. Here we want to investigate how the resource of quantum randomness can be impacted by correlations and how predictions are altered by approximations.

Randomness is in itself a valuable resource for vastly different fields of science spanning game theory, chaos theory and cryptography. However, classical sources cannot generate true randomness since they might depend on prior information [66]. After all, classical mechanics is a deterministic theory and thus predictable. On the other hand, quantum theory provides a fundamental source of randomness. For example, the outcome of an unbiased measurement of an observable of a quantum system in a basis complementary to the basis in which it was prepared is *a priori* unpredictable.

In that sense, one can think of a plethora of quantum systems that one could use for extracting randomness. The majority of current quantum random number generators is of optical nature, e.g. photon counting or phase noise of lasers. Another major branch consists of electronic setups, e.g. noise generation in Zener diodes or electronic shot noise [67]. Both branches share the feature that the system used to generate quantum randomness is fundamentally and intrinsically coupled to the electromagnetic field. As such, the quantum system can become correlated with the electromagnetic field. In principle, those correlations can be exploited by adversaries to remotely make an educated guess on the outcome of the measurement without having physical access to the quantum system. In order to understand how randomness extraction can get compromised by the coupling between the quantum system used for randomness generation and the electromagnetic field, we want to study a very simple example from atomic physics: preparing a hydrogen-like atom in a given state and measuring in a complementary basis. Specifically, this setup resembles the

common method of using trapped ions to generate randomness [68, 69].

One may think that if the preparation and the measurement are done fast enough, no information about the outcome of the measurement can possibly be leaked to the electromagnetic field; given that the atom is in its ground state (so as to minimize spontaneous emission) and placed in the vacuum of the electromagnetic field in absence of charges or currents. In fact, this first intuition happens to be confirmed under the common approximations in quantum optics, namely the rotating-wave approximation and single-mode approximation [48]. A quick quantum-optical calculation shows that an adversary cannot increase their chances of guessing the outcome of the measurement correctly if the joint state of atom and field is in its ground state.

However, this intuition, and the calculation that backs it up, are not revealing the full story: If the coupling strength between the atom and the field is strong enough (strong-coupling in quantum optics [70, 71, 72] or ultra-strong coupling in superconducting circuits [73]), or if the time between preparation and measurement is short enough, the most common approximations (that happen to violate the local covariance of the interaction and thus render quantum optics non-relativistic [74]), such as the single-mode approximation, break down [48].

An idealized model on a fully relativistic footing has been analyzed already within the context of the UDW interaction model in 1+1 dimensions [48]. It was found that information is always leaked to the quantum field due to interactions of the detector-field system which entangle the detector and the field even when they start in their respective ground states, and even if the time between preparation and measurement is small. Moreover it turned out that a superposition of ground and excited state of the detector is the optimal state in maximizing the randomness extracted.

In this chapter we go beyond the UDW model employed in [48], and we consider a hydrogen-like atom interacting with a fully relativistic electromagnetic field via an effective dipole coupling in 3+1 dimensions. This will fulfill several purposes: First, it will allow us to put some of the approximations of quantum optics and the intuition behind it under the scrutiny in the regime where they are usually applied. Second, we consider the full anisotropic nature of the atomic transitions, as well as the exchange of angular momentum between the atom and the field.

The structure of this chapter is as follows: In Section 3.1 we will provide the physical setup and give a measure of quantum randomness. The amount randomness that is generated for different switching functions is presented in Section 3.2. We will also show a comparison to different UDW interaction prescriptions. Finally, in Sec. 3.3 we will summarize our findings.

3.1 Setup

In the remainder of this chapter, we will use natural units ($c = \hbar = \epsilon_0 = 1$). We will consider a fully featured hydrogen-like atom coupled dipolarly to the electromagnetic field (cf. Sec. 2.2) and, in particular, we will not use the rotating-wave approximation (whose limitations were pointed out in [74, 59, 60, 61, 62]). We will focus on the randomness that can be extracted from a general electric dipolar transition between two levels of the atom: a ground state $|g\rangle_{\text{A}}$ and an excited state $|e\rangle_{\text{A}}$.

For choosing the initial state of the field, an intuitive approach would be to consider the case where no field excitations are present near the atom if we wanted the atom to not be correlated with the field. If there were 'field quanta' around the atom, surely the probability of finding the atom in one or another state would be biased towards the excited state (through photon absorption with the field) and an adversary could use that to predict the outcome of a measurement on the atom with more than 50% accuracy, thus compromising the extraction of randomness from the atom. We would expect then that preparing the field in the vacuum state would be the best way to circumvent the bias of the probability to find the atom in the ground or excited state. For these reasons, in the same spirit as in [48], we will consider that the electromagnetic field is in the vacuum state. However, even in the vacuum we expect atom-field interactions to create correlations between atom and field, which in turn can reduce the extracted randomness.

We will employ the effective dipole model of (2.16) to study finite time interactions. For our setup, however, we will only consider that sector of the theory that effects atomic transitions between $|g\rangle_{\text{A}}$ and $|e\rangle_{\text{A}}$:

$$\hat{H}^{\text{eff}}_{I,eg}(t) \coloneqq \chi(t) \int_{\mathbb{R}^3} \mathrm{d}^3\boldsymbol{x}\ \hat{\boldsymbol{d}}(\boldsymbol{x},t) \cdot \hat{\boldsymbol{E}}(\boldsymbol{x},t), \tag{3.1}$$

where we defined $\hat{\boldsymbol{d}}_{eg} \coloneqq \hat{\boldsymbol{d}}$. We will, further, assume that initially field and detector are uncorrelated and hence in a product state of the form

$$\hat{\rho}_0 = |\Psi\rangle_{\text{A}}\langle\Psi| \otimes |0\rangle_{\text{F}}\langle 0|\,, \tag{3.2}$$

where $|\Psi\rangle_{\text{A}}$ is some arbitrary superposition of the two relevant energy eigenstates of the atom, and, as noted before, the field is in the vacuum state. That the initial state is of that particular form may be justified as it corresponds to the leading order term of the dressed ground state, or alternatively one can view it as as result of measurements on the atom.

Generating randomness from an atomic probe (i.e. with two energy levels) is conceptually easy: one prepares an initial state of the atom in a basis that is part of a set of mutually

unbiased bases, and then performs a von-Neumann measurement in a complementary basis of the same set. However, even theoretically, this protocol for extracting randomness is too naive: atoms are always intrinsically coupled to the electromagnetic field. In between the preparation of the atom and the projective measurement, the atom interacts with the electromagnetic field which will generally correlate both, giving an adversary with access to the field means to make an educated guess on the result of the measurement. Contrary to intuition, the acquisition of correlations between the field and the state of the atom can happen even if the time between preparation and projection is small, and even if both atom and field start in the ground state [48, 74]. These correlations serve as a bias that can be exploited by an adversary who has access to the field to infer the measurement outcome better than just by chance. In order to prevent this, two options are at our disposal. First, one can try to change the initial state of the atom to minimize these correlations, and secondly a different measurement basis might allow us to re-establish an unbiased situation.

Let us formalize the problem, following the approach of [48]: The joint system (atom-field) is prepared in its initial state in some basis at some time. Following preparation, atom and field interact with each other, and after some time σ the von-Neumann measurement $\{\hat{P}_x\}$ will be performed in some other arbitrary basis on the atom with the objective of generating randomness. From this measurement one obtains the result $x = \{0, 1\}$, eigenvalues of some observable $\hat{X}$. This yields the new total state $\hat{\rho}^x_{\hat{\mathrm{X}}\mathrm{F}} = |x\rangle_{\mathrm{A}}\langle x| \otimes \hat{\tau}^x_{\mathrm{F}}$. The state of the field after the projection ($\hat{\tau}^x_{\mathrm{F}}$) can be obtained by tracing out the atomic degrees of freedom and is given by

$$\hat{\tau}^x_{\mathrm{F}} = \frac{\mathrm{tr}_{\mathrm{A}}\left(\hat{P}_x \hat{\rho}_{\mathrm{AF}}\right)}{\mathrm{tr}\left(\hat{P}_x \hat{\rho}_{\mathrm{AF}}\right)}. \tag{3.3}$$

This state can possibly be accessed by an adversary in order to infer the measurement result x. Note however that we will be interested in an ensemble measurement, where we denote $\hat{\rho}_{\mathrm{XF}} = \sum_x p_X(x)\hat{\rho}^x_{\mathrm{XF}}$ as the statistical ensemble of the possible measurement outcomes.

The conditional min-entropy [66, 75, 76] will be used to quantify a lower bound on the extracted randomness by an adversary with access to the quantum field after the initial measurement and is defined as

$$H_{\min}(X|F)_{\hat{\rho}_{\mathrm{XF}}} = -\log_2\left[P_g(X|F)_{\hat{\rho}_{\mathrm{XF}}}\right], \tag{3.4}$$

where $P_g(X|F)_{\hat{\rho}_{\mathrm{XF}}}$ denotes the probability of guessing correctly the outcome of a measurement on the random variable X associated with the observable $\hat{X}$ given access to the partial state of the field F.

The choice of the min-entropy as a figure of merit to quantify randomness is justified by the following rationale: Since the min-entropy takes the value k if all outcomes of a distribution occur at most with probability 2^{-k}, we have a necessary condition to generate k random bits from the distribution. More generally, the distribution only has to be ϵ-close to a distribution that has min-entropy k [77]. The min-entropy also constitutes a much better estimator of randomness than the Shannon entropy, which coincides with the min-entropy for homogeneous (flat) distributions. The reason is that the Shannon entropy yields the gain of information about a distribution obtained per individual sampling after taking the average over (asymptotically infinitely) many independent samples, whereas the min-entropy quantifies the gain of information when taking only one sample in the 'worst-case' scenario [78]. Due to this averaging, we cannot conclude that having access to a random variable with a high Shannon entropy leaves us in possession of a good randomness source. Therefore, the min-entropy functions as a more conservative estimator of randomness. Indeed, the min-entropy is always bounded from above by the Shannon entropy. Accordingly, it is known that the Shannon entropy often significantly overestimates the amount of randomness obtainable from a random variable [77].

Another point to take into account is the fact that the quantum field is infinite-dimensional. From the point of view of randomness extraction, the issue of the infinite-dimensionality of the field can be reduced to a problem of finite number of degrees of freedom since, by construction, the atom accounts for a finite number of energy eigenstates. For example, in this chapter we consider the conservative case where we quantify the randomness that can be extracted from only two atomic levels connected by an electric dipole transition, such that the field can excite the ground state of the atom only to one higher energy state (in the same fashion as it was done in [48] for a scalar field). We can write the final pure state of the joint system after interaction via Schmidt decomposition as

$$|\tilde{\Psi}\rangle_{\mathrm{AF}} = \sqrt{\lambda_0}\,|0\rangle_{\mathrm{A}} \otimes |f_0\rangle_{\mathrm{F}} + \sqrt{\lambda_1}\,|1\rangle_{\mathrm{A}} \otimes |f_1\rangle_{\mathrm{F}}\,, \tag{3.5}$$

where $\{|f_i\rangle_{\mathrm{F}}\}$ are two orthonormal basis states out of the field's infinite-dimensional Hilbert space, and $\{|i\rangle_{\mathrm{A}}\}$ are eigenstates of $\hat{X}$. *A priori* these basis states are not known, and their precise form is not even needed to arrive at an analytic expression for the amount of generated randomness. If the adversary wants to implement a protocol to optimize the guessing probability for the measurement outcome, then they would indeed need to construct $\{|f_i\rangle_{\mathrm{F}}\}$ by a Schmidt decomposition algorithm, and may involve many (possibly infinite) field modes. However, we do not concern ourselves with finding that specific decomposition as doing so is the adversary's task. Rather, our objective is to reduce their ability to make educated guesses on the randomly generated data by probing the

field. Thus, we should keep the most conservative assumptions on the adversary's ability. Considering that the min-entropy is invariant under local isometries [79], we can devise a unitary operation that transfers the information from the field to an ancillary qubit E in possession of the adversary, e.g. swapping entanglement between field and E. Therefore, the new final joint state reads

$$|\tilde{\Psi}\rangle_{\mathrm{AE}} = \sqrt{\lambda_0}\,|0\rangle_{\mathrm{A}} \otimes |0\rangle_{\mathrm{E}} + \sqrt{\lambda_1}\,|1\rangle_{\mathrm{A}} \otimes |1\rangle_{\mathrm{E}}\,. \tag{3.6}$$

Accordingly, after the von-Neumann measurement on atom A, the ensemble corresponding to the different outcomes is

$$\hat{\rho}^x_{\mathrm{AE}} = \sum_x |x\rangle_{\mathrm{A}}\langle x| \otimes \hat{\tau}^x_{\mathrm{E}}, \tag{3.7}$$

with the qubit E being, for the outcome x, in the state

$$\hat{\tau}^x_{\mathrm{E}} = \frac{\mathrm{tr}_{\mathrm{A}}\left(\hat{P}_x\hat{\rho}_{\mathrm{AE}}\right)}{\mathrm{tr}\left(\hat{P}_x\hat{\rho}_{\mathrm{AE}}\right)}. \tag{3.8}$$

The probability of guessing correctly the outcome is equivalent to the optimal success probability of the adversary to distinguish the states of the qubit $\hat{\tau}^x_{\mathrm{E}}$ [76, 48]:

$$\begin{aligned} P_g\big(X|E\big)_{\hat{\rho}_{\mathrm{AE}}} &= \max_{\hat{\mathcal{E}}} \sum_x p_X(x)\,{}_{\mathrm{E}}\langle x|\,\hat{\mathcal{E}}(\hat{\tau}^x_{\mathrm{E}})\,|x\rangle_{\mathrm{E}} \\ &= \max_{\hat{\Pi}_x} \sum_x p_X(x)\,\mathrm{tr}\Big(\hat{\Pi}_x\hat{\tau}^x_{\mathrm{E}}\Big), \end{aligned} \tag{3.9}$$

where we optimize over CPTP maps $\hat{\mathcal{E}}$ or equivalently over POVMs $\{\hat{\Pi}_x = \hat{\mathcal{E}}^\dagger(|x\rangle_{\mathrm{E}}\langle x|)\}$, and we assumed that the adversary is aware of the measurement basis in $\hat{X}$. By the Helstrom bound [80] for the minimum-error probability of distinguishing two states by optimizing over POVMs we find [48]

$$P_g\big(X|E\big)_{\hat{\rho}_{\mathrm{AE}}} = \frac{1}{2}\left(1 + \|p_X(0)\hat{\tau}^0_{\mathrm{E}} - p_X(1)\hat{\tau}^1_{\mathrm{E}}\|_1\right), \tag{3.10}$$

where $\|\hat{O}\|_1 = \mathrm{tr}\,\sqrt{\hat{O}^\dagger\hat{O}}$ is the Schatten 1-norm. Counteracting the adversary to yield the maximum amount of randomness $H^*_{\min}$ which can be extracted from the atom, we have to optimize over all von-Neumann measurements on atom A. Any arbitrary complex two-dimensional projector decomposition can be written as a linear combination of projectors of the form $\hat{P}_i = |m_i\rangle_{\mathrm{A}}\langle m_i|$ with

$$\begin{aligned} |m_0\rangle_{\mathrm{A}} &= \cos\theta\,|0\rangle_{\mathrm{A}} + e^{\mathrm{i}\phi}\sin\theta\,|1\rangle_{\mathrm{A}}\,, \\ |m_1\rangle_{\mathrm{A}} &= \sin\theta\,|0\rangle_{\mathrm{A}} - e^{\mathrm{i}\phi}\cos\theta\,|1\rangle_{\mathrm{A}}\,. \end{aligned} \tag{3.11}$$

Then we find that $p_X(x)\hat{\tau}_{\mathrm{E}}^x = |n_x\rangle_{\mathrm{E}}\langle n_x|$, where

$$\begin{aligned} |n_0\rangle_{\mathrm{E}} &= \sqrt{\lambda_0}\,{}_{\mathrm{A}}\langle m_0|0\rangle_{\mathrm{A}}\,|0\rangle_{\mathrm{E}} + \sqrt{\lambda_1}\,{}_{\mathrm{A}}\langle m_0|1\rangle_{\mathrm{A}}\,|1\rangle_{\mathrm{E}}\,, \\ |n_1\rangle_{\mathrm{E}} &= \sqrt{\lambda_0}\,{}_{\mathrm{A}}\langle m_1|0\rangle_{\mathrm{A}}\,|0\rangle_{\mathrm{E}} + \sqrt{\lambda_1}\,{}_{\mathrm{A}}\langle m_1|1\rangle_{\mathrm{A}}\,|1\rangle_{\mathrm{E}}\,. \end{aligned} \tag{3.12}$$

This allows us to write the optimized guessing probability, by using Eq. (3.10), as [48]

$$\begin{aligned} P_g^*\big(X|E\big)_{\hat{\rho}_{\mathrm{AE}}} &= \min_{\{|m_i\rangle_{\mathrm{A}}\}} \frac{1}{2}\left(1+\sqrt{1-4\,|{}_{\mathrm{E}}\langle n_0|n_1\rangle_{\mathrm{E}}|^2}\right) \\ &= \frac{1}{2}\left(1+\sqrt{1-(\lambda_0-\lambda_1)^2}\right) \\ &= \frac{1}{2}+\sqrt{\frac{1}{4}-\left(\frac{1}{2}\,\mathrm{tr}\,(\hat{\rho}_{\mathrm{A}}^2)-\frac{1}{4}\right)}, \end{aligned} \tag{3.13}$$

where $\hat{\rho}_{\mathrm{A}}$ is the reduced density matrix of the atom after its interaction with the field from preparation to measurement. Finally we find the expression for the optimized min-entropy [48]:

$$H_{\min}^* = -\log_2\left(\frac{1}{2}+\sqrt{\frac{1-\mathrm{tr}\,(\hat{\rho}_{\mathrm{A}}^2)}{2}}\right), \tag{3.14}$$

using Eq. (3.4). Thus, it is sufficient to know the state of the atom after the interaction to fully quantify the extractable randomness.

3.2 Extracted Randomness

We assume that the initial state of the field is its ground state $|0\rangle_{\mathrm{F}}$ and the atom is in some superposition of its energy eigenstates $|\Psi\rangle_{\mathrm{A}_i} = a\,|g\rangle_{\mathrm{A}} + \sqrt{1-a^2}\,|e\rangle_{\mathrm{A}}$, where we restrict a to be real and $a=1$ ($a=0$) corresponds to the ground state (excited state). For instance, $|g\rangle_{\mathrm{A}}$ could be the $1s$ state and $|e\rangle_{\mathrm{A}}$ the $2p_z$ state. Hence the initial state of the atom reads

$$\hat{\rho}_{\mathrm{A}_i} = \begin{pmatrix} a^2 & a\sqrt{1-a^2} \\ a\sqrt{1-a^2} & 1-a^2 \end{pmatrix} \tag{3.15}$$

in the $\{|g\rangle_{\mathrm{A}}, |e\rangle_{\mathrm{A}}\}$ basis. The change in the atomic state $\Delta\hat{\rho}$ can be computed from (2.36) using (2.34). In Appendix A.1 the derivation is explicitly shown in general form for arbitrary atomic transitions and switching functions. In particular, the final results for the exemplary $1s \to 2p_z$ atomic transition (Appendix A.2) is given for the following switching functions (Appendix A.3):

1. Gaussian switching $\chi^{\mathrm{G}}(t) = e^{-t^2/\sigma^2}$,
2. sudden Heaviside top-hat switching $\chi^{\mathrm{S}}(t) = \Theta(t)\Theta(-t+\sigma)$,
3. Dirac delta switching $\chi^{\mathrm{D}}(t) = C\delta(t)$,

where σ is the interaction time scale and the constant C is needed for correct dimensionality. This yields for the change in the atomic state to second order in perturbation theory respectively

$$\begin{aligned}\Delta\hat{\rho}^{\mathrm{G}} =&\frac{24576(a_0 e\sigma)^2}{\pi}\int_0^\infty \mathrm{d}|\boldsymbol{k}|\frac{|\boldsymbol{k}|^3 e^{-\frac{1}{2}\sigma^2(|\boldsymbol{k}|+\Omega)^2}}{\left(4a_0^2|\boldsymbol{k}|^2+9\right)^6}\Bigg\{2\left[(1-a^2)e^{2|\boldsymbol{k}|\sigma^2\Omega}-a^2\right]\begin{pmatrix}1&0\\0&-1\end{pmatrix}\\&+\Bigg(a\sqrt{1-a^2}\left[e^{2|\boldsymbol{k}|\sigma^2\Omega}\mathrm{erf}\left(\frac{\mathrm{i}\sigma(|\boldsymbol{k}|-\Omega)}{\sqrt{2}}\right)-\mathrm{erf}\left(\frac{\mathrm{i}\sigma(|\boldsymbol{k}|+\Omega)}{\sqrt{2}}\right)-\left(1-e^{|\boldsymbol{k}|\sigma^2\Omega}\right)^2\right]\\&\times\begin{pmatrix}0&0\\1&0\end{pmatrix}+\mathrm{H.c.}\Bigg)\Bigg\},\end{aligned} \tag{3.16}$$

$$\begin{aligned}\Delta\hat{\rho}^{\mathrm{S}} =&\frac{49152(a_0 e)^2}{\pi^2}\int_0^\infty\frac{\mathrm{d}|\boldsymbol{k}||\boldsymbol{k}|^3}{\left(4a_0^2|\boldsymbol{k}|^2+9\right)^6\left(|\boldsymbol{k}|^2-\Omega^2\right)^2}\Big\{\Big[4|\boldsymbol{k}|\Omega+2a^2(|\boldsymbol{k}|-\Omega)^2\cos(\sigma(|\boldsymbol{k}|+\Omega))\\&+2\left(1-2a^2\right)\left(|\boldsymbol{k}|^2+\Omega^2\right)+2(a^2-1)\cos(\sigma(|\boldsymbol{k}|-\Omega))(|\boldsymbol{k}|+\Omega)^2\Big]\begin{pmatrix}1&0\\0&-1\end{pmatrix}\\&+\Bigg(\Big[e^{2\mathrm{i}\sigma\Omega}(|\boldsymbol{k}|^2-\Omega^2)+|\boldsymbol{k}|^2(2\mathrm{i}\sigma\Omega-1)+4\Omega e^{\mathrm{i}\sigma\Omega}(\Omega\cos(|\boldsymbol{k}|\sigma)-\mathrm{i}|\boldsymbol{k}|\sin(|\boldsymbol{k}|\sigma))\\&-\Omega^2(3+2\mathrm{i}\sigma\Omega)\Big]a\sqrt{1-a^2}\begin{pmatrix}0&0\\1&0\end{pmatrix}+\mathrm{H.c.}\Bigg)\Big\},\end{aligned} \tag{3.17}$$

$$\Delta\hat{\rho}^{\mathrm{S}}_{\Omega=0} =\frac{512e^2}{295245\pi^2}\left(1-2a^2\right)\left[24-\sqrt{\pi}G^{2,1}_{1,3}\left(\begin{smallmatrix}0\\0,5,\frac{1}{2}\end{smallmatrix}\middle|\,\frac{9\sigma^2}{16a_0^2}\right)\right]\begin{pmatrix}1&0\\0&-1\end{pmatrix}, \tag{3.18}$$

$$\Delta\hat{\rho}^{\mathrm{D}} =\frac{128C^2e^2}{10935\pi^2a_0^2}(1-2a^2)\begin{pmatrix}1&0\\0&-1\end{pmatrix}, \tag{3.19}$$

where $G^{m,n}_{p,q}\left(\begin{smallmatrix}a_1,\ldots,a_p\\b_1,\ldots,b_q\end{smallmatrix}\middle|\,z\right)$ is the Meijer G-function, $\mathrm{erf}(z)$ is the error function, a_0 is the generalized Bohr radius, and $\Omega := \Omega_{eg} = E_e - E_g$. Eq. (3.18), obtained from (3.17) for degenerate atomic transitions ($\Omega = 0$), corresponds to gapless sudden switching.

We have now obtained the time evolved density matrix of the atom from the time of preparation to the time when the measurement is performed for the different switching functions considered, namely Gaussian (3.16), sudden (3.17)-(3.18), and delta (3.19). With this information at hand, we can calculate the number of bits of randomness that can be

generated with each measurement. We will present the results for Gaussian switching, gapless sudden switching and delta switching separately.

The first step is to choose physically meaningful values for the parameters of the problem. As a baseline, we start with the parameters $e \approx 137^{-1/2} \approx 8.54 \cdot 10^{-2}$, $\Omega \approx 3.73$ eV, $a_0 \approx 2.68 \cdot 10^{-4}$ eV^{-1}. These have been chosen such that the atomic radius corresponds to the Bohr radius, e to the standard electric charge in vacuum (the square root of the fine structure constant in natural units) and $a_0\Omega \approx 0.001$ is of the same order as for a typical transition from the ground state to the first excited state in a hydrogen-like atom [81]. By varying a_0, e, Ω we will study how the generated randomness is dependent on these parameters.

3.2.1 Gaussian Switching: $\chi^{\mathrm{G}}(t) = e^{-t^2/\sigma^2}$

For a Gaussian switching function, the amount of randomness that can be generated as a function of the interaction time σ and initial superposition parameter a is shown in Fig. 3.1. As a general feature we note that for shorter interaction times the amount of randomness is compromised more severely. In fact, we see that for the regular free-space coupling of Fig. 3.1a, Gaussian switching provides a good source of randomness for interaction times above $\approx 10^{-2}$ eV^{-1}, which in principle tells us that an adiabatic switching (smooth switching that depends only on one timescale, such as Gaussian) prevents the generation of atom-field correlations well enough to guarantee a reliable extraction of randomness. However, this is not true for regimes of strong coupling: as we will comment on below, the amount of randomness extracted decays fast with the interaction strength and becomes relevant for strong coupling strengths. Remarkably, and contrary to intuition the ground state is not the most secure choice of initial atom preparation for short interaction times. It turns out that an equal superposition of ground and excited state is most resilient and in fact yields min-entropy very close to 1 bit. Moreover, the initial guess that the excited state of the atom may be the worst preparation (because of its probability of spontaneously decay) is not the complete picture. Surprisingly, the ground state is almost as bad a choice as the excited state in terms of generation of randomness.

This stresses our claim: for fast randomness generation the equal superposition state provides the best possible initialization of the system. Nonetheless, as we would expect, for the late interaction time regime we recover that the ground state yields maximum randomness generation whereas all other state preparations, including excited state and equal superposition, experience a decrease in randomness for longer interaction times (see Fig. 3.2).

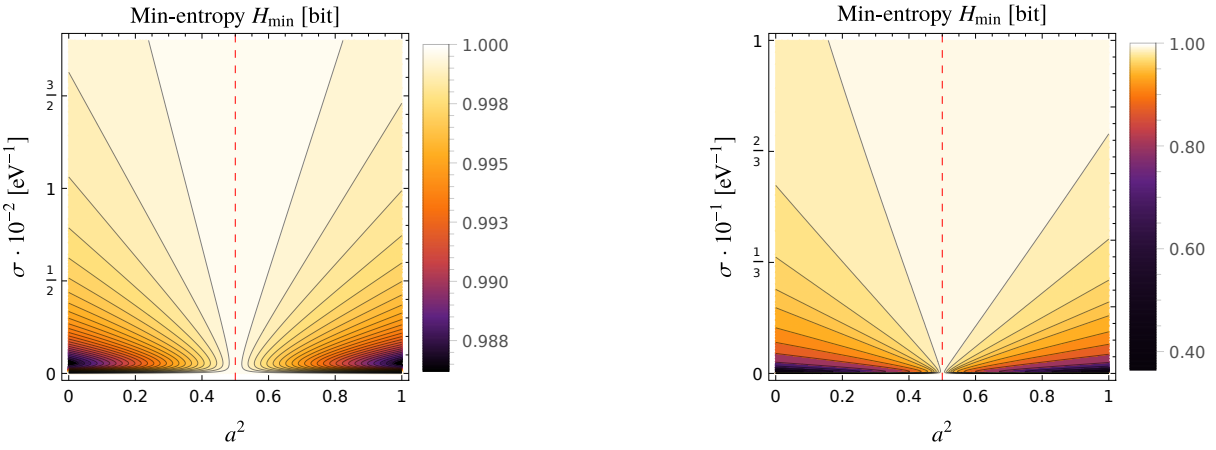

Figure 3.1: Min-entropy $H_{\min}$ plotted against duration of interaction σ and atomic initial superposition a ($a = 0$ corresponds to $|e\rangle_{\mathrm{A}}$ and $a = 1$ to $|g\rangle_{\mathrm{A}}$) for Gaussian switching with the parameters $a_0 = 2.68 \cdot 10^{-4}$ eV^{-1}, $\Omega = 3.73$ eV, and (a) free-space coupling $e = 8.54 \cdot 10^{-2}$ or (b) strong coupling $e = 5$. $H_{\min} = 1$ bit coincides with maximal randomness and is never absolutely reached. The highest amount of randomness can be found for an equal superposition $a = 1/\sqrt{2}$ (red dashed line). The ground and the excited state are the least favored preparations for short interactions.

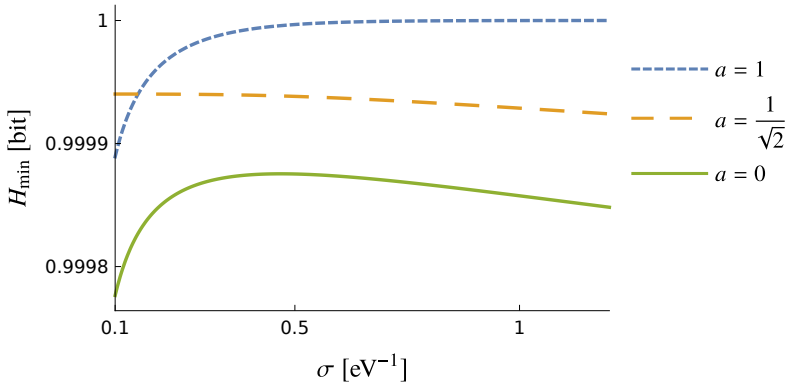

Figure 3.2: Min-entropy $H_{\min}$ for longer times σ with parameters $a_0 = 2.68 \cdot 10^{-4}$ eV^{-1}, $\Omega = 3.73$ eV, $e = 8.54 \cdot 10^{-2}$ for the ground ($a = 1$) and excited state ($a = 0$), and equal superposition ($a = 1/\sqrt{2}$) in the case of Gaussian switching. The ground state recovers $H_{\min} = 1$ bit, the other initial atomic preparations witness a fall-off of the extracted randomness.

In Fig. 3.3 we show the dependence of the extracted randomness on the parameters e, a_0 and Ω. The stronger the coupling e between atom and field the less randomness will be generated overall since it results in the enhancements of acquired atom-field correlations. The extracted randomness falls off more quickly for states that are closer to being either of the two energy eigenstates. This is particularly relevant as shown in Fig. 3.1b: in regimes of strong coupling the loss of randomness at short times can still be relatively significant for timescales of 10^{-1} eV^{-1}.

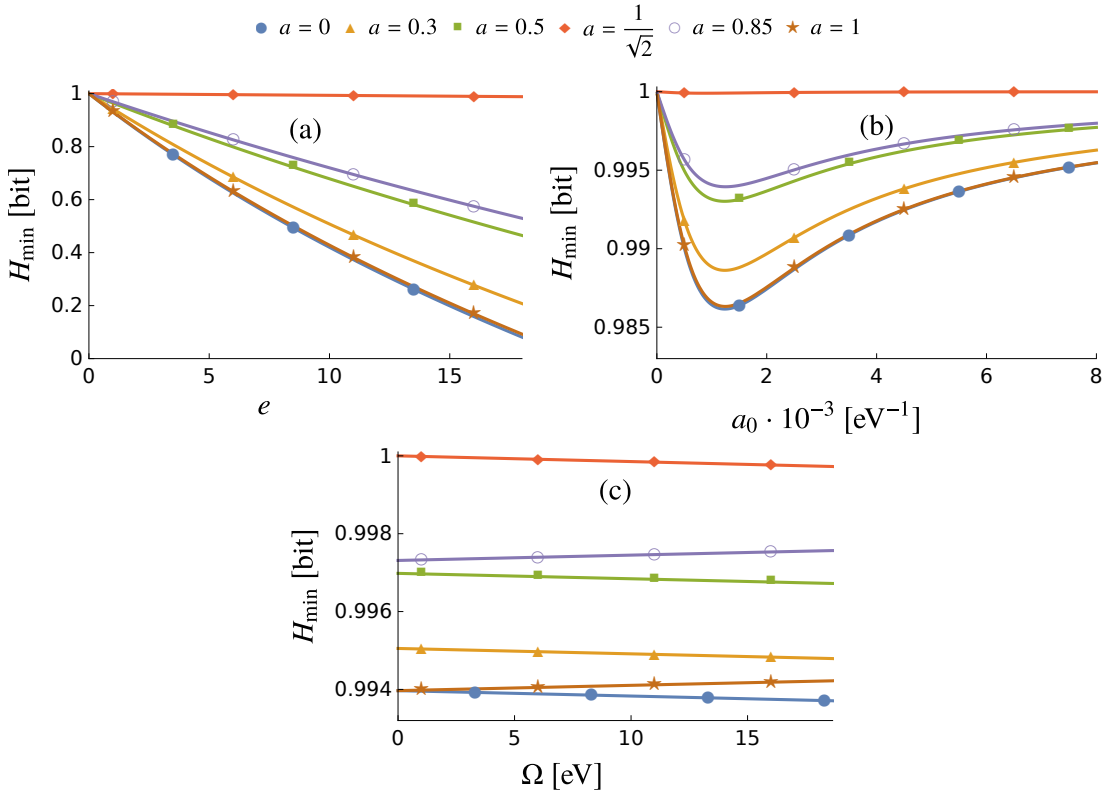

Figure 3.3: Extracted min-entropy as a function of the parameters (a) electric charge e, (b) atomic radius a_0, and (c) energy gap Ω for a fixed interaction time $\sigma = 2.5 \cdot 10^{-3}$ eV^{-1} and different atomic state parameters a in the case of Gaussian switching. For (a) we fix $a_0 = 2.68 \cdot 10^{-4}$ eV^{-1}, $\Omega = 3.73$ eV, in (b) it is $e = 8.54 \cdot 10^{-2}$, $\Omega = 3.73$ eV, and in (c) it is $a_0 = 2.68 \cdot 10^{-4}$ eV^{-1}, $e = 8.54 \cdot 10^{-2}$.

For the dependence on the atomic radius we find that for large values of a_0 the generated randomness asymptotically approaches a constant value after passing through a minimum.

The depth of the minimum is larger for states that are closer to either of the energy eigenstates. Hence the equal superposition of them shows to be very close to constant.

The extracted randomness decreases with larger values for the energy gap Ω for atomic states with parameter $a \leq 1/\sqrt{2}$ and increases for the remaining states. Hence the ground state or in general states with the major probability of being in the ground state after preparation become more secure when the gap between the energy eigenstates increases. This is consistent with the intuition that a larger gap makes it more difficult for the ground state to get excited through a counter-rotating process (emitting excitations that could be captured by an adversary). At the same time, increasing the gap increases the probability that the excited states decayed emitting light, which in turn can be captured to infer the measurement outcome. An equal superposition state is overall most resistant to variations in these parameters and, moreover, is close to being constant in all three parameter cases.

3.2.2 Sudden Switching: $\chi^{\mathbf{s}}(t) = \Theta(t)\Theta(-t+\sigma)$

We consider here the case of an infinitely fast switching on and off, modelled by a square function. For the sudden top-hat switching we will study the case of degenerate atomic transitions ($\Omega = 0$) due to numerical simplicity. The min-entropy portraits a different picture (see Fig. 3.4a) than for the case of Gaussian switching. It is still true that an equal superposition of ground and excited state is the most secure state to generate randomness for general interaction times. However, short interaction times between field and atom yield a larger min-entropy than longer interaction times. On the other hand, for later times the min-entropy varies very little with the interaction time for fixed a. It suggests that the amount of randomness that can be extracted takes an asymptotic value for fixed a. In this case, we observe that it is preferable to perform the measurement very fast in order to avoid the loss of randomness coming from the regime of long interaction times. This stands in contrast to the Gaussian switching where it is better to choose a longer interaction time between atom and electromagnetic field.

From Eq. (3.18) it is obvious that to second order in perturbation theory the equal superposition provides us with a state that yields $H_{\min} = 1$ bit since that state is a fixed point in time evolution (does not vary in time) for the degenerate transition case.

In Fig. 3.4(b,c) the dependence of the min-entropy on its parameters e and a_0 is shown for fixed times σ. As in the case of Gaussian switching, a stronger coupling implies a decrease of randomness. It also holds that states prepared close to being in an equal superposition show a slower decrease in the min-entropy than for states which are prepared close to being in an energy eigenstate. Moreover, for small atomic radii a_0 the randomness

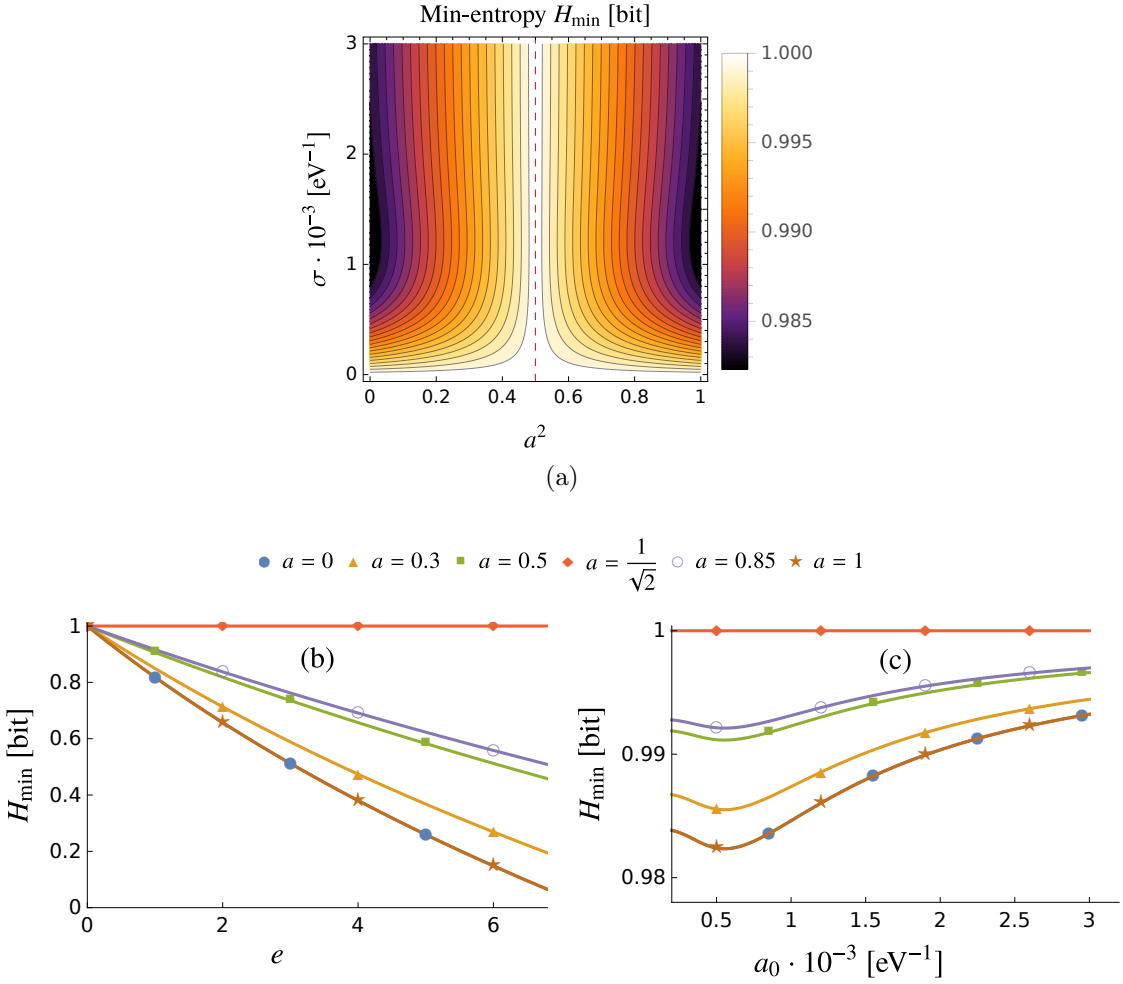

Figure 3.4: (a) Min-entropy $H_{\min}$ plotted against interaction time σ and atomic initial superposition a with $a_0 = 2.68 \cdot 10^{-4}$ eV^{-1}, $e = 8.54 \cdot 10^{-2}$ for gapless sudden switching. The dashed line corresponds to equal superposition and yields a maximum of $H_{\min} = 1$ bit. Ground/excited state witness the least amount of randomness. (b, c) Min-entropy as a function of the parameters (b) electric charge e and (c) atomic radius a_0 for a fixed interaction time $\sigma = 2.5 \cdot 10^{-3}$ eV^{-1} and different state parameters a for sudden switching. In (b) we keep $a_0 = 2.68 \cdot 10^{-4}$ eV^{-1} fixed and for (c) we have $e = 8.54 \cdot 10^{-2}$.

shows a minimum and increases then asymptotically to a constant value, depending on a. In summary, the equal superposition provides the optimal state to extract randomness as it is in fact independent of the parameters to leading order in perturbation theory.

3.2.3 Delta Switching: $\chi^{\mathrm{D}}(t) = C\delta(t)$

We consider here the effect of a fast kick of the system, modelled by a delta coupling. This can be seen as the limit of a succession of thinner Gaussian (or top-hat) functions of equal area (recall that this way of interpreting the delta as a limit is important for the results at hand, as discussed in detail in [82], and in Appendix A.3).

Studying the delta switching, we take $C = \sigma = 2.5 \times 10^{-3}$ eV^{-1} (reading (3.19) we note that C acts in the same way as the coupling constant). The particular choice for C means that the time-integrated switching function is proportional to σ, as was in the case for Gaussian and sudden switching.. Eq. (3.19) shows that once again the equal superposition yields perfect randomness extraction $H_{\min} = 1$ bit. This can be seen in Fig. 3.5.

Fig. 3.5a shows that the min-entropy peaks at equal superposition of the atom's initial state and quickly decreases at either side, resulting in a much larger loss of randomness than for any of the previously studied switching functions. Moreover the peak becomes narrower the stronger the coupling between atom and field is, spoiling quickly any randomness extraction if it is not in an equal superposition state. From Fig. 3.5(b,c) we see that, as expected, a stronger coupling between atom and electromagnetic field causes larger correlations and reduces the min-entropy. In addition, the dependence on the atomic radius displays an increase to an asymptotic value of the min-entropy. In contrast to the two previous switching functions, the delta switching shows much larger variations in the min-entropy.

3.2.4 Comparison with Scalar Field Models

Let us now compare our results to earlier studies where the atom was modeled as an UDW detector coupled to a scalar field $\phi(\boldsymbol{x}, t)$ (see Sec. 2.1). We recall that UDW model has been shown to capture the fundamental features to leading order of light-matter interactions as long as there is no exchange of orbital angular momentum [24, 25, 26]. We will consider two different kinds of UDW detectors, namely the original UDW model of Eq. (2.2) and a derivative coupling (that we will denote as UDW$_{\mathrm{d}}$) [83]. The respective Hamiltonians are

$$H_{\mathrm{UDW}} = \lambda\chi(t) \int \mathrm{d}\boldsymbol{x}^3 F(\boldsymbol{x})\hat{\mu}(t)\hat{\phi}(t, \boldsymbol{x}), \tag{3.20}$$

$$H_{\mathrm{UDW_d}} = \lambda_{\mathrm{d}}\chi(t) \int \mathrm{d}\boldsymbol{x}^3 F(\boldsymbol{x})\hat{\mu}(t)\partial_t\hat{\phi}(t, \boldsymbol{x}), \tag{3.21}$$

where we choose, cf. Eq. (2.30), for the detector's monopole moment $\hat{\mu}(t) = \hat{\sigma}^+ e^{\mathrm{i}\Omega t} + \hat{\sigma}^- e^{-\mathrm{i}\Omega t}$ (with $\hat{\sigma}^+ = |e\rangle_{\mathrm{A}}\langle g| = (\hat{\sigma}^-)^\dagger$). Further, $F(\boldsymbol{x})$ is the *ad hoc* included spatial smearing function

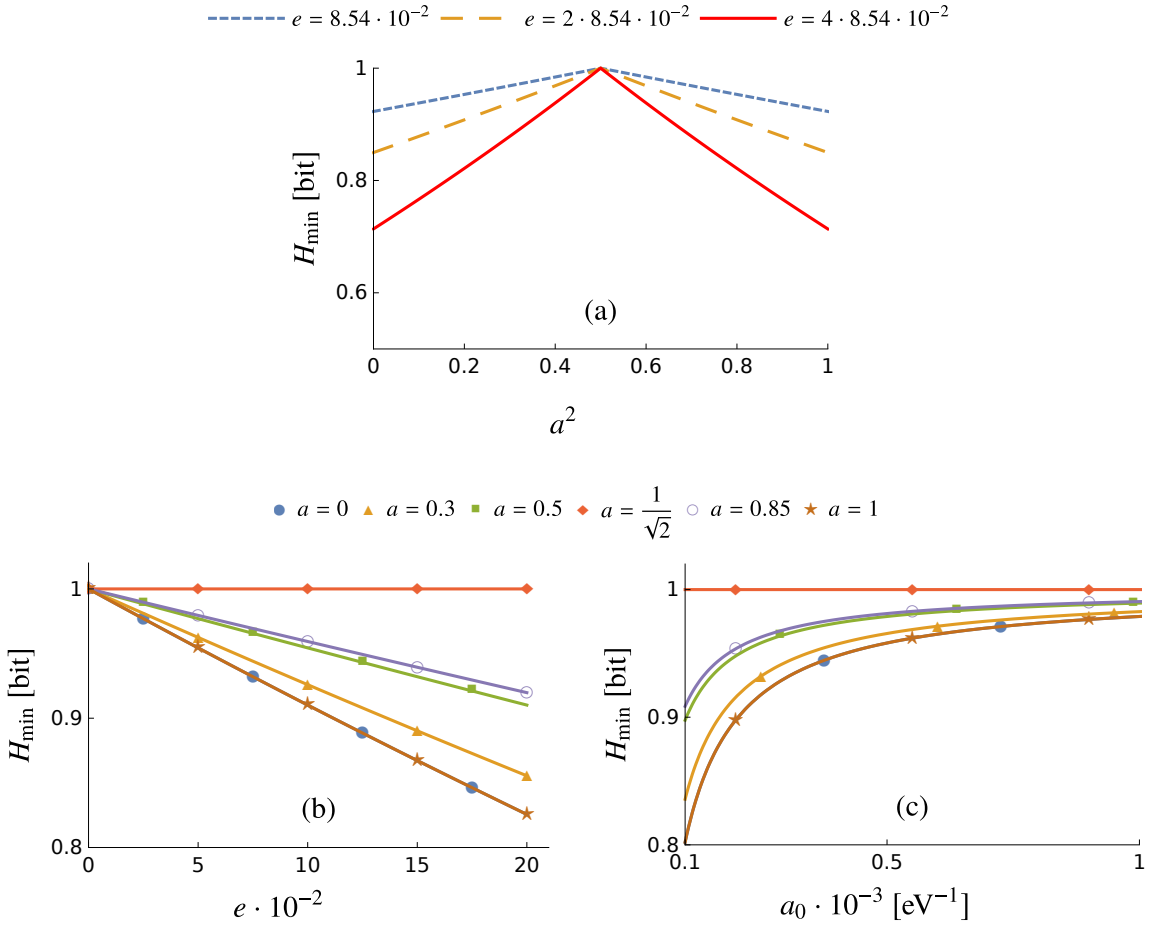

Figure 3.5: (a) Min-entropy $H_{\min}$ plotted against atomic initial superposition a with the atomic radius $a_0 = 2.68 \cdot 10^{-4}$ eV^{-1} for delta switching and different values of the coupling strength e. At equal superposition $a = 1/\sqrt{2}$ the extracted randomness has its maximum with $H_{\min} = 1$ bit. (b, c) Extracted min-entropy as a function of the parameters (b) electric charge e and (c) atomic radius a_0 for different atomic state parameters a in the case of delta switching. In (b) a_0 is taken to be $2.68 \cdot 10^{-4}$ eV^{-1}, and in (c) the coupling constant is $8.54 \cdot 10^{-4}$.

of the detector. In particular, (3.21) has been used in previous literature to analyze the loss of randomness due to coupling to relativistic fields [48], so it makes sense to compare the results of the simplified scalar model with the dipole model employed here.

The difference between the EM coupling and these two models has been analyzed in the past in the context of entanglement harvesting [24]. The $\mathrm{UDW_d}$ model can be thought of as a scalar analogue of the dipole coupling by noting that in the Coulomb gauge $\boldsymbol{E} = -\partial_t \boldsymbol{A}$ and one may perhaps expect that it should resemble the dipole interaction to some extent (as discussed in [48]). Both scalar models do not allow transitions where there is exchange of angular momentum. In particular, the $1s \to 2p_z$ transition is not permitted. Same as in [24] we will consider the closest scalar analogue to the $1s \to 2p_z$ dipole transition, that is $1s \to 2s$.

The change in the density matrix of the atomic state after an interaction of time σ takes for the scalar couplings the form

$$\Delta\hat{\rho}_{\mathrm{UDW}} = -\frac{32768}{\pi}\left(a_0^2\lambda\sigma\right)^2\int_0^\infty \mathrm{d}|\boldsymbol{k}|\frac{|\boldsymbol{k}|^5 e^{-\frac{1}{2}\sigma^2(|\boldsymbol{k}|+\Omega)^2}}{(4a_0^2|\boldsymbol{k}|^2+9)^6}\hat{\sigma}_z, \tag{3.22}$$

$$\Delta\hat{\rho}_{\mathrm{UDW_d}} = -\frac{32768}{\pi}\left(a_0^2\lambda_{\mathrm{d}}\sigma\right)^2\int_0^\infty \mathrm{d}|\boldsymbol{k}|\frac{|\boldsymbol{k}|^7 e^{-\frac{1}{2}\sigma^2(|\boldsymbol{k}|+\Omega)^2}}{(4a_0^2|\boldsymbol{k}|^2+9)^6}\hat{\sigma}_z, \tag{3.23}$$

with $\hat{\sigma}_z$ being the Pauli-Z operator. The scalar models were derived by assuming a Gaussian switching function and the initial ground state of the detector ($a = 1$). In addition the smearing function was chosen as the scalar version of the smearing vector: $F(\boldsymbol{x}) = \psi_{2s}(\boldsymbol{x})\psi_{1s}(\boldsymbol{x})$. Consequently, we have to analyze the electric dipole model in the respective configuration slice. It should be noted that the coupling constants of the different couplings do not all have the same dimensionality. In particular, for the dipole and direct scalar interaction we find $[e] = 0 = [\lambda]$, whilst for the derivative coupling $[\lambda_{\mathrm{d}}] = -1$ (in mass dimensions). We choose the parameters $a_0 = 2.68 \cdot 10^{-4}$ eV^{-1}, $e = \lambda = 10^{-3}$, $\lambda_{\mathrm{d}} = 10^{-3}$ eV^{-1}, $\Omega = 3.73$ eV, taking into account that for stronger couplings the perturbative expansion of the $\mathrm{UDW_d}$ model breaks down by virtue of the additional $|\boldsymbol{k}|^2$ dependence in (3.23).

In Fig. 3.6 one finds that the derivative model vastly underestimates the extracted randomness for early times and is off by up to over 40 %. On the other hand the UDW model slightly overestimates it for short interaction times by the order of 10^{-2} %. For long interaction times both scalar models approach the realistic dipole model.

3.3 Summary

We quantified a lower bound for the randomness that can be extracted from a hydrogen-like atom coupled to the electromagnetic field. Here, we did not make any use of the usual

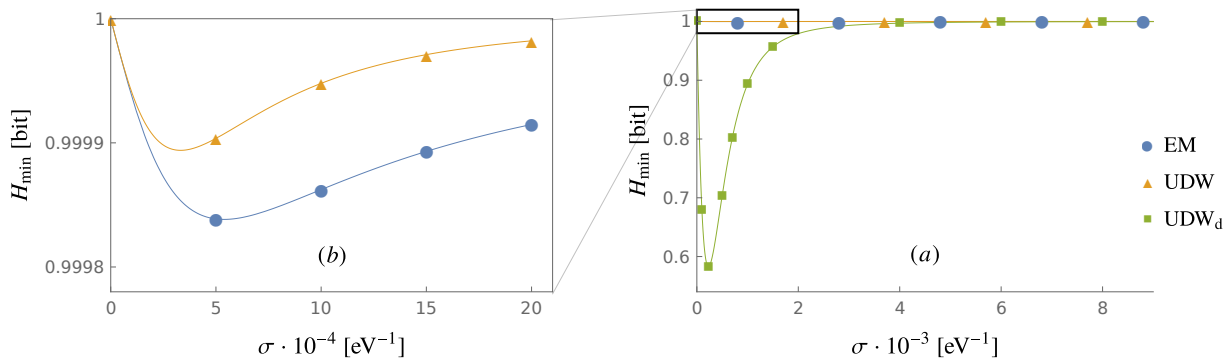

Figure 3.6: (a) Min-entropy $H_{\min}$ plotted against duration of interaction σ with parameters $a_0 = 2.68 \cdot 10^{-4}$ eV^{-1}, $e = \lambda = 10^{-3}$, $\lambda_d = 10^{-3}$ eV^{-1}, $\Omega = 3.73$ eV in the $1s$ ground state ($a = 1$) for Gaussian switching of the electric dipole model (EM: final state $2p_z$), scalar coupling (UDW) and coupling to the time derivative of the scalar field (UDW$_d$) with final state $2s$. (b) Corresponds to a zoomed-in region of (a) marked by the black box.

simplifications within the effective dipole interaction, i.e. the rotating-wave approximation or the single-mode approximation. In that context, we showed how the amount of entanglement between the atom and the electromagnetic field deviates in special-relativistic quantum regimes from non-relativistic scenarios. Conversely, protocols that use entanglement as a resource can benefit from the regimes we identified as particularly bad for randomness extraction where entanglement was considered malicious.

We analyzed how much information an adversary with access to the EM field but not the atom can obtain about a supposedly random measurement outcome. We found (consistently with studies that considered simplified scalar field interaction models [48]) that generally the ground state of the atom and the vacuum state of the field is not the optimal state to generate randomness out of a succession of preparation and measurement in unbiased bases for the atomic state basis.

We have analyzed a variety of switching regimes and found that for the switching function as well as the duration of the interaction between atom and electromagnetic field there are two possibilities for choosing the optimal state in terms of randomness generation: For short time between preparation and measurement in the unbiased basis, the equal superposition between ground and excited atomic states yields the optimal randomness. For sudden preparation and measurement (preparation times and measurement times much shorter than the inverse of the frequency of the atomic transition), the equal superposition between ground and excited yields the best results even for long times between preparation

and measurement. In contrast, for adiabatic switching and long times, the ground state of the atom yields the optimal randomness generation.

Furthermore, we also showed that in the cases where the equal superposition is optimal, the ground state is one of the two worst choices (together with the excited atomic state) in order to generate randomness, something that contradicts the intuition coming from the rotating-wave approximation that basically would suggest that 'if everything is in the ground state, the field and the atom will remain uncorrelated'.

Finally, we compared the dipole model of the electromagnetic field coupled to the atom to simplified scalar models. We found that both the UDW coupling [23] and the derivative coupling [83] provide a good approximation for the full electromagnetic model for long enough interaction times. For short interaction times, the UDW model is a better approximation than the derivative coupling, which significantly deviates from the full electromagnetic calculation. Due to the distinct dimension of the $\mathrm{UDW_d}$ coupling constant, there is an additional level of ambiguity in the choice of its value.

Even though the hydrogenoid atom as a testbed for randomness is not the atomic species commonly used in experiments for randomness generation [67], examining its behavior allows to draw conclusions for more feasible scenarios: Ions also couple dipolarly to the electromagnetic field and hence they will show very similar features to the ones we identified in this chapter. In that way the atom functions as a class representative for a wide array of experiments.

Chapter 4

Accelerated Atoms in Optical Cavities

In the previous chapter we studied light-matter interactions in free space with a focus on the dipole model. As a second study of effective interaction models, we will consider in this chapter atoms that are confined to an optical cavity, with a focus on the UDW Hamiltonian. In particular, we wish take a closer look at the impact that approximations have on physical predictions. This is motivated by the fact that in the study of atoms inside optical cavities sometimes approximations coming from quantum optical considerations are employed. For example, it is common to carry out the single-mode approximation (or perhaps in some cases a few-mode approximation) where the number of modes in the cavity is reduced to a subset of close-to-resonance modes that the atom interacts with. Another common approximation is to consider 1+1D cavities neglecting the fact that the cavities are implemented in 3+1 dimensional spacetime. This last consideration may in principle seem reasonable in the case of, for instance, optical fibers that are very long as compared to their cross section.

The number of cases where these approximations are used is considerable. For instance, among others, [84, 85, 86, 87, 88, 89, 90, 91] for the single- or few-mode approximation, or, e.g., [72, 84, 92, 93, 94, 95, 96, 97, 98] for the usage of 1+1D cavities. While simplifying the problem, sometimes the rationale for these simplifications remains to be justified, above all in relativistic regimes. In a similar spirit, in [96] the authors investigate in 1+1D the validity of the single-mode approximation inside a cavity with a stationary qubit, but still within a 1+1D framework and limited to the ultra-strong coupling regime.

In this chapter we will analyze if the common approximations of quantum optics are valid in the weak coupling limit in a 3+1 dimensional cavity setup for a moving two-level particle detector. In particular, we will analyze the soundness of the single- and few-mode

approximation as well as of a non-relativistic approximation on the detector's trajectory. Further, we will begin to discuss the approximation of reducing the 3+1D model to a 1+1D problem for long cavities of small cross section (this shall be treated in much more depth in the next chapter). This is particularly relevant in the context of the Unruh effect [27, 28, 22] within a cavity, i.e. for relativistic trajectories of accelerated particle detectors in cavities. Specifically, this is of importance in the light of relatively recent proposals for experiments to detect the Unruh effect involving optical cavities [84, 85, 99, 100, 101, 102]. We will characterize when and how those approximations are acceptable and, in particular, we will see that the few-mode approximation cannot generally be justified for moving atoms in cavities when relativistic trajectories are considered (such as those commensurate with the Unruh effect).

The structure of this chapter is as follows. In Sec. 4.1 we will provide the setup and the objectives in more details. In Sec. 4.2 we will examine the single-mode approximation for different modes of motion. We will then study in Sec. 4.3 the validity of the non-relativistic approximation. Further, in Sec. 4.4, we will provide brief physical arguments on the dimensional reduction approximation which will be treated in much more depth in Chapter 5. Lastly, we will sum up our findings in Sec. 4.5.

4.1 Setup

We wish to analyze the effects of the detector on the quantum field inside the cavity as well as the detector's response due to its acceleration. The scenario is depicted in Fig. 4.1. The first thing we will analyze is in which field modes the energy is deposited after the detector crossed the cavity depending on the detector's initial state and its trajectory. Moreover, as a measure of the validity of the single-mode or few-mode approximation, we will study the detector's transition probabilities after it crossed the cavity and how much the predictions of the single- and few-mode approximation deviate from the exact results. In addition to the analysis above, we will further compare the state of the field after the cavity is crossed by an accelerated detector to the case where the detector is moving with constant velocity. This will show if the state of the field has any unique signature deriving from the acceleration as opposed to non-accelerated detectors.

Secondly, we will examine if a non-relativistic (Galilean) approximation of the detector's trajectory will be reliable for low detector accelerations. This particular approximation is expected to greatly simplify the mathematical complexity. Finally, we will investigate if it is possible to use a 1+1D model to reproduce the 3+1D model where the length of the cavity is much larger than its radius, (i.e. an 'optical fiber' experiment), both in the case

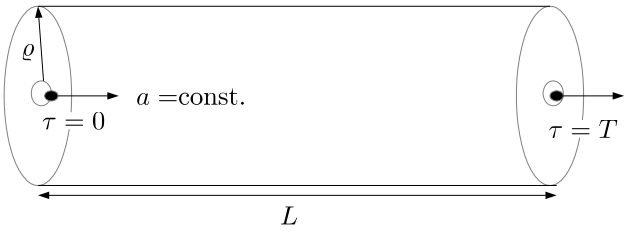

Figure 4.1: Detector moving with constant proper acceleration a through a cylindrical cavity of length L.

of a massless 1+1D model and in the refined case of a massive 1+1D model whose mass results from the effective reduced dimensions of spacetime.

We will employ the UDW interaction Hamiltonian (2.2):

$$\hat{H}_{\text{UDW}}(\tau) = \hbar c \lambda \chi(\tau) \hat{\mu}(\tau) \hat{\phi}(t(\tau), \boldsymbol{x}(\tau)), \tag{4.1}$$

where we choose (cf. (2.30)) $\hat{\mu}(\tau) = e^{\mathrm{i}\Omega\tau}\hat{\sigma}^{+} + e^{-\mathrm{i}\Omega\tau}\hat{\sigma}^{-}$ with $\hat{\sigma}^{+/-}$ being the SU(2) ladder operators, and τ is the proper time of the detector. We further assumed for simplicity that the detector is spatially localized at a point. The time-dependent coupling is chosen to be $\chi(\tau) = 1\ \forall \tau \in [0, T]$ where 0 and T correspond to the times at which the detector enters and exits the cavity in the detector's frame respectively (see Fig. 4.1). Note that there are no UV divergences despite the finiteness of the interaction. This is due to the choice of Dirichlet boundary conditions.

Further, we will model the optical cavity as a cylinder with Dirichlet boundary conditions. As we show in Appendix B.1, the massless Klein-Gordon can be solved in cylindrical coordinates. The resulting quantized scalar field reads

$$\hat{\phi}(t, r, \varphi, z) = \sum_{\substack{m=0 \\ n,\ell=1}}^{\infty} \left(u_{m\ell n} \hat{a}_{m\ell n} + u^{*}_{m\ell n} \hat{a}^{\dagger}_{m\ell n} \right), \tag{4.2}$$

where the creation and annihilation operators $\hat{a}^{\dagger}_{m\ell n}$ and $\hat{a}_{m\ell n}$ obey the canonical commutation relations. Further, n is the longitudinal quantum number, and m and ℓ are the quantum numbers corresponding to transversal degrees of freedom. The field modes $u_{m\ell n}$

have the form

$$u_{mn\ell}(t,r,\varphi,z) = A_{m\ell n} e^{\mathrm{i}m\varphi} e^{-\mathrm{i}\omega t} \sin\!\left(\frac{n\pi}{L}z\right) J_m\left(\frac{x_{m\ell}}{R}r\right), \tag{4.3}$$

$$A_{m\ell n} = c^{1/2}\left(R\sqrt{L\pi\omega}J_{m+1}(x_{m\ell})\right)^{-1}, \tag{4.4}$$

$$\omega = c\sqrt{\frac{x_{m\ell}^2}{R^2} + \frac{n^2\pi^2}{L^2}}, \tag{4.5}$$

with $x_{m\ell}$ being the ℓ-th zero of the m-th Bessel function of the first kind J_m.

Finally, we assume that the field is initially in the vacuum state, and that field and detector start out uncorrelated:

$$\hat{\rho}_0 = \hat{\rho}_{\mathrm{D}} \otimes |0\rangle_{\mathrm{F}}\langle 0| \,. \tag{4.6}$$

For the initial state of the detector we assume it is either in the ground state $|g\rangle$ or in the excited state $|e\rangle$. We can compute the final field state to second order in the coupling λ from Eq. (2.37).

4.2 Validity of a Single (or Few) Mode Approximation

We begin first assessing the (in)validity of the single-mode approximation in relativistic scenarios. We will do this in two ways:

1. We will compute what modes become non-negligibly excited – i.e. to determine the spectrum – in the field after an accelerated detector crossed the cavity in the longitudinal direction.

2. We will calculate by how much the few-mode approximation fails to predict the transition probabilities of such a detector.

Then we will repeat the analysis with the detector following a constant-velocity trajectory. As we will see, it is not true that most field excitations remain confined to near-resonant modes.

4.2.1 Single-Mode Approximation for Accelerated Detectors

We consider a detector initially at rest at the entrance of the cavity $(t, r, \varphi, z) = 0$, and its subsequent constant proper acceleration a in the longitudinal direction z. The detector's worldline in the cavity frame parametrized by its proper time τ is

$$z(\tau) = \frac{c^2}{a}\left(\cosh(a\tau/c) - 1\right), \; t(\tau) = \frac{c}{a}\sinh(a\tau/c), \; r, \varphi = 0. \tag{4.7}$$

Hence, the field's mode functions (4.3) become

$$u_{m\ell n}(\tau) = \delta_{m0} A_{m\ell n} \exp\left(-\mathrm{i}\frac{\omega c}{a}\sinh(a\tau/c)\right) \sin\left(\frac{c^2 n\pi}{aL}\left(\cosh(a\tau/c) - 1\right)\right), \tag{4.8}$$

where all contributions with $m \neq 0$ vanish since for $r = 0$ we have that $J_m(0) = \delta_{m0}$. The (detector's proper time) duration of the interaction in the cavity is $T = \operatorname{arccosh}(aL + 1)/a$.

As can be seen in Appendix B.2.1, the number expectation value of field modes with quantum number $m = 0$ is

$$N_{\ell n} = c^2\lambda^2 \left| \int_0^T \mathrm{d}\tau e^{\pm \mathrm{i}\Omega\tau} u^*_{0ln}(\tau) \right|^2, \tag{4.9}$$

where, again, $\ell, n \geq 1$, and the $\pm$ is there to notate that for the $+$ sign the initial state of the detector is the ground state and the $-$ sign yields the result for the detector initially in the excited state. We show as well in Appendix B.2.1 that, to leading order, $\sum_{\ell,n} N_{\ell n}$ equals the detector's transition probabilities after cavity crossing (again, this means that with a $+$ we start in $|g\rangle$ and we will get the vacuum excitation probability, and with a $-$ we start in $|e\rangle$ and get the probability of spontaneous emission). We denote the vacuum excitation probability $\mathcal{P}^+$ and the probability of spontaneous emission $\mathcal{P}^-$. Therefore, we can choose as a measure of the validity of the single- or few-mode approximation

$$\frac{N_{\mathrm{res}}}{\sum_{n,\ell=1}^{\infty} N_{\ell n}} = \frac{\mathcal{P}^{\pm}_{\mathrm{res}}}{\mathcal{P}^{\pm}}, \tag{4.10}$$

where the subscript 'res' indicates the contribution of the resonant field mode (a single or a few if they are close in energy). This ratio is easy to justify: it tells us the relative magnitude of the contribution of the resonant mode(s) with respect to the full calculation where the single-mode approximation is not carried out.

In Fig. 4.2 the distribution of excitations in the field modes is displayed for different accelerations for both detector settings. As can be clearly seen, for non-relativistic setups

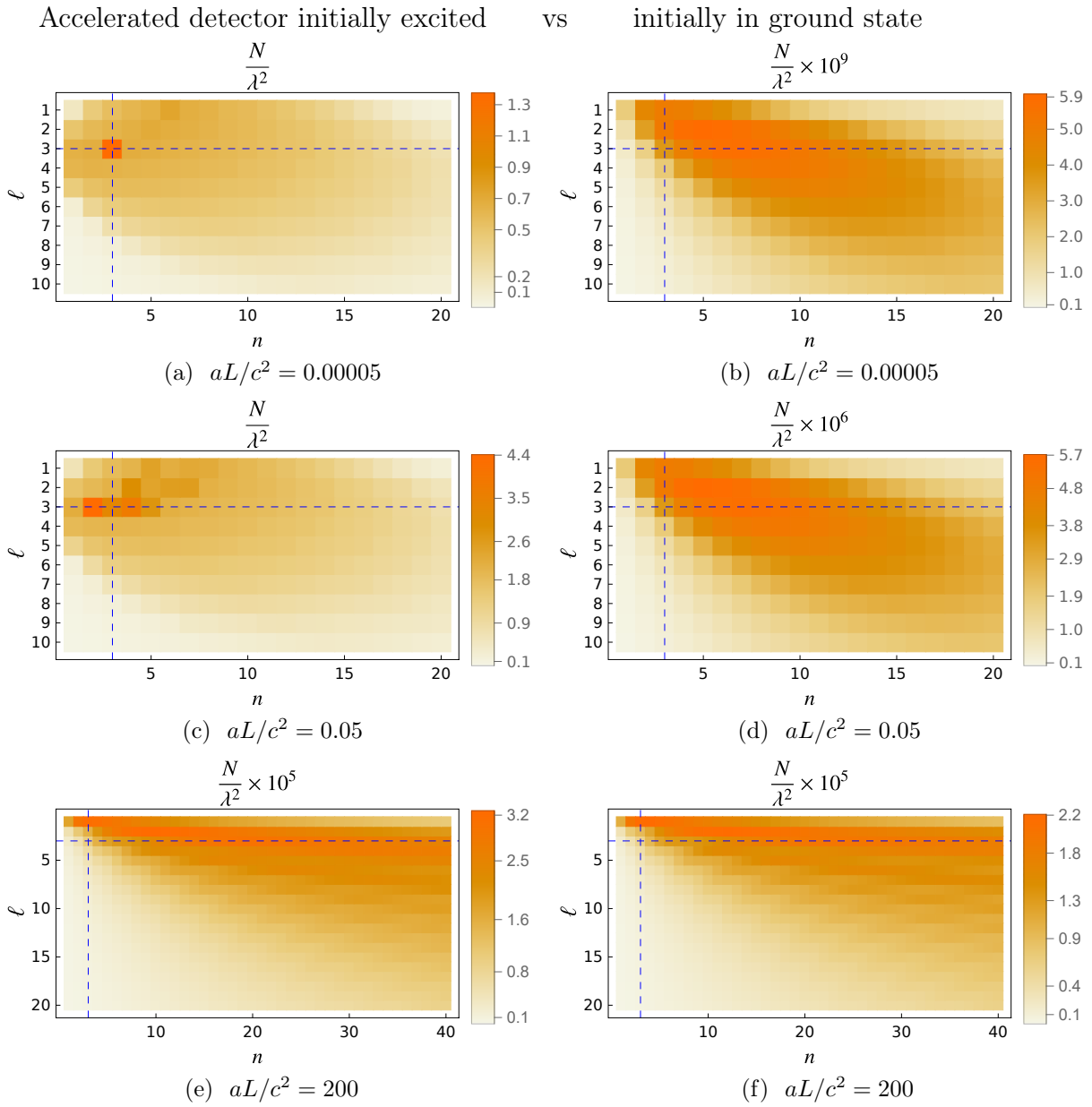

(a) $aL/c^2 = 0.00005$ (b) $aL/c^2 = 0.00005$

(c) $aL/c^2 = 0.05$ (d) $aL/c^2 = 0.05$

(e) $aL/c^2 = 200$ (f) $aL/c^2 = 200$

Figure 4.2: Number expectation N versus mode numbers n and ℓ for different detector accelerations. Parameters are $R/L = 0.5$, $\Omega R/c = 10$, $\Omega L/c = 20$ so that the detector's energy gap is resonant with $(m, \ell, n) = (0, 3, 3)$ (intersection of dashed lines). (a, b) $aL/c^2 = 0.00005$ (final velocity $\sim 0.01c$); (c, d) $aL/c^2 = 0.05$ (final velocity $\sim 0.3c$); (e, f) $aL/c^2 = 200$ (final velocity $\sim 0.99c$). With higher accelerations, the resonance of the excited case exhibits a Doppler shift that broadens the peak.

Parameters	$R/L = 1/2$, $\Omega L/c = 5.75$, resonant with $(\ell, n) = (1, 1)$					
aL/c^2	5×10^{-5}	5×10^{-4}	5×10^{-3}	5×10^{-2}	5×10^{-1}	200
$\frac{\mathcal{P}^-_{\rm res}}{\mathcal{P}^-} \leq$	1.00	1.00	1.00	0.97	0.48	7×10^{-5}
$\frac{\mathcal{P}^+_{\rm res}}{\mathcal{P}^+} \leq$	6.6×10^{-3}	6.5×10^{-3}	6.5×10^{-3}	6.4×10^{-3}	5.2×10^{-3}	6.8×10^{-5}
Parameters	$R/L = 1/2$, $\Omega L/c = 20$, resonant with $(\ell, n) = (3, 3)$					
aL/c^2	5×10^{-5}	5×10^{-4}	5×10^{-3}	5×10^{-2}	5×10^{-1}	200
$\frac{\mathcal{P}^-_{\rm res}}{\mathcal{P}^-} \leq$	0.89	0.8	0.42	0.13	0.06	3.3×10^{-5}
$\frac{\mathcal{P}^+_{\rm res}}{\mathcal{P}^+} \leq$	6.2×10^{-4}	6.2×10^{-4}	6.2×10^{-4}	6.2×10^{-4}	5.4×10^{-4}	2.9×10^{-5}
Parameters	$R/L = 1/2$, $\Omega L/c = 50$, 10 resonant modes					
aL/c^2	5×10^{-5}	5×10^{-4}	5×10^{-3}	5×10^{-2}	5×10^{-1}	200
$\frac{\mathcal{P}^-_{\rm res}}{\mathcal{P}^-} \leq$	0.99	0.98	0.53	0.09	0.06	5.5×10^{-4}
$\frac{\mathcal{P}^+_{\rm res}}{\mathcal{P}^+} \leq$	1.5×10^{-3}	1.5×10^{-3}	1.5×10^{-3}	1.5×10^{-3}	1.4×10^{-3}	5.4×10^{-4}

Table 4.1: 3+1D: Determining the validity of the single- and few-mode approximation by finding an upper bound to the ratio of the resonant contribution to the total spontaneous emission probability $\mathcal{P}^-$ and vacuum excitation probability $\mathcal{P}^+$, respectively. The resonant modes have been chosen such that they differ at most 2 % energetically from the detector gap Ω. We have taken as the cut-offs for the sums over n and ℓ 10^4 and 200, respectively.

($aL/c^2 \ll 1$) in the case of the detector initially in the excited state the excitations peak in the vicinity of the resonant frequency $\omega \approx \Omega$. However, for larger accelerations, and hence larger final velocities, excitations can be found far away from the resonance due to the relativistic Doppler effect. If the detector starts out in the ground state, there is no peak around the resonant frequencies at all. Moreover, the ground state configuration has number expectation values which are several orders of magnitude less than for the case where the detector is initially excited.

In Table 4.1 we present upper bounds for the transition probabilities. We define resonant modes as such modes that are less than 2 % different from the detector's gap Ω.

The table shows that for an excited detector in non-relativistic regimes the non-resonant contribution may be negligible, depending on the set of parameters. Nonetheless, going to relativistic accelerations will significantly increase the non-resonant contribution, as was expected from the Doppler shift, and it will also add a mode spread of the energy deposited in the field. In principle, this renders the single-mode or few-mode approximation invalid in the excited case for high accelerations. If the detector enters the cavity in its ground state, matters look even worse: the resonant contribution is negligible for all regimes, and thus we cannot expect a single-mode (and even few-mode) approximation to be justified.

Lastly, we show in Appendix B.3 a further study of the validity of the single-mode approximation depending on the different parameters of the problem.

4.2.2 Single-Mode Approximation for Constant-Velocity Detectors

We compare our results now to the case of constant velocity $\bar{v}$ ($a = 0$) in order to clarify which signatures are due to acceleration and which are a mere artifact of the velocity. To that end, we choose as the detector's worldline

$$z(\tau) = \gamma\bar{v}\tau,\ t(\tau) = \gamma\tau,\ r, \varphi = 0. \tag{4.11}$$

We find accordingly the mode functions (4.3):

$$u_{m\ell n}(\tau) = \delta_{m0} A_{m\ell n} e^{-\mathrm{i}\omega\gamma\tau} \sin\Big(\frac{n\pi}{L}\gamma\bar{v}\tau\Big), \tag{4.12}$$

where again all contributions with $m \neq 0$ vanish. The length of interaction as given by the proper time is $T' = L/\gamma\bar{v}$, and we choose the velocity such that the detector will require the same time (with respect to the cavity frame) as the uniformly accelerated one to traverse the cavity:

$$\bar{v} = \left(1 + \frac{2c^2}{aL}\right)^{-1/2}. \tag{4.13}$$

We may then analytically solve the integral for the number expectation values (see (4.9)):

$$N_{\ell n} = c^3\lambda^2 \frac{2\pi(n\bar{v})^2}{\omega L^3 (R\gamma J_1(x_{0\ell}))^2} \frac{1 + (-1)^{n+1}\cos\Big(\Big(\omega \pm \frac{\Omega}{\gamma}\Big)\frac{L}{\bar{v}}\Big)}{\left[\Big(\omega \pm \frac{\Omega}{\gamma}\Big)^2 - \big(\frac{n\pi\bar{v}}{L}\big)^2\right]^2}, \tag{4.14}$$

where again the top sign denotes the initial ground state and the bottom sign the initial excited state of the detector. Interestingly, $N_{\ell n}$ can be zero due to its oscillatory behavior if

$$\left(\omega \pm \frac{\Omega}{\gamma}\right) \frac{L}{\bar{v}} = \pi p, \tag{4.15}$$

given that $\omega \pm \Omega/\gamma \neq 0$ and $p + n =$ even, or for all even n if $\omega - \Omega/\gamma = 0$, i.e. if a corresponding (Lorentz transformed) field mode is exactly resonant with the detector's gap and the detector is initially excited. This is a manifestation of the phenomenon called 'mode invisibility', that was introduced in [103] and has been also used in quantum optics for non-demolition measurements [104, 105].

In Fig. 4.3 we show the results for constant velocity. For both detector initializations (ground and excited state), the distribution is clearly distinguishable from the constant acceleration setting. Considering constant velocity, the distribution of number expectation values is sensitive to the velocity, having zeros as discussed before. For an initially excited detector, a relativistic Doppler broadening of the initial resonance can again be observed. Further, the initial ground state detector does not exhibit a resonance in the distribution, rendering any single-mode approximation invalid for any regime.

In Fig. 4.4 one can see an upper bound to the ratio of the resonant contribution to the spontaneous emission probability, given an exemplary parameter setting. Here, as was in the case for a uniformly accelerated detector, the single-mode approximation does not reproduce the distribution to a good fidelity for relativistic trajectories, and even for low velocities caution is required due to the oscillating behavior.

4.3 Validity of a Non-Relativistic Approximation

Another approximation that we will assess is the consideration that the trajectory of the detector undergoes non-relativistic motion and the trajectory is approximated by a Galilean motion of constant acceleration. This greatly simplifies the mathematical treatment of the dynamics. However, as we will see, it is not enough that the final speed of the detector is non-relativistic to carry out this approximation: this approximation also fails to assess the number of excitations deposited in high enough energy modes regardless of the speed of the detector.

In the non-relativistic limit for $a\tau \ll c$ the worldline (4.7) approximates to

$$z(\tau) = \frac{a\tau^2}{2} + \mathcal{O}\left((a\tau)^2\right), \; t = \tau + \mathcal{O}\left((a\tau)^3\right). \tag{4.16}$$

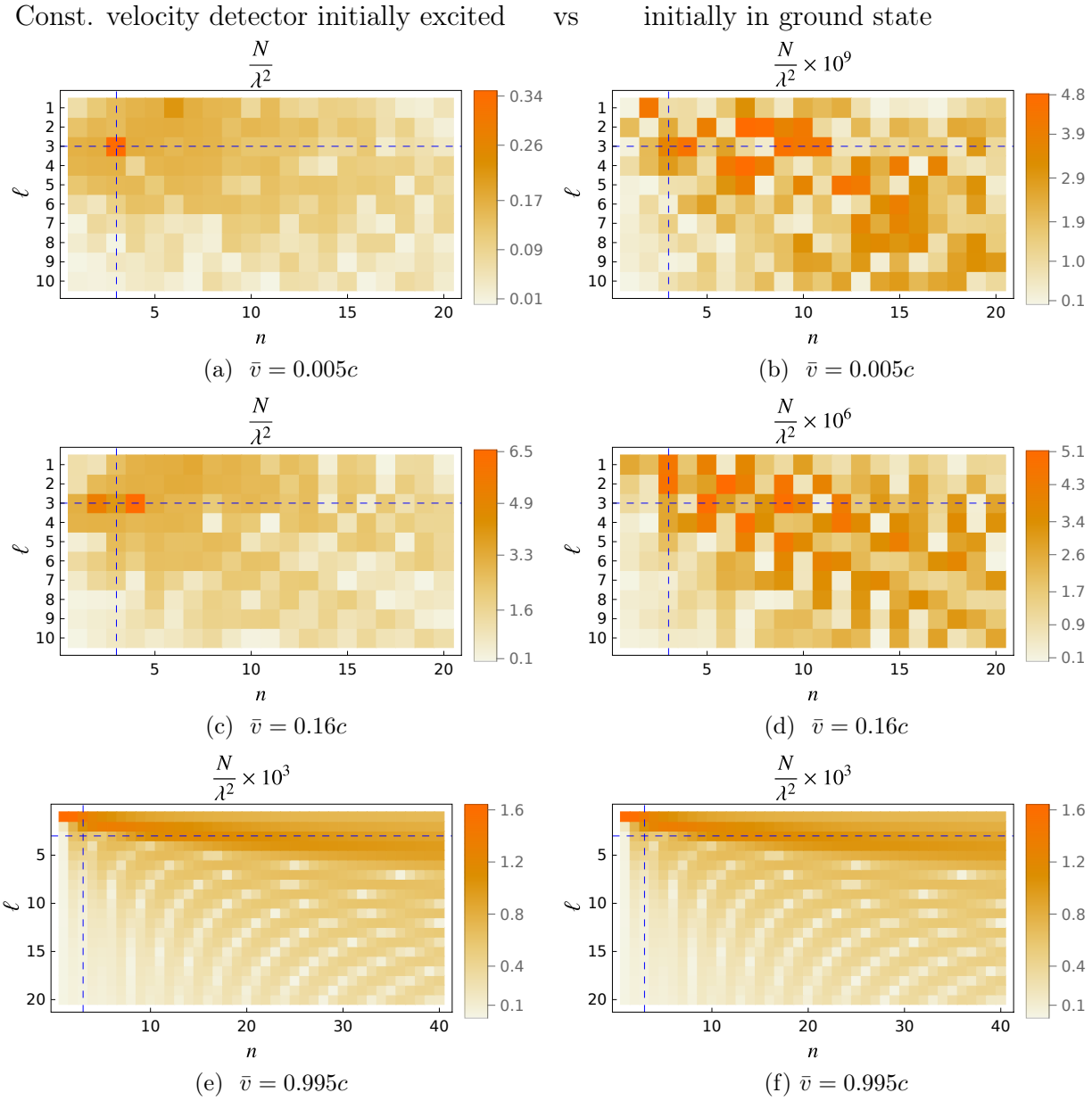

(a) $\bar{v} = 0.005c$ (b) $\bar{v} = 0.005c$

(c) $\bar{v} = 0.16c$ (d) $\bar{v} = 0.16c$

(e) $\bar{v} = 0.995c$ (f) $\bar{v} = 0.995c$

Figure 4.3: Number expectation N versus mode numbers n and ℓ for different detector velocities. Parameters are $R/L = 0.5$, $\Omega R/c = 10$, $\Omega L/c = 20$ so that the detector is resonant with $(m, \ell, n) = (0, 3, 3)$ (intersection of dashed lines). (a, b) Velocity $\bar{v} = 0.005c$ (corresponds to $aL/c^2 = 0.00005$); (c, d) $\bar{v} = 0.16c$ (corresponds to $aL/c^2 = 0.05$); (e, f) $\bar{v} = 0.995c$ (corresponds to $aL/c^2 = 200$). The detector traverses the cavity in the same times (in the cavity frame) as for the corresponding cases of an accelerated detector.

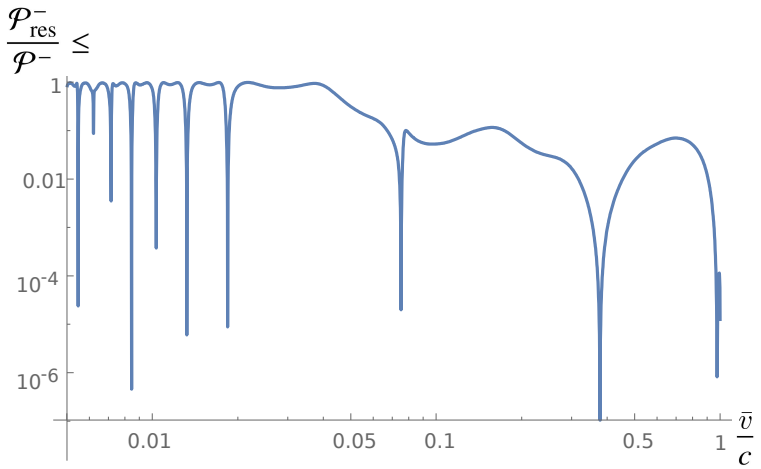

Figure 4.4: Estimating an upper bound to the ratio of the resonant contribution to the spontaneous emission probability $\mathcal{P}^-_{\text{res}}/\mathcal{P}^-$ for varying constant velocity $\bar{v}$ in a log-log plot. Parameters are $R/L = 0.5$, $\Omega L/c = 20$. The detector's energy gap is resonant with $(m, \ell, n) = (0, 3, 3)$. We have chosen as the cut-offs for the sums over n and ℓ 2000 and 100, respectively.

Under this approximation, one can find an analytic solution to the integrals of Eq. (4.9) by noting that (where + denotes again the initial detector ground state, and − the initial excited state)

$$\begin{aligned} D_{\pm}(\ell, n) \coloneqq & \int_0^T \mathrm{d}\tau e^{\mathrm{i}\tau(\omega\pm\Omega)} \sin\left(\frac{a\pi n\tau^2}{2L}\right) \\ = & \frac{(-1)^{\frac{1}{4}}\sqrt{L}}{2\sqrt{2an}} \left\{ e^{\frac{\mathrm{i}L}{2\pi an}(\omega\pm\Omega)^2} \left[\mathrm{erf}\left(\frac{\frac{1+\mathrm{i}}{2}(\pi anT - L(\omega\pm\Omega))}{\sqrt{\pi anL}} \right) + \mathrm{erf}\left(\frac{\frac{1+\mathrm{i}}{2}\sqrt{L}(\omega\pm\Omega)}{\sqrt{\pi an}} \right) \right] \right. \\ & \left. + \mathrm{i}e^{-\frac{\mathrm{i}L}{2\pi an}(\omega\pm\Omega)^2} \left[\mathrm{erf}\left(\frac{\frac{\mathrm{i}-1}{2}(L(\omega\pm\Omega) + \pi anT)}{\sqrt{\pi anL}} \right) - \mathrm{erf}\left(\frac{\frac{\mathrm{i}-1}{2}\sqrt{L}(\omega\pm\Omega)}{\sqrt{\pi an}} \right) \right] \right\}. \end{aligned} \tag{4.17}$$

We then can write, recalling that only $m = 0$ is non-vanishing,

$$N^{\text{NR}}_{\ell n} \approx c^2\lambda^2 |A_{0\ell n}|^2 |D_{\pm}(\ell, n)|^2. \tag{4.18}$$

The relative error Δ due to the non-relativistic approximation (denoted by superscript

NR) for the expectation value of the number operator in the different field modes $N_{\ell n}$ is

$$\Delta(\ell, n) = 1 - \frac{N_{\ell n}^{\mathrm{NR}}}{N_{\ell n}}. \tag{4.19}$$

In Fig. 4.5 we plot the relative error for different proper accelerations a. For an initially excited detector and for low mode numbers n and ℓ, the error has a peak at the most resonant modes. In general all field modes, for low accelerations, that are close in energy to the detector's gap from below will show an underestimation in the number expectation values. Secondly, for modes with larger values of n and ℓ, the non-relativistic approximation systematically overestimates the number expectation values. Decreasing the proper acceleration reduces, as expected, the relative error. Nonetheless, for a fixed acceleration the approximation incurs a run-away error from the exact values as one increases further the mode numbers ℓ or n. This implies that for high enough mode numbers the approximation will fail for any fixed acceleration. If the detector starts out in the ground state, there is no such peaking of the relative error. Nonetheless, there is a general overestimation of the number expectation values in the non-relativistic approximation. Towards larger values of n and ℓ this overestimation increases, and again results in a diverging relative error for unbounded mode numbers. Overall, the non-relativistic approximation is only reliable for low accelerations in the case of modes with low values of n and ℓ if the detector is initially in the ground state, and for modes which are close in energy to the detector's gap (but not resonant) for an initially excited detector.

4.4 One-Dimensional Approximation to Long and Thin Cavities

Another common approximation that we see in the literature is to model an optical cavity through a 1+1 dimensional cavity instead of the more realistic 3+1 dimensional model. The question we want to address is: can we approximate a very long and thin cavity (think of an optical fiber) by just a 1+1 dimensional cavity?

In more concrete words: we call 'optical fiber limit' the limit of a very thin and very long cylindrical cavity. For $R \ll L$, we want to see whether the model is effectively that of a scalar field in 1+1 dimensions. In that case the main contribution to the dynamics would be dominated by the field modes with $\ell = 1$ (recall ℓ is the label of the radial modes). This is so because for fixed $\Omega L/c$, as we take the optical fiber limit even the lowest-energy radial mode will become far off-resonant with the detector gap, i.e. $\omega \gg \Omega$. In particular, the

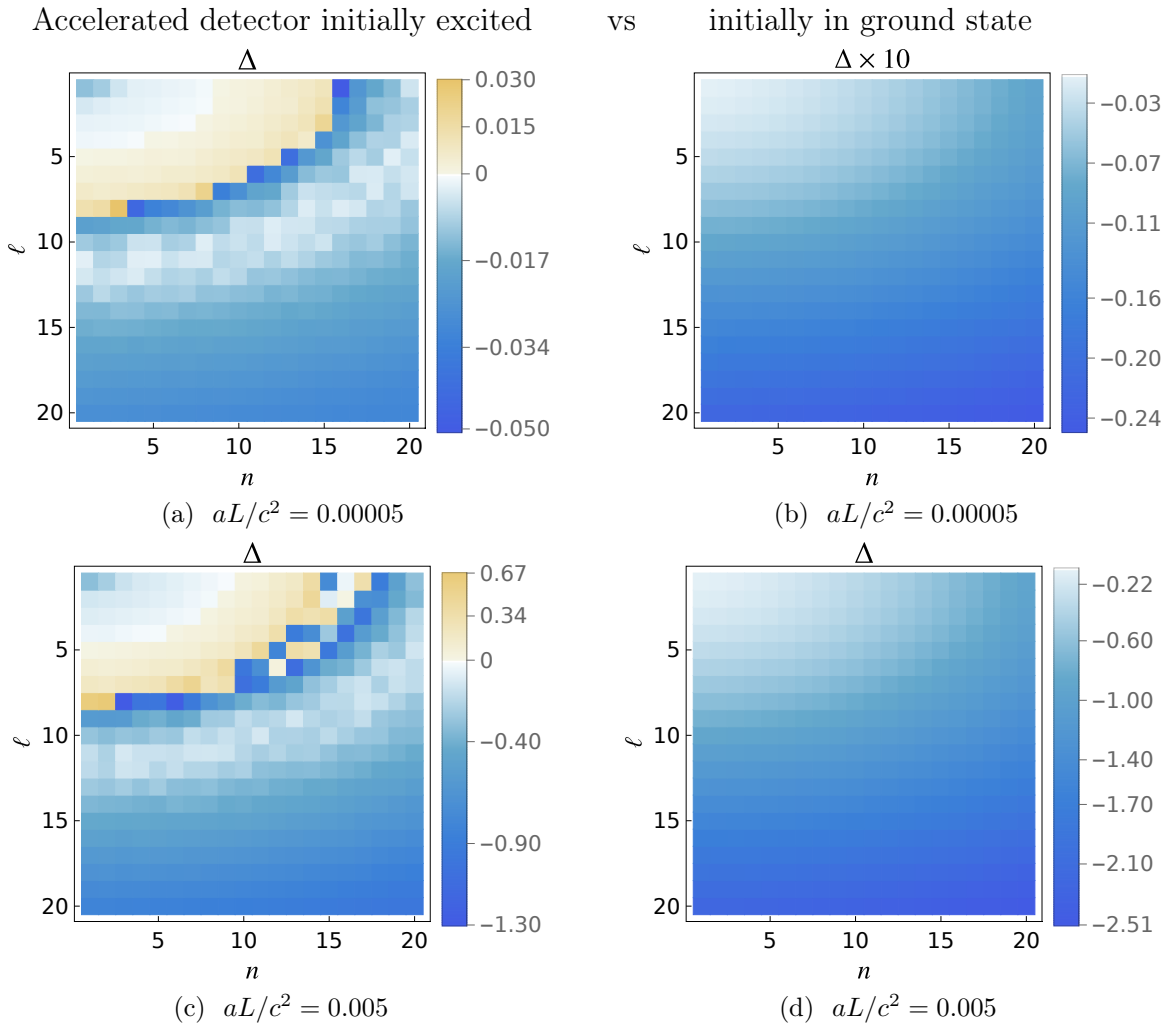

(a) $aL/c^2 = 0.00005$ (b) $aL/c^2 = 0.00005$

(c) $aL/c^2 = 0.005$ (d) $aL/c^2 = 0.005$

Figure 4.5: Relative error Δ in number of excitations due to a non-relativistic approximation versus mode numbers n and ℓ. Parameters are $R/L = 0.5$, $\Omega L/c = 50$. (a, b) $aL/c^2 = 0.00005$ (final velocity $\sim 0.01c$); (c, d) $aL/c^2 = 0.005$ (final velocity $\sim 0.1c$). The following field modes are in a 2 % difference from the detector's gap: $\{(\ell, n)|(\ell, n) = (1, 16), (3, 15), (4, 14), (5, 13), (6, 11), (7, 8-9), (8, 2-4)\}$. For the excited case, the number expectation values are underestimated for modes close to resonance for low accelerations; for higher accelerations this gets Doppler shifted in ℓ direction. The higher energetic modes are overestimated resulting in a run-away relative difference even for low acceleration. For the ground state case, all number expectation values are overestimated with the relative difference being lowest for low energy modes. Even for low accelerations, the error is diverging when going to higher values of ℓ or n.

energy spacing corresponding to modes with different quantum numbers ℓ is significant. This can be seen from (4.5) as for sufficiently low quantum numbers n in the optical fiber limit

$$\omega \approx c\frac{x_{0\ell}}{R} = \omega_0 \frac{x_{0\ell}}{x_{01}}, \tag{4.20}$$

where we have defined $\omega_0 \coloneqq cx_{01}/R$. However, as we will observe, the first few radial modes with $\ell > 1$ may still be moderately excited by detector crossing. This, in turn, would mean that the typical dimensional reduction approach of modelling the 3+1 dimensional problem as a single scalar field in 1+1 dimensions is not sound. In general, as we will see, choosing a single *massless* field in the lower dimensional setting is even less sound due to the effective masses associated with each ℓ in 1+1 dimensions. Before we investigate this in more detail, though, we will take a step back and study dimensional reduction from a more general standpoint in the next chapter. That is, we will develop the methods and tools to perform the dimensional reduction approximation for arbitrary boundary conditions and cavity geometries with axial symmetry. Afterwards, in Sec. 5.4, we will be in the position to come back to our study of (moving) atoms inside a cylindrical cavity and assess the validity of the dimensional reduction at this concrete example.

4.5 Summary

We have studied the imprint on the quantum field as well as transition probabilities after an accelerated detector crossed an optical cavity. In particular we looked at relativistic and non-relativistic regimes and found that a sharp localization in the field modes that gets excited can only be given for initially excited detectors with non-relativistic accelerations. However, even in these settings, we saw that assuming a single-mode or few-mode approximation will not always – depending on the specific parameters of detector and cavity – yield a satisfactory reproduction of the full physics. Moreover, as soon as we enter the relativistic regime or have a detector initially in the ground state, a restriction of the relevant field modes to one or a few will even in principle fail to predict the correct results.

We compared the results to the signature of the field if a detector moves with constant velocity and found that the distributions can be distinguished in order to extract the acceleration-induced influence on the field state after the detector crossed the cavity. Due to mode invisibility, even non-relativistic velocities for initially excited detectors may not guarantee the validity of the single-mode approximation. In all other regimes, similarly to the acceleration case, the approximation fails to correctly predict observables. Furthermore,

we have shown that a non-relativistic approximation on the trajectory of a detector crossing an optical cavity yields incorrect results for any fixed acceleration; in particular for high-energy field modes.

Chapter 5

Dimensional Reduction

In this chapter, we wish to approach the problem of dimensional reduction, which we began to discuss in the last chapter, from a more general perspective. There is an intuitive sense in which a long, thin cavity (e.g., a fiber optic cable) can be modeled as an approximately one dimensional system. But how exactly does this dimensional reduction work technically? And under exactly what conditions is such an approximation valid?

We will show that a $D+1$ dimensional quantum scalar field inside a cavity can be mapped (without any approximation) to an infinite collection of massive $1+1$ dimensional quantum fields, which we call subfields. We will discuss this *subfield decomposition* in sufficient generality to apply it to a wide variety of cavity geometries and boundary conditions. After this, we will identify the dimensional reduction approximation as the approximation made by ignoring all but one of these subfields.

It is important to note that since the subfields are generically massive (even if the $D+1$ field is massless), one cannot in general approximate a 3+1 dimensional field in a very long, very thin optical fiber by a *massless* $1+1$ dimensional field, as is often done. When done properly, and in the regimes where this is possible, the dimensional reduction approximates the 3+1 dimensional cavity by a single $1+1$ dimensional theory with a mass given by the transverse mode scales.

As we will discuss, the subfield decomposition tells us the strength with which the detector couples to each of the subfields. These coupling strengths are fixed entirely by the size and shape of the detector in the $D+1$ dimensional description. Thus, the dimensional reduction approximation – which, recall, couples the detector to only one subfield – is equivalent to an approximation on the detector's shape. Thus the question of which

subfields are relevant to the detector's dynamics reduces to the question of which changes in the detector's shape will only minimally affect its evolution.

This chapter is organized as follows. In Sec. 5.1, for the case of Dirichlet boundary conditions, we show how the interaction of a detector with a $D+1$ dimensional theory can be written in terms an infinite number of (massive) subfields, and how the detector couples to each individually. In Sec. 5.2, we generalize the results for a wide range of boundary conditions and cavity geometries. In Sec. 5.3 we discuss the relation between performing a dimensional reduction approximation and changing the detector's shape and size. Further, in Sec. 5.4 we show at the setup from Chapter 4, i.e. for a cylindrical cavity, when the dimensional reduction can be justified in different regimes. Finally, we summarize our results in Sec. 5.5.

5.1 Dimensional Reduction of Cavities with Axial Symmetry

Consider a real, potentially massive[1], free scalar field $\hat{\phi}(t, x_1, \ldots, x_{D-1}, x_D)$ in $D+1$ dimensions, with $D \geq 2$. We are particularly interested in such a field living in a cavity with an axial symmetry with arbitrary cross-section Γ (see Fig. 5.1). To this end, we partition the spatial dimensions as $\boldsymbol{x} = (\boldsymbol{y}, z)$ with $\boldsymbol{y} = (x_1, \ldots, x_{D-1})$ and $z = x_D$. We take the cavity to be extended along its axial coordinate z from $z = 0$ to $z = L$. In the transverse coordinates, $\boldsymbol{y}$, we take the cavity to have an arbitrary shape defined by $\boldsymbol{y} \in \Gamma$ where $\Gamma \subset \mathbb{R}^{D-1}$ is a bounded domain. For instance, if Γ defines a triangle then the cavity is a triangular prism. If Γ defines a disk, then the cavity is cylindrical.

We will leave the boundary conditions in the z direction (at $z = 0$ and $z = L$) unspecified: e.g. Dirichlet, Neumann, periodic, etc. For sake of introduction, we will in this section take the field to obey Dirichlet boundary conditions in the $\boldsymbol{y}$ directions, i.e. $\hat{\phi}(t, \boldsymbol{y}, z) = 0 \ \forall \boldsymbol{y} \in \partial\Gamma$. In Sec. 5.2 we will discuss the generalization to other transverse boundary conditions.

[1]Note that we allow the field to be massive to increase the generality of our consideration. None of the conclusions or techniques discussed in this chapter depend critically on having $M \neq 0$.

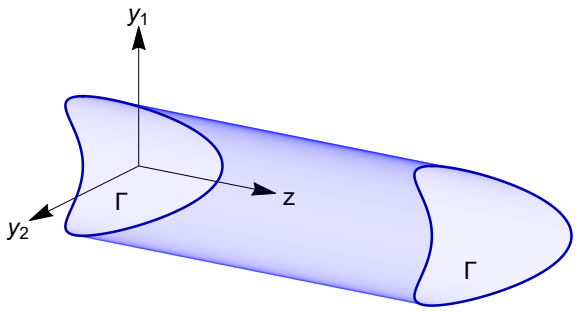

Figure 5.1: An example of a cavity with axial symmetry.

The field's free Hamiltonian written in these $(\boldsymbol{y}, z)$ coordinates is

$$\begin{aligned}\hat{H}_{\text{F}} =& \frac{1}{2}\int \mathrm{d}^D x \, \left(c^2 \hat{\pi}(t,\boldsymbol{x})^2 + |\nabla\hat{\phi}(t,\boldsymbol{x})|^2 + \frac{M^2c^2}{\hbar^2}\hat{\phi}(t,\boldsymbol{x})^2\right) \\ =& \frac{1}{2}\int_\Gamma \mathrm{d}^{D-1} y \int_0^L \mathrm{d}z \left(c^2\, \hat{\pi}(t,\boldsymbol{y},z)^2 + |\nabla\hat{\phi}(t,\boldsymbol{y},z)|^2 + \frac{M^2c^2}{\hbar^2}\hat{\phi}(t,\boldsymbol{y},z)^2\right),\end{aligned} \tag{5.1}$$

where M is the field's mass, and $\hat{\pi}(t,\boldsymbol{y},z)$ is the canonically conjugate momentum to $\hat{\phi}(t,\boldsymbol{y},z)$, satisfying the equal-time canonical commutation relations

$$[\hat{\phi}(t,\boldsymbol{y}_1,z_1), \hat{\pi}(t,\boldsymbol{y_2},z_2)] = \mathrm{i}\hbar\, \mathbb{1}\, \delta(\boldsymbol{y}_1-\boldsymbol{y}_2)\, \delta(z_1-z_2). \tag{5.2}$$

The UDW Hamiltonian (2.2) correspondingly reads in these coordinates

$$\hat{H}_{\text{UDW}} = \hbar c\lambda\, \chi(t) \int_\Gamma \mathrm{d}^{D-1} y \int_0^L \mathrm{d}z\, F(\boldsymbol{y},z)\, \hat{\mu}(t) \otimes \hat{\phi}(t,\boldsymbol{y},z). \tag{5.3}$$

One may expect that if the cavity is a *very thin fiber*, then one should be able to approximate the interaction of the detector and the $D+1$ dimensional field by a simpler interaction of the detector and an effectively $1+1$ dimensional field. Concretely, let R be a characteristic lengthscale of Γ [2]. One might expect the dimensional reduction criteria to be $L \gg R$. Certainly, in this regime the cavity *looks* one-dimensional from the outside, but is this what the detector sees from inside?

Our approach to answering this question is as follows: First we will show how the $D+1$ dimensional field in a cavity can be recast (with no approximations) as an infinite collection

[2] For instance, if Γ is a disk, R could be its radius. If Γ defines a polygon, R could be its inradius.

of uncoupled 1+1 dimensional fields (what we will call *subfields*). We will then identify how the detector interacts with each of these $1+1$ dimensional subfields. Viewed in this light, the desired dimensional reduction can be identified as making an approximation in which the detector couples to only one (or maybe a few) of these subfields. Perhaps surprisingly, we will see that the dimensional reduction condition is not as simple as $L \gg R$, it also involves the size/shape of the detector as well as the duration of its interaction with the field and the initial field state.

5.1.1 Subfield Decomposition

To map the $D+1$ dimensional quantum field into a set of simpler 1+1 dimensional fields, we first split the derivative ∇ in (5.1) into its axial and transversal components ($\nabla = \partial_z + \nabla_\Gamma$). This yields for the free field Hamiltonian

$$\hat{H}_{\text{F}} = \frac{1}{2}\int_\Gamma \mathrm{d}^{D-1}y \int_0^L \mathrm{d}z \left(c^2 \hat{\pi}(t,\boldsymbol{y},z)^2 + (\partial_z \hat{\phi}(t,\boldsymbol{y},z))^2 + |\nabla_\Gamma\, \hat{\phi}(t,\boldsymbol{y},z)|^2 + \frac{M^2c^2}{\hbar^2}\hat{\phi}(t,\boldsymbol{y},z)^2 \right). \tag{5.4}$$

Integration by parts in the transverse directions $\boldsymbol{y}$ gives

$$\hat{H}_{\text{F}} = \frac{1}{2}\int_\Gamma \mathrm{d}^{D-1}y \int_0^L \mathrm{d}z \left(c^2 \hat{\pi}(t,\boldsymbol{y},z)^2 + (\partial_z \hat{\phi}(t,\boldsymbol{y},z))^2 + \hat{\phi}(t,\boldsymbol{y},z)\left(\Delta_\Gamma + \frac{M^2c^2}{\hbar^2}\right)\hat{\phi}(t,\boldsymbol{y},z) \right), \tag{5.5}$$

where Δ_Γ is the Dirichlet Laplacian over Γ, that is the Laplacian restricted to operating on functions that vanish on $\partial\Gamma$. Note that we have used the boundary condition over Γ to remove the boundary term.

We next find the eigenfunctions $\psi_j(\boldsymbol{y})$ and eigenvalues λ_j of this transversal Laplacian. These obey

$$\Delta_\Gamma\, \psi_j(\boldsymbol{y}) = -\lambda_j \psi_j(\boldsymbol{y}), \quad \psi_j(\boldsymbol{y}) = 0 \quad \forall y \in \partial\Gamma \tag{5.6}$$

for integers $j \geq 1$. Since Γ is bounded, we know the Dirichlet Laplacian has an unbounded discrete positive spectrum, $0 < \lambda_1 \leq \lambda_2 \leq \lambda_3 \leq \cdots \to \infty$, and that its eigenfunctions form an orthonormal basis with respect to the L^2 inner product [106].

Several example geometries will be considered in detail in Sec. 5.2. For now, and to start building intuition, let us focus on the simple case of a rectangular cavity. Let

$\Gamma = [0, L_1] \times [0, L_2] \times \cdots \times [0, L_{D-1}]$ for a $D-1$ dimensional rectangular cavity. The eigenfunctions and eigenvalues of the Dirichlet Laplacian are then

$$\psi_{n_1 \ldots n_{D-1}}(\boldsymbol{y}) = \prod_{k=1}^{D-1} \sqrt{\frac{2}{L_k}} \sin\left(\frac{n_k \, \pi \, y_k}{L_k}\right), \tag{5.7}$$

$$\lambda_{n_1 \ldots n_{D-1}} = \sum_{k=1}^{D-1} \left(\frac{n_k \, \pi}{L_k}\right)^2, \tag{5.8}$$

for integers $n_k \geq 1$. Note that these eigenvalues have multiple indices, $n_1, \ldots, n_d$. In order to be converted into the single-index form of Eq. (5.6), these eigenvalues would need to be listed and sorted.

We can expand the field operators for each t and z in terms of these eigenfunctions as

$$\hat{\phi}(t, \boldsymbol{y}, z) = \sum_{j=1}^{\infty} \hat{\phi}_j(t, z) \, \psi_j(\boldsymbol{y}), \tag{5.9}$$

$$\hat{\pi}(t, \boldsymbol{y}, z) = \sum_{j=1}^{\infty} \hat{\pi}_j(t, z) \, \psi_j(\boldsymbol{y}), \tag{5.10}$$

where

$$\hat{\phi}_j(t, z) \coloneqq \int_{\Gamma} \mathrm{d}^{D-1} y \; \hat{\phi}(t, \boldsymbol{y}, z) \, \psi_j(\boldsymbol{y}), \tag{5.11}$$

$$\hat{\pi}_j(t, z) \coloneqq \int_{\Gamma} \mathrm{d}^{D-1} y \; \hat{\pi}(t, \boldsymbol{y}, z) \, \psi_j(\boldsymbol{y}) \tag{5.12}$$

are $1+1$ dimensional fields which we will dub "subfields". Indeed these subfields obey the equal-time canonical commutation relations

$$[\hat{\phi}_i(t, z_1), \hat{\pi}_j(t, z_2)] = \mathrm{i} \, \hbar \, \mathbb{1} \, \delta(z_1 - z_2) \delta_{ij}. \tag{5.13}$$

The field's free Hamiltonian (5.1) can be written in terms of the subfields as

$$\hat{H}_{\mathrm{F}} = \sum_{j=1}^{\infty} \frac{1}{2} \int \mathrm{d}z \left(c^2 \, \hat{\pi}_j(t, z)^2 + (\partial_z \hat{\phi}_j(t, z))^2 + \left(\frac{M^2 c^2}{\hbar^2} + \lambda_j\right) \hat{\phi}_j(t, z)^2 \right). \tag{5.14}$$

Note that the subfields are all uncoupled from each other and each have an effective mass M_j given by

$$M_j = \frac{\hbar}{c} \sqrt{\frac{M^2 c^2}{\hbar^2} + \lambda_j}. \tag{5.15}$$

Or equivalently,

$$(Mc^2)^2 = (M_j c^2)^2 - (\hbar\, c\, k_j)^2, \quad \text{where } \lambda_j =: k_j^2. \tag{5.16}$$

Note that even if the original field were massless, $M = 0$, the subfields are still effectively massive since $\lambda_j > 0$ (due to the transverse Dirichlet boundary conditions). Neglecting this effective mass yields incorrect predictions for detectors coupling to quantum fields in cavities.

The masses of these subfields can be thought of as being due to a confinement effect. We note that light inside of an idealized box, i.e. being small and massless with perfectly reflecting walls, behaves inertially [107]. That is, the light-box behaves in many ways exactly like a massive particle would. In actuality, our field in a cavity is confined (at least in the transverse directions). This confinement does not go away as the cavity becomes "more one-dimensional", indeed the field is *more* confined in this limit/regime. As we will discuss more in-depth soon, as the transverse scale of the cavity R becomes increasingly small, the eigenvalues λ_j (and therefore the subfield masses M_j) become increasingly large. Said differently, the cavity's transverse geometry remains present and is encoded in the subfield masses.

5.1.2 The Detector's Interaction with the Subfields

Now that we have decomposed the $D+1$ dimensional field into these uncoupled $1+1$ dimensional subfields, we can investigate how the detector couples to each subfield. Recall that our goal is to identify under what conditions we might be able to approximate the detector's interaction with the full field by an interaction with only one (or maybe a few) of these $1+1$ dimensional subfields.

The UDW interaction Hamiltonian (5.3) can be straightforwardly written in terms of the subfields as

$$\hat{H}_{\text{I}} = \sum_{j=1}^{\infty} \hbar c \lambda\, \chi(t) \int_0^L \mathrm{d}z\, F_j(z)\, \hat{\mu}(t) \otimes \hat{\phi}_j(t,z), \tag{5.17}$$

where

$$F_j(z) \coloneqq \int_\Gamma \mathrm{d}^{D-1}y\; F(\boldsymbol{y}, z)\, \psi_j(\boldsymbol{y}) \tag{5.18}$$

is the detector's effective smearing function for the j^{th} subfield. Note that for a generic smearing function $F(\boldsymbol{y}, z)$ the detector will couple to every subfield to varying degrees.

Given this, we may ask: under what conditions is a single (or few) subfield approximation justified? We will consider this question in detail in Sec. 5.3 but we can already see two hints as to why we might be able to ignore the subfields with very high index j.

First, if the detector's smearing function is relatively smooth, then we can expect the detector to couple very weakly to subfields with high index j; the corresponding eigenfunction $\psi_j(\boldsymbol{y})$ will be highly oscillatory and so have little overlap with the relatively smooth $F(\boldsymbol{y}, z)$. A slight caveat is, however, that particle detectors are often modeled as being point-like, i.e., not smooth. We will address this point in Sec. 5.4.

Second, these high-j subfields will have high eigenvalues λ_j and therefore high effective masses M_j. If the subfield's effective mass is large compared to the energy scales associated with the detector-field coupling we expect that the coupling will not provide "enough energy" to excite (or absorb energy from) highly massive subfields. This would effectively decouple subfields with large j from the detector. The intricacy here is that in the $R \to 0$ limit where we intuitively expect to get dimensional reduction, *all* of the subfield masses will diverge. In this limit the detector's interaction with every subfield will be "frozen out". More on this in Sec. 5.4.

Before exploring in detail exactly when a single-subfield approximation is justified, let us first discuss how this *subfield decomposition* can be achieved for more general cavity geometries and boundary conditions.

5.2 General Boundary Conditions

As we showed in the previous section, one can reduce a $D+1$ dimensional field in an axially symmetric cavity to an infinite collection of uncoupled effectively massive $1+1$ dimensional fields. We demonstrated this for a cavity with rectangular cross-section and Dirichlet boundary conditions on $\partial\Gamma$. It turns out this reduction can be done much more generally.

Indeed, the only properties of the Dirichlet Laplacian that we used are that it has a discrete spectrum and that its eigenfunctions form a complete orthonormal basis. If Γ is open, bounded, connected and has a piecewise smooth boundary, then the Neumann Laplacian and Robin Laplacian also have these properties [108, 109, 106]. We could even consider periodic boundary conditions for Γ. More generally we could take Γ to be any compact manifold. This possibility will be discussed further on in this section. This widens the scope of the above subfield decomposition to include a huge number of different transverse geometries and boundary conditions. All that changes case-to-case are the

eigenvalues λ_j (and so the effective masses M_j) and the eigenfunctions $\psi_j(\boldsymbol{y})$ (and so the effective smearing functions $F_j(z)$).

One key difference between different boundary conditions is their allowance or disallowance of a "constant" eigenfunction with eigenvalue $\lambda = 0$, i.e. a zero-mode. For instance, this will always happen in the Neumann case and never in the Dirichlet case [110]. When there is a subfield with $\lambda = 0$ and when the $D+1$ dimensional field is massless, $M = 0$, then there can be a single massless subfield.

The relationship between the eigenvalues of the Laplacians and the geometry of Γ deserves some further comment. In particular, any eigenvalue of the Robin Laplacian is lower and upper bounded by the corresponding eigenvalues (labeled by j) of the Neumann and Dirchlet Laplacian. This is a consequence of the Courant minmax principle [108, 106]. The Courant principle further implies domain monotonicity for Dirichlet boundary conditions (however not for Robin and Neumann) so that $\lambda_j(\Gamma_1) \geq \lambda_j(\Gamma_2)$ if $\Gamma_1 \subset \Gamma_2$ [106]. Further, while the distribution of the eigenvalues λ_j is fixed by the shape of Γ and the boundary conditions, the reverse is not true. These eigenvalues do not carry complete information about the shape of Γ [111] (one cannot always hear the shape of a drum). However, the works by Kempf et al. prove that the spectrum of the Laplacian does carry a great deal of information about the shape [112, 113]. A standard example of the relationship between the spectrum of the Laplacian and the shape of its domain is Weyl's law [114, 115] which tells us that for large j the eigenvalue λ_j scales as

$$\lambda_j \sim 4\pi^2 \left(\frac{j}{V_d \ |\Gamma|} \right)^{2/d}, \tag{5.19}$$

where $d = D - 1$ is the dimension of the domain Γ, V_d is the volume of the unit-ball in $\mathbb{R}^d$ and $|\Gamma|$ is the d-dimensional volume of Γ.

Note that since $|\Gamma| \sim R^d$ (where we recall R is the characteristic length scale of Γ) we have that $\lambda_j \sim R^{-2}$ for small R. Thus for all j we have that $M_j \to \infty$ as $R \to 0$ (unless of course for $\lambda_j = 0$ and $M = 0$ such that $M_j = 0$). Then in the thin-cavity limit, every subfield has an infinite effective mass (except for potentially one subfield with $M = 0$). If one is to take this limit, it must be handled carefully. In particular, approximating the detector's interaction as being with a single $1+1$ dimensional, *massless* field becomes increasingly inappropriate as $R \to 0$.

This close connection between the effective masses of the subfields and the cavity's geometry leads to the exciting possibility of extracting detailed geometric information from measurements of our detector. Given sufficient measurement data from a detector with a known shape $F(\boldsymbol{y}, z)$ but in an unknown geometry, it is not unreasonable to imagine

that we could extract from this data some approximate values for M_j and $F_j(z)$. From these we can approximately determine λ_j and $\psi_j(\boldsymbol{y})$ which together tell us approximately about the geometry of Γ and its boundary conditions.

As an extreme (but hopefully delighting) example consider a cosmology with $d = D-1$ compactified spatial dimensions and one[3] extended spatial direction. The inhabitants of such a cosmos may be completely unaware of these compactified dimensions. Such inhabitants would likely interpret their particle physics experiments as indicating the existence of a finite collection of $1+1$ dimensional fields with some distribution of masses. Once these inhabitants learn of the compactified dimensions (maybe taking inspiration from string theory) they can reinterpret these $1+1$ dimensional fields as the subfields of a single $D+1$ dimensional field. By noting the scaling of M_j for high j they could (by Weyl's law) determine the number of compactified dimensions and the d dimensional volume of Γ. By guessing the geometry of Γ they would be able to predict the masses of new yet-to-be-discovered subfields (that they may perhaps call strings?).

Connecting back to quantum optics, this tells us that it may be possible to determine similar geometric information about a fiber optic cable from the response of a detector embedded in it. For instance, one could estimate the cross sectional area of the cable or detect slight imperfections in the cable's shape.

5.2.1 Example Geometries

For reference, we will now list the eigenfunction and eigenvalues of the Laplacian for several simple geometries and boundary conditions.

As we mentioned in Sec. 5.1, $\Gamma = [0, L_1] \times [0, L_2] \times \cdots \times [0, L_d]$ for a $d = D-1$ dimensional rectangle, and so the eigenfunctions and eigenvalues of the Dirichlet Laplacian are

$$\psi_{n_1 \ldots n_d}(\boldsymbol{y}) = \prod_{k=1}^{d} \sqrt{\frac{2}{L_k}} \sin\left(\frac{n_k \, \pi \, y_k}{L_k}\right), \tag{5.20}$$

$$\lambda_{n_1 \ldots n_d} = \sum_{k=1}^{d} \left(\frac{n_k \, \pi}{L_k}\right)^2, \tag{5.21}$$

for integers $n_k \geq 1$. The eigenfunctions and eigenvalues of the Neumann Laplacian in this

[3]Note that although we focus here on only one extended longitudinal dimension, there is essentially no barrier to extend the results to cases with multiple extended spatial directions.

geometry are

$$\psi_{n_1 \ldots n_d}(\boldsymbol{y}) = \prod_{k=1}^{d} A(k, n_k) \cos\left(\frac{n_k \, \pi \, y_k}{L_k}\right), \tag{5.22}$$

$$\lambda_{n_1 \ldots n_d} = \sum_{k=1}^{d} \left(\frac{n_k \, \pi}{L_k}\right)^2, \tag{5.23}$$

for integers $n_k \geq 0$ and where $A(k, n)$ is $\sqrt{2/L_k}$ for $n \neq 0$ and $\sqrt{1/L_k}$ for $n = 0$.

For a disk with radius R the eigenfunctions and eigenvalues of the Dirichlet Laplacian are

$$\psi_{m\ell}(r, \varphi) = \frac{1}{\sqrt{\pi} R J_{m+1}(x_{m\ell})} \exp(\mathrm{i} m \varphi) \, J_m(x_{m\ell} \, r/R), \tag{5.24}$$

with eigenvalues $\lambda_{m\ell} = (x_{m\ell}/R)^2$ where J_m is the m-th Bessel function of the first kind and $x_{m\ell}$ is the ℓ-th zero of the m-th Bessel function. Note that each of the above expressions (except for $m = 0$) gives us two eigenfuctions, namely its real and imaginary parts. The eigenfunctions and eigenvalues of the Neumann Laplacian for a disk can be found in [106].

The eigenvalues of the Dirichlet, Neumann and Robin Laplacians for an equilateral triangle and many other related geometries are known in closed form [116, 117, 118]. Moreover, much is known about how the spectrum of the Laplacian changes under perturbations to the domain. In the case of Dirichlet boundary conditions, the perturbed spectrum converges to the original spectrum for a wide variety of deformations [108, 119, 106]. The Neumann Laplacian, on the other hand, can be very sensitive to general perturbations [106, 120, 119] which makes numerical stability difficult. Indeed, on certain bounded domains the Neumann spectrum may not even be discrete [121].

5.3 Subfield Truncation as a Modification of Detector Shape

In the previous sections we have discussed how one can (with no approximation) rewrite the interaction of a detector with a single $D + 1$ dimensional field into the interaction of a detector with an infinite collection of $1 + 1$ dimensional fields (which we called subfields). Under what conditions can we approximate this situation as a detector interacting with only one (or perhaps a few) subfields?

This approximation can be straightforwardly achieved by truncating the sum over j in the interaction Hamiltonian Eq. (5.17) to include only $j \in J$ for some finite set of positive integers J. Crucially, this truncation is equivalent to modifying the detector's smearing function as

$$F(\boldsymbol{y}, z) = \sum_{j=1}^{\infty} F_j(z)\psi_j(\boldsymbol{y}) \to F^{(\mathrm{TR})}(\boldsymbol{y}, z) := \sum_{j \in J} F_j(z)\psi_j(\boldsymbol{y}). \tag{5.25}$$

A detector that has *a priori* such a truncated smearing function does not couple to subfields with $j \notin J$. This also means that we can truncate the field's free Hamiltonian (5.14) without further approximation. In other words, from the perspective of the detector, the subfields with $j \notin J$ are completely invisible. Therefore if we exclude them from the description of the field, any prediction on the detector will not be altered. In summary: the effects of subfield truncation can be understood entirely in terms of modifying the "shape" of the detector.

But how well can the truncation of the subfield sum describe the actual physics of a detector in a thin cavity? One may intuit that this truncation will be justified if the corresponding change of the detector's shape, i.e.,

$$\Delta F^{(\mathrm{TR})}(\boldsymbol{y}, z) := F(\boldsymbol{y}, z) - F^{(\mathrm{TR})}(\boldsymbol{y}, z), \tag{5.26}$$

is "small enough": that is, if $F(\boldsymbol{y}, z)$ and $F^{(\mathrm{TR})}(\boldsymbol{y}, z)$ are roughly the same. Let us proceed uncritically (without delving into what "small" means) temporarily and see what we find.

For a single-subfield approximation to work we would need that $F(\boldsymbol{y}, z) \approx f(z)\psi_j(\boldsymbol{y})$ for some $f(z)$ and j. That is, such an approximation would be justified only if the detector's smearing function $F(\boldsymbol{y}, z)$ is sufficiently "near" to a harmonic mode of the Laplacian on Γ and "far" from all the other harmonic modes. Such a detector would need to have non-negligible spatial support over the whole cavity since every harmonic mode of Γ is supported over the whole cavity. However, smearing functions for realistic detectors (e.g., atoms with shapes roughly given by atomic orbitals) look nothing like these harmonic modes, they are far too localized. By this argument it may seem that a single-subfield approximation is never justified for realistic atomic detectors.

Indeed, in quantum optics, atoms are taken to be extremely localized, often being modeled as point-like with $F(\boldsymbol{x}) \approx \delta(\boldsymbol{x} - \boldsymbol{x}_0)$ for some $\boldsymbol{x}_0$. In this case, the severity of above described issues are drastically increased. No detector can simultaneously be highly localized (be delta-like) and couple to exactly one subfield (be ψ_j-like). In order for a point-like approximation and a single-subfield approximation to hold simultaneously the

detector's smearing function would have to be simultaneously "close" to two very different spatial distributions: $f(z)\psi_j(\boldsymbol{y})$ and $\delta(\boldsymbol{x}-\boldsymbol{x}_0)$. If we compare these distributions with the L^2 norm, these functions are infinitely far apart, i.e. $||f(z)\psi_j(\boldsymbol{y})-\delta(\boldsymbol{x}-\boldsymbol{x}_0)||_2=\infty$. Moreover, with respect to the L^1 norm we have

$$||f(z)\psi_j(\boldsymbol{y})-\delta(\boldsymbol{x}-\boldsymbol{x}_0)||_1=||f(z)\psi_j(\boldsymbol{y})||_1+||\delta(\boldsymbol{x}-\boldsymbol{x}_0)||_1 \tag{5.27}$$

since $f(z)\psi_j(\boldsymbol{y})$ has no "volume" over $\boldsymbol{x}_0$. That is, these two distributions saturate the triangle inequality; they are as far apart as possible given their finite L^1 norms. Surely, the smearing function $F(\boldsymbol{x})$ cannot be simultaneously close to two such distant distributions. By this argument, it appears that the point-like approximation and the single-subfield approximation are incompatible.

But surely this conclusion is suspect. In quantum optics it is common to take both the point-like approximation and the $1+1$ dimensional approximation and nothing seems to go horribly wrong there. Indeed, as we will now discuss there is something subtly wrong with the above argument; In infinite dimensional vector spaces, the notions of "near" and "far" require careful qualification. Different norms do give radically different notions of what it means to be "far". Above we saw that $f(z)\psi_j(\boldsymbol{y})$ and $\delta(\boldsymbol{x}-\boldsymbol{x}_0)$ are far apart with respects to both the L^2 and L^1. However, before we started discussing distances in terms of the L^2 and L^1 norms, we should have asked, "why are these the relevant norms for the comparison in this particular physical scenario?" Indeed, what is a very different shape for our eyes (or for our mathematical intuition based on the L^1 and L^2 norms) may not be that different from the perspective of a detector coupling to the field.

To analyze the difference in detector response for the exact smearing and the truncated one, we may evaluate therefore the relative difference in physical observables such as transition probabilities $\mathcal{P}$:

$$\Delta_{\mathcal{P}} \coloneqq \frac{|\mathcal{P}-\mathcal{P}^{(\text{TR})}|}{\mathcal{P}}. \tag{5.28}$$

This figure of merit is more appropriate to analyze how "blind" the detector is to the truncation of the smearing function. Indeed, it is built directly from the difference the truncation causes in the detector's response. It also naturally takes into account the "contextual details" of the detector's interaction, i.e. the state of the field and the coupling strength's dependence on time.

Despite the failure of the L^1 and L^2 norms to predict when a single-subfield approximation may be valid, we maintain our earlier claim that this approximation can be understood entirely in terms of modifying the shape of the detector. There must be some

better context-sensitive norm with which we can appropriately judge the smallness of $\Delta F^{(\text{TR})}(\boldsymbol{y}, z)$. Indeed, we can identify two such norms using the transition probabilities. The transition probabilities for a (stationary) detector to leading order in the coupling can be written as, see e.g. [55],

$$\mathcal{P}^{\pm} = c^2\lambda^2 \int \mathrm{d}t \int \mathrm{d}^D x \int \mathrm{d}t' \int \mathrm{d}^D x' \chi(t)\, F(\boldsymbol{x})\, \chi(t')\, F(\boldsymbol{x'}) e^{\mp \mathrm{i}\Omega(t-t')}\, W_\phi(t, t'; \boldsymbol{x}, \boldsymbol{x}'), \quad (5.29)$$

where, as in the previous chapter, $\mathcal{P}^{\pm}$ are the vacuum excitation/spontaneous emission probability for the detector, and where

$$W_\phi(t, t'; \boldsymbol{x}, \boldsymbol{x}') \coloneqq \mathrm{Tr}(\hat{\rho}_{\text{F}}\, \hat{\phi}(t, \boldsymbol{x})\, \hat{\phi}(t', \boldsymbol{x}')) \quad (5.30)$$

is the field's Wightman function with $\hat{\rho}_{\text{F}}$ being the initial field state.

By using transition probabilities, we can maintain our earlier claim that the subfield approximation can be understood entirely in terms of modifying the shape of the detector. Indeed, from Eq. (5.29) we can identify two such context-sensitive norms in order to judge the smallness of $\Delta F^{(\text{TR})}(\boldsymbol{y}, z)$:

$$\frac{\mathcal{P}^{\pm}}{\lambda^2} = c^2 \int \mathrm{d}^D x \int \mathrm{d}^D x'\, K_{\pm}(\boldsymbol{x}, \boldsymbol{x}')\, F(\boldsymbol{x})\, F(\boldsymbol{x}') =: ||F||^2_{\pm}, \quad (5.31)$$

with kernels $K_{\pm}(\boldsymbol{x}, \boldsymbol{x}')$ given by

$$K_{\pm}(\boldsymbol{x}, \boldsymbol{x}') \coloneqq \int \mathrm{d}t \int \mathrm{d}t'\, \chi(t)\chi(t') e^{\mp \mathrm{i}\Omega(t-t')} W_\phi(t, t'; \boldsymbol{x}, \boldsymbol{x}'). \quad (5.32)$$

These norms naturally take into account the detector's switching function $\chi(t)$ and the state of the field through the field's Wightman function. Moreover, one can check that we have

$$\frac{||F(\boldsymbol{y}, z) - F^{(\text{TR})}(\boldsymbol{y}, z)||^2_{\pm}}{||F(\boldsymbol{y}, z)||^2_{\pm}} = \frac{|\mathcal{P}^{\pm} - (\mathcal{P}^{\pm})^{(\text{TR})}|}{\mathcal{P}^{\pm}}. \quad (5.33)$$

That is, the relative error in these new norms is exactly the relative error in the transition probabilities. This confirms that, ultimately, the way that the detector "sees" space (i.e., changes in shape) is through the $||F||_{\pm}$ norms rather than trough the L^1 or L^2 norms. This framing resolves the above raised issue: How can $F(x)$ be near to both $f(z)\psi_j(\boldsymbol{y})$ and $\delta(\boldsymbol{x} - \boldsymbol{x}_0)$ if they are so far apart? The answer is that $f(z)\psi_j(\boldsymbol{y})$ and $\delta(\boldsymbol{x} - \boldsymbol{x}_0)$ are not so far apart with respect to the norms which are actually relevant for the dynamics.

We can conclude that we have to consider the change of predictions of physical observables, as compared to norms that are irrespective of the physical process, if we want to evaluate the impact of truncating the number of subfields. In the next section, for the concrete example of the cylindrical cavity from Chapter 4, we will see in more detail under what conditions the change in transition probabilities is small.

5.4 Dimensional Reduction for a Cylindrical Cavity

In this section, we want to further understand under what conditions the $1+1$ dimensional reduction is an adequate approximation by going back to the cavity geometry of Section 4.1. Recall, we consider a cylindrical cavity of radius R and length L with Dirichlet boundary conditions. The solution to the 3+1 dimensional Klein-Gordon equation yields the following mode decomposition of the quantized scalar field,

$$\hat{\phi}(t,r,\varphi,z) = \sum_{\substack{m=0\\n,\ell=1}}^{\infty} \left(u_{m\ell n}\, \hat{a}_{m\ell n} + u^*_{m\ell n}\, \hat{a}^\dagger_{m\ell n} \right), \tag{5.34}$$

where the field modes satisfying Dirichlet boundary conditions are

$$u_{m\ell n}(t,r,\varphi,z) = A_{m\ell n} e^{\mathrm{i}m\varphi} e^{-\mathrm{i}\omega t} \sin\left(\frac{n\pi}{L} z\right) J_m\left(\frac{x_{m\ell}}{R} r\right), \tag{5.35}$$

$$A_{m\ell n} = c^{1/2} \left(R\sqrt{L\pi\omega} J_{m+1}(x_{m\ell}) \right)^{-1}, \tag{5.36}$$

$$\omega = c\sqrt{\frac{x^2_{m\ell}}{R^2} + \frac{n^2\pi^2}{L^2}}, \tag{5.37}$$

where x_{ml} is the ℓ-th zero of the m-th Bessel function of the first kind, J_m. Note that the field modes are orthonormalized with respect to the Klein-Gordon inner product.

Following the procedure laid out in Section 5.1, we can rewrite this scenario as one in which the detector interacts with an infinite collection of $1+1$ dimensional fields. The transverse profiles of these subfields are given by (5.24). In this geometry the subfields are labeled by both m and ℓ. These subfields have effective masses, $M_{m\ell} \coloneqq \frac{\hbar}{c}\sqrt{\lambda_{m\ell}} = \frac{\hbar x_{m\ell}}{cR}$, and mode decompositions,

$$\hat{\phi}_{m\ell}(t,z) = \sum_{n=1}^{\infty} \left(\tilde{u}_{m\ell,n}(t,z)\hat{a}_n + \tilde{u}^*_{m\ell,n}(t,z)\hat{a}^\dagger_n \right), \tag{5.38}$$

where

$$\tilde{u}_{m\ell,n}(t,z) = \sqrt{\frac{c}{\tilde{\omega}L}} e^{-\mathrm{i}\tilde{\omega}t} \sin\left(\frac{n\pi}{L} z\right) \tag{5.39}$$

and

$$\tilde{\omega} = c\sqrt{\left(\frac{M_{m\ell}c}{\hbar}\right)^2 + \left(\frac{n\pi}{L}\right)^2}. \tag{5.40}$$

We assume for now that the detector is localized on the axis of symmetry with a spherically symmetric spatial profile. Thus, only subfields with $m = 0$ will be contributing. Consequently, the $3+1$ dimensional theory decomposes into an infinite number of $1+1$ dimensional massive theories, where the UDW Hamiltonian reads

$$\hat{H}_{\text{UDW}} = \sum_{\ell=1}^{\infty} \hbar c\lambda\, \chi(t) \int_0^L \mathrm{d}z\, F_{0\ell}(z)\, \hat{\mu}(t) \otimes \hat{\phi}_{0\ell}(t,z). \tag{5.41}$$

Since the dimensional reduction is usually justified for one spatial dimension being much larger than the remaining dimensions, we want to examine in the following sections the regime where $R \ll L$. Furthermore we assume $\sigma/R \ll 1$, where σ is the detector's characteristic length scale. This implies that the detector is localized far away from the cavity boundaries. From the previous discussion it should become clear that the best possible approximation for a 3+1D cavity with a lower dimensional one is certainly not that of a 1+1D massless field. In the next sections we will investigate how the subfields and their respective masses can reproduce the full theory in more detail.

As a preliminary remark, the mode functions of the 3+1 dimensional theory and the 1+1 dimensional theory for a given ℓ (i.e., for a given effective mass $M_{0\ell}$ in the lower dimensional theory), when the detector in $3+1$ dimensions stays on the axis of symmetry, are equal up to an (ℓ-dependent) proportionality constant, cf. (5.35):

$$\tilde{u}_{0\ell,n}(t,z) = \sqrt{\pi} J_1(x_{0\ell}) R\, u_{0\ell n}(t,0,0,z). \tag{5.42}$$

Notice that the two mode functions depend on different powers of R. The effective 1+1 dimensional case inherits dependence on R through the effective mass $M_{0\ell}$. For $R \ll L$, $\tilde{u}_{0\ell,n}(t,z) \propto \sqrt{R}$ and $u_{0\ell n}(t,0,0,z) \propto R^{-1/2}$. Further, as can be seen from (5.35), taking the limit $R/L \to 0$ will increase the frequency of the oscillatory behavior resulting in enhanced cancellations of positive and negative contributions. Therefore, the deposited energy in the field modes of the 3+1 as well as the 1+1 dimensional model will become smaller as the quantity $R/L \to 0$. In the next two sections we want to study with how few subfields we can reconstruct the full 3+1 dimensional process in different scenarios: for moving, point-like detectors and for stationary, spatially extended detectors.

5.4.1 Dimensional Reduction with Moving Point-like Detectors

We will continue here where we left off in Sec. 4.4: a point-like detector traversing the cavity on its axis of symmetry. Then, the UDW Hamiltonian (5.41) takes the form

$$\hat{H}_{\text{UDW}} = \sum_{\ell=1}^{\infty} \frac{\hbar c \lambda \, \chi(t)}{\sqrt{\pi} J_1(x_{0\ell}) R} \, \hat{\mu}(\tau) \otimes \hat{\phi}_{0\ell}(t(\tau), z(\tau)). \tag{5.43}$$

Let us study the transition probabilities of the detector after leaving the cavity, and conclude whether it is the same for the full theory (5.43) and a truncated version thereof. In particular, we want to investigate if there are scenarios where a single-subfield approximation, i.e. a dimensional reduction approximation, is valid. We, therefore, will begin by setting the detector's energy gap to be either resonant with the first subfield, i.e. with $\ell = 1$, or off-resonant with any subfield, i.e. $\hbar\Omega \ll M_{01}c^2$. Intuitively, for these assumptions, a single subfield ($\ell = 1$) should suffice to obtain correct predictions, at least in the non-relativistic regime. From our results of Chapter 4 it should be clear that the number of modes relevant to reconstruct transition probabilities is significantly larger for excitation than de-excitation processes. Hence, we will focus in the first step on vacuum excitation probabilities as the worst-case scenario. This will illustrate that a naive dimensional reduction approximation where we only consider one subfield (even if massive) can fail.

In 1+1 dimensions, the excitation probability $\tilde{\mathcal{P}}_l^+$, for a fixed subfield ℓ, after the detector crosses the cavity is to leading order (cf. Appendix B.2.1):

$$\tilde{\mathcal{P}}_l^+ = c^2\lambda^2 \sum_{n=1}^{\infty} \left| \int_0^T \mathrm{d}\tau e^{\mathrm{i}\Omega\tau} \tilde{u}_{0\ell,n}(t(\tau), z(\tau))^* \right|^2, \tag{5.44}$$

where the ℓ dependence is implicit in the frequencies $\tilde{\omega}$ which depend on the mass $M_{0\ell}$. Using (5.42), we can compare (5.44) to the probability of excitation $\mathcal{P}^+$ in the 3+1 dimensional model (cf. (B.25)):

$$\mathcal{P}^+ = \sum_{\ell=1}^{\infty} \mathcal{P}_l^+ = \sum_{\ell=1}^{\infty} \frac{1}{\pi J_1(x_{0\ell})^2 R^2} \tilde{\mathcal{P}}_l^+, \tag{5.45}$$

where $\mathcal{P}_l^+$ without tilde is the collective contribution of all modes to the excitation probability for a given ℓ:

$$\mathcal{P}_l^+ = c^2\lambda^2 \sum_{n=1}^{\infty} \left| \int_0^T \mathrm{d}\tau e^{\mathrm{i}\Omega\tau} u_{0\ell n}(t(\tau), 0, 0, z(\tau))^* \right|^2. \tag{5.46}$$

Let us remark first that the pre-factors in the probabilities of Eq. (5.45) depend on R and radial quantum number ℓ, and thus cannot be obtained by starting naively from a 1+1 dimensional theory. Note also that the dimensions for the coupling λ are different when starting in one spatial dimension as opposed to the three dimensional case. Further, if the excitation probability for the detector in 3+1 dimensions has significant contributions only for $\ell = 1$, then the single-subfield model is a good approximation in the optical fiber limit to describe the detector response. As an estimator of the validity of the approximation, we will work here with the relative magnitude $\mathcal{F}$ of the $\ell > 1$ subfield contributions to the full probability with respect to the contribution that comes from the subfield with $\ell = 1$ which constitutes the dimensional reduction approximation as discussed above.

The estimator is difficult to evaluate in the case of a moving detector but we can easily derive a lower bound to it by evaluating the partial sum up to N_{sub}:

$$\mathcal{F} = \frac{\sum_{\ell=2}^{\infty} \mathcal{P}_l^+}{\mathcal{P}_1^+} \geq \frac{\sum_{\ell=2}^{N_{\text{sub}}} (\mathcal{P}_l^+)^{(N_{\text{long}})}}{\mathcal{P}_1^+}, \tag{5.47}$$

where $(\mathcal{P}_l^+)^{(N_{\text{long}})}$ indicates that the sum in n is truncated at N_{long}. For simplicity, we will consider now a detector with small constant velocity v, which will allow to feasibly perform the sum numerically. The contribution from the each subfield ℓ to the excitation probability in the 3+1 dimensional model takes the following form (see (4.14)):

$$(\mathcal{P}_l^+)^{(N_{\text{long}})} = \sum_{n=1}^{N_{\text{long}}} \frac{2\lambda^2 c^3 \pi (n\bar{v})^2}{\tilde{\omega} L^3 (R\gamma J_1(x_{0\ell}))^2} \frac{1 + (-1)^{n+1} \cos\left(\left(\tilde{\omega} + \frac{\Omega}{\gamma}\right)\frac{L}{v}\right)}{\left[\left(\tilde{\omega} + \frac{\Omega}{\gamma}\right)^2 - \left(\frac{n\pi v}{L}\right)^2\right]^2}. \tag{5.48}$$

The results are shown in Table 5.1. We find that $\mathcal{F}$ does not seem to have the limit zero when taking $R/L \to 0$, and that therefore the dimensional reduction will not reproduce the results correctly as the excitation probability for the 3+1 dimensional case has in fact non-negligible contributions coming from $\ell > 1$ – already in the regime of non-relativistic velocities. We can conclude that there exist regimes where the (massive) single-subfield approximation cannot work. In particular, from our observations in Chapter 4, considering relativistic detector trajectories, where many modes of the 3+1 dimensional field are excited, will especially spoil any validity of the single-subfield approximation.

5.4.2 Dimensional Reduction with Extended Stationary Detectors

In the previous section, we studied a point-like detector traversing a cylindrical cavity. We showed that there exist regimes where the dimensional reduction approximation, i.e. only

Parameters	$\bar{v} = 0.005c$, $\Omega L/c = 20$					
R/L	5×10^{-1}	10^{-2}	10^{-3}	10^{-4}	10^{-5}	10^{-6}
$\mathcal{F} \geq$	151.47	4.9	4.15	4.11	4.05	3.16
Parameters	$\bar{v} = 0.005c$, Ω resonant with $\tilde{\omega}_{\ell=1,n=1}$					
R/L	5×10^{-1}	10^{-2}	10^{-3}	10^{-4}	10^{-5}	10^{-6}
$\mathcal{F} \geq$	31.31	16.42	17	16.88	16.65	12.11

Table 5.1: Estimating the validity of single-subfield approximation by considering the ratio of excitation probabilities $\mathcal{F}$ as a function of R/L for constant non-relativistic velocity $\bar{v} = 0.005c$ in the 3+1D model. We have chosen 1) $\Omega L/c = 20$ so that the detector is increasingly off-resonant with any field modes for $R/L \to 0$, and 2) Ω to be always most resonant with the first mode of the first subfield. The cut-offs for the sums over n and ℓ are $N_{\text{long}} = 10^8$ and $N_{\text{sub}} = 250$, respectively. Importantly, (the lower bound to) $\mathcal{F}$ does not seem to approach zero in the limit $R/L \to 0$.

taking into account one subfield, breaks down. Moreover, we only considered a sudden switching function (which was naturally imposed by the detector's passing through the cavity).

In the following we will investigate with how many subfields, instead of just one, we can reliably reconstruct the higher dimensional physics. We will study different adiabatic and non-adiabatic switching functions and, to simplify matters, we will assume that the detector is stationary. Further, we generalize the detector's spatial profile to be Gaussian (instead of point-like) with central localisation at $z = L/2$, $r = 0$:

$$F(r, \varphi, z) = \frac{1}{\sqrt{2\pi\sigma^2}^3} \exp\left(-\frac{r^2}{2\sigma^2}\right) \exp\left(-\frac{\left(z - \frac{L}{2}\right)^2}{2\sigma^2}\right), \tag{5.49}$$

which is L^1-normalized for a detector strongly localized inside the cavity. Following the procedure around Eq. (5.18), the reduced smearing functions become[4]

$$F_{0\ell}(z) = \frac{1}{\sqrt{2}\pi\sigma R J_1(x_{0\ell})} \exp\left(-\frac{\sigma^2 x_{0\ell}^2}{2R^2}\right) \exp\left(-\frac{\left(z - \frac{L}{2}\right)^2}{2\sigma^2}\right), \tag{5.50}$$

where $F_{m\ell} = 0$ for $m \neq 0$ due to the axial symmetry. These reduced smearing functions go into the UDW Hamiltonian of Eq. (5.41).

[4]Note that assuming the localization of the detector to be much smaller than the cavity dimensions, we can extend the integrals involving the Gaussians to the whole space.

One may expect that truncating the infinite sum could yield a good approximation to the detector dynamics. In particular, in the previous section we particularized to the case where the sum is truncated to one subfield. Let us generalize these results by studying the speed at which the transition probabilities of the detector converge as we consider the effect of more summands in Eq. (5.41).

The number of excitations $N_{\ell n}$ in modes (ℓ, n) of the $3+1$ dimensional model to leading order in perturbation theory is for a Gaussian and a sudden box switching function, respectively, given by (analogous to the expression in Appendix B.2)

$$\begin{aligned}
N_{\ell n} =& c^2\lambda^2 \left| \int_{\mathbb{R}} \mathrm{d}t \chi(t) e^{\pm \mathrm{i}\Omega t} \int_{\mathbb{R}^3} \mathrm{d}^3x F(r,z) u^*_{0\ell,n}(t,r,\varphi,z) \right|^2 \\
=& c^3\lambda^2 \left| \int_{\mathbb{R}} \mathrm{d}t \chi(t) e^{\mathrm{i}(\pm\Omega+\tilde{\omega})t} \int_{\mathbb{R}} \mathrm{d}z \frac{F_{0\ell}(z)}{\sqrt{L\omega}} \sin\left(\frac{n\pi}{L}z\right) \right|^2 \\
=& \frac{c^3\lambda^2}{L\omega\pi R^2 J_1(x_{0\ell})^2} e^{-(\pi n\sigma/L)^2} e^{-(\sigma M_{0\ell} c/\hbar)^2} \sin^2\left(\frac{n\pi}{2}\right) \\
& \times \begin{cases} 2\pi T^2 e^{-T^2(\pm\Omega+\tilde{\omega})^2}, & \chi(t) = \exp(-t^2/(2T^2)) \\ 2\frac{1-\cos(T(\Omega\pm\tilde{\omega}))}{(\Omega\pm\omega)^2}, & \chi(t) = \theta(t) - \theta(t-T) \end{cases},
\end{aligned} \tag{5.51}$$

where the $+$ sign indicates the initial ground state of the detector and the $-$ sign indicates that the detector is initially excited. Then the vacuum excitation probability $\mathcal{P}^+$ and the spontaneous emission probability $\mathcal{P}^-$ are obtained via

$$\mathcal{P}^\pm = \sum_{\ell,n=1}^{\infty} N_{\ell n} = \sum_{\ell=1}^{\infty} \tilde{\mathcal{P}}^\pm_\ell \frac{e^{-(\sigma M_{0\ell} c/\hbar)^2}}{\pi R^2 J_1(x_{0\ell})^2}, \tag{5.52}$$

where the $1+1$ dimensional transition probabilities are defined as

$$\begin{aligned}
\tilde{\mathcal{P}}^\pm_\ell =& \sum_{n=1}^{\infty} \frac{\lambda^2 c^3}{L\tilde{\omega}} e^{-(\pi n\sigma/L)^2} \sin^2\left(\frac{n\pi}{2}\right) \\
& \times \begin{cases} 2\pi T^2 e^{-T^2(\pm\Omega+\tilde{\omega})^2}, & \chi(t) = \exp(-t^2/(2T^2)) \\ 2\frac{1-\cos(T(\Omega\pm\tilde{\omega}))}{(\Omega\pm\tilde{\omega})^2}, & \chi(t) = \theta(t) - \theta(t-T) \end{cases}.
\end{aligned} \tag{5.53}$$

Again, the $3+1$ dimensional transition probabilities of a detector coupled to a single massless scalar field are recast as the infinite sum of $1+1$ dimensional subfields with effective masses $M_\ell = \hbar x_{0\ell}/(cR)$. Recall, we assumed that $R \ll L$ and $\sigma \ll R$. Two points should be repeated here: First, the factors in Eq. (5.52) multiplying the $1+1$ dimensional

contributions to the probabilities are non-negligible: it would be wrong to just model the long cavity starting from a 1+1 dimensional theory naively without doing the dimensional reduction. Second, the frequencies Eq. (5.40) become $\tilde{\omega} \approx M_{0\ell}c^2/\hbar$ when $R \ll L$ for small enough n. For those large masses it will be very energetically costly to excite the fields and this suggests that the high mass subfields (as compared to the other scales of the problem) will be frozen out and not contribute to the detector dynamics. We will see how this is the case below.

Considering the case of Gaussian switching first, Eq. (5.51) together with the assumption $R \ll L$ imply that the decay of subfield contributions is governed by

$$e^{-\frac{\sigma^2 x_{0\ell}^2}{R^2}} e^{-T^2(\pm\Omega+\tilde{\omega})^2} \sim e^{-(\sigma M_{0\ell}c/\hbar)^2} e^{-T^2(\pm\Omega+M_{0\ell}c^2/\hbar)^2} \tag{5.54}$$

for $cT/R \gtrsim 1$, i.e., exponentially suppressed with the effective mass of the subfields[5]. This suppression is lower bounded by the spontaneous emission scenario. Thus, we should expect that few subfields will be required for convergence, and that for vacuum excitation processes convergence sets in more quickly. However, when $cT/R \ll 1$, fast convergence in the number of subfields is only possible if Eq (5.54) is negligible for all but a small set of subfields. For the case of spontanous emission (the minus sign in front of Ω) this happens only if $T\Omega \gg \sigma/R$. In general, we expect thus the convergence in the spontaneous emission case to be slower than the vacuum excitation one.

To quantify the required number N_{sub} of subfields, i.e. how many $1+1$ dimensional fields we need to consider for sufficient accuracy in the detector dynamics, we consider the relative difference between the exact transition probability and a truncated version with only N_{sub} summands as per Eq. (5.28). In this case, the relative difference can be written as

$$\Delta_{\mathcal{P}^\pm}(N_{\text{sub}}) = 1 - \frac{1}{\mathcal{P}^\pm} \sum_{\ell=1}^{N_{\text{sub}}} \tilde{\mathcal{P}}_\ell^\pm \frac{e^{-\sigma^2 M_{0\ell}^2 c^2/\hbar^2}}{\pi R^2 J_1(x_{0\ell})^2}. \tag{5.55}$$

In Fig. 5.2 we plot the relative difference as a function of ΩT for different truncations of the sum in Eq. (5.55) and for different parameter configurations. We see that for vacuum excitations, as the evolution time becomes longer, the truncated sum of 1+1 dimensional terms approximates the exact calculation better. Indeed, for vacuum excitation processes, even a single-subfield approximation is valid for long times. That can be explained with

[5]This strong suppression is a consequence of the smooth Gaussian switching. As we will see, the suppression will not be as strong for any other switching as it goes with the Fourier transform of the switching function.

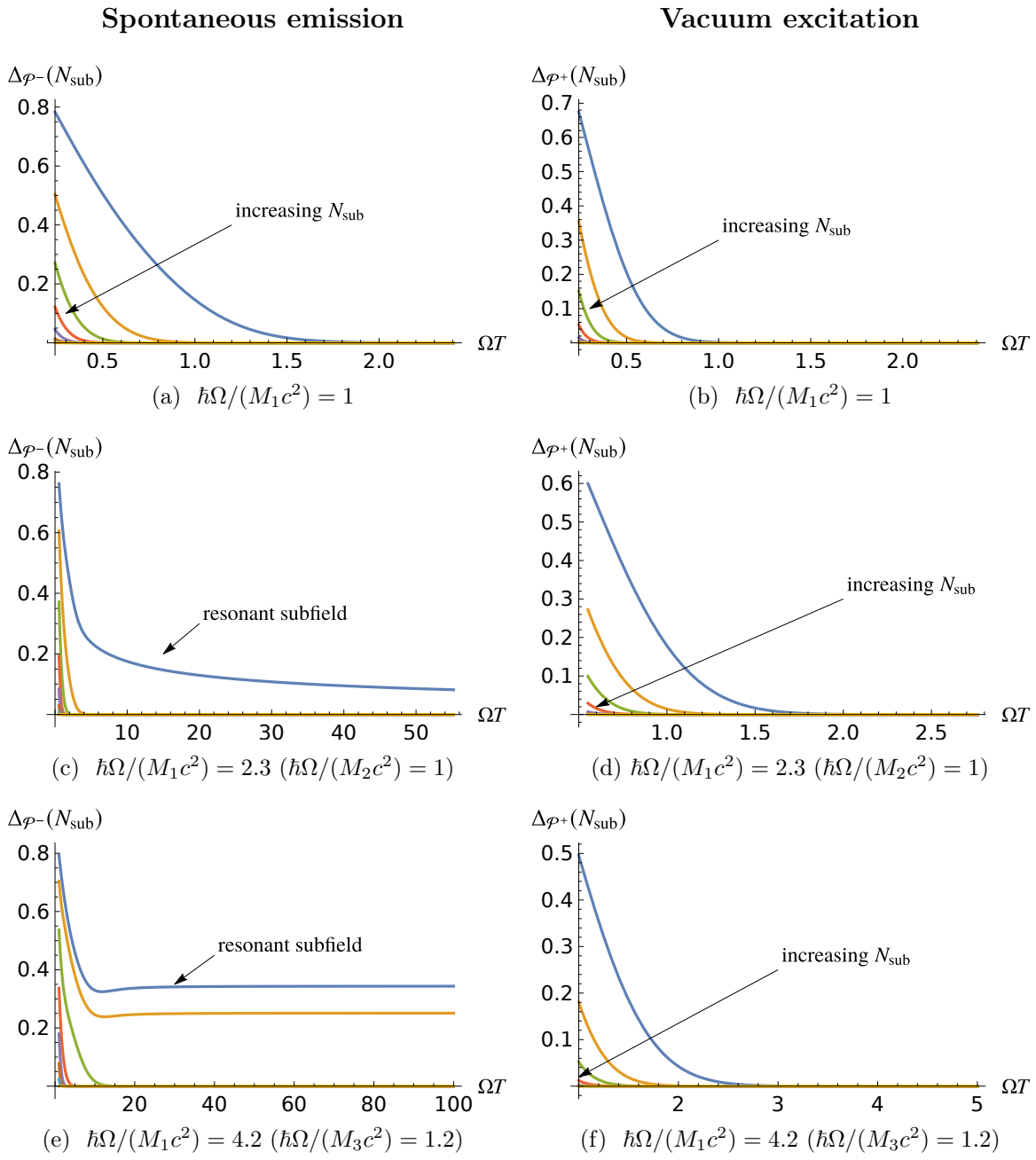

(a) $\hbar\Omega/(M_1c^2) = 1$ (b) $\hbar\Omega/(M_1c^2) = 1$

(c) $\hbar\Omega/(M_1c^2) = 2.3$ $(\hbar\Omega/(M_2c^2) = 1)$ (d) $\hbar\Omega/(M_1c^2) = 2.3$ $(\hbar\Omega/(M_2c^2) = 1)$

(e) $\hbar\Omega/(M_1c^2) = 4.2$ $(\hbar\Omega/(M_3c^2) = 1.2)$ (f) $\hbar\Omega/(M_1c^2) = 4.2$ $(\hbar\Omega/(M_3c^2) = 1.2)$

Figure 5.2: Relative difference $\Delta_{\mathcal{P}^\pm}(N_{\rm sub})$ as a function of ΩT for Gaussian switching. Parameters are $L/R = 10^3$ and (a)–(d) $\sigma/R = 10^{-2}$; (e, f) $\sigma/R = 10^{-6}$. Most-resonant subfield in (a, b) is $\ell = 1$; in (c, d) $\ell = 2$; in (e, f) $\ell = 3$. In (c, e) we first considered the resonant subfield and subsequently added the subfields from $\ell = 1$ onwards.

(5.54) which suppresses higher order summands strongly with increasing ℓ. For spontaneous emission, however, the number of subfields is largely governed by being in resonance, i.e. $\Omega - \tilde{\omega}$ being close to zero. The determining parameter is $\hbar\Omega/(M_{01}c^2)$, i.e. the ratio of the detector's transition energy to the mass of the least massive subfield. We find that for increasing values of $\hbar\Omega/(M_{01}c^2)$ the convergence for a fixed number of subfields becomes slower in time. In fact, even in the long-time regime one or a few subfields will not in general suffice for spontaneous emission probabilities if $\hbar\Omega/(M_{01}c^2)$ is large since more subfields will be close to resonance.

Let us consider now the Gaussian switching case with a point-like detector

$$F^{\delta}(r,z) = \frac{1}{2\pi r}\delta(r)\delta(z - L/2) \tag{5.56}$$

such that $F^{\delta}(r,z)$ is L^1-normalized. Note that, unlike in the previous section – which considered sudden switching – we keep the Gaussian switching for this point-like limit. The number of excitations can be obtained from (4.9):

$$N^{\delta}_{\ell n} = \lim_{\sigma\to 0} N_{\ell n}. \tag{5.57}$$

Therefore, the suppression factor in Eq. (5.54) becomes

$$e^{-T^2(\pm\Omega + M_{0\ell}c^2/\hbar)^2}, \tag{5.58}$$

i.e. there is no longer a suppression factor due to the detector size. Nonetheless, since we chose $\sigma = 10^{-2}R$ in Fig. 5.2, the dominant contribution to the decay of (5.54) came from the remaining exponential in (5.58) – at least in the long time regime when $\hbar\Omega \geq M_{01}c^2$. Hence, we do not expect any qualitative differences in the number of required subfields for long times when comparing to the spatially extended case.

Finally, let us now examine the relative difference in the case of a Gaussian smearing but a sudden switching function (as opposed to the adiabatic Gaussian switching above, see Eq. (5.53)). As seen in Fig. 5.3, the transition probability presents oscillatory behavior as a function of ΩT. We find that, already far off-resonance, one needs more subfields as compared to the adiabatic switching case. We also see that the relative difference does not approach zero as a function of ΩT for a fixed number of subfields, highlighting how the suddenness of the switching prevents a few-subfield approximation even in the long-time regime.

So far we have solely considered detectors that were positioned in the cavity's center, canceling the contribution from any subfields with $m \neq 0$. We will now study the influence

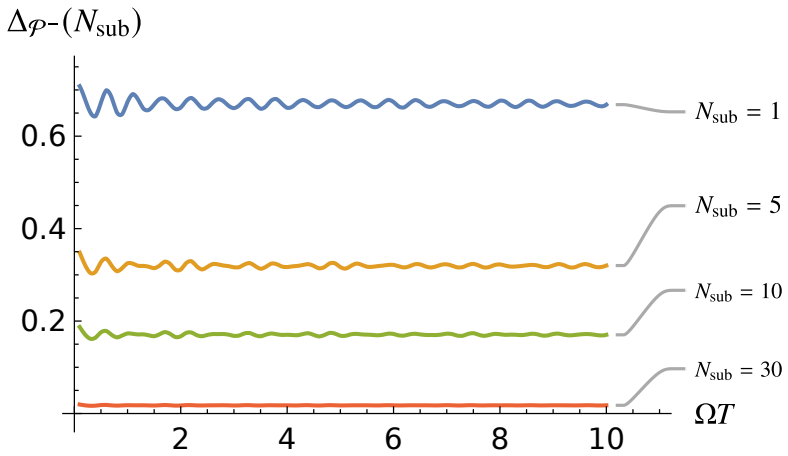

Figure 5.3: Relative difference $\Delta_{\mathcal{P}^-}(N_{\text{sub}})$ as a function of ΩT for sudden switching in the case of spontaneous emission. Parameters are $L/R = 10^3$, $\sigma/R = 10^{-2}$, and $\hbar\Omega/(M_{01}c^2) = 0.004$. As compared to the Gaussian switching, many more subfields are needed to significantly reduce the relative difference. Note that since we consider $\hbar\Omega \ll M_{01}c^2$, emission and excitation probabilities are near-identical and so we only plotted one transition process.

on the convergence of the subfield sum if we relax this assumption. Before that, let us look at the case where the detector is still centered on the axis of symmetry but not around $z = L/2$. If the detector is centred around $z = z_0 \in (0, L)$ while still assuming that $z_0 \gg \sigma$ and $L - z_0 \gg \sigma$, then we have to carry out the following replacement in Eq. (4.9)

$$\sin^2\left(\frac{n\pi}{2}\right) \longrightarrow \sin^2\left(\frac{nz_0\pi}{L}\right), \tag{5.59}$$

i.e. in general the even modes in n will not vanish. Nonetheless, the convergence in the number of subfields is not affected. If, however, we position the detector outside of the axis of symmetry of the cavity, for example, without loss of generality $(r, \varphi) = (r_0, 0)$, the spatial smearing (5.49) will read

$$F(r, \varphi, z) = \frac{1}{\sqrt{2\pi\sigma^2}^3} \exp\left(-\frac{(z - \frac{L}{2})^2}{2\sigma^2}\right) \exp\left(-\frac{r^2 + r_0^2 - 2r_0 r\cos\varphi}{2\sigma^2}\right). \tag{5.60}$$

Consequently, we find that the transition probability is obtained by Eq. (5.52) but making

the following substitution in the number of excitations in Eq. (4.9):

$$e^{-\frac{\sigma^2 x_{0\ell}^2}{R^2}} \longrightarrow e^{-\frac{r_0^2}{\sigma^2}} \left| \int_0^\infty \mathrm{d}r\, r \frac{e^{-\frac{r^2}{2\sigma^2}}}{\sigma^2} I_m\left(\frac{r_0 r}{\sigma^2}\right) J_m\left(\frac{x_{ml}}{R} r\right) \right|^2 , \tag{5.61}$$

where I_m is the modified Bessel function of the first kind, and the integral is generally non-zero for $m > 0$. The convergence in the subfield sum with $m > 0$ is subtle and depends on the specific parameters. In general, more than just the leading $m = 0$ subfield will be required. Hence it is reasonable to say that the analysis of particle detectors in the absence of axial symmetry cannot be dimensionally reduced to the coupling with a few 1+1D subfields in general.

5.5 Summary

In this chapter we showed how one can decompose a $3 + 1$ dimensional quantum field inside a cavity into an infinite collection of $1 + 1$ dimensional quantum fields, which we call subfields. We have discussed this subfield decomposition in sufficient generality to apply to a wide variety of cavity geometries and boundary conditions. It is important to note that this subfield decomposition is exact, not an approximation. Using the subfield decomposition, we were able to identify the proper dimensional reduction approximation as the approximation made by ignoring all but one of these subfields.

One first thing that we clarify is that a naive reduction of a very long, very thin cavity to a massless 1+1 dimensional field in a cavity is not acceptable in most regimes. This is important because this kind of intuitive (but inaccurate) dimensional reduction has arguably been commonplace in the body of literature on the light-matter interaction.

One benefit of viewing dimensional reduction in this way is that we can now access a gradation of approximations by considering different numbers of 1+1 dimensional subfields. This perspective also casts light on which features of the cavity's geometry survive the dimensional reduction and how these features shape the effective $1 + 1$ dimensional subfields; a triangular cavity and a cylindrical one remain distinguishable in the dimensional reduction limit. In particular, each subfield has an effective mass which encodes information about the cavity's transverse geometry.

Once we made this subfield decomposition, we then investigated exactly how a localized detector system couples to each of these subfields. In particular, we have shown that the strength with which the detector couples to each of these subfields is fixed entirely by the

size and shape of the detector in the $3+1$ dimensional description. Thus, the dimensional reduction approximation (which takes the detector to couple to only one subfield) can be understood in terms of making an approximation on the detector's shape.

Roughly, any given subfield might be irrelevant to the detector for one of three reasons: 1) this subfield has a high effective mass (due to the cavity's transverse shape), or 2) it does not couple strongly to the detector (due to the detector's size and shape), or 3) the time profile of the interaction strength suppresses the coupling to some of the subfields. For the dimensional reduction approximation to be justified, these three possibilities must conspire to allow us to eliminate all but one subfield from our consideration. That is, in order for us to justify a dimensional reduction approximation we must think carefully about not only the cavity's shape, but also the shape of the detector within that cavity and its switching function (its "shape in time"). To explore concretely when this approximation is justified we have provided a numerical study with typical setups in optical cavities and superconducting circuits.

Chapter 6

The Multipolar Coupling Hamiltonian

Now that we have studied effective models, their applications and approximations in a variety of aspects, let us take a step back and re-evaluate the light-matter interaction by starting from the Lagrangian and fully disclose our assumptions. The interaction of matter with light presents two important challenges when trying to find simple models to describe it: the relativistic, covariant, vector nature of light, and the fact that electromagnetism is a gauge theory. Regarding the relativistic nature of the theory, in atomic physics and quantum optics, matter is usually treated non-relativsitically (atoms are, to a good approximation, systems of bound nuclei and low-energy electrons), and thus for simplicity one combines in the same model a relativistic field interacting with a non-relativistic atom.

The gauge dependence of the theory is trickier. It has been a source of issues in simple models of light-matter interaction. Directly using minimal coupling $\hat{\boldsymbol{p}} \cdot \hat{\boldsymbol{A}}$ between charged particles and the EM field together with gauge independent atomic wavefunctions leads to nonphysical, gauge-dependent atomic transition probabilities [122, 35, 57]. These issues have been the subject of a great deal of studies and can be partially overcome by recasting the interaction in terms of a multipolar Hamiltonian. This is achieved through combinations of canonical and gauge transformations in order to express the interaction in terms of well-known textbook charge-in-a-Coulomb-potential terms and the observable fields $\hat{\boldsymbol{E}}$ and $\hat{\boldsymbol{B}}$ rather than $\hat{\boldsymbol{A}}$. This can be done for external classical fields with the Goeppert-Mayer transformation [30], as well as for quantized electromagnetic (radiation) fields [31, 123, 36, 124]. In the quantum electromagnetic case, the class of transformations employed to arrive at a multipolar Hamiltonian is known as Power-Zienau-Woolley (PZW) transformations. This is the origin of the ubiquitously used 'dipole approximation' $\hat{\boldsymbol{d}} \cdot \hat{\boldsymbol{E}}$. However, there are a number of subtleties to deal with before arriving at this simple dipole coupling Hamiltonian. These subtleties can be relevant in quantum optics, and particularly

so in the context of RQI when we model the interaction of a microscopic, moving atomic probe with the electromagnetic field. In those cases, the multipolar Hamiltonian with quantized fields, even in the dipole approximation, contains the so-called Röntgen term[1] which couples the center-of-mass (COM) degrees of freedom of the atom with its internal degrees of freedom and the electromagnetic field – and that is not commonly considered in RQI studies. However, if one wants to model atomic physics, these kind of terms can only be neglected in a few select scenarios.

Indeed, in [36] it was argued that the Röntgen term is required for energy-momentum conservation and gauge invariant forces. This is a consequence of the mechanical momentum not coinciding with the canonical momentum of the COM position for ions. It has been shown, further, that the Röntgen term is already necessary to leading order in the velocity, v/c, so as to avoid a nonphysical angular distribution of spontaneously emitted photons [37, 38]. In [126] and [127] it was then shown that the total spontaneous emission rate (as given by Fermi's Golden rule) for a classical COM under uniform motion requires the inclusion of the Röntgen term. Features of this Röntgen term have also been explored in [128] for classical fields and classical COM degrees of freedom. The contribution is usually smaller than radiation-pressure forces, but it is nonetheless required for correct physical results. In [39] it was shown that for a quantum COM the time derivative of the expectation value of the canonical momentum of the COM is observer dependent, at odds with the necessary covariance of predictions. The resolution (at least to leading order) was found in the inclusion of the atomic binding energy terms in the Hamiltonian. As noted in [39], a dynamical mass-energy term coupled to the COM momentum is a feature missing from the multipolar Hamiltonian. Sonnleitner and Barnett go on in [129] to include a low-order relativistic correction for the multipolar Hamiltonian which remedies the absence of the missing dynamical mass-energy.

A number of subtleties in the multipole (including dipole) approximation appear when carefully considering the role of gauge transformations in the light-matter interaction, and the fact that atoms can actually have a spatial extension since they are not point-like objects (even in the dipole approximation). Although there has been a plethora of previous work on multipole approximations (above all considering either classical EM fields e.g. [128] and/or semiclassical atoms e.g. [126, 127], with only a few fully quantum setups, e.g., [39]), the considerations of gauge issues, finite size of the atomic wavefunction (even for dipoles) and possible quantum delocalization of the COM are not commonly combined in any previous work known to us.

[1]The term is named after Wilhelm Conrad Röntgen who experimentally verified that an electrically neutral, moving dielectric generates an electromagnetic force [125].

The few works that consider a more complete approach regarding gauge and the quantum nature of the interaction (e.g., [39]) do particularize to eigenstates of the COM and also consider the rotating-wave approximation, which is incompatible with most RQI setups [62, 74]. Furthermore, within the context of RQI, gauge and COM dynamics considerations are not usually present in most of the traditional light-matter interaction models, making it useful to contextualize the particle detector models used in RQI with a complete description of the light-matter interaction.

In this chapter, we wish to analyze effective models that can capture realistic dynamics of a first-quantized atom interacting with the quantum EM field. This includes a quantized COM, the quantum nature of the atomic multipole operator, and neither assuming the single-mode nor rotating-wave approximation, nor taking a discrete field-momentum spectrum in free space. We will take into account recent results by Stritzelberger and Kempf [130] (followed up on in [131]) where they studied precisely the influence on the atomic dynamics of the initial delocalization of the COM. We will extend those studies to show the extra considerations that one needs in order for the predictions of the model to be gauge-independent and to include the effect of Röntgen terms. As a particular example, we will illustrate the effect of the Röntgen term in atomic transition rates in the presence of initial COM delocalization. This is particularly relevant because, with the exception of [132], the effect of Röntgen-like terms have not been considered in the light-matter interaction in any previous RQI studies known to the authors. However, even in [132] the interaction Hamiltonian is prescribed from the single-particle scenario in [133], which ignores the subtleties that appear in the case that atoms are modelled as multi-charged objects [129]. While this could in principle be a functional effective model, it is potentially subject to the subtleties related to the gauge nature of electromagnetism that we analyze in this chapter, above all when computing leading-order relativistic corrections.

In particular, we will show that there is only one scenario where one can neglect the Röntgen term: when one considers the atomic COM degrees of freedom to be classical, the atoms are tightly localized, and there exists a common rest frame for all the moving atoms in which the Röntgen term vanishes. This is for example the case of entanglement harvesting for comoving inertial atoms (see, e.g., [46]), or a single atom when we work in the detector's COM frame for not very relativistic trajectories. If the atomic COM is treated as quantum, or when there is no common rest frame, this additional term cannot be neglected. We will also discuss the higher order terms that appear in the case of more relativistic trajectories of the COM.

As we will see, the inclusion of the Röntgen term entangles, generally, internal and external atomic (as well as field) degrees of freedom. There has been a volume of literature that studies the use of entanglement between internal and external degrees of freedom

for quantum information tasks, see for instance [134, 135, 136, 137, 138, 139, 140]. In this light, studying the impact of the Röntgen dynamics with respect to entanglement generation could yield new insights and protocols in RQI.

This will set the stage for Chapter 7 where we compare these considerations to the usually employed effective light-matter interaction models. Thus, we will discuss the limitations of the effective dipolar coupling $e\hat{\boldsymbol{r}} \cdot \hat{\boldsymbol{E}}(\hat{\boldsymbol{r}})$ and scalar-analogue models such as the UDW model. In the case of scalar-analogue models, we will argue that a coupling of COM and radiation degrees of freedom has to be included in most scenarios if one wants to capture the atomic dynamics.

The structure of this chapter is as follows: In Sec. 6.1, we will present the derivation of the non-relativistic multipolar Hamiltonian. We will study the phenomenological implications of this model in Sec. 6.2. Further, in Sec. 6.3 we will discuss the sub-leading-order correction term to the multipolar Hamiltonian. Lastly, in Sec. 6.4 we will summarize our findings.

6.1 Derivation

Our objective in this section is to explicitly derive the multipolar coupling Hamiltonian from the two-particle minimal coupling. We will do so for a fully quantized model – including the quantization of both the field and COM of the atom. More concretely, we combine the quantization of the field, the COM of the atom and the relative motion (internal) degrees of freedom to derive the dipole coupling Hamiltonian in the (approximated) gauge in which the relative degree of freedom wavefunctions correspond exactly to the textbook-problem of a charge trapped in a Coulomb potential (hydrogenoid atom). It is important to recall that the atomic wavefunctions are not gauge-invariant [35, 57], and only under very strict considerations are the internal atomic wavefunctions the textbook hydrogen-like ones.

Although we are (to a large extent) revisiting old-known problems, the particular approach to deriving these results from the Hamiltonian formalism with a fully quantum framework that we take is (to the authors' knowledge) not available in previous literature. Operating directly from the Hamiltonian formalism we avoid introducing an *ad hoc* change of the canonical commutation relations of the field operators [34] (something common in past derivations of the multipolar Hamiltonian, e.g. [31, 123, 36]), which allows for a pedagogically easier treatment. We will also analyze all the terms that are typically neglected in simplified particle detector models employed in RQI, such as the orbital magnetic dipole and Röntgen terms [123, 36, 37], paying special attention to the discussion about gauge and localization.

Concretely, we consider a hydrogen atom interacting with the electromagnetic field described by the gauge-dependent potentials $(U, \boldsymbol{A})$. The atom consists of a proton (with mass m_p and associated position $\boldsymbol{r}_p$) and an electron (with mass m_e and position $\boldsymbol{r}_e$). Both constituents will be treated as spinless[2]. A relativistic-friendly approach would start then from the general classical Lagrangian with the minimal coupling prescription [129]:

$$\begin{aligned} L = &- \sum_{i=e,p} m_i c^2 \sqrt{1 - \dot{\boldsymbol{r}}_i^2/c^2} + \frac{\epsilon_0}{2} \int_{\mathbb{R}^3} \mathrm{d}^3\boldsymbol{x} \left((\partial_t \boldsymbol{A}_{\mathrm{tot}} + \nabla U_{\mathrm{tot}})^2 - c^2 \left(\nabla \times \boldsymbol{A}_{\mathrm{tot}} \right)^2 \right) \\ &+ \int_{\mathbb{R}^3} \mathrm{d}^3\boldsymbol{x} \left(\boldsymbol{j} \cdot \boldsymbol{A}_{\mathrm{tot}} - \rho U_{\mathrm{tot}} \right), \end{aligned} \tag{6.1}$$

where $\boldsymbol{A}_{\mathrm{tot}}, U_{\mathrm{tot}}$ includes the vector and scalar potentials generated by the charges, and ρ, $\boldsymbol{j}$ are the charge and current densities, respectively. Solving the dynamics for this Lagrangian is involved. Indeed, Currie, Jordan, and Sudarshan showed that there exists no (classical) fully-relativistic canonical theory for interacting particles [143][3]. Accordingly, the problem is generally reduced to an expansion about the particle velocities $\dot{\boldsymbol{r}}_i$ in some inertial frame. Changing to the Hamiltonian picture and after quantization we get the minimal coupling Hamiltonian at leading order in velocities. Besides the standard free-field Hamiltonian, this reads [52, Ch. 4]

$$\hat{H} = \sum_{i=e,p} \left[\frac{(\hat{\boldsymbol{p}}_i + e_i \hat{\boldsymbol{A}}(t, \hat{\boldsymbol{r}}_i))^2}{2m_i} - e_i \hat{U}(t, \hat{\boldsymbol{r}}_i) \right] - \frac{e^2}{4\pi\epsilon_0 |\hat{\boldsymbol{r}}|}, \tag{6.2}$$

where the last term corresponds to the electrostatic Coulomb energy with $\hat{\boldsymbol{r}} = \hat{\boldsymbol{r}}_e - \hat{\boldsymbol{r}}_p$, and we are considering the field in the interaction picture with explicit time dependence. The sub-leading relativistic correction, called the Darwin Hamiltonian [129], is of the form

$$\hat{H}_{\mathrm{D}} = \frac{\hat{\boldsymbol{\pi}}_e^4}{8m_e^3c^2} + \frac{\hat{\boldsymbol{\pi}}_p^4}{8m_p^3c^2} + \frac{e^2}{16\pi\varepsilon_0 c^2 m_e m_p} \left[\hat{\boldsymbol{\pi}}_e \cdot \frac{1}{|\hat{\boldsymbol{r}}|} \hat{\boldsymbol{\pi}}_p + (\hat{\boldsymbol{\pi}}_e \cdot \hat{\boldsymbol{r}}) \frac{1}{|\hat{\boldsymbol{r}}|^3} (\hat{\boldsymbol{r}} \cdot \hat{\boldsymbol{\pi}}_p) + (e \leftrightarrow p) \right], \tag{6.3}$$

[2]The inclusion of spin via the Dirac equation yields (to order $\mathcal{O}(c^{-2})$) the Breit Hamiltonian, [141] and [142, Ch. 2].

[3]The fact that boost generators depend on the interaction generally means that classical particle trajectories no longer transform under Lorentz transformations [144]. There are different directions for interpreting this *no interaction* theorem: The question of whether the particle position can be a canonical variable – or, is $\boldsymbol{r}$ a physical observable representing particle position? – was considered, see e.g. [145]. Another interpretation of this theorem is that the particle-based description should be replaced with a field-based approach, see e.g. [146]. This is done when one considers the particles to be excitations of some quantum matter field in quantum field theory.

where $\hat{\boldsymbol{\pi}}_i := \hat{\boldsymbol{p}}_i + e_i \hat{\boldsymbol{A}}(\hat{\boldsymbol{r}}_i)$ is the mechanical momentum. In Sec. 6.3, once we derived the dipolar Hamiltonian, we will come back and discuss the phenomenological implications of $\hat{H}_{\rm D}$.

For simplicity, in this section we shall be concerned with general scenarios where the atomic COM describes non-relativistic motion. This means that we will neglect the Darwin term and any other higher order corrections associated with the relativistic motion of the charges. While this does not cover all interesting regimes in RQI, it does cover several relevant regimes directly such as, for instance, most entanglement harvesting scenarios [45, 46, 147].

We can therefore start from the standard leading-order minimal coupling Hamiltonian in Eq. (6.2). For convenience, we choose the Coulomb gauge where there is no scalar potential and $[\hat{\boldsymbol{p}}_i, \hat{\boldsymbol{A}}(t, \hat{\boldsymbol{r}}_i)] = 0$ [51].

When working with the minimal coupling Hamiltonian we have to be careful with the gauge freedom of the field. In particular, we need to make a consistent choice of atomic wavefunctions when we choose a particular gauge in order to have gauge-independent predictions. For example, in the Coulomb gauge, the atomic wavefunctions of a hydrogen atom are very different from the textbook hydrogen orbitals (see e.g., [122, 35, 57]). Additional complications appear as we are working with a two-particle atom. We cannot simply assume that there is a gauge where the internal atomic wavefunctions are the textbook atomic orbitals and then transform them to whatever gauge we are considering. As we will see, there is no such gauge [148]. Moreover, in general one cannot directly neglect the $\hat{\boldsymbol{A}}^2$ terms. This is only possible in certain regimes (see, e.g., [149]).

It would be convenient to express the Hamiltonian solely in terms of gauge-invariant field observables, and also choose canonical coordinates so that we have the hydrogenic orbitals when we take the position representation for the internal atomic degrees of freedom. The canonical transformation that achieves these two goals is a Power-Zienau-Woolley (PZW) transformation [36]. This transformation applied to the Coulomb-gauge Hamiltonian yields the so-called multipolar coupling Hamiltonian.

Concretely[4], let us define the atomic center-of-mass and relative-motion position operators:

$$\hat{\boldsymbol{R}} = \frac{m_e \hat{\boldsymbol{r}}_e + m_p \hat{\boldsymbol{r}}_p}{M}, \quad \hat{\boldsymbol{r}} = \hat{\boldsymbol{r}}_e - \hat{\boldsymbol{r}}_p, \tag{6.4}$$

[4]Recall, we will derive the Hamiltonian directly via the Hamiltonian formalism treating all degrees of freedom as quantum, cf. e.g. [51].

where $M = m_e + m_p$ is the total mass. Similarly the total momentum of the COM, and the momentum of the relative motion associated with the reduced mass $\mu = m_e m_p/M$ read, respectively,

$$\hat{\boldsymbol{P}} = \hat{\boldsymbol{p}}_e + \hat{\boldsymbol{p}}_p, \quad \hat{\boldsymbol{p}} = \frac{m_p}{M}\hat{\boldsymbol{p}}_e - \frac{m_e}{M}\hat{\boldsymbol{p}}_p. \tag{6.5}$$

These two new sets of operators satisfy the canonical commutation relations amongst each other: $[\hat{\boldsymbol{R}}, \hat{\boldsymbol{P}}] = \mathrm{i}\hbar\mathbb{1} = [\hat{\boldsymbol{r}}, \hat{\boldsymbol{p}}]$. The Hamiltonian (6.2) re-expressed in terms of COM and relative coordinates yields [51]

$$\begin{aligned}\hat{H} =& \frac{\hat{\boldsymbol{P}}^2}{2M} + \frac{\hat{\boldsymbol{p}}^2}{2\mu} - \frac{1}{4\pi\epsilon_0}\frac{e^2}{|\hat{\boldsymbol{r}}|} - \frac{e}{\mu}\left\{\frac{\mu}{m_e}\hat{\boldsymbol{A}}\left(t, \hat{\boldsymbol{R}} + \frac{m_p}{M}\hat{\boldsymbol{r}}\right) + \frac{\mu}{m_p}\hat{\boldsymbol{A}}\left(t, \hat{\boldsymbol{R}} - \frac{m_e}{M}\hat{\boldsymbol{r}}\right)\right\}\cdot\hat{\boldsymbol{p}} \\ & - \frac{e}{M}\left\{\hat{\boldsymbol{A}}\left(t, \hat{\boldsymbol{R}} + \frac{m_p}{M}\hat{\boldsymbol{r}}\right) - \hat{\boldsymbol{A}}\left(t, \hat{\boldsymbol{R}} - \frac{m_e}{M}\hat{\boldsymbol{r}}\right)\right\}\cdot\hat{\boldsymbol{P}} \\ & + \frac{e^2}{2m_e}\hat{\boldsymbol{A}}^2\left(t, \hat{\boldsymbol{R}} + \frac{m_p}{M}\hat{\boldsymbol{r}}\right) + \frac{e^2}{2m_p}\hat{\boldsymbol{A}}^2\left(t, \hat{\boldsymbol{R}} - \frac{m_e}{M}\hat{\boldsymbol{r}}\right).\end{aligned} \tag{6.6}$$

The non-relativistic quantum treatment of the atom requires the COM and relative momenta to be bounded. Since the motion of an electron 'around' a proton is typically non-relativistic, considering the relative motion to be non-relativistic is generally a very reasonable assumption. However, for the state of the atomic COM to be in a non-relativistic regime, the state should not have any non-negligible overlap with generalized eigenstates of momentum beyond some scale where relativistic corrections would be necessary.

In order to arrive at the multipolar Hamiltonian, we insert resolutions of identity in the COM and relative position bases (taking a position representation for $\boldsymbol{R}$ and $\boldsymbol{r}$), and expand the vector field around the center-of-mass coordinate $\boldsymbol{R}$. For our purposes, we will only consider the dipolar contributions:

$$\hat{\boldsymbol{A}}(t, \boldsymbol{R} + \delta\boldsymbol{r}) \approx \hat{\boldsymbol{A}}(t, \boldsymbol{R}) + (\delta\boldsymbol{r}\cdot\boldsymbol{\nabla}_{\boldsymbol{R}})\hat{\boldsymbol{A}}(t, \boldsymbol{R}). \tag{6.7}$$

When applied to Eq. (6.6) we will have that either $\delta\boldsymbol{r} = \frac{m_p}{M}\boldsymbol{r}$ or $\delta\boldsymbol{r} = -\frac{m_e}{M}\boldsymbol{r}$ depending on the term. As we will discuss more in depth later on, the spatial support in the relative coordinate $\boldsymbol{r}$ for atomic scales is given approximately by the scale of Bohr radius a_0 associated with the reduced mass μ. Hence, the second-order term is suppressed with respect to the leading order by a factor $\sim a_0|\boldsymbol{k}_{\mathrm{UV}}|$, with $|\boldsymbol{k}_{\mathrm{UV}}|$ being the maximum wave vector of the vector field. It may be determined by the atomic smearing and the time-dependent coupling between atom and field, or by a dominant atomic transition process [57]. Ultimately, the Compton wavelength will yield the upper bound in order to stay in the non-relativistic

quantum description of the atom [52, Ch. 3]. Note that since we consider a quantum COM, or also in the case of motion of a classical COM, the second order term is required even at the dipole level [51].

In the dipole regime where Eq. (6.7) applies, $\hat{H}$ approximates to [51]

$$\hat{H}^{(1)} = \int_{\mathbb{R}^3} \mathrm{d}^3\boldsymbol{R} \int_{\mathbb{R}^3} \mathrm{d}^3\boldsymbol{r} \left\{ \frac{1}{2M} \left[\hat{\boldsymbol{P}} - e\,(\boldsymbol{r}\cdot\boldsymbol{\nabla}_{\boldsymbol{R}})\,\hat{\boldsymbol{A}}(t,\boldsymbol{R}) \right]^2 + \frac{1}{2\mu} \left[\hat{\boldsymbol{p}} - e\hat{\boldsymbol{A}}(t,\boldsymbol{R}) - e\frac{\Delta m}{M}\,(\boldsymbol{r}\cdot\boldsymbol{\nabla}_{\boldsymbol{R}})\,\hat{\boldsymbol{A}}(t,\boldsymbol{R}) \right]^2 - \frac{e^2}{4\pi\epsilon_0|\boldsymbol{r}|} \right\} |\boldsymbol{R}\rangle\langle\boldsymbol{R}| \otimes |\boldsymbol{r}\rangle\langle\boldsymbol{r}|\,, \tag{6.8}$$

where $\Delta m = m_p - m_e$. The Hamiltonian (6.8) is the generator of time translations to the joint atom-field state $|\Psi\rangle$ governed by the Schrödinger equation

$$\mathrm{i}\hbar\frac{\partial\,|\Psi\rangle}{\partial t} = \hat{H}^{(1)}\,|\Psi\rangle\,, \tag{6.9}$$

with the field being in the interaction picture. We will now write the interaction Hamiltonian in terms of gauge-invariant field operators such that the internal atomic Hamiltonian admits the usual hydrogenic wavefunction solutions. To accomplish this, we perform a canonical transformation generated by the self-adjoint operator [51]

$$\hat{\Lambda}^{(1)}(t,\hat{\boldsymbol{R}},\hat{\boldsymbol{r}}) = \int_{\mathbb{R}^3} \mathrm{d}^3\boldsymbol{R}\;|\boldsymbol{R}\rangle\langle\boldsymbol{R}| \left[\hat{\boldsymbol{r}}\cdot\hat{\boldsymbol{A}}(t,\boldsymbol{R}) + \frac{\Delta m}{2M}(\hat{\boldsymbol{r}}\cdot\boldsymbol{\nabla}_{\boldsymbol{R}}) \left(\hat{\boldsymbol{r}}\cdot\hat{\boldsymbol{A}}(t,\boldsymbol{R}) \right) \right]. \tag{6.10}$$

This transformation is, in general, not a gauge transformation. We already saw earlier in Sec. 2.2 that for the effective dipole model one can indeed use a gauge transformation to go from one-particle minimal coupling to the multipolar Hamiltonian – but not in the current two-particle case. Note that the procedure of first performing the dipole approximation (6.7) and then performing the canonical transformation $\hat{\mathcal{U}}_{\hat{\Lambda}^{(1)}} \coloneqq \exp[-\frac{i}{\hbar}e\hat{\Lambda}^{(1)}]$ is equivalent to first performing a transformation with the Dirac-Heisenberg line function

$$\hat{\Lambda}(t,\hat{\boldsymbol{R}},\hat{\boldsymbol{r}}) = \hat{\boldsymbol{r}}\cdot\int_0^1 \mathrm{d}\lambda\,\hat{\boldsymbol{A}}\left(t,\hat{\boldsymbol{R}} - \left(\frac{m_e}{M} - \lambda\right)\hat{\boldsymbol{r}}\right), \tag{6.11}$$

and then performing a Taylor expansion in the electromagnetic vector potential [51]. Furthermore (6.11) is identical (order by order) to the standard PZW transformation [36] (as we show in Appendix C.1):

$$\hat{\Lambda}^{\mathrm{PZW}} = \sum_{i=e,p} \frac{e_i}{|e|}(\hat{\boldsymbol{r}}^i - \hat{\boldsymbol{R}})\cdot\int_0^1 \mathrm{d}\lambda\,\hat{\boldsymbol{A}}\left(t,\hat{\boldsymbol{R}} + \lambda(\hat{\boldsymbol{r}}^i - \hat{\boldsymbol{R}})\right). \tag{6.12}$$

Using (6.10) we define the canonically transformed state $|\tilde{\Psi}\rangle$ through

$$|\Psi\rangle = \exp\left(\frac{\mathrm{i}}{\hbar} e\hat{\Lambda}^{(1)}(t, \hat{\boldsymbol{R}}, \hat{\boldsymbol{r}})\right)|\tilde{\Psi}\rangle. \tag{6.13}$$

This means that the left-hand side of (6.9) can be written as

$$\mathrm{i}\hbar\frac{\partial\,|\Psi\rangle}{\partial t} = -e\frac{\partial\hat{\Lambda}^{(1)}}{\partial t}e^{\frac{\mathrm{i}}{\hbar}e\hat{\Lambda}^{(1)}}|\tilde{\Psi}\rangle + e^{\frac{\mathrm{i}}{\hbar}e\hat{\Lambda}^{(1)}}\mathrm{i}\hbar\frac{\partial|\tilde{\Psi}\rangle}{\partial t}, \tag{6.14}$$

while the right-hand side of (6.9) reads

$$\hat{H}^{(1)}\,|\Psi\rangle = \hat{H}^{(1)}\exp\left(\frac{\mathrm{i}}{\hbar}e\hat{\Lambda}^{(1)}\right)|\tilde{\Psi}\rangle. \tag{6.15}$$

Regrouping all the extra terms in the left-hand-side into the right-hand side allows us to find the form of the canonically transformed Hamiltonian

$$\hat{\tilde{H}}^{(1)} = \exp\left(-\frac{\mathrm{i}}{\hbar}e\hat{\Lambda}^{(1)}\right)\left[\hat{H}^{(1)} + e\frac{\partial\hat{\Lambda}^{(1)}}{\partial t}\right]\exp\left(\frac{\mathrm{i}}{\hbar}e\hat{\Lambda}^{(1)}\right). \tag{6.16}$$

As we will see later, $\hat{\tilde{H}}^{(1)}$ will be the Hamiltonian we are seeking: a function of the electric and magnetic field operators, and for which the internal atomic dynamics admits as a solution the textbook hydrogen wavefunctions. Notice that the canonically transformed (PZW-transformed) Hamiltonian is not unitarily equivalent to the minimal coupling Hamiltonian (after the dipole approximation). As we will discuss soon, the extra term (associated with the time-dependence of $\hat{\Lambda}$) is related with self-energy and will be responsible for a shift on the energy levels (such as the Lamb shift).

To implement the canonical transformation, we need the commutation relations between the vector potential and its different derivatives. In terms of the usual plane-wave expansion, the vector potential in the interaction picture takes the form (recall Eq. (2.17))

$$\hat{\boldsymbol{A}}(t, \boldsymbol{x}) = \sum_{s=1}^{2}\int_{\mathbb{R}^3}\frac{\mathrm{d}^3\boldsymbol{k}}{(2\pi)^{\frac{3}{2}}}\sqrt{\frac{\hbar}{2\epsilon_0 c|\boldsymbol{k}|}}\left(\hat{a}_{\boldsymbol{k},s}\boldsymbol{\epsilon}_{\boldsymbol{k},s}e^{-\mathrm{i}c|\boldsymbol{k}|t}e^{\mathrm{i}\boldsymbol{k}\cdot\boldsymbol{x}} + \mathrm{H.c.}\right), \tag{6.17}$$

where we denoted as $\{\boldsymbol{\epsilon}_{\boldsymbol{k},s}\}_{s=1}^{2}$ an arbitrary set of two orthonormal transverse polarization vectors that together with the normalized wave vector $\boldsymbol{e}_{\boldsymbol{k}} = \boldsymbol{k}/|\boldsymbol{k}|$ form an orthonormal

basis. Therefore we find that the equal-time commutator between two components of the vector potential is

$$\left[\hat{A}^i(t,\boldsymbol{x}),\hat{A}^j(t,\boldsymbol{x}')\right]=\int_{\mathbb{R}^3}\frac{\mathrm{d}^3\boldsymbol{k}}{(2\pi)^3}\frac{\hbar}{2\epsilon_0 c|\boldsymbol{k}|}(\delta^{ij}-e^i_{\boldsymbol{k}}e^j_{\boldsymbol{k}})\left(e^{\mathrm{i}\boldsymbol{k}\cdot(\boldsymbol{x}-\boldsymbol{x}')}-e^{-\mathrm{i}\boldsymbol{k}\cdot(\boldsymbol{x}-\boldsymbol{x}')}\right), \tag{6.18}$$

by use of the completeness relations [52, Ch. 3]

$$\sum_{s=1}^{2}\epsilon^i_{\boldsymbol{k},s}\epsilon^j_{\boldsymbol{k},s}=\delta^{ij}-e^i_{\boldsymbol{k}}e^j_{\boldsymbol{k}}. \tag{6.19}$$

By differentiation, we find the remaining commutators required for the dipole approximation (we can stop at the first spatial derivatives). The details of the calculations can be found in Appendix C.2. We use the transverse delta function [150]

$$\delta^{ij,(\mathrm{tr})}(\boldsymbol{x})=\frac{1}{(2\pi)^3}\int_{\mathbb{R}^3}\mathrm{d}^3\boldsymbol{k}\,(\delta^{ij}-e^j_{\boldsymbol{k}}e^j_{\boldsymbol{k}})e^{\mathrm{i}\boldsymbol{k}\cdot\boldsymbol{x}}. \tag{6.20}$$

The only commutators that are non-zero in the coincidence limit are then

$$\left[\hat{A}^i(t,\boldsymbol{x}),\partial_t\hat{A}^j(t,\boldsymbol{x}')\right]=\frac{\mathrm{i}\hbar}{\epsilon_0}\delta^{ij,(\mathrm{tr})}(\boldsymbol{x}-\boldsymbol{x}'), \tag{6.21}$$

$$\left[\partial_l\hat{A}^i(t,\boldsymbol{x}),\partial_t\partial_m\hat{A}^j(t,\boldsymbol{x}')\right]=\frac{\mathrm{i}\hbar}{\epsilon_0}\frac{\partial^2\delta^{ij,(\mathrm{tr})}(\boldsymbol{x}-\boldsymbol{x}')}{\partial x^l\partial x'^m}. \tag{6.22}$$

Eq. (6.21) and (6.22) contribute to the commutator of the generator $\hat{\Lambda}^{(1)}$ with its time derivative. Moreover, they yield divergent contributions in the coincidence limit which will give rise to the self-energy of the atom. They appear only in the quantum case and its divergences can be renormalized and regularized through smeared spatial profiles.

To find the new Hamiltonian (6.16), we commute the old Hamiltonian with the canonical transformation operator. There will be two kinds of contributions: those that come from commuting with $\hat{H}^{(1)}$ and those that come from commuting with $\partial_t\hat{\Lambda}$. Since the calculation can get cumbersome, let us compute the two non-trivial terms in $\hat{H}^{(1)}$ as well as the contributions from the commutator with $\partial_t\hat{\Lambda}$ separately.

First consider the commutation of the canonical transformation with the first summand of $\hat{H}^{(1)}$ in Eq. (6.8). To that end, let us take initially the simpler commutation (without the square) given by

$$\begin{aligned}&\int_{\mathbb{R}^3}\mathrm{d}^3\boldsymbol{R}\,|\boldsymbol{R}\rangle\langle\boldsymbol{R}|\left[\hat{\boldsymbol{P}}-e\,(\hat{\boldsymbol{r}}\cdot\boldsymbol{\nabla}_{\boldsymbol{R}})\,\hat{\boldsymbol{A}}(t,\boldsymbol{R})\right]\hat{\mathcal{U}}^\dagger_{\hat{\Lambda}^{(1)}}|\tilde{\Psi}\rangle\\ =&\int_{\mathbb{R}^3}\mathrm{d}^3\boldsymbol{R}\,|\boldsymbol{R}\rangle\langle\boldsymbol{R}|\,\hat{\mathcal{U}}^\dagger_{\hat{\Lambda}^{(1)}}\left[\hat{\boldsymbol{P}}+e\boldsymbol{\nabla}_{\boldsymbol{R}}\hat{\Lambda}^{(1)}-e\,(\hat{\boldsymbol{r}}\cdot\boldsymbol{\nabla}_{\boldsymbol{R}})\,\hat{\boldsymbol{A}}(t,\boldsymbol{R})\right]|\tilde{\Psi}\rangle,\end{aligned} \tag{6.23}$$

with $\boldsymbol{\nabla}_{\boldsymbol{R}}\hat{\Lambda}^{(1)}(t,\boldsymbol{R},\boldsymbol{r}) = \boldsymbol{\nabla}_{\boldsymbol{R}}\big[\boldsymbol{r}\cdot\hat{\boldsymbol{A}}(t,\boldsymbol{R})\big]$ to leading order [51]. This term arises from position representation, i.e. $\langle\boldsymbol{R}|\,\hat{\boldsymbol{P}}\hat{O}\,|\Psi\rangle = -\mathrm{i}\hbar\boldsymbol{\nabla}_{\boldsymbol{R}}\langle\boldsymbol{R}|\,\hat{O}\,|\Psi\rangle$. Using

$$\hat{\boldsymbol{B}} = \boldsymbol{\nabla}\times\hat{\boldsymbol{A}}, \tag{6.24}$$

$$\hat{\boldsymbol{r}}\times\hat{\boldsymbol{B}} = \boldsymbol{\nabla}(\hat{\boldsymbol{r}}\cdot\hat{\boldsymbol{A}}) - (\hat{\boldsymbol{r}}\cdot\boldsymbol{\nabla})\hat{\boldsymbol{A}}, \tag{6.25}$$

and recovering the square, we arrive at

$$\int_{\mathbb{R}^3}\mathrm{d}^3\boldsymbol{R}\,|\boldsymbol{R}\rangle\langle\boldsymbol{R}|\left[\hat{\boldsymbol{P}} - e\,(\hat{\boldsymbol{r}}\cdot\boldsymbol{\nabla}_{\boldsymbol{R}})\,\hat{\boldsymbol{A}}(t,\boldsymbol{R})\right]^2\hat{\mathcal{U}}^{\dagger}_{\hat{\Lambda}^{(1)}}|\tilde{\Psi}\rangle = \hat{\mathcal{U}}^{\dagger}_{\hat{\Lambda}^{(1)}}\left[\hat{\boldsymbol{P}} + e\hat{\boldsymbol{r}}\times\hat{\boldsymbol{B}}(t,\hat{\boldsymbol{R}})\right]^2|\tilde{\Psi}\rangle. \tag{6.26}$$

Similarly, for the next summand of $\hat{H}^{(1)}$, we need [51]

$$\begin{aligned}
&\int_{\mathbb{R}^3}\mathrm{d}^3\boldsymbol{R}\int_{\mathbb{R}^3}\mathrm{d}^3\boldsymbol{r}\,|\boldsymbol{R}\rangle\langle\boldsymbol{R}|\otimes|\boldsymbol{r}\rangle\langle\boldsymbol{r}|\left[\hat{\boldsymbol{p}} - e\hat{\boldsymbol{A}}(t,\boldsymbol{R}) - e\frac{\Delta m}{M}\,(\boldsymbol{r}\cdot\boldsymbol{\nabla}_{\boldsymbol{R}})\,\hat{\boldsymbol{A}}(t,\boldsymbol{R})\right]\hat{\mathcal{U}}^{\dagger}_{\hat{\Lambda}^{(1)}}|\tilde{\Psi}\rangle\\
&= \int_{\mathbb{R}^3}\mathrm{d}^3\boldsymbol{R}\int_{\mathbb{R}^3}\mathrm{d}^3\boldsymbol{r}\,|\boldsymbol{R}\rangle\langle\boldsymbol{R}|\otimes|\boldsymbol{r}\rangle\langle\boldsymbol{r}|\,\hat{\mathcal{U}}^{\dagger}_{\hat{\Lambda}^{(1)}}\left[\hat{\boldsymbol{p}} - e\hat{\boldsymbol{A}}(t,\boldsymbol{R}) - e\frac{\Delta m}{M}\,(\boldsymbol{r}\cdot\boldsymbol{\nabla}_{\boldsymbol{R}})\,\hat{\boldsymbol{A}}(t,\boldsymbol{R})\right.\\
&\quad\left.+e\boldsymbol{\nabla}_{\boldsymbol{r}}\hat{\Lambda}^{(1)}\right]|\tilde{\Psi}\rangle,
\end{aligned} \tag{6.27}$$

where, using Eq. (6.10), we get

$$\boldsymbol{\nabla}_{\boldsymbol{r}}\hat{\Lambda}^{(1)}(t,\boldsymbol{R},\boldsymbol{r}) = \hat{\boldsymbol{A}}(t,\boldsymbol{R}) + \frac{\Delta m}{2M}\left\{\boldsymbol{\nabla}_{\boldsymbol{R}}\left[\boldsymbol{r}\cdot\hat{\boldsymbol{A}}(t,\boldsymbol{R})\right] + (\boldsymbol{r}\cdot\boldsymbol{\nabla}_{\boldsymbol{R}})\hat{\boldsymbol{A}}(t,\boldsymbol{R})\right\}.$$

Thus, recovering the square, and using (6.24) and (6.25), we have

$$\begin{aligned}
&\int_{\mathbb{R}^3}\mathrm{d}^3\boldsymbol{R}\int_{\mathbb{R}^3}\mathrm{d}^3\boldsymbol{r}\,|\boldsymbol{R}\rangle\langle\boldsymbol{R}|\otimes|\boldsymbol{r}\rangle\langle\boldsymbol{r}|\left[\hat{\boldsymbol{p}} - e\hat{\boldsymbol{A}}(t,\boldsymbol{R}) - e\frac{\Delta m}{M}\,(\boldsymbol{r}\cdot\boldsymbol{\nabla}_{\boldsymbol{R}})\,\hat{\boldsymbol{A}}(t,\boldsymbol{R})\right]^2\hat{\mathcal{U}}^{\dagger}_{\hat{\Lambda}^{(1)}}|\tilde{\Psi}\rangle\\
&= \hat{\mathcal{U}}^{\dagger}_{\hat{\Lambda}^{(1)}}\left[\hat{\boldsymbol{p}} + \frac{e}{2}\frac{\Delta m}{M}(\hat{\boldsymbol{r}}\times\hat{\boldsymbol{B}}(t,\hat{\boldsymbol{R}}))\right]^2|\tilde{\Psi}\rangle.
\end{aligned} \tag{6.28}$$

This concludes the calculations regarding $\hat{H}^{(1)}$ as the Coulomb potential stays trivially the same. In the last step to find the new Hamiltonian, we have to evaluate $\hat{\mathcal{U}}_{\hat{\Lambda}^{(1)}}(\partial_t\hat{\Lambda})$. By using the following identity [151]

$$\frac{\partial}{\partial t}e^{-\beta\hat{\Lambda}} = -\int_0^{\beta}e^{-(\beta-u)\hat{\Lambda}}\frac{\partial\hat{\Lambda}}{\partial t}e^{-u\hat{\Lambda}}\mathrm{d}u, \tag{6.29}$$

and a Baker-Campbell-Hausdorff (BCH) formula we find

$$e^{-\frac{i}{\hbar}e\hat{\Lambda}^{(1)}}\frac{\partial\hat{\Lambda}^{(1)}}{\partial t}e^{\frac{i}{\hbar}e\hat{\Lambda}^{(1)}}=\frac{\partial\hat{\Lambda}^{(1)}}{\partial t}-\frac{\mathrm{i}e}{2\hbar}\left[\hat{\Lambda}^{(1)},\frac{\partial\hat{\Lambda}^{(1)}}{\partial t}\right]. \tag{6.30}$$

Note that the second term on the right-hand side is a multiple of the identity for the field Hilbert space, and since it only depends on the position operators (and not the momenta) the higher order BCH terms in (6.30) cancel exactly. Using $\hat{\boldsymbol{E}}=-\partial_t\hat{\boldsymbol{A}}$, we have [51]

$$\frac{\partial\hat{\Lambda}^{(1)}}{\partial t}=-\int_{\mathbb{R}^3}\mathrm{d}^3\boldsymbol{R}\;|\boldsymbol{R}\rangle\langle\boldsymbol{R}|\left[\hat{\boldsymbol{r}}\cdot\hat{\boldsymbol{E}}(t,\boldsymbol{R})+\frac{\Delta m}{2M}(\hat{\boldsymbol{r}}\cdot\boldsymbol{\nabla}_{\boldsymbol{R}})\left(\hat{\boldsymbol{r}}\cdot\hat{\boldsymbol{E}}(t,\boldsymbol{R})\right)\right]. \tag{6.31}$$

There are only two non-vanishing contributions to the commutator of Eq. (6.30) coming from (6.21) and (6.22):

$$\begin{aligned}
2\mathrm{i}\hbar\hat{\Delta}&:=\left[\hat{\Lambda}^{(1)},\frac{\partial\hat{\Lambda}^{(1)}}{\partial t}\right]\\
&=\int_{\mathbb{R}^3}\mathrm{d}^3\boldsymbol{R}\int_{\mathbb{R}^3}\mathrm{d}^3\boldsymbol{r}\;|\boldsymbol{R}\rangle\langle\boldsymbol{R}|\otimes|\boldsymbol{r}\rangle\langle\boldsymbol{r}|\,r_ir_j\left(\left[\hat{A}^i(t,\boldsymbol{R}),\partial_t\hat{A}^j(t,\boldsymbol{R})\right]\right.\\
&\qquad\left.+\left(\frac{\Delta m}{2M}\right)^2r^lr^m\left[\partial_l\hat{A}^i(t,\boldsymbol{R}),\partial_t\partial_m\hat{A}^j(t,\boldsymbol{R})\right]\right)\\
&=\frac{\mathrm{i}\hbar}{3\pi^2\epsilon_0}\int_0^{|\boldsymbol{k}_{\mathrm{UV}}|}\mathrm{d}|\boldsymbol{k}|\,|\boldsymbol{k}|^2\int_{\mathbb{R}^3}\mathrm{d}^3\boldsymbol{r}\;|\boldsymbol{r}\rangle\langle\boldsymbol{r}|\left(|\boldsymbol{r}|^2+\frac{1}{5}\left(\frac{\Delta m}{2M}\right)^2|\boldsymbol{r}|^4\right),
\end{aligned} \tag{6.32}$$

where, again, we have a UV cutoff $|\boldsymbol{k}_{\mathrm{UV}}|$ as in the initial dipole expansion of the field that removes the $\delta^{(\mathrm{tr})}(0)$ divergences. Eq. (6.32) corresponds to self-energies which have to be regularized by a cutoff since we initially assumed point charges constituting the atom. They are relevant for Lamb-like energy shifts [8].

Combining Eq. (6.26), (6.28) and (6.30), we have now an expression for the transformed Hamiltonian Eq. (6.16):

$$\begin{aligned}
\hat{\tilde{H}}^{(1)}=\int_{\mathbb{R}^3}\mathrm{d}^3\boldsymbol{R}\int_{\mathbb{R}^3}\mathrm{d}^3\boldsymbol{r}\;|\boldsymbol{R}\rangle\langle\boldsymbol{R}|\otimes|\boldsymbol{r}\rangle\langle\boldsymbol{r}|\left(\frac{[\hat{\boldsymbol{P}}+e\boldsymbol{r}\times\hat{\boldsymbol{B}}(t,\boldsymbol{R})]^2}{2M}+\frac{\left[\hat{\boldsymbol{p}}+\frac{e}{2}\frac{\Delta m}{M}\boldsymbol{r}\times\hat{\boldsymbol{B}}(t,\boldsymbol{R})\right]^2}{2\mu}\right.\\
\left.-\frac{e^2}{4\pi\epsilon_0|\boldsymbol{r}|}+e^2\hat{\Delta}-e\boldsymbol{r}\cdot\hat{\boldsymbol{E}}(t,\boldsymbol{R})-\frac{e}{2}\frac{\Delta m}{M}\left(\boldsymbol{r}\cdot\boldsymbol{\nabla}_{\boldsymbol{R}}\right)\left[\boldsymbol{r}\cdot\hat{\boldsymbol{E}}(t,\boldsymbol{R})\right]\right).
\end{aligned} \tag{6.33}$$

As we will be working in the weak-coupling limit, let us discuss and order the terms of Eq. (6.34) according to the two physically relevant small parameters: 1) the coupling strength e, and 2) the length-scale of atomic internal-state localization in terms of the Bohr radius a_0. The latter appears through the vanishing of the atomic wavefunctions for distances from the COM much farther than the Bohr radius.

Expanding the squares, we can then write Eq. (6.33) as a sum of terms with different powers of the small parameters of the problem:

$$\begin{aligned}\hat{\tilde{H}}^{(1)} =& \frac{\hat{\boldsymbol{P}}^2}{2M} + \underbrace{\frac{\hat{\boldsymbol{p}}^2}{2\mu} - \frac{e^2}{4\pi\epsilon_0|\hat{\boldsymbol{r}}|}}_{\text{Hydrogen Hamiltonian}} \underbrace{- e\hat{\boldsymbol{r}}\cdot\hat{\boldsymbol{E}}(t,\hat{\boldsymbol{R}})}_{\substack{\text{Electric dipole}\\ \mathcal{O}(ea_0)}} + \underbrace{e\left\{\frac{\hat{\boldsymbol{P}}}{2M}, \hat{\boldsymbol{r}}\times\hat{\boldsymbol{B}}(t,\hat{\boldsymbol{R}})\right\}_+}_{\substack{\text{COM Röntgen term}\\ \mathcal{O}(ea_0)}} \\ & \underbrace{+e\left\{\frac{\hat{\boldsymbol{p}}}{2\mu}, \hat{\boldsymbol{r}}\times\hat{\boldsymbol{B}}(t,\hat{\boldsymbol{R}})\right\}_+}_{\substack{\text{Relative Röntgen term (Orbital magnetic dipole)}\\ \mathcal{O}(ea_0^2)}} \underbrace{-\frac{e\Delta m}{2M}\int_{\mathbb{R}^3} \mathrm{d}^3\boldsymbol{R}\,|\boldsymbol{R}\rangle\langle\boldsymbol{R}|\,(\hat{\boldsymbol{r}}\cdot\boldsymbol{\nabla}_{\boldsymbol{R}})\,(\hat{\boldsymbol{r}}\cdot\hat{\boldsymbol{E}}(t,\boldsymbol{R}))}_{\substack{\text{Electric quadrupole}\\ \mathcal{O}(ea_0^2)}} \\ & + \underbrace{\frac{e^2}{8\mu}(\hat{\boldsymbol{r}}\times\hat{\boldsymbol{B}}(t,\hat{\boldsymbol{R}}))^2}_{\substack{\text{Diamagnetic term}\\ \mathcal{O}(e^2a_0^2)}} + \underbrace{e^2\hat{\Delta}}_{\substack{\text{Self-energy}\\ \mathcal{O}(e^2a_0^2)}} \\ =:& \hat{H}_0 + \hat{H}_I + \hat{H}_{M1} + \hat{H}_{E2} + \hat{H}_{\text{dia}} + \hat{H}_{\text{self}}. \end{aligned} \tag{6.34}$$

Let us analyze the different terms one by one. First, we have the unperturbed free atomic Hamiltonian $\hat{H}_0$ (where the solutions of the relative degrees of freedom are the hydrogenic wavefunctions $\psi_{nlm}(\boldsymbol{r})$ with an effective mass μ, i.e. the reduced mass) of the form

$$\hat{H}_0 = \frac{\hat{\boldsymbol{P}}^2}{2M} + \frac{\hat{\boldsymbol{p}}^2}{2\mu} - \frac{1}{4\pi\epsilon_0}\frac{e^2}{|\hat{\boldsymbol{r}}|}. \tag{6.35}$$

To leading order $\mathcal{O}(ea_0)$ we then find the electric dipole interaction and the Röntgen term associated with the COM motion:

$$\hat{H}_I = -e\hat{\boldsymbol{r}}\cdot\hat{\boldsymbol{E}}(t,\hat{\boldsymbol{R}}) + e\left\{\frac{\hat{\boldsymbol{P}}}{2M}, \hat{\boldsymbol{r}}\times\hat{\boldsymbol{B}}(t,\hat{\boldsymbol{R}})\right\}_+. \tag{6.36}$$

The terms of order $\mathcal{O}(ea_0^2)$ are 1) the electric quadrupole interaction and 2) a *Röntgen term* associated with the currents induced by the internal atomic motion, which results in

a magnetic dipole coupling with orbital angular momentum degrees of freedom:

$$\hat{H}_{E2} = -\frac{e\Delta m}{2M}\int_{\mathbb{R}^3} \mathrm{d}^3\boldsymbol{R}\,|\boldsymbol{R}\rangle\langle\boldsymbol{R}|\,(\hat{\boldsymbol{r}}\cdot\boldsymbol{\nabla}_{\boldsymbol{R}})\,(\hat{\boldsymbol{r}}\cdot\hat{\boldsymbol{E}}(t,\boldsymbol{R})), \tag{6.37}$$

$$\hat{H}_{M1} = e\left\{\frac{\hat{\boldsymbol{p}}}{2\mu}, \hat{\boldsymbol{r}}\times\hat{\boldsymbol{B}}(t,\hat{\boldsymbol{R}})\right\}_+ . \tag{6.38}$$

The highest order terms in (6.34) with respect to the small parameters are of order $\mathcal{O}(e^2a_0^2)$. These are called the diamagnetic and self-energy contributions, respectively:

$$\hat{H}_{\mathrm{dia}} = \frac{e^2}{8\mu}(\hat{\boldsymbol{r}}\times\hat{\boldsymbol{B}}(t,\hat{\boldsymbol{R}}))^2, \tag{6.39}$$

$$\hat{H}_{\mathrm{self}} = e^2\hat{\Delta}. \tag{6.40}$$

The combined Hamiltonian at leading order in the small parameters is thus

$$\hat{\tilde{H}}^{(1)} = \hat{H}_0 + \hat{H}_I + \mathcal{O}(e^2, a_0^2). \tag{6.41}$$

This is the Hamiltonian that we will be studying from here onwards. We will now express the interaction Hamiltonian $\hat{H}_I$ in terms of the hydrogen wavefunctions and COM momentum eigenstates, and in the interaction picture generated by $\hat{H}_0$. Eq. (6.36) can be rewritten as

$$\hat{H}_I = -e\hat{\boldsymbol{r}}\cdot\left[\hat{\boldsymbol{E}}(t,\hat{\boldsymbol{R}}) + \frac{\hat{\boldsymbol{P}}\times\hat{\boldsymbol{B}}(t,\hat{\boldsymbol{R}}) - \hat{\boldsymbol{B}}(t,\hat{\boldsymbol{R}})\times\hat{\boldsymbol{P}}}{2M}\right]. \tag{6.42}$$

Eq. (6.42) has a very similar structure to Eq. (2.13). Thus we can (equivalently to the derivation of Sec. 2.2) take the position representation on the relative coordinate by inserting the identity in terms of $\hat{\boldsymbol{r}}$ generalized eigenstates, and write the atomic dipole operator in the interaction picture of the relative degrees of freedom as

$$\hat{\boldsymbol{d}} \coloneqq e\hat{\boldsymbol{r}} = \sum_{\boldsymbol{a}>\boldsymbol{b}} \hat{\boldsymbol{d}}_{\boldsymbol{ab}}(t,\boldsymbol{r}) \tag{6.43}$$

where the partial dipole between two hydrogenic internal levels $|\boldsymbol{a}\rangle$ and $|\boldsymbol{b}\rangle$ (recall that $\{|\boldsymbol{a}\rangle = |(n,l,m)\rangle\}$) is

$$\hat{\boldsymbol{d}}_{\boldsymbol{ab}}(t,\boldsymbol{r}) = e\boldsymbol{F}_{\boldsymbol{ab}}(\boldsymbol{r})e^{\mathrm{i}\Omega_{\boldsymbol{ab}}\tau}\,|\boldsymbol{a}\rangle\langle\boldsymbol{b}| + \mathrm{H.c.} \tag{6.44}$$

The spatial smearing vector is given by $\boldsymbol{F_{ab}}(\boldsymbol{r}) = \boldsymbol{r}\Psi^*_{\boldsymbol{a}}(\boldsymbol{r})\Psi_{\boldsymbol{b}}(\boldsymbol{r})$, and $\hbar\Omega_{\boldsymbol{ab}} = E_{\boldsymbol{a}} - E_{\boldsymbol{b}}$ is the energy difference between the states $|\boldsymbol{a}\rangle$ and $|\boldsymbol{b}\rangle$. In contrast to the effective model in Sec. 2.2, the wavefunctions are associated with the reduced mass μ instead of the electron mass m_e.

Notice that while the electric dipole in (6.44) is smeared with the internal hydrogenic orbitals, the localization of the interaction is not given by these wavefunctions, unlike in the effective model in Eq. (2.14). Indeed, if we were to evaluate expectations of $\hat{H}_I$ on a given state of the system, it is the COM localization (the initial state of the COM as a distribution of $\hat{\boldsymbol{R}}$ generalized eigenstates) what gives the spatial localization of the interaction with the field. Of course, the spread of this localization will be bounded from below by the atomic orbital wavefunctions support, but we find that it is the center-of-mass localization that gives the spatial extension to the atom in the dipole approximation.

It is convenient to take a momentum representation for the COM degrees of freedom in (6.42). We note that for all COM states $|\Psi_{\text{COM}}\rangle$

$$\langle \boldsymbol{P}|\, e^{\pm \mathrm{i}\boldsymbol{k}\cdot\hat{\boldsymbol{R}}}\, |\Psi_{\text{COM}}\rangle = \langle \boldsymbol{P} \mp \boldsymbol{k}|\Psi_{\text{COM}}\rangle\,, \tag{6.45}$$

and we can identify thus

$$\langle \boldsymbol{P}|\, e^{\pm \mathrm{i}\boldsymbol{k}\cdot\hat{\boldsymbol{R}}} = \langle \boldsymbol{P} \mp \boldsymbol{k}|\,. \tag{6.46}$$

Also, we recall Eq. (2.18), (2.19):

$$\hat{\boldsymbol{E}}(t,\boldsymbol{x}) = \sum_{s=1}^{2}\int_{\mathbb{R}^3}\frac{\mathrm{d}^3\boldsymbol{k}}{(2\pi)^{\frac{3}{2}}}\sqrt{\frac{\hbar c|\boldsymbol{k}|}{2\epsilon_0}}\left(\mathrm{i}\hat{a}_{\boldsymbol{k},s}\boldsymbol{\epsilon}_{\boldsymbol{k},s}e^{-\mathrm{i}\omega t}e^{\mathrm{i}\boldsymbol{k}\cdot\boldsymbol{x}} + \text{H.c.}\right), \tag{6.47}$$

$$\hat{\boldsymbol{B}}(t,\boldsymbol{x}) = \sum_{s=1}^{2}\int_{\mathbb{R}^3}\frac{\mathrm{d}^3\boldsymbol{k}}{(2\pi)^{\frac{3}{2}}}\sqrt{\frac{\hbar|\boldsymbol{k}|}{2c\epsilon_0}}\left(\mathrm{i}\hat{a}_{\boldsymbol{k},s}(\boldsymbol{e}_{\boldsymbol{k}}\times\boldsymbol{\epsilon}_{\boldsymbol{k},s})e^{-\mathrm{i}\omega t}e^{\mathrm{i}\boldsymbol{k}\cdot\boldsymbol{x}} + \text{H.c.}\right), \tag{6.48}$$

where $\boldsymbol{e}_{\boldsymbol{k}} = \boldsymbol{k}/|\boldsymbol{k}|$ is the normalized wave vector. Then, the interaction Hamiltonian (6.42) in the full Hilbert space interaction picture is given by

$$\begin{aligned}\hat{H}_I = -\int_{\mathbb{R}^3}\mathrm{d}^3\boldsymbol{r}\,\hat{\boldsymbol{d}}(t,\boldsymbol{r})\cdot\sum_{s=1}^{2}\int_{\mathbb{R}^3}\frac{\mathrm{d}^3\boldsymbol{k}}{(2\pi)^{3/2}}\sqrt{\frac{\hbar c|\boldsymbol{k}|}{2\epsilon_0}}\int\mathrm{d}^3\boldsymbol{P}\\ \times\left[\mathrm{i}\hat{a}_{\boldsymbol{k},s}e^{-\mathrm{i}c|\boldsymbol{k}|t}\boldsymbol{\alpha}_{\boldsymbol{k},s,\boldsymbol{P}}\,|\boldsymbol{P}(t)\rangle\langle(\boldsymbol{P}-\boldsymbol{k})(t)| + \text{H.c.}\right],\end{aligned} \tag{6.49}$$

where we define through the free COM time evolution

$$|\boldsymbol{P}(t)\rangle = \exp\left(\frac{\mathrm{i}}{\hbar}t\frac{\boldsymbol{P}^2}{2M}\right)|\boldsymbol{P}\rangle\,, \tag{6.50}$$

and

$$\boldsymbol{\alpha}_{\boldsymbol{k},s,\boldsymbol{P}} \coloneqq \boldsymbol{\epsilon}_{\boldsymbol{k},s} - \frac{(\boldsymbol{e}_{\boldsymbol{k}} \times \boldsymbol{\epsilon}_{\boldsymbol{k},s}) \times (\boldsymbol{P} - \hbar\boldsymbol{k}/2)}{Mc} = \boldsymbol{\epsilon}_{\boldsymbol{k},s}\left[1 - \frac{\boldsymbol{P}\cdot\boldsymbol{e}_{\boldsymbol{k}} - \hbar|\boldsymbol{k}|/2}{Mc}\right] + \boldsymbol{e}_{\boldsymbol{k}}\frac{\boldsymbol{P}\cdot\boldsymbol{\epsilon}_{\boldsymbol{k},s}}{Mc}. \tag{6.51}$$

From this, one can see that there is an effective change of the center-of-mass momentum $\boldsymbol{P}$ by $\hbar\boldsymbol{k}/2$ per every plane-wave 'component' of the field expansion, as was also noted in [39].

Eq. (6.49) is the final result of our derivation of the interaction Hamiltonian in the interaction picture. It shows that considering a fully quantized atom, the interaction couples all the degrees of freedom: the (hydrogenic) relative-motion degrees of freedom, the COM, and the electromagnetic field. This in turn means that even if the initial state of internal, external and field degrees of freedom is separable, the interaction will in general create a non-separable state of these three subsystems.

For a quantum COM, the wavefunction disperses, so one cannot generally find a frame where the momentum of the COM is exactly zero since momentum eigenstates are unphysical. The best one can do is cancel its expectation value, but the COM of any localized atom will still disperse. Thus it is not possible to neglect the Röntgen contribution in those cases where the COM is a quantum degree of freedom. This is not a problem if the COM degrees of freedom are considered classical – there the Röntgen contribution vanishes in the COM comoving frame. Of course, these terms will emerge even in the classical case if we describe the system in frames where the atom is in motion.

6.2 Phenomenological Example: Transition Rates

In the following, we will treat the dipolar and Röntgen interaction terms as a perturbation of the hydrogenic Hamiltonian, so that we can work with the unperturbed internal atomic wavefunctions as a basis to apply perturbation theory.

Computing transition rates is something well-known and addressed many times before in the literature (see, e.g., [128]). We include this result mainly for illustration and completeness but we also generalize it considering initial states that are not necessarily COM-momentum eigenstates (which we argued are unnormalizable and unphsyically delocalized). To our knowledge, this assumption has not commonly been relaxed in previous literature about the multipolar Hamiltonian.

Consider initially (at time $t = 0$) a state of the whole system $|i, \varphi, 0\rangle \coloneqq |i\rangle \otimes |\varphi\rangle \otimes |0\rangle$, where $|i\rangle$ is an energy eigenstate of the internal atomic dynamics, $|0\rangle$ is the EM vacuum, and

we allow for the COM to have an arbitrary momentum distribution: $|\varphi\rangle = \int \mathrm{d}^3\boldsymbol{P}\,\varphi(\boldsymbol{P})\,|\boldsymbol{P}\rangle$. We wish then to compute the transition probability to a different atomic energy level, that is, to a final state $|f\rangle$ at time t_f, where $|f\rangle$ is an energy eigenstate of the internal atomic dynamics. For that we will need to sum over all possible final states for the field and COM degrees of freedom. To that end we expand in a Dyson series the time evolution operator to first order

$$\hat{\mathcal{U}} = \mathbb{1} + \hat{\mathcal{U}}^{(1)} + \mathcal{O}\left(e^2\right), \tag{6.52}$$

where $\hat{\mathcal{U}}^{(1)} = -\frac{\mathrm{i}}{\hbar}\int_0^{t_f}\mathrm{d}t\,\hat{H}_I(t)$ corresponds to a finite time evolution (cf. Eq. (2.33)). The probability for that process to happen at leading order is

$$P_{\text{tot}} = \int_{\mathbb{R}^3}\mathrm{d}^3\boldsymbol{P}_f\sum_{s=1}^{2}\int_{\mathbb{R}^3}\mathrm{d}^3\boldsymbol{k}\left|\int_{\mathbb{R}^3}\mathrm{d}^3\boldsymbol{P}\,\varphi(\boldsymbol{P})\,\langle f,\boldsymbol{P}_f,1_{\boldsymbol{k},s}|\hat{\mathcal{U}}^{(1)}|i,\boldsymbol{P},0\rangle\right|^2 + \mathcal{O}\left(e^4\right).$$

We make use of the following resolution of the identity in the COM and field Hilbert space, respectively, [65, Ch. 7]

$$\mathbb{1}_{\text{COM}} = \int_{\mathbb{R}^3}\mathrm{d}^3\boldsymbol{P}\,|\boldsymbol{P}\rangle\langle\boldsymbol{P}|\,, \tag{6.53}$$

$$\mathbb{1}_f = |0\rangle\langle 0| + \sum_{n=1}^{\infty}\sum_{s=1}^{2}\int_{\mathbb{R}^3}\mathrm{d}^3\boldsymbol{k}\,|n_{\boldsymbol{k},s}\rangle\langle n_{\boldsymbol{k},s}| + \ldots \tag{6.54}$$

The total probability thus reads

$$\begin{aligned}
P_{\text{tot}} &= \int_{\mathbb{R}^3}\mathrm{d}^3\boldsymbol{P}\,\varphi(\boldsymbol{P})\int_{\mathbb{R}^3}\mathrm{d}^3\boldsymbol{P}'\,\varphi^*(\boldsymbol{P}')\,\langle i,\boldsymbol{P}',0|\hat{\mathcal{U}}^{(1)\dagger}|f\rangle\langle f|\hat{\mathcal{U}}^{(1)}|i,\boldsymbol{P},0\rangle + \mathcal{O}\left(e^4\right)\\
&= \frac{e^2}{\hbar^2}\int_{\mathbb{R}^3}\mathrm{d}^3\boldsymbol{P}\int_{\mathbb{R}^3}\mathrm{d}^3\boldsymbol{P}'\,\varphi(\boldsymbol{P})\varphi^*(\boldsymbol{P}')\int_0^{t_f}\mathrm{d}t\int_0^{t_f}\mathrm{d}t' e^{\mathrm{i}(\Omega_{fi}t+\Omega_{if}t')}\int_{\mathbb{R}^3}\mathrm{d}^3\boldsymbol{r}\int_{\mathbb{R}^3}\mathrm{d}^3\boldsymbol{r}'\int_{\mathbb{R}^3}\mathrm{d}^3\boldsymbol{Q}\\
&\quad\times\int_{\mathbb{R}^3}\mathrm{d}^3\boldsymbol{Q}'\int_{\mathbb{R}^3}\frac{\mathrm{d}^3\boldsymbol{k}}{(2\pi)^3}\frac{\hbar c|\boldsymbol{k}|}{2\epsilon_0}e^{\mathrm{i}c|\boldsymbol{k}|(t-t')}\,\langle\boldsymbol{P}'|\boldsymbol{Q}'(t)\rangle\,\langle(\boldsymbol{Q}'-\boldsymbol{k})(t')|(\boldsymbol{Q}-\boldsymbol{k})(t)\rangle\,\langle\boldsymbol{Q}(t)|\boldsymbol{P}\rangle\\
&\quad\times\sum_{s=1}^{2}\sum_{a,b=1}^{3}F^a_{fi}(\boldsymbol{r})F^b_{if}(\boldsymbol{r}')\alpha^a_{\boldsymbol{k},s,\boldsymbol{Q}}\alpha^b_{\boldsymbol{k},s,\boldsymbol{Q}'} + \mathcal{O}\left(e^4\right).
\end{aligned} \tag{6.55}$$

The inner products in Eq. (6.55) can be thought of as enforcing momentum conservation deltas that yield upon integration $\boldsymbol{P} = \boldsymbol{P}' = \boldsymbol{Q} = \boldsymbol{Q}'$. Assume now that we are considering

a spontaneous decay, i.e. $\Omega \coloneqq \Omega_{if} = -\Omega_{fi} > 0$. Hence, substituting (6.50), Eq. (6.55) becomes

$$P_{\text{tot}} = \frac{e^2}{\hbar^2}\frac{\hbar c}{2\epsilon_0}\int_0^{t_f}\mathrm{d}t\int_0^{t_f}\mathrm{d}t' e^{-\mathrm{i}\Omega(t-t')}\sum_{a,b=1}^{3}\int_{\mathbb{R}^3}\mathrm{d}^3\boldsymbol{r}\, F_{fi}^a(\boldsymbol{r})\int_{\mathbb{R}^3}\mathrm{d}^3\boldsymbol{r}'\, F_{if}^b(\boldsymbol{r}')\int_{\mathbb{R}^3}\mathrm{d}^3\boldsymbol{P}\,|\varphi(\boldsymbol{P})|^2$$
$$\times\int_{\mathbb{R}^3}\frac{\mathrm{d}^3\boldsymbol{k}}{(2\pi)^3}|\boldsymbol{k}|e^{\mathrm{i}(t-t')\left[\frac{\hbar\boldsymbol{k}^2-2\boldsymbol{P}\cdot\boldsymbol{k}}{2M}+c|\boldsymbol{k}|\right]}\sum_{s=1}^{2}\alpha^a_{\boldsymbol{k},s,\boldsymbol{P}}\alpha^b_{\boldsymbol{k},s,\boldsymbol{P}}+\mathcal{O}\left(e^4\right), \tag{6.56}$$

where the summands $\hbar^2\boldsymbol{k}^2/2M - \hbar\boldsymbol{P}\cdot\boldsymbol{k}/M$ correspond to a recoil and Doppler shift, respectively. As is commonplace in the literature, we can take the limit $t_f \to \infty$ if we use (Dirac's) Fermi's golden rule for the transition rate $\Gamma \coloneqq \lim_{t_f\to\infty}\frac{\mathrm{d}P}{\mathrm{d}t_f}$:

$$\Gamma = \frac{e^2}{8\pi^2\hbar\epsilon_0}\sum_{a,b=1}^{3}\int_{\mathbb{R}^3}\mathrm{d}^3\boldsymbol{r}\, F_{fi}^a(\boldsymbol{r})\int_{\mathbb{R}^3}\mathrm{d}^3\boldsymbol{r}'\, F_{if}^b(\boldsymbol{r}')\int_{\mathbb{R}^3}\mathrm{d}^3\boldsymbol{P}\,|\varphi(\boldsymbol{P})|^2\int_{\mathbb{R}^3}\mathrm{d}^3\boldsymbol{k}\,|\boldsymbol{k}|\sum_{s=1}^{2}\alpha^a_{\boldsymbol{k},s,\boldsymbol{P}}\alpha^b_{\boldsymbol{k},s,\boldsymbol{P}}$$
$$\times\,\delta\left(\frac{\hbar\boldsymbol{k}^2-2\boldsymbol{P}\cdot\boldsymbol{k}}{2M}+c|\boldsymbol{k}|-\Omega\right)+\mathcal{O}\left(e^4\right), \tag{6.57}$$

From now on, we will assume that $\varphi(\boldsymbol{P}) = \varphi(|\boldsymbol{P}|)$ such that we can reach closed forms for the integrals. We further define $P \coloneqq |\boldsymbol{P}|$, $k \coloneqq |\boldsymbol{k}|$, and $z \coloneqq \boldsymbol{e}_{\boldsymbol{P}}\cdot\boldsymbol{e}_{\boldsymbol{k}}$ (where $\boldsymbol{e}_{\boldsymbol{P}} = \boldsymbol{P}/P$). With the help of (6.51) and (6.19), we then recast the sum over polarizations in terms of powers of k and P:

$$\begin{aligned}\sum_{s=1}^{2}\alpha^a_{\boldsymbol{k},s,\boldsymbol{P}}\alpha^b_{\boldsymbol{k},s,\boldsymbol{P}} =&(\delta^{ab}-e^a_{\boldsymbol{k}}e^b_{\boldsymbol{k}})+\frac{\hbar k}{2Mc}\left[2(\delta^{ab}-e^a_{\boldsymbol{k}}e^b_{\boldsymbol{k}})-\frac{P}{Mc}(2\delta^{ab}z-e^a_{\boldsymbol{P}}e^b_{\boldsymbol{k}}-e^b_{\boldsymbol{P}}e^a_{\boldsymbol{k}})\right]\\&-\frac{P}{Mc}(2\delta^{ab}z-e^a_{\boldsymbol{P}}e^b_{\boldsymbol{k}}-e^b_{\boldsymbol{P}}e^a_{\boldsymbol{k}})+\left(\frac{\hbar k}{2Mc}\right)^2(\delta^{ab}-e^a_{\boldsymbol{k}}e^b_{\boldsymbol{k}})\\&+\left(\frac{P}{Mc}\right)^2\left[z(\delta^{ab}z-e^a_{\boldsymbol{P}}e^b_{\boldsymbol{k}}-e^b_{\boldsymbol{P}}e^a_{\boldsymbol{k}})+e^a_{\boldsymbol{k}}e^b_{\boldsymbol{k}}\right].\end{aligned} \tag{6.58}$$

Then in spherical coordinates for $\boldsymbol{k}$ and $\boldsymbol{P}$, with Θ_k and Θ_P being the respective solid angles, we re-express the integral over $\boldsymbol{k}$ and the angular part of the integral over $\boldsymbol{P}$ in

(6.57) as

$$\begin{aligned}
&\int_{S^2} \mathrm{d}\Theta_P \int_{S^2} \mathrm{d}\Theta_k \int_0^\infty \mathrm{d}k\, k^3 \delta\left(\frac{\hbar k^2 - 2Pkz}{2M} + ck - \Omega\right) \sum_{s=1}^{2} \alpha^a_{\boldsymbol{k},s,\boldsymbol{P}} \alpha^b_{\boldsymbol{k},s,\boldsymbol{P}} \\
&= \frac{8\pi}{3}\delta^{ab}\left\{\frac{\hbar^2\pi\Omega^5}{M^2c^8}\left[1 + 7\left(\frac{P}{Mc}\right)^2\right] + \frac{4\hbar\pi\Omega^4}{Mc^6}\left[1 - 3\frac{\hbar\Omega}{Mc^2} + \left(\frac{P}{Mc}\right)^2\left(5 - 28\frac{\hbar\Omega}{Mc^2}\right)\right]\right. \\
&\quad \left. + \frac{\pi\Omega^3}{c^4}\left[4 - 10\frac{\hbar\Omega}{Mc^2} + 21\left(\frac{\hbar\Omega}{Mc^2}\right)^2 + \frac{2}{3}\left(\frac{P}{Mc}\right)^2\left(20 - 21\cdot 5\frac{\hbar\Omega}{Mc^2} + 18\cdot 21\left(\frac{\hbar\Omega}{Mc^2}\right)^2\right)\right]\right\} \\
&\quad - \delta^{ab}\frac{16\pi^2\Omega^3}{9c^4}\left(\frac{P}{Mc}\right)^2\left[12 - 50\frac{\hbar\Omega}{Mc^2} + 147\left(\frac{\hbar\Omega}{Mc^2}\right)^2\right] + \mathcal{O}\left(\left(\frac{\hbar\Omega}{Mc^2}\right)^6, \left(\frac{P}{Mc}\right)^4\right) \\
&=: \frac{32\pi^2 M}{3\hbar^3}\delta^{ab} g(P),
\end{aligned} \tag{6.59}$$

where we have implicitly defined the function $g(P)$ in the last step. To solve the integral over k in (6.59), upon substitution of (6.58), we use that, for general a_i,

$$\int_0^\infty \mathrm{d}k\, k^3 \delta\left(\frac{\hbar k^2 - 2Pkz}{2M} + ck - \Omega\right)(a_2 k^2 + a_1 k + a_0) = \theta(Pz - Mc(1-\kappa)) \sum_{i=0}^{2} \frac{a_i \kappa^{3+i}}{\hbar^{3+i}}, \tag{6.60}$$

where $\kappa := \sqrt{\left(1 - \frac{Pz}{Mc}\right)^2 + \frac{2\hbar\Omega}{Mc^2}}$, and we also used that $P \ll Mc$. Finally, we expand in powers of $P \ll Mc$ as well as $\hbar\Omega/Mc^2$ before performing the angular integrals but after the integral over k. To evaluate the angular integrals we use

$$\int_{S^2} \mathrm{d}\Theta_k \left(\delta^{ab} - e^a_{\boldsymbol{k}} e^b_{\boldsymbol{k}}\right) = \frac{8\pi}{3}\delta^{ab}. \tag{6.61}$$

The expansion in powers of $P \ll Mc$ is justified since we are working in the non-relativistic regime. However, it is important to note that relativistic corrections of powers higher or equal to P/Mc are not consistent with the approximation made at the level of Eq. (6.41) since we already neglected the sub-leading order terms there. Indeed, these relativistic corrections have to be accompanied by the corresponding corrections to the Hamiltonian in order to be consistent (as we will discuss in more detail in Sec. 6.3). We will nevertheless keep the sub-leading corrections in these expressions to analyze qualitatively the dynamics that they generate, but we need to keep in mind that extra corrections from the Darwin terms (Eq. (6.3)) would need to be included as well if we want to get numerically accurate

predictions. The expansion in powers of $\hbar\Omega/Mc^2$ is justified for hydrogenic atoms since the energy of the transitions is much smaller than the rest mass of the atom.

Note that in the case of vacuum excitation processes, i.e. $\Omega \to -\Omega$, Eq. (6.59) vanishes as the argument of the delta is always positive (we require $P \ll Mc$ to be consistent with the non-relativistic approximation made). However, the fact that the delta argument could be negative outside the non-relativistic approximation suggests that when we properly include the Darwin correction it may be possible to get 'Cherenkov' excitations even in the infinite time limit, as pointed out in [130].

Concentrating on the sub-leading order in transition frequencies then yields

$$g(P) = P_0^2 \left(1 - \frac{3}{2}\frac{\hbar\Omega}{Mc^2} + \frac{2}{3}\left(\frac{P}{Mc}\right)^2\right) + \mathcal{O}\left(\left(\frac{\hbar\Omega}{Mc^2}\right)^5, \left(\frac{P}{Mc}\right)^4\right), \tag{6.62}$$

where we defined

$$P_0^2 = \left(\frac{\hbar\Omega}{Mc^2}\right)^3 M^2c^2. \tag{6.63}$$

Let us analyze what kind of phenomenology the sub-leading corrections generate when we do not consider eigenstates of the COM momentum as initial states and instead consider a COM with a momentum wavefunction $\varphi(P)$. With these definitions, the transition rate yields to leading order

$$\Gamma = \frac{e^2\Omega^3}{3\pi\hbar\epsilon_0 c^3} |\langle i|\hat{\boldsymbol{r}}|f\rangle|^2 4\pi \int_0^\infty \mathrm{d}P\, |\varphi(P)|^2 \left(1 - \frac{3}{2}\frac{\hbar\Omega}{Mc^2} + \frac{2}{3}\left(\frac{P}{Mc}\right)^2\right),$$

where we used that $\sum_{a,b=1}^3 F^a_{fi}(\boldsymbol{r})F^b_{if}(\boldsymbol{r}')\alpha^a_{\boldsymbol{k},s,\boldsymbol{P}}\alpha^b_{\boldsymbol{k},s,\boldsymbol{P}} \longrightarrow \sum_{a=1}^3 F^a_{fi}(\boldsymbol{r})F^a_{if}(\boldsymbol{r}')$ in terms of the internal atomic degrees of freedom.

Let us specialize now to the case of $|i\rangle = |1s\rangle$, i.e. $(n,l,m) = (1,0,0)$, and $|f\rangle = |2p_z\rangle$, i.e. $(n,l,m) = (2,1,0)$. Hence $\hbar\Omega/(Mc^2) \approx 10^{-8}$, and $P_0 \approx 10^{-30}$ kg m/s such that $P_0/Mc \approx 10^{-12}$. Therefore, one can check that the expansion (6.62) is valid for $P \lesssim 10^{11}P_0$ such that $P/Mc \lesssim 0.1$. The internal hydrogenic matrix element yields

$$|\langle 1s|\hat{\boldsymbol{r}}|2p_z\rangle|^2 = \sum_{a=1}^3 \left|\int_{\mathbb{R}^3} \mathrm{d}^3\boldsymbol{r}\, F^a_{2p_z,1s}(\boldsymbol{r})\right|^2 = \frac{2^{15}}{3^{10}}a_0^2. \tag{6.64}$$

We consider, additionally, an initial momentum distribution for the COM of $\varphi(P) = (2\pi\sigma_P^2)^{3/4}\exp(-P^2/4\sigma_P^2)$ so that $|\varphi\rangle$ is L^2-normalized to one, σ_P being the uncertainty

in momentum. To leading order in the expansion of coupling strength, momentum and transition frequency, we arrive at

$$\Gamma = \frac{e^2 a_0^2 \Omega^3}{3\pi\epsilon_0 \hbar c^3} \frac{2^{15}}{3^{10}} \left(1 - \frac{3}{2}\frac{\hbar\Omega}{Mc^2} + \frac{2}{3}\left(\frac{\sigma_P}{Mc}\right)^2\right) =: \Gamma_0 \left(1 - \frac{3}{2}\frac{\hbar\Omega}{Mc^2} + \frac{2}{3}\left(\frac{\sigma_P}{Mc}\right)^2\right), \tag{6.65}$$

where $\Gamma_0 \approx 6.27 \cdot 10^8/s$ is the well-known hydrogen transition rate expression with no extra corrections [142, Ch. 4]. The correction due to Ω in a typical transition of hydrogen is of order 10^{-9}. It is straightforward to see that in the limit of an initial eigenstate in the COM momentum, i.e. $\sigma_P \to 0$, Γ_0 is still shifted due to the finite transition frequency that originated due to the Röntgen term. The transition rate in this limit coincides with the results of [39]. The expansion is valid for $\sigma_p \ll Mc = h/\lambda_C$, λ_C being the Compton wavelength of the atom. Of course we recall that the corrections proportional to $(\sigma_P/Mc)^2$ will be accompanied by Darwin corrections at the same order. Note finally that averaging over all $2p$ states, i.e. $m \in \{-1, 0, 1\}$, would yield the same rate as given by (6.65).

6.3 Leading Order Relativistic Corrections

As discussed at the beginning of Sec. 6, if we are interested in the leading-order correction for relativistic atomic trajectories, we need to include the Darwin Hamiltonian (6.3). We include in this section a brief summary of the discussion in [129] about how the leading order relativistic corrections would modify the dynamics. Following the same procedure of quantization and PZW transformation as in Sec. 6, from the minimal coupling Hamiltonian (6.2) with the Darwin correction (6.3) one would arrive at the Hamiltonian [129]

$$\begin{aligned}\hat{H} =& \frac{\hat{\boldsymbol{P}}^2}{2M}\left[1 - \frac{\hat{\boldsymbol{P}}^2}{4M^2c^2} - \frac{1}{Mc^2}\left(\frac{\hat{\boldsymbol{p}}}{2\mu} - \frac{e^2}{4\pi\epsilon_0|\hat{\boldsymbol{r}}|}\right)\right] - \frac{\left(\hat{\boldsymbol{P}}\cdot\hat{\boldsymbol{p}}\right)^2}{2M^2\mu c^2} + \frac{e^2}{4\pi\varepsilon_0|\hat{\boldsymbol{r}}|}\frac{(\hat{\boldsymbol{P}}\cdot\hat{\boldsymbol{r}}/|\hat{\boldsymbol{r}}|)^2}{2M^2c^2} \\ &- \frac{\Delta m}{2\mu M^2c^2}\left[\left(\hat{\boldsymbol{P}}\cdot\hat{\boldsymbol{p}}\right)\frac{\hat{\boldsymbol{p}}^2}{\mu} - \frac{e^2}{8\pi\varepsilon_0|\hat{\boldsymbol{r}}|}\left(\hat{\boldsymbol{P}}\cdot\hat{\boldsymbol{p}} + \frac{1}{|\hat{\boldsymbol{r}}|^2}(\hat{\boldsymbol{P}}\cdot\hat{\boldsymbol{r}})\,(\hat{\boldsymbol{r}}\cdot\hat{\boldsymbol{p}}) + \text{H.c.}\right)\right] + \hat{H}_{\text{A}} + \hat{H}_I,\end{aligned} \tag{6.66}$$

where, again, $\Delta m = m_p - m_e$, and the free internal atomic Hamiltonian

$$\hat{H}_{\text{A}}(\hat{\boldsymbol{r}}, \hat{\boldsymbol{p}}) = \frac{\hat{\boldsymbol{p}}^2}{2\mu}\left(1 - \frac{m_e^3 + m_p^3}{M^3}\frac{\hat{\boldsymbol{p}}^2}{4\mu^2c^2}\right) - \frac{e^2}{4\pi\varepsilon_0}\left[\frac{1}{r} + \frac{1}{2\mu Mc^2}\left(\hat{\boldsymbol{p}}\cdot\frac{1}{|\hat{\boldsymbol{r}}|}\hat{\boldsymbol{p}} + \hat{\boldsymbol{p}}\cdot\hat{\boldsymbol{r}}\frac{1}{|\hat{\boldsymbol{r}}|^3}\hat{\boldsymbol{r}}\cdot\hat{\boldsymbol{p}}\right)\right]$$

no longer assumes the analytically tractable hydrogenic wavefunctions as solutions but a more complicated form. $\hat{H}_I$ is given by (6.42), i.e. the dipolar and Röntgen interaction

to leading order. Significantly, the cross-coupling between COM and internal degrees of freedom of the atom takes a complicated form. For instance, what was the free COM Hamiltonian in the non-relativistic approximation is replaced by the rather non-trivial terms in Eq. (6.66) that now have corrections coming from $\hat{\boldsymbol{P}}^2$ and couples the COM to the momentum and position operators of the relative motion.

It is possible in this case to apply a canonical transformation[5] $\{\hat{\boldsymbol{R}}, \hat{\boldsymbol{r}}, \hat{\boldsymbol{p}}\} \longrightarrow \{\hat{\boldsymbol{Q}}, \hat{\boldsymbol{q}}, \hat{\boldsymbol{\rho}}\}$ that simplfies the form of the corrected Hamiltonian:

$$\hat{\boldsymbol{r}} = \hat{\boldsymbol{q}} - \frac{\Delta m}{2\mu M^2 c^2}[(\hat{\boldsymbol{q}}\cdot\hat{\boldsymbol{P}})\hat{\boldsymbol{\rho}} + \text{H.c.}] - \frac{\hat{\boldsymbol{q}}\cdot\hat{\boldsymbol{P}}}{2M^2c^2}\hat{\boldsymbol{P}}, \tag{6.67}$$

$$\hat{\boldsymbol{p}} = \hat{\boldsymbol{\rho}} + \frac{\Delta m}{2M^2c^2}\left[\frac{\hat{\boldsymbol{\rho}}^2}{\mu}\hat{\boldsymbol{P}} - \frac{e^2}{4\pi\varepsilon_0|\hat{\boldsymbol{q}}|}\left(\hat{\boldsymbol{P}} - \frac{(\hat{\boldsymbol{P}}\cdot\hat{\boldsymbol{q}})\hat{\boldsymbol{q}}}{|\hat{\boldsymbol{q}}|^2}\right)\right] + \frac{\hat{\boldsymbol{\rho}}\cdot\hat{\boldsymbol{P}}}{2M^2c^2}\hat{\boldsymbol{P}}, \tag{6.68}$$

$$\hat{\boldsymbol{R}} = \hat{\boldsymbol{Q}} - \frac{\Delta m}{2M^2c^2}\left[\left(\frac{\hat{\boldsymbol{\rho}}^2}{2\mu}\hat{\boldsymbol{q}} + \text{H.c.}\right) - \frac{e^2}{4\pi\varepsilon_0|\hat{\boldsymbol{q}}|}\hat{\boldsymbol{q}}\right] - \frac{1}{4M^2c^2}[(\hat{\boldsymbol{q}}\cdot\hat{\boldsymbol{P}})\hat{\boldsymbol{\rho}} + (\hat{\boldsymbol{P}}\cdot\hat{\boldsymbol{\rho}})\hat{\boldsymbol{q}} + \text{H.c.}]. \tag{6.69}$$

However, the new variables $\{\hat{\boldsymbol{Q}}, \hat{\boldsymbol{q}}, \hat{\boldsymbol{\rho}}\}$ mix relative motion and COM degrees of freedom. Whereas, the COM momentum is still associated with $\hat{\boldsymbol{P}}$, the remaining new variables lose their original physical meaning of separating internal and external degrees of freedom. After neglecting terms suppressed by $1/M^4c^4$, the form of the Hamiltonian becomes [129, 152]:

$$\hat{\tilde{H}} = \frac{\hat{\boldsymbol{P}}^2}{2M}\left(1 - \frac{\hat{H}_{\text{A}}(\hat{\boldsymbol{q}}, \hat{\boldsymbol{p}})}{Mc^2}\right) + \hat{H}_{\text{A}}(\hat{\boldsymbol{q}}, \hat{\boldsymbol{\rho}}) + \hat{H}_I, \tag{6.70}$$

$$\hat{H}_I = -e\hat{\boldsymbol{q}}\cdot\hat{\boldsymbol{E}}(t, \hat{\boldsymbol{Q}}) + e\left\{\frac{\hat{\boldsymbol{P}}}{2M}, \hat{\boldsymbol{q}}\times\hat{\boldsymbol{B}}(t, \hat{\boldsymbol{Q}})\right\}_+. \tag{6.71}$$

where the interaction is carried over now in terms of the new canonical variables, and the coupling between COM and internal atomic degrees of freedom is more tractable. Additionally, the COM contribution is no longer quartic in the COM momentum.

6.4 Summary

In this chapter we relaxed the simplification of a classical COM and quantized all atomic and field degrees of freedom. Even though we worked in the dipole approximation, we

[5] For the corresponding treatment of the Breit Hamiltonian with spin degrees of freedom, see [152].

had to consider the sub-leading correction terms of the vector field expansion around the COM. This was due to the dynamical nature of the COM degrees of freedom and would result in the Röntgen term. Going from the two-particle minimal coupling Hamiltonian to the multipolar Hamiltonian was achieved through a Power-Zienau-Woolley transformation which, however, was not a gauge transformation. In the new representation of the Hamiltonian, only the dipole and Röntgen terms survived to leading order, i.e. linear in the coupling constant and the Bohr radius. Importantly, the localization of the interaction was given by the COM and not, as in the case of the effective dipole model, through the electronic wavefunctions. We also noted that the multipolar Hamiltonian accounts for recoil and Doppler shifts. We computed, further, an example atomic transition probability for an initially delocalized COM, and found correction terms that were quadratic in the momentum uncertainty and linear in the energy difference between the two atomic states of the transition. Finally, we discussed sub-leading terms to the multipolar Hamiltonian that are introduced by the Darwin correction.

Chapter 7

Revisiting Effective Models

After having studied the nuances related to taking into account the COM dynamics, one realizes quickly that it would be truly challenging to consider scenarios where the COM trajectories undergo arbitrarily accelerated relativistic motion since the coupling of internal and external degrees of freedom becomes increasingly complicated. This poses the question whether we can use effective models that a) allow for the COM motion to be relativistic b) are computationally tractable and c) are reasonable approximations that at least capture the main phenomenology of an interaction between matter and light. This is what we will study in the following.

The structure of this chapter is as follows: In Sec. 7.1 we will examine the transformation properties of the effective dipole model. Additionally, in Sec. 7.2 we will present modifications to the UDW model that are in analogy to the multipolar Hamiltonian with a quantized atomic COM. Lastly, in Sec. 7.3 we will summarize our results.

7.1 Approximate Dipole Model with Classical Center-of-Mass Motion

Under the considerations of the previous chapter, let us come back to the effective dipole model from Sec. 2.2. Now it becomes clear that we are neglecting the quantum nature of the COM and along with it the dynamics in form of the Röntgen term of the COM. However, in contrast to the multipolar Hamiltonian, we can consider relativistic, and externally prescribed trajectories of the atom. Furthermore, if this model holds any value for probing of the electromagnetic field, the predictions should be generally covariant for different

observers. This is in distinction to the multipolar Hamiltonian that can only guarantee Galilei covariance. One would expect that although this model may not give the accurate numbers associated with a particular atomic physics experiment, it may still hold some of the core phenomenology of the light-matter interaction and provide a simple yet covariant model to measure the electromagnetic field. Neglecting the Röntgen term for the COM would be akin to considering that a) the COM is a classical degree of freedom and b) the mass of the nucleus is much larger than that of the electron.

We recall that this effective model is prescribed in the center-of-mass frame of the atom, where the atom does not move, and hence there are no COM Röntgen terms. We denote as τ the proper time of the atom's COM rest frame $(\tau, \boldsymbol{\xi})$. As is common in particle detector models, we take the atom to be Fermi-Walker transported as the interatomic forces preserve its spatial coherence [47]. It is convenient to quantize the field in an inertial frame that we will call the 'lab' frame of coordinates $(t, \boldsymbol{x})$. For general spacetimes characterized by the metric g the interaction Hamiltonian that generates translations with respect to the COM proper time (in the interaction picture) reads

$$\hat{H}_I^{\mathrm{eff},\tau} = \chi(\tau) \sum_{\boldsymbol{a}>\boldsymbol{b}} \int_{\Sigma_\tau} \mathrm{d}^3\boldsymbol{\xi} \sqrt{-g}\; \hat{\boldsymbol{d}}_{\boldsymbol{ab}}(\tau, \boldsymbol{\xi}) \cdot \hat{\boldsymbol{E}}\left(t(\tau, \boldsymbol{\xi}), \boldsymbol{x}(\tau, \boldsymbol{\xi})\right) =: \int_{\Sigma_\tau} \mathrm{d}^3\boldsymbol{\xi}\, \hat{h}_I^{\mathrm{eff}}(\tau, \boldsymbol{\xi}), \tag{7.1}$$

where the time dependence of the coupling is prescribed in the COM rest frame and encoded in χ, and where we defined the Hamiltonian density $\hat{h}_I^{\mathrm{eff}}(\tau, \boldsymbol{\xi})$.

7.1.1 Covariance of Predictions

If the model holds any value as a relativistic probe of the electromagnetic field, its predictions in flat spacetime should be Lorentz covariant. To show explicitly that they are, we take (7.1) and analyze how the Hamiltonian transforms under changes of reference frame. For Minkowski spacetime in any coordinates associated with internal frames we have that $\sqrt{-g} = 1$. Assuming that the atom is undergoing inertial motion, we can compute the Hamiltonian that generates translations with respect to the lab frame using the transformation properties under general Lorentz transformations. The covariance of the model demands that [58]

$$\hat{\mathcal{U}} = \mathcal{T} \exp\left(\frac{-\mathrm{i}}{\hbar} \int_{\mathbb{R}^4 \times \mathbb{R}} \mathrm{d}^3\boldsymbol{\xi}\, \mathrm{d}\tau\, \hat{h}_I^{\mathrm{eff}}(\tau, \boldsymbol{\xi})\right) = \mathcal{T} \exp\left(\frac{-\mathrm{i}}{\hbar} \int_{\mathbb{R}^3 \times \mathbb{R}} \mathrm{d}^3\,\boldsymbol{x}\, \mathrm{d}t\, \hat{h}_I^{\mathrm{eff}}(\tau(t, \boldsymbol{x}), \boldsymbol{\xi}(t, \boldsymbol{x}))\right). \tag{7.2}$$

In the Hamiltonian (7.1), the electric field is as seen from the COM frame. However, it is quantized in the lab frame. To write the Hamiltonian that generates translations with respect to the lab frame's time t we need to transform the electric field. Let us assume then that the atomic COM moves on a trajectory $\boldsymbol{x}(t) = vt$ with velocity v with respect to the lab frame. The electric field changes under Lorentz transformations via [153, Ch. 26]

$$\hat{\boldsymbol{E}}(t(\tau,\boldsymbol{\xi}), x((\tau,\boldsymbol{\xi})) \to \gamma\left(\hat{\boldsymbol{E}}(t,\boldsymbol{x}) + \boldsymbol{v}\times\hat{\boldsymbol{B}}(t,\boldsymbol{x})\right) + (1-\gamma)\left(\hat{\boldsymbol{E}}(t,\boldsymbol{x})\cdot\boldsymbol{e}_v\right)\boldsymbol{e}_v,$$

where $\boldsymbol{e}_v = \boldsymbol{v}/|\boldsymbol{v}|$. The Lorentz-transformed Hamiltonian generating translations with respect to time t is thus

$$\begin{aligned}\hat{H}_I^{\mathrm{eff},t} =& \sum_{\boldsymbol{a}>\boldsymbol{b}}\int_{\mathbb{R}^3}\mathrm{d}^3\boldsymbol{x}\,\chi(\tau(t,\boldsymbol{x}))\,\hat{\boldsymbol{d}}'_{\boldsymbol{ab}}(\tau(t,\boldsymbol{x}),\boldsymbol{\xi}(t,\boldsymbol{x}))\\ &\times\left\{\gamma[\hat{\boldsymbol{E}}(t,\boldsymbol{x}) + \boldsymbol{v}\times\hat{\boldsymbol{B}}(t,\boldsymbol{x})] + (1-\gamma)\left(\hat{\boldsymbol{E}}(t,\boldsymbol{x})\cdot\boldsymbol{e}_v\right)\boldsymbol{e}_v\right\}. \end{aligned} \tag{7.3}$$

Naturally, a Röntgen term arises for the classical COM through the Lorentz transformation. The transformed dipole moment reads

$$\hat{\boldsymbol{d}}'_{\boldsymbol{ab}}(\tau(t,\boldsymbol{x}),\boldsymbol{\xi}(t,\boldsymbol{x})) = e\boldsymbol{F}_{ab}(\xi(t,\boldsymbol{x}))e^{\mathrm{i}\Omega_{\boldsymbol{ab}}\tau(t,\boldsymbol{x})}|\boldsymbol{a}\rangle\langle\boldsymbol{b}| + \mathrm{H.c.} \tag{7.4}$$

Although it is not necessary to prove that this is covariant because it was made covariant by construction, there is some value in explicitly showing its covariance and how to deal with changes of reference frame in the context of this effective light-matter interaction. With this in mind let us compute the transition probability of the atom in the COM frame and the lab frame, explicitly showing how they coincide.

7.1.2 Example - Vacuum Excitation Probability

We will showcase a simple example to demonstrate that the previous considerations yield Lorentz-invariant predictions. Let us consider an atom whose COM is comoving with the lab frame. We will compute the transition probability from a $|1s\rangle$ state to the excited state $|2p_z\rangle$. Let us do this calculation using two different coordinate systems: one comoving with the atomic COM and the lab frame, and another one moving at a constant speed with respect to the lab frame, showing how both results coincide. This will also allow us to compute very useful quantities along the way such as the Wightman tensor for the electric and magnetic fields.

Wightman Functions

We will give first the electromagnetic Wightman functions which will be used to compute the subsequent transition probabilities (the derivations can be found in Appendix C.3). We begin with the two-point function of the electric field which is of the form

$$W_E^{ij}[t,t';\boldsymbol{x},\boldsymbol{x}'] = \langle 0|\,\hat{E}^i(t,\boldsymbol{x})\hat{E}^j(t',\boldsymbol{x}')\,|0\rangle = \frac{\hbar c}{2\epsilon_0}\int_{\mathbb{R}^3}\frac{\mathrm{d}^3\boldsymbol{k}}{(2\pi)^3}|\boldsymbol{k}|e^{-\mathrm{i}c|\boldsymbol{k}|(t-t')}e^{\mathrm{i}\boldsymbol{k}\cdot(\boldsymbol{x}-\boldsymbol{x}')}\left(\delta^{ij}-e^i_{\boldsymbol{k}}e^j_{\boldsymbol{k}}\right). \tag{7.5}$$

This can be put in relation to the magnetic-field Wightman tensor:

$$W_B^{ij}[t,t';\boldsymbol{x},\boldsymbol{x}'] = \langle 0|\,\hat{B}^i(t,\boldsymbol{x})\hat{B}^j(t',\boldsymbol{x}')\,|0\rangle = \frac{1}{c^2}W_E^{ij}[t,t';\boldsymbol{x},\boldsymbol{x}']. \tag{7.6}$$

The two cross-field Wightman functions can be similarly related:

$$\begin{aligned} W_{BE}^{ij}[t,t';\boldsymbol{x},\boldsymbol{x}'] &= \langle 0|\,\hat{B}^i(t,\boldsymbol{x})\hat{E}^j(t',\boldsymbol{x}')\,|0\rangle \\ &= -\frac{\hbar}{2\epsilon_0}\int_{\mathbb{R}^3}\frac{\mathrm{d}^3\boldsymbol{k}}{(2\pi)^3}|\boldsymbol{k}|e^{-\mathrm{i}c|\boldsymbol{k}|(t-t')}e^{\mathrm{i}\boldsymbol{k}\cdot(\boldsymbol{x}-\boldsymbol{x}')}\epsilon^{ijk}(e_{\boldsymbol{k}})_k \\ &= W_{EB}^{ji}[t,t';\boldsymbol{x},\boldsymbol{x}'], \end{aligned} \tag{7.7}$$

where all the details can be seen in Appendix C.3. We additionally give an explicit form for the different electromagnetic Wightman functions after performing the integral over $\boldsymbol{k}$. The following expansion in terms of spherical harmonics Y_{lm} and spherical Bessel functions of the first kind j_l will be of use [154]:

$$\boldsymbol{k} = \sqrt{\frac{2\pi}{3}}|\boldsymbol{k}|\left(Y_{11}(\boldsymbol{e}_{\boldsymbol{k}})-Y_{1-1}(\boldsymbol{e}_{\boldsymbol{k}}),\mathrm{i}[Y_{11}(\boldsymbol{e}_{\boldsymbol{k}})-Y_{1-1}(\boldsymbol{e}_{\boldsymbol{k}})],\sqrt{2}Y_{10}(\boldsymbol{e}_{\boldsymbol{k}})\right), \tag{7.8}$$

$$e^{\mathrm{i}\boldsymbol{k}\cdot\boldsymbol{x}} = \sum_{l=0}^{\infty}\sum_{m=-l}^{l}4\pi\mathrm{i}^l j_l(|\boldsymbol{k}||\boldsymbol{x}|)Y_{lm}(\boldsymbol{e}_{\boldsymbol{k}})Y^*_{lm}(\boldsymbol{e}_{\boldsymbol{x}}) = \sum_{l=0}^{\infty}\sum_{m=-l}^{l}4\pi\mathrm{i}^l j_l(|\boldsymbol{k}||\boldsymbol{x}|)Y^*_{lm}(\boldsymbol{e}_{\boldsymbol{k}})Y_{lm}(\boldsymbol{e}_{\boldsymbol{x}}). \tag{7.9}$$

Then, the two independent Wightman functions W_E and W_{BE} (with implicit pole prescription, and where we denote derivatives of Dirac's delta by $\dot{\delta}, \ddot{\delta}$) are:

$$
\begin{aligned}
&W_E^{ij}[t,t';\boldsymbol{x},\boldsymbol{x}'] \\
&= \frac{\hbar c}{2(2\pi)^2\epsilon_0}\left[\frac{8[\tilde{r}^2(2X^{ij}+\delta^{ij})-c^2(t'-t)^2\delta^{ij}]}{(\tilde{r}^2-c^2(t'-t)^2)^3} + \mathrm{i}\pi\left\{\frac{\ddot{\delta}(\tilde{r}-c(t'-t))-\ddot{\delta}(\tilde{r}+c(t'-t))}{\tilde{r}}X^{ij}\right.\right. \\
&\quad + \left(\frac{\delta(\tilde{r}-c(t'-t))-\delta(\tilde{r}+c(t'-t))}{\tilde{r}^3} - \frac{\dot{\delta}(\tilde{r}-c(t'-t))-\dot{\delta}(\tilde{r}+c(t'-t))}{\tilde{r}^2}\right) \\
&\quad \left.\left.\times\,(3X^{ij}+2\delta^{ij})\right\}\right], \\
&W_{BE}^{ij}[t,t';\boldsymbol{x},\boldsymbol{x}'] = -\frac{\hbar}{2(2\pi)^2\epsilon_0}\beta\epsilon^{ijk}(e_{\boldsymbol{x}}-e_{\boldsymbol{x}'})_k,
\end{aligned}
\tag{7.10}
$$

where we defined $|\boldsymbol{x}-\boldsymbol{x}'|=\tilde{r}$, $e_{\boldsymbol{x}}=\boldsymbol{x}/|\boldsymbol{x}|$, and

$$
X^{ij} = (e_{\boldsymbol{x}}-e_{\boldsymbol{x}'})^i(e_{\boldsymbol{x}}-e_{\boldsymbol{x}'})^j-\delta^{ij}, \tag{7.11}
$$

$$
\begin{aligned}
\beta =& \frac{16c(t'-t)\tilde{r}}{(\tilde{r}^2-c^2(t'-t)^2)^3} \\
&+\mathrm{i}\pi\left[\frac{\ddot{\delta}(\tilde{r}-c(t'-t))+\ddot{\delta}(\tilde{r}+c(t'-t))}{\tilde{r}^2} - \frac{\dot{\delta}(\tilde{r}-c(t'-t))+\dot{\delta}(\tilde{r}+c(t'-t))}{\tilde{r}^3}\right].
\end{aligned}
\tag{7.12}
$$

These results can be confirmed for the real part in [155, Ch. 9] and for the imaginary part [52, Ch. 3] (by noting that that the imaginary part of the Wightman function corresponds to the commutators of the respective fields).

Calculation in the COM/Lab Frame

Let us first calculate the transition probability assuming that the atom is at rest in the lab frame. Without loss of generality we can assume that rest and lab frame are identical, i.e. $(t,\boldsymbol{x})=(\tau,\boldsymbol{\xi})$. We can then perform a perturbative analysis and compute the Dyson series of the time evolution operator to first order:

$$
\hat{\mathcal{U}} = \mathbb{1} + \hat{\mathcal{U}}^{(1)} + \mathcal{O}\left(e^2\right), \tag{7.13}
$$

where, as usual, $\hat{\mathcal{U}}^{(1)} = -\frac{\mathrm{i}}{\hbar}\int_{-\infty}^{\infty} \mathrm{d}t \hat{H}_I^{\mathrm{eff,\,t}}$. The vacuum excitation probability for the initial joint ground state reads

$$\begin{aligned}
\mathcal{P} &= \sum\!\!\!\!\!\!\int_{\text{out}} |\,\langle 2p_z, \text{out}|\hat{\mathcal{U}}|1s,0\rangle\,|^2 \\
&= \sum\!\!\!\!\!\!\int_{\text{out}} \langle 1s,0|\hat{\mathcal{U}}^{(1)\dagger}|2p_z,\text{out}\rangle\ \langle 2p_z,\text{out}|\hat{\mathcal{U}}^{(1)}|1s,0\rangle + \mathcal{O}\left(e^4\right) \\
&= \frac{e^2}{\hbar^2}\int_{\mathbb{R}}\mathrm{d}t\int_{\mathbb{R}}\mathrm{d}t'\,\chi(t)\chi(t')e^{\mathrm{i}\Omega_{2p_z1s}(t'-t)}\int_{\mathbb{R}^3}\mathrm{d}^3\boldsymbol{x}\int_{\mathbb{R}^3}\mathrm{d}^3\boldsymbol{x}'\,\boldsymbol{F}_{2p_z1s,i}(\boldsymbol{x})W_E^{ij}[t,t';\boldsymbol{x},\boldsymbol{x}']\boldsymbol{F}_{2p_z1s,j}(\boldsymbol{x}') \\
&\quad + \mathcal{O}\left(e^4\right), \qquad (7.14)
\end{aligned}$$

where we used the resolution of identity in terms of the field states $|\text{out}\rangle$. Using Eq. (7.5), we can write

$$\begin{aligned}
\mathcal{P} = \frac{e^2 c}{2(2\pi)^3\epsilon_0\hbar}\int_{\mathbb{R}^3}\mathrm{d}^3\boldsymbol{k}\,|\boldsymbol{k}|\left|\int_{\mathbb{R}}\mathrm{d}t\,\chi(t)e^{-\mathrm{i}(\Omega_{2p_z1s}+c|\boldsymbol{k}|)t}\right|^2 \\
\times\left[\left|\int_{\mathbb{R}^3}\mathrm{d}^3\boldsymbol{x}\,e^{\mathrm{i}\boldsymbol{k}\cdot\boldsymbol{x}}\boldsymbol{F}_{2p_z1s}(\boldsymbol{x})\right|^2 - \left|\int_{\mathbb{R}^3}\mathrm{d}^3\boldsymbol{x}\,e^{\mathrm{i}\boldsymbol{k}\cdot\boldsymbol{x}}\boldsymbol{F}_{2p_z1s}(\boldsymbol{x})\cdot\boldsymbol{e}_{\boldsymbol{k}}\right|^2\right] + \mathcal{O}\left(e^4\right).
\end{aligned}$$

For simplicity and also comparison with results from Chapter 3, we can further assume that the time-dependent coupling is of Gaussian adiabatic nature, i.e. $\chi(t) = \exp(-(t/\sigma)^2)$ with σ being the time scale of interaction. The calculation parallels the one from Appendix A.1, where we use Eq. (7.8) and (7.9), and the fact that for $f_{lm} \in \mathbb{C}$ it is satisfied that (by use of Parseval's theorem)

$$\int_{S^2}\mathrm{d}\Theta_k\left|\sum_{l=0}^{\infty}\sum_{m=-l}^{l} f_{lm}Y_{lm}(\boldsymbol{e}_{\boldsymbol{k}})\right|^2 = \sum_{l=0}^{\infty}\sum_{m=-l}^{l}|f_{lm}|^2\,. \qquad (7.15)$$

The probability can then be evaluated to

$$\mathcal{P} = 49152\frac{(ea_0\sigma)^2 c}{\pi\hbar\epsilon_0}\int_0^{\infty}\mathrm{d}|\boldsymbol{k}|\frac{|\boldsymbol{k}|^3 e^{-\frac{1}{2}\sigma^2(c|\boldsymbol{k}|+\Omega_{2p_z1s})^2}}{\left(4a_0^2|\boldsymbol{k}|^2+9\right)^6} + \mathcal{O}\left(e^4\right). \qquad (7.16)$$

Using natural units for a hydrogen atom (the generalization to an hydrogenoid atom is straightforward) with $c = \hbar = \epsilon_0 = 1, e \approx 137^{-1/2}$, $a_0 \approx 2.68\times10^{-4}$ eV^{-1}, $\Omega_{2pz1s} \approx 10.2$ eV, we plot the vacuum excitation probability in Fig. 7.1 which will be our reference point for the calculations of the next section.

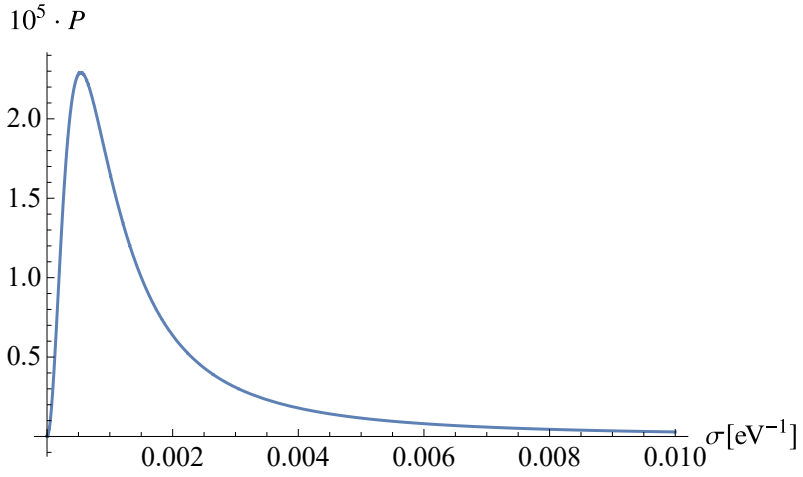

Figure 7.1: Rescaled vacuum excitation probability to the first excited state $2p_z$ for a stationary hydrogen atom and stationary observer as a function of the time scale of the interaction σ ($e \approx 137^{-1/2}$, $a_0 \approx 2.68 \times 10^{-4}$ eV^{-1}, and $\Omega_{2p_z 1s} \approx 10.2$ eV).

Calculation for a Boosted Observer

Now we will compare the previous result with the probability as computed by an observer that moves in the z direction as seen from the lab frame with velocity v. This corresponds to a Lorentz boost in the z direction, i.e. $\{c\tau = \cosh\eta\, ct - \sinh\eta\, x_3, \xi_3 = \cosh\eta\, x_3 - \sinh\eta\, ct\}$ with rapidity η. As the electric field transforms via (7.3), the electric-field Wightman tensor in the probability expression of (7.14) transforms as,

$$
\begin{aligned}
&W_E^{ij}[t,t';\boldsymbol{x},\boldsymbol{x}'] \rightarrow \\
&\gamma^2\Big(W_E^{ij}[t,t';\boldsymbol{x},\boldsymbol{x}'] + \epsilon_{abi}\epsilon_{cdj}v^a v^c W_B^{bd}[t,t';\boldsymbol{x},\boldsymbol{x}'] + \epsilon_{abi}v_a W_{BE}^{bj}[t,t';\boldsymbol{x},\boldsymbol{x}'] \\
&\quad + \epsilon_{cdj}v^c W_{EB}^{id}[t,t';\boldsymbol{x},\boldsymbol{x}']\Big) + (1-\gamma)^2 (e_v)_a (e_v)_b W_E^{ab}[t,t';\boldsymbol{x},\boldsymbol{x}'](e_v)^i (e_v)^j \\
&+ \gamma(1-\gamma)\Big[W_E^{ia}[t,t';\boldsymbol{x},\boldsymbol{x}'](e_v)_a(e_v)^j + W_E^{aj}[t,t';\boldsymbol{x},\boldsymbol{x}'](e_v)_a(e_v)^i + \epsilon_{abi}v^a W_{BE}^{bc}[t,t';\boldsymbol{x},\boldsymbol{x}'] \\
&\quad + \epsilon_{cdj}v^c W_{EB}^{ad}[t,t';\boldsymbol{x},\boldsymbol{x}'](e_v)_a(e_v)^i\Big].
\end{aligned}
\tag{7.17}
$$

We can then use $v_a = v\delta_{a3}$, and the relations (7.5), (7.6) and (7.7) to arrive at

$$
W_E[t,t';\boldsymbol{x},\boldsymbol{x}'] \rightarrow \frac{\hbar c}{2\epsilon_0}\int_{\mathbb{R}^3}\frac{\mathrm{d}^3\boldsymbol{k}}{(2\pi)^3}|\boldsymbol{k}|e^{-\mathrm{i}c|\boldsymbol{k}|(t-t')}e^{\mathrm{i}\boldsymbol{k}\cdot(\boldsymbol{x}-\boldsymbol{x}')}M, \tag{7.18}
$$

where

$$M = \begin{pmatrix} \gamma^2\left(1-e^3_{\boldsymbol{k}}\frac{v}{c}\right)^2 - e^1_{\boldsymbol{k}}e^1_{\boldsymbol{k}} & -e^1_{\boldsymbol{k}}e^2_{\boldsymbol{k}} & \gamma e^1_{\boldsymbol{k}}\left(\frac{v}{c}-e^3_{\boldsymbol{k}}\right) \\ -e^1_{\boldsymbol{k}}e^2_{\boldsymbol{k}} & \gamma^2\left(1-e^3_{\boldsymbol{k}}\frac{v}{c}\right)^2 - e^2_{\boldsymbol{k}}e^2_{\boldsymbol{k}} & \gamma e^2_{\boldsymbol{k}}\left(\frac{v}{c}-e^3_{\boldsymbol{k}}\right) \\ \gamma e^1_{\boldsymbol{k}}\left(\frac{v}{c}-e^3_{\boldsymbol{k}}\right) & \gamma e^2_{\boldsymbol{k}}\left(\frac{v}{c}-e^3_{\boldsymbol{k}}\right) & 1-e^3_{\boldsymbol{k}}e^3_{\boldsymbol{k}} \end{pmatrix}. \tag{7.19}$$

The excitation probability therefore becomes

$$\begin{aligned}\mathcal{P} =& \frac{e^2 c}{2\epsilon_0\hbar}\int_{\mathbb{R}^3}\frac{\mathrm{d}^3\boldsymbol{k}}{(2\pi)^3}|\boldsymbol{k}|\iint_{\mathbb{R}^2}\mathrm{d}t\mathrm{d}t' e^{-\mathrm{i}c|\boldsymbol{k}|(t-t')}\iint_{\mathbb{R}^6}\mathrm{d}^3\boldsymbol{x}\mathrm{d}^3\boldsymbol{x}' e^{\mathrm{i}\boldsymbol{k}\cdot(\boldsymbol{x}-\boldsymbol{x}')}\chi(\tau(t,\boldsymbol{x}))\chi(\tau(t',\boldsymbol{x}')) \\ & \times e^{\mathrm{i}\Omega_{2p_z1s}(\tau(t',\boldsymbol{x}')-\tau(t,\boldsymbol{x}))}\boldsymbol{F}_{2p_z1s}(\boldsymbol{\xi}(t,\boldsymbol{x}))\cdot M\cdot\boldsymbol{F}_{2p_z1s}(\boldsymbol{\xi}(t',\boldsymbol{x}'))+\mathcal{O}\left(e^4\right).\end{aligned} \tag{7.20}$$

With the change of variables $\{ct = \cosh\eta\, c\tau + \sinh\eta\,\xi_3, x_3 = \cosh\eta\,\xi_3 + \sinh\eta\, c\tau\}$ (applied twice), which is equivalent to the inverse Lorentz transformation (and thus non-singular), we get exactly the same result as in the proper frame of the atom for the transition probability in Eq. (7.16). Similarly one can check numerically that Eq. (7.20) reproduces Fig. 7.1. It is clear then that, since the model is covariant, choosing a convenient frame (the atomic rest frame in this example) significantly simplifies the calculations.

7.2 Implications for the Unruh-DeWitt Model

One of the most common scalar approximations to the light-matter interaction is the UDW model presented in Section 2.1. This model can certainly approximate the interaction under the effective dipole model where we consider a 'heavy' atom with a classical COM even when the atomic motion is relativistic as discussed in a number of previous papers [26, 58, 24].

For the effective dipole model, we can always describe the interaction in the comoving frame of the atom where there would be no Röntgen term, and the corresponding Röntgen terms in other frames emerge out of the reference frame transformations as described in Sec. 7.1. However, after the analysis of the dynamics of the atomic COM and the internal degrees of freedom of the atom, one may wonder whether the usual scalar approximations to the light-matter interaction (such as the UDW model) can be 'upgraded' to phenomenologically capture (still with a simple scalar model) the effect of the missing Röntgen terms outside of the 'infinitely heavy' proton approximation of the effective dipole model. This is particularly relevant when one has a quantum COM which is necessarily delocalized in momentum as momentum eigenstates are nonphysical.

Based on the interaction Hamiltonian (6.36) we propose the following scalar analogue of the dipole interaction:

$$\hat{H}_{\text{Scalar}} = \hat{H}_{\text{mono}} + \hat{H}_{\text{Rö}}. \tag{7.21}$$

That is, the sum of a monopole moment like in the UDW model and a scalar-analogue Röntgen term. This monopole term has the peculiarity that spatial localization is given in terms of the COM wavefunction (as was also argued in [130]). The new monopole interaction then reads

$$\hat{H}_{\text{mono}} = \hbar c \lambda \hat{\mu} \otimes \int_{\mathbb{R}^3} \mathrm{d}^3\boldsymbol{R}\; \hat{\phi}(\boldsymbol{R})\, |\boldsymbol{R}\rangle\langle\boldsymbol{R}| \,. \tag{7.22}$$

We also need to add an effective coupling of the internal, COM, and field degrees of freedom mimicking the Röntgen interaction of (6.36). This interaction is vectorial in its core, so it is very difficult to capture its behaviour in a scalar model. As we will see, a qubit UDW detector is not naturally well-suited to build such an analogy outside the 1+1-dimensional case. Further, we need an analogue of the magnetic field operator to build up our Röntgen facsimile.

Our analogy starts with the $D+1$ dimensional scalar field as an expansion in plane wave modes

$$\hat{\phi}(t,\boldsymbol{x}) = \int \frac{\mathrm{d}^D\boldsymbol{k}}{(2\pi)^{D/2}} \sqrt{\frac{c}{2\omega}} \left(e^{-\mathrm{i}\omega t + \mathrm{i}\boldsymbol{k}\cdot\boldsymbol{x}} \hat{a}_{\boldsymbol{k}} + \text{H.c.}\right) \tag{7.23}$$

and the electric field (2.18). We have also a relation between the magnetic and electric field through the Maxwell equation $\partial_0 \hat{\boldsymbol{E}} = c\boldsymbol{\nabla} \times \hat{\boldsymbol{B}}$ (without external currents). Finding a scalar analogue of this equation that is so remarkably vectorial in nature will come at the price of some ambiguities and choices in the model. From the Heisenberg equation of motion we know that $\partial_0 \hat{\phi} = \hat{\pi}$, where

$$\hat{\pi}(t,\boldsymbol{x}) = -\int \frac{\mathrm{d}^D\boldsymbol{k}}{(2\pi)^{D/2}} \sqrt{\frac{\omega}{2c}} \left(\mathrm{i}e^{-\mathrm{i}\omega t + \mathrm{i}\boldsymbol{k}\cdot\boldsymbol{x}} \hat{a}_{\boldsymbol{k}} + \text{H.c.}\right) \tag{7.24}$$

is the canonical momentum operator to $\hat{\phi}$. As there is necessarily a limitation in the alignment of scalar and vector theory, we suggest here to find an operator $\boldsymbol{\nabla}\hat{X}$ mimicking the magnetic field such that $\hat{\pi} = c\,(\boldsymbol{\nabla}\hat{X}) \cdot \boldsymbol{\epsilon}$ is satisfied, for some spatial direction $\boldsymbol{\epsilon}$.

In $1+1$ dimensions it is straightforward to find the operator

$$\partial_x \hat{X}(t,\boldsymbol{x}) = -\partial_x \hat{\phi}(t,\boldsymbol{x}), \tag{7.25}$$

being nothing else than the spatial derivative of the field operator itself. Therefore, an analogous construction in $1+1$ dimensions for the Röntgen term of the UDW model would read

$$\hat{H}_{\text{Rö}} = -\hbar c\tilde{\lambda} \int_{\mathbb{R}} \mathrm{d}R \left\{ \frac{\hat{P}}{2M}, \hat{\mu} \cdot \partial_R \hat{\phi}(R) \right\}_+ |R\rangle\langle R| \,, \tag{7.26}$$

where we introduced the coupling constant $\tilde{\lambda}$ with units $[\tilde{\lambda}] = [\lambda]/T$ – this additional factor of time T is needed for the correct dimensionality.

To better capture an analogy to the Röntgen term in 3+1 dimensions let us model from here on the internal detector degrees of freedom through a quantum harmonic oscillator (as it is also common for UDW detectors [156, 157, 158, 159, 160]) with respective position and momentum operators $\hat{\boldsymbol{q}}$ and $\hat{\boldsymbol{p}}_q$. We suggest then that our analogue magnetic field should be $-\boldsymbol{\nabla}\hat{\phi}$. Therefore, an analogous construction for the Röntgen term of the UDW model could be

$$\hat{H}_{\text{Rö}} = -\hbar c\tilde{\lambda} \int_{\mathbb{R}^3} \mathrm{d}^3\boldsymbol{R} \left\{ \frac{\hat{\boldsymbol{P}}}{2M}, \hat{\boldsymbol{q}} \times \boldsymbol{\nabla}_{\boldsymbol{R}} \hat{\phi}(\boldsymbol{R}) \right\}_+ |\boldsymbol{R}\rangle\langle\boldsymbol{R}| \,. \tag{7.27}$$

Notice that, same as in the full non-relativistic light-matter interaction of Chapter 6 this term couples the internal degrees of freedom of the atom simultaneously with both the COM degrees of freedom and the field. This coupling cannot be expected to be any less significant for relativistic studies where the relativistic corrections induce additional couplings between all these degrees of freedom. Adding to the usual monopole coupling a term analogous to the Röntgen dynamics is thus necessary if one wants to mimic light-matter interactions where the COM is treated as a quantum degree of freedom.

The particular choice for the scalar Röntgen term depends on the properties of the full electromagnetic theory one wishes to study. After all, the scalar simplification cannot account for all the properties at once. In particular, the choice of (7.27) does not have the correct behavior under the parity operator. One could remedy this by replacing the operator $\hat{\boldsymbol{q}}$ by an axial vector such as the detector's orbital angular momentum. On the other hand, this would require us to couple different detector degrees of freedom in the dipole and Röntgen analogue terms, respectively. Other choices for the relevant detector degrees of freedom and for an analogue for the magnetic field operator are possible and depend on the specific purposes of the intended study.

7.3 Summary

In this final chapter, we revisited the usefulness of effective models with a classical atomic COM. We recognized that, even though we neglect atomic dynamics related to the COM degrees of freedom, we have a means to study relativistic setups in a qualitative fashion. In particular, we showed for the effective dipole model that predictions are covariant under changes of reference frames. Even though we neglected the Röntgen interaction in the beginning, a classical analogue naturally arises after transforming from the COM frame to any non-comoving frame. In that context, we gave an account of all the different electromagnetic Wightman functions. Further, the property of covariance allowed us to compute observables in a suitably simple frame. Lastly, we gave a scalar-analogue model for the Röntgen interaction which can be incorporated into the UDW model. After all, the UDW model is supposed to be the simplified version of the dipolar interaction and should incorporate all the leading order effects when considering a quantum COM.

Chapter 8

Conclusions

In this thesis, we studied common Hamiltonian models of quantum optics and RQI with a special focus on approximations within and comparison between models – in particular under relativistic considerations. In Chapter 2 we gave an account of common light-matter interaction models of quantum optics and RQI when the atomic COM is treated as a classical degree of freedom. We saw that the dipolar coupling Hamiltonian is of central relevance in the study of light-matter interactions. It allows us to derive quantum optical models like the Jaynes-Cummings and Dicke model after performing a number of simplifications – in particular the rotating-wave and single-mode approximation. We also connected the dipolar coupling to the UDW model that serves as the most common tool in RQI by neglecting the vector degrees of freedom of electromagnetism. In this chapter it should have become clear that the usefulness of these effective models, and especially in comparison to the dipole model, relies strongly on the validity of the employed simplifications. The single-mode and the rotating-wave approximation require special attention, not least due to their wide-spread use in the literature.

Chapter 3 was then devoted to the study of quantum randomness generation in free space within the dipole model. We argued that a rotating-wave approximation would lead to the intuition that the ground state is generally the most preferable state to generate quantum randomness. We saw, appropriately, that for adiabatic coupling processes the atomic ground state only is the best choice for long interaction times (as is congruent with the approximation). However, in the case of non-adiabatic processes the equal superposition of two particular atomic states is, even for long times, the optimal choice. We then compared the dipole interaction predictions to two different UDW coupling prescriptions – the usual UDW model and a derivative coupling. Importantly, both models agreed with the dipole model for long interaction times. For short times, however, in the studied ex-

ample the derivative coupling deviated significantly by up to around 40 %. This favors the standard UDW model as an analogue to the electromagnetic dipole coupling – at least in this example scenario. More importantly though, it shows that scalar analogue models can mimic the dipole model astonishingly well under the right choice of conditions.

In Chapter 4 we focused on atoms traversing an optical cavity. We investigated a number of different simplifications that are commonly applied in the context of cavities. Firstly, we examined the single-mode approximation for accelerated and constant-velocity detectors. We found that the single-mode approximation can only be justified for non-relativistic atomic trajectories when considering de-excitation processes. Due to Doppler shifts, selecting one or a few field modes is never warranted in relativistic regimes. For initial ground-state detectors, on the other hand, the single-mode approximation cannot even be justified in the non-relativistic regime. Distinctively, for detectors with constant velocities we discovered that mode invisibility can, already in the non-relativistic regime for de-excitation processes, hamper the approximation, and special care is needed for the specific parameters under consideration. Further, we studied the non-relativistic approximation and found that, for any detector acceleration, only modes with sufficiently low quantum numbers are accurately described. Indeed, high-energy modes observe a diverging relative error.

The results of this chapter become particularly relevant considering that there are proposals to assess Unruh and Hawking effect-related phenomena using atoms and optical cavities. The main point is that some of the most common approximations made in quantum optics have to be questioned for any experiments involving relativistic effects – but possibly already for non-relativistic regimes.

In Chapter 5, we examined the question of whether a very long and thin cavity can be described by a one-dimensional system. We showed that one can recast (without any approximation) the higher dimensional quantum field inside the cavity as an infinite sum of lower dimensional fields with effective masses – which we call subfields. The dimensional reduction approximation is therefore identified with ignoring all but one of these subfields. We observed further that any truncation of the subfield sum results in the modification of the detector's spatial profile. Coming back to the geometry from Chapter 4, we showed under which circumstances we can truncate the sum to reconstruct the full transition probabilities. In particular, we found that the non-adiabaticity of the coupling, the detector's resonance with a subfield, and the detector's spatial profile as well as its trajectory can spoil the validity of the approximation. Importantly, this means that only in very few select scenarios one can actually do a "naive", i.e. with a single-subfield, dimensional reduction approximation. Using a single *massless* 1+1 dimensional field is, however, *a priori* ill-suited to describe higher dimensional cavity fields that do not have a zero mode.

We believe the tools of this chapter can be adopted in quantum optics as a quantifiable standard by which dimensional reduction approximations are justified. Moreover, we believe that the connection between a cavity's transverse geometry and the effective mass of the subfields deserves further study. For instance, consider detecting the shape (or defects in the shape) of optical cavities: suppose that one has developed a protocol for estimating the masses of $1+1$ dimensional fields from measurements of localized detectors coupled to these fields. This exact same protocol applied to localized detectors in a $3+1$ dimensional cavity would yield detailed information about the cavity's transverse shape.

Finally, in Chapter 6, we included the quantum nature of the atomic COM in the description of light-matter interactions. The goal of this chapter was to highlight 1) the gauge subtleties of a fully quantized atom, and 2) the usually neglected interaction terms that are leading order and of relevance when including COM dynamics, such as the Röntgen term. We examined in detail the different parts of the derivation of the multipolar Hamiltonian at the lowest order approximation, i.e. the dipole interaction, for non-relativistic COM motion. We showed that there exists no gauge transformation from the two-particle minimal coupling to the multipolar Hamiltonian, and argued that the resulting representation is physically motivated: in it we can interpret the interaction as a hydrogen-like atom which is perturbed by the quantum electromagnetic field. Further, we discussed the individual terms and explained that at leading order the dipole term is accompanied by the Röntgen term, which entangles all atomic and field degrees of freedom. In particular, we argued that the Röntgen term cannot be avoided through a choice of reference frame in the quantized COM case. At the example of transition rates, we showed that COM delocalization and the Röntgen term modify physical observables. Significantly, even if we assume that the atomic COM is initially in an unphysical momentum eigenstate, observable predictions are affected by the Röntgen term for any non-degenerate atomic transition.

In the final chapter, Chapter 7, we revisited the effective light-matter models and examined how they can keep their status as useful tools in the study of light-matter interaction. We showed that they can be used to consider relativistic trajectories of atoms in a simple way – given one accepts the implications of neglecting part of the atomic dynamics and using a classical COM. We observed that the effective dipole model produces Lorentz-covariant predictions under changes of reference frame, which is in contrast to the non-relativistic multipolar Hamiltonian that obeys only Galilei invariance. Crucially, this provides the means to study relativistic atomic trajectories beyond scalar models and allows us to consider more general physical processes that, for instance, involve the exchange of angular momentum between an atom and the EM field. In the context of scalarized theories, we argued that the UDW model should be viewed as the analogue to the leading order interaction of the multipolar Hamiltonian. Consequently, we proposed a modification

to the standard UDW model to account for COM dynamics induced by the Röntgen term which is at the same order as the dipole term. Even though this required assumptions in the analogy between scalar and EM model, it will allow us to study the Röntgen term in a simplified setting whilst keeping its key features. Concerning RQI, we anticipate that the Röntgen term will be of importance when, for example, studying vacuum entanglement harvesting, i.e. the process where space-like separated atoms become entangled by interacting locally with a quantum field in its vacuum state, see for instance [45, 46, 131, 147]. In particular, even for initially well-localized atoms, we expect that entanglement harvesting will be suppressed as compared to results that assumed a classical atomic COM.

Modifications to the UDW model beyond the non-relativistic dipole approximation may be pursued in different directions. As we presented in Sec. 6.3 a subleading correction term to the multipolar Hamiltonian, an analogue to the Darwin Hamiltonian may be built. This, however, cannot yield a fully relativistic treatment and would favor instead a non-perturbative treatment to allow for ultra-relativistic regimes. Further, spin degrees of freedom have been neglected due to their sub-leading effects. They are expected, of course, to be relevant in relativistic regimes. Here, a scalar analogue along the lines of a Breit Hamiltonian [141] and [142, Ch. 2] may be of promising nature.

The purpose of this thesis was to deliver a detailed link between simple particle detector models – commonly applied in quantum field theory in curved and flat spacetimes as well as in RQI – and atomic physics by pointing out the subtleties of approximations, gauge transformations and the choice of physical variables. Further, we investigated the influence of quantum COM delocalization on light-matter interactions to understand the phenomenology that has thus far been neglected in effective models. Additional studies are expected to focus further, e.g. [161], on the impact that a delocalized atom has on protocols in RQI. In summary, the essence of this thesis is to understand the impact and limitations of approximations that are frequently or implicitly part of many models in quantum optics and RQI. These simplifications, as we saw throughout, cannot be justified in many different scenarios. On the one hand, approximations often break down in relativistic regimes, which we may associate with very short interaction times as compared to the internal atomic dynamics. This was the case for the rotating-wave, single-mode approximation and the dimensional reduction as well. However, even in non-relativistic regimes these assumptions may not be adequate. This depends to a large degree on the dynamics, in particular on the specific physical observable we are interested in and how non-adiabatic the process is. On the other hand, the assumption of a classical COM is only commensurate with the fully quantized model in the limit of an infinitely heavy atomic mass. Therefore, in real-life setups the Röntgen term is always required at the dipole level in order to ensure physically consistent predictions, as already pointed out in [37, 38]. Naturally, considering

that every approximation has its limit, the issue of how complicated our models must be arises. Are minuscule correction terms worth a greatly enhanced model complexity? We might respond to this in two ways. First, these small correction terms often hide novel and fascinating physics – not to speak of model consistencies, such as causality, that may be broken by approximations. And second, it was exactly the purpose of this thesis to bring attention to these details. Assumptions may become so implicit in our models that rarely the need to question them emerges. After all, they may be necessary to allow for simple order-of-magnitude predictions but at the same time the regime of validity must be kept in mind. In the end, in our investigation of these approximations we frequently had to simplify matters ourselves, such as assuming a non-relativistic COM or point-like detectors. And it is clear that the implications of those choices need to be considered in detail as well.

References

[1] R. Lopp and E. Martín-Martínez. "Quantum delocalization, gauge, and quantum optics: Light-matter interaction in relativistic quantum information". In: *Phys. Rev. A* 103.1 (2021), p. 013703. DOI: 10.1103/PhysRevA.103.013703.

[2] R. Lopp and E. Martín-Martínez. "Light, matter, and quantum randomness generation: A relativistic quantum information perspective". In: *Opt. Commun.* 423 (2018), pp. 29–47. DOI: 10.1016/j.optcom.2018.03.056.

[3] R. Lopp, E. Martín-Martínez, and D. N. Page. "Relativity and quantum optics: accelerated atoms in optical cavities". In: *Class. Quantum Gravity* 35.22 (2018), p. 224001. DOI: 10.1088/1361-6382/aae750.

[4] D. Grimmer, R. Lopp, and E. Martín-Martínez. "Dimensional reduction of cavities with axial symmetry: Are optical fibers really one-dimensional?" In: *ArXiv e-prints* (2021). arXiv: 2104.00745.

[5] N. Bohr. "I. On the constitution of atoms and molecules". In: *Philos. Mag.* 26.151 (1913), pp. 1–25. DOI: 10.1080/14786441308634955.

[6] N. Bohr. "The Spectra of Helium and Hydrogen". In: *Nature* 92.2295 (1913), pp. 231–232. DOI: 10.1038/092231d0.

[7] P. Dirac. "The quantum theory of the electron". In: *Proc. R. Soc. Lond. A* 117.778 (1928), pp. 610–624. DOI: 10.1098/rspa.1928.0023.

[8] W. Lamb and R. Retherford. "Fine Structure of the Hydrogen Atom by a Microwave Method". In: *Phys. Rev.* 72.3 (1947), pp. 241–243. DOI: 10.1103/PhysRev.72.241.

[9] W. Heitler. *The quantum theory of radiation*. Vol. 5. International Series of Monographs on Physics. Oxford: Oxford University Press, 1936.

[10] H. J. Kimble and L. Mandel. "Theory of resonance fluorescence". In: *Phys. Rev. A* 13.6 (1976), pp. 2123–2144. DOI: 10.1103/PhysRevA.13.2123.

[11] H. J. Carmichael and D. F. Walls. "A quantum-mechanical master equation treatment of the dynamical Stark effect". In: *J. Phys. B: At. Mol. Opt. Phys.* 9.8 (1976), pp. 1199–1219. DOI: 10.1088/0022-3700/9/8/007.

[12] H. J. Kimble, M. Dagenais, and L. Mandel. "Photon Antibunching in Resonance Fluorescence". In: *Phys. Rev. Lett.* 39.11 (1977), pp. 691–695. DOI: 10.1103/PhysRevLett.39.691.

[13] D. Meschede, H. Walther, and G. Müller. "One-Atom Maser". In: *Phys. Rev. Lett.* 54.6 (1985), pp. 551–554. DOI: 10.1103/PhysRevLett.54.551.

[14] M. Weidinger et al. "Trapping States in the Micromaser". In: *Phys. Rev. Lett.* 82.19 (1999), pp. 3795–3798. DOI: 10.1103/PhysRevLett.82.3795.

[15] Y. Mu and C. M. Savage. "One-atom lasers". In: *Phys. Rev. A* 46.9 (1992), pp. 5944–5954. DOI: 10.1103/PhysRevA.46.5944.

[16] J. McKeever et al. "Experimental realization of a one-atom laser in the regime of strong coupling". In: *Nature* 425.6955 (2003), pp. 268–271. DOI: 10.1038/nature01974.

[17] P. Lougovski et al. "Strongly driven one-atom laser and decoherence monitoring". In: *Phys. Rev. A* 76.3 (2007), p. 033802. DOI: 10.1103/PhysRevA.76.033802.

[18] H. Walther. "Entanglement and superposition states in the micromaser". In: *Phil. Trans. R. Soc. A* 355.1733 (1997), pp. 2343–2351. DOI: 10.1098/rsta.1997.0131.

[19] W. Paul and H. Steinwedel. *Verfahren zur Trennung bzw. zum getrennten Nachweis von Ionen verschiedener spezifischer Ladung*. DE 944900, 1953.

[20] C. Yu et al. "Atom-Interferometry Measurement of the Fine Structure Constant". In: *Ann. Phys.* 531.5 (2019), p. 1800346. DOI: 10.1002/andp.201800346.

[21] J. B. Fixler et al. "Atom Interferometer Measurement of the Newtonian Constant of Gravity". In: *Science* 315.5808 (2007), pp. 74–77. DOI: 10.1126/science.1135459.

[22] W. G. Unruh. "Notes on black-hole evaporation". In: *Phys. Rev. D* 14.4 (1976), pp. 870–892. DOI: 10.1103/PhysRevD.14.870.

[23] B. DeWitt. *General Relativity: an Einstein Centenary Survey*. Cambridge University Press, edited by S. W. Hawking and W. Israel, 1979.

[24] A. Pozas-Kerstjens and E. Martín-Martínez. "Entanglement harvesting from the electromagnetic vacuum with hydrogenlike atoms". In: *Phys. Rev. D* 94.6 (2016), p. 064074. DOI: 10.1103/PhysRevD.94.064074.

[25] Á. M. Alhambra, A. Kempf, and E. Martín-Martínez. "Casimir forces on atoms in optical cavities". In: *Phys. Rev. A* 89.3 (2014), p. 033835. DOI: 10.1103/PhysRevA.89.033835.

[26] E. Martín-Martínez, M. Montero, and M. del Rey. "Wavepacket detection with the Unruh-DeWitt model". In: *Phys. Rev. D* 87.6 (2013), p. 064038. DOI: 10.1103/PhysRevD.87.064038.

[27] S. A. Fulling. "Nonuniqueness of Canonical Field Quantization in Riemannian Space-Time". In: *Phys. Rev. D* 7.10 (1973), pp. 2850–2862. DOI: 10.1103/PhysRevD.7.2850.

[28] P. C. W. Davies. "Scalar production in Schwarzschild and Rindler metrics". In: *J. Phys. A: Math. Gen.* 8.4 (1975), p. 609. DOI: 10.1088/0305-4470/8/4/022.

[29] S. Grundmann et al. "Zeptosecond birth time delay in molecular photoionization". In: *Science* 370.6514 (2020), pp. 339–341. DOI: 10.1126/science.abb9318.

[30] M. Goeppert-Mayer. "Über Elementarakte mit zwei Quantensprüngen". In: *Ann. Phys.* 401.3 (1931), pp. 273–294. DOI: 10.1002/andp.19314010303.

[31] M. Babiker and R. Loudon. "Derivation of the Power-Zienau-Woolley Hamiltonian in quantum electrodynamics by gauge transformation". In: *Proc. R. Soc. A* 385.1789 (1983), pp. 439–460. DOI: 10.1098/rspa.1983.0022.

[32] E. T. Jaynes and F. W. Cummings. "Comparison of quantum and semiclassical radiation theories with application to the beam maser". In: *Proc. IEEE* 51.1 (1963), pp. 89–109. DOI: 10.1109/PROC.1963.1664.

[33] H. Paul. "Induzierte Emission bei starker Einstrahlung". In: *Ann. Phys.* 466.7-8 (1963), pp. 411–412. DOI: 10.1002/andp.19634660710.

[34] D. H. Kobe and R. D. Gray. "Operator gauge transformations in nonrelativistic quantum electrodynamics: Application to the multipolar Hamiltonian". In: *Il Nuovo Cimento B* 86 (1985), pp. 155–170. DOI: 10.1007/BF02721529.

[35] M. O. Scully and M. S. Zubairy. *Quantum Optics*. Cambridge University Press, 1997. DOI: 10.1017/CBO9780511813993.

[36] C. Baxter, M. Babiker, and R. Loudon. "Canonical approach to photon pressure". In: *Phys. Rev. A* 47.2 (1993), pp. 1278–1287. DOI: 10.1103/PhysRevA.47.1278.

[37] M. Wilkens. "Spurious velocity dependence of free-space spontaneous emission". In: *Phys. Rev. A* 47.1 (1993), pp. 671–673. DOI: 10.1103/PhysRevA.47.671.

[38] M. Wilkens. "Significance of Röntgen current in quantum optics: Spontaneous emission of moving atoms". In: *Phys. Rev. A* 49.1 (1994), pp. 570–573. DOI: 10.1103/PhysRevA.49.570.

[39] M. Sonnleitner, N. Trautmann, and S. M. Barnett. "Will a Decaying Atom Feel a Friction Force?" In: *Phys. Rev. Lett.* 118.5 (2017), p. 053601. DOI: 10.1103/PhysRevLett.118.053601.

[40] R. D. Sorkin. "Impossible measurements on quantum fields". In: *Directions in General Relativity: An International Symposium in Honor of the 60th Birthdays of Dieter Brill and Charles Misner*. Cambridge University Press, 1993, pp. 293–305.

[41] D. M. T. Benincasa et al. "Quantum information processing and relativistic quantum fields". In: *Class. Quantum Gravity* 31.7 (2014), p. 075007. DOI: 10.1088/0264-9381/31/7/075007.

[42] H. Halvorson and R. Clifton. "No Place for Particles in Relativistic Quantum Theories?" In: *Ontological Aspects of Quantum Field Theory*. Ed. by M. Kuhlmann, H. Lyre, and A. Wayne. World Scientific, 2002. Chap. 10. DOI: 10.1142/5117.

[43] P. Candelas and D. W. Sciama. "Irreversible Thermodynamics of Black Holes". In: *Phys. Rev. Lett.* 38.23 (1977), pp. 1372–1375. DOI: 10.1103/PhysRevLett.38.1372.

[44] G. W. Gibbons and S. W. Hawking. "Cosmological event horizons, thermodynamics, and particle creation". In: *Phys. Rev. D* 15.10 (1977), pp. 2738–2751. DOI: 10.1103/PhysRevD.15.2738.

[45] A. Valentini. "Non-local correlations in quantum electrodynamics". In: *Phys. Lett. A* 153.6 (1991), pp. 321–325. DOI: 10.1016/0375-9601(91)90952-5.

[46] A. Pozas-Kerstjens and E. Martín-Martínez. "Harvesting correlations from the quantum vacuum". In: *Phys. Rev. D* 92.6 (2015), p. 064042. DOI: 10.1103/PhysRevD.92.064042.

[47] E. Martín-Martínez, T. R. Perche, and B. de S. L. Torres. "General relativistic quantum optics: Finite-size particle detector models in curved spacetimes". In: *Phys. Rev. D* 101.4 (2020), p. 045017. DOI: 10.1103/PhysRevD.101.045017.

[48] L. P. Thinh, J.-D. Bancal, and E. Martín-Martínez. "Certified randomness from a two-level system in a relativistic quantum field". In: *Phys. Rev. A* 94.2 (2016), p. 022321. DOI: 10.1103/PhysRevA.94.022321.

[49] B. Peropadre et al. "Switchable Ultrastrong Coupling in Circuit QED". In: *Phys. Rev. Lett.* 105.2 (2010), p. 023601. DOI: 10.1103/PhysRevLett.105.023601.

[50] P. Kirton et al. "Introduction to the Dicke Model: From Equilibrium to Nonequilibrium, and Vice Versa". In: *Adv. Quantum Technol.* 2.1-2 (2019), p. 1800043. DOI: 10.1002/qute.201800043.

[51] W. Schleich. "Atom-Field Interaction". In: *Quantum Optics in Phase Space*. John Wiley and Sons, Ltd. Chap. 14, pp. 381–412. DOI: 10.1002/3527602976.ch14.

[52] C. Cohen-Tannoudji, J. Dupont-Roc, and G. Grynberg. *Photons and Atoms: Introduction to Quantum Electrodynamics*. John Wiley and Sons, Ltd, 1997. DOI: 10.1002/9783527618422.

[53] M. Bartelmann et al. *Theoretische Physik*. Springer Berlin Heidelberg, 2014. DOI: 10.1007/978-3-642-54618-1.

[54] B. F. Svaiter and N. F. Svaiter. "Inertial and noninertial particle detectors and vacuum fluctuations". In: *Phys. Rev. D* 46.12 (1992), pp. 5267–5277. DOI: 10.1103/PhysRevD.46.5267.

[55] J. Louko and A. Satz. "How often does the Unruh-DeWitt detector click? Regularization by a spatial profile". In: *Class. Quantum Gravity* 23.22 (2006), pp. 6321–6343. DOI: 10.1088/0264-9381/23/22/015.

[56] L. Sriramkumar and T. Padmanabhan. "Finite-time response of inertial and uniformly accelerated Unruh-DeWitt detectors". In: *Class. Quantum Gravity* 13.8 (1996), pp. 2061–2079. DOI: 10.1088/0264-9381/13/8/005.

[57] N. Funai, J. Louko, and E. Martín-Martínez. "$\hat{\boldsymbol{p}} \cdot \hat{\boldsymbol{A}}$ vs $\hat{\boldsymbol{x}} \cdot \hat{\boldsymbol{E}}$: Gauge invariance in quantum optics and quantum field theory". In: *Phys. Rev. D* 99.6 (2019), p. 065014. DOI: 10.1103/PhysRevD.99.065014.

[58] E. Martín-Martínez and P. Rodriguez-Lopez. "Relativistic quantum optics: The relativistic invariance of the light-matter interaction models". In: *Phys. Rev. D* 97.10 (2018), p. 105026. DOI: 10.1103/PhysRevD.97.105026.

[59] G. Compagno et al. "Virtual Field, Causal Photon Absorption and Photodetectors". In: *EPL* 9.3 (1989), pp. 215–220. DOI: 10.1209/0295-5075/9/3/005.

[60] G. Compagno, R. Passante, and F. Persico. "Virtual Photons, Causality and Atomic Dynamics in Spontaneous Emission". In: *J. Mod. Opt.* 37.8 (1990), pp. 1377–1382. DOI: 10.1080/09500349014551511.

[61] A. A. Clerk and J. E. Sipe. "Nonlocality and the Rotating Wave Approximation". In: *Found. Phys.* 28.4 (1998), pp. 639–651. DOI: 10.1023/A:1018717823725.

[62] N. Funai and E. Martín-Martínez. "Faster-than-light signaling in the rotating-wave approximation". In: *Phys. Rev. D* 100.6 (2019), p. 065021. DOI: 10.1103/PhysRevD.100.065021.

[63] K. Hepp and E. H. Lieb. "On the superradiant phase transition for molecules in a quantized radiation field: the dicke maser model". In: *Ann. Phys.* 76.2 (1973), pp. 360–404. DOI: 10.1016/0003-4916(73)90039-0.

[64] R. H. Dicke. "Coherence in Spontaneous Radiation Processes". In: *Phys. Rev.* 93.1 (1954), pp. 99–110. DOI: 10.1103/PhysRev.93.99.

[65] M. E. Peskin and D. V. Schroeder. *An Introduction to Quantum Field Theory*. Westview Press, 1995.

[66] D. Frauchiger, R. Renner, and M. Troyer. "True randomness from realistic quantum devices". In: *ArXiv e-prints* (2013). arXiv: 1311.4547.

[67] M. Herrero-Collantes and J. C. Garcia-Escartin. "Quantum random number generators". In: *Reviews of Modern Physics* 89.1, 015004 (2017), p. 015004. DOI: 10.1103/RevModPhys.89.015004.

[68] S. Olmschenk et al. "Manipulation and detection of a trapped Yb^+ hyperfine qubit". In: *Phys. Rev. A* 76.5, 052314 (2007), p. 052314. DOI: 10.1103/PhysRevA.76.052314.

[69] S. Pironio et al. "Random numbers certified by Bell's theorem". In: *Nature* 464 (2010), pp. 1021–1024. DOI: 10.1038/nature09008.

[70] A. Blais et al. "Cavity quantum electrodynamics for superconducting electrical circuits: An architecture for quantum computation". In: *Phys. Rev. A* 69.6, 062320 (2004), p. 062320. DOI: 10.1103/PhysRevA.69.062320.

[71] K. Cicak et al. "Low-loss superconducting resonant circuits using vacuum-gap-based microwave components". In: *Applied Physics Letters* 96.9, 093502 (2010), p. 093502. DOI: 10.1063/1.3304168.

[72] A. Wallraff et al. "Strong coupling of a single photon to a superconducting qubit using circuit quantum electrodynamics". In: *Nature* 431 (2004), pp. 162–167. DOI: 10.1038/nature02851.

[73] T. Niemczyk et al. "Circuit quantum electrodynamics in the ultrastrong-coupling regime". In: *Nature Physics* 6 (2010), pp. 772–776. DOI: 10.1038/nphys1730.

[74] E. Martín-Martínez. "Causality numbers of particle detector models in QFT and quantum optics". In: *Phys. Rev. D* 92.10 (2015), p. 104019. DOI: 10.1103/PhysRevD.92.104019.

[75] L. Reyzin. "Some Notions of Entropy for Cryptography". In: *Information Theoretic Security*. Ed. by S. Fehr. Springer Berlin Heidelberg, 2011, pp. 138–142. DOI: 10.1007/978-3-642-20728-0_13.

[76] R. Konig, R. Renner, and C. Schaffner. "The Operational Meaning of Min- and Max-Entropy". In: *IEEE Transactions on Information Theory* 55.9 (2009), pp. 4337–4347. DOI: 10.1109/TIT.2009.2025545.

[77] M. Skorski. "How Much Randomness Can Be Extracted from Memoryless Shannon Entropy Sources?" In: *Information Security Applications*. Ed. by H. Kim and D. Choi. Springer International Publishing, 2016, pp. 75–86. DOI: 10.1007/978-3-319-31875-2_7.

[78] R. Shaltiel. "An Introduction to Randomness Extractors". In: *Automata, Languages and Programming*. Ed. by L. Aceto, M. Henzinger, and J. Sgall. Springer Berlin Heidelberg, 2011, pp. 21–41. DOI: 10.1007/978-3-642-22012-8_2.

[79] M. Tomamichel, R. Colbeck, and R. Renner. "Duality Between Smooth Min- and Max-Entropies". In: *IEEE Trans. Inf. Theory* 56.9 (2010), pp. 4674–4681. DOI: 10.1109/TIT.2010.2054130.

[80] C. W. Helstrom. "Quantum detection and estimation theory". In: *J. Stat. Phys.* 1.2 (1969), pp. 231–252. DOI: 10.1007/BF01007479.

[81] P. J. Mohr, D. B. Newell, and B. N. Taylor. "CODATA Recommended Values of the Fundamental Physical Constants: 2014". In: *Rev. Mod. Phys.* 88.3 (2016), p. 035009. DOI: 10.1103/RevModPhys.88.035009.

[82] A. Pozas-Kerstjens, J. Louko, and E. Martín-Martínez. "Degenerate detectors are unable to harvest spacelike entanglement". In: *Phys. Rev. D* 95.10 (2017), p. 105009. DOI: 10.1103/PhysRevD.95.105009.

[83] W. G. Unruh and W. H. Zurek. "Reduction of a wave packet in quantum Brownian motion". In: *Phys. Rev. D* 40.4 (1989), pp. 1071–1094. DOI: 10.1103/PhysRevD.40.1071.

[84] M. O. Scully et al. "Enhancing Acceleration Radiation from Ground-State Atoms via Cavity Quantum Electrodynamics". In: *Phys. Rev. Lett.* 91.24 (2003), p. 243004. DOI: 10.1103/PhysRevLett.91.243004.

[85] A. Belyanin et al. "Quantum electrodynamics of accelerated atoms in free space and in cavities". In: *Phys. Rev. A* 74.2 (2006), p. 023807. DOI: 10.1103/PhysRevA.74.023807.

[86] D. A. Steck et al. “Feedback cooling of atomic motion in cavity QED”. In: *Phys. Rev. A* 74.1 (2006), p. 012322. DOI: 10.1103/PhysRevA.74.012322.

[87] S. V. Prants, L. E. Kon’kov, and I. L. Kirilyuk. “Semiclassical interaction of moving two-level atoms with a cavity field: From integrability to Hamiltonian chaos”. In: *Phys. Rev. E* 60.1 (1999), pp. 335–346. DOI: 10.1103/PhysRevE.60.335.

[88] R. Miller et al. “Trapped atoms in cavity QED: coupling quantized light and matter”. In: *J. Phys. B: At. Mol. Opt. Phys.* 38.9 (2005), S551. DOI: 10.1088/0953-4075/38/9/007.

[89] B. Deb and S. Sen. “Interaction of a moving two-level atom with a single-mode quantized cavity field”. In: *Phys. Rev. A* 56.3 (1997), pp. 2470–2472. DOI: 10.1103/PhysRevA.56.2470.

[90] L. García-Álvarez et al. “Entanglement of superconducting qubits via acceleration radiation”. In: *Sci. Rep.* 7, 657 (2017), p. 657. DOI: 10.1038/s41598-017-00770-z.

[91] A. C. Doherty et al. “Trapping of single atoms with single photons in cavity QED”. In: *Phys. Rev. A* 63.1 (2000), p. 013401. DOI: 10.1103/PhysRevA.63.013401.

[92] A. Dragan, I. Fuentes, and J. Louko. “Quantum accelerometer: Distinguishing inertial Bob from his accelerated twin Rob by a local measurement”. In: *Phys. Rev. D* 83.8 (2011), p. 085020. DOI: 10.1103/PhysRevD.83.085020.

[93] A. Ahmadzadegan, R. B. Mann, and E. Martín-Martínez. “Measuring motion through relativistic quantum effects”. In: *Phys. Rev. A* 90.6 (2014), p. 062107. DOI: 10.1103/PhysRevA.90.062107.

[94] W. Zhu, Z. H. Wang, and D. L. Zhou. “Multimode effects in cavity QED based on a one-dimensional cavity array”. In: *Phys. Rev. A* 90.4 (2014), p. 043828. DOI: 10.1103/PhysRevA.90.043828.

[95] D. E. Chang et al. “Cavity QED with atomic mirrors”. In: *New J. Phys.* 14.6 (2012), p. 063003. DOI: 10.1088/1367-2630/14/6/063003.

[96] C. Sánchez Muñoz, F. Nori, and S. De Liberato. “Resolution of superluminal signalling in non-perturbative cavity quantum electrodynamics”. In: *Nat. Commun.* 9.1 (2018), p. 1924. DOI: 10.1038/s41467-018-04339-w.

[97] J. S. Ben-Benjamin et al. “Unruh acceleration radiation revisited”. In: *Int. J. Mod. Phys. A* 34.28 (2019), p. 1941005. DOI: 10.1142/S0217751X19410057.

[98] I. Lizuain et al. “Zeno physics in ultrastrong-coupling circuit QED”. In: *Phys. Rev. A* 81.6 (2010), p. 062131. DOI: 10.1103/PhysRevA.81.062131.

[99] B. L. Hu, A. Roura, and S. Shresta. "Vacuum fluctuations and moving atoms/detectors: from the Casimir–Polder to the Unruh–Davies–DeWitt–Fulling effect". In: *J. Opt. B: Quantum Semiclass. Opt.* 6.8 (2004), S698. DOI: 10.1088/1464-4266/6/8/011.

[100] O. Levin, Y. Peleg, and A. Peres. "Unruh effect for circular motion in a cavity". In: *J. Phys. A: Math. Gen.* 26.12 (1993), p. 3001. DOI: 10.1088/0305-4470/26/12/035.

[101] M. O. Scully et al. "Quantum optics approach to radiation from atoms falling into a black hole". In: *Proc. Natl. Acad. Sci. U.S.A.* 115.32 (2018), pp. 8131–8136. DOI: 10.1073/pnas.1807703115.

[102] S. Vriend, D. Grimmer, and E. Martín-Martínez. "The Unruh effect in slow motion". In: *ArXiv e-prints* (2020). arXiv: 2011.08223.

[103] M. Onuma-Kalu, R. B. Mann, and E. Martín-Martínez. "Mode invisibility and single-photon detection". In: *Phys. Rev. A* 88.6 (2013), p. 063824. DOI: 10.1103/PhysRevA.88.063824.

[104] M. Onuma-Kalu, R. B. Mann, and E. Martín-Martínez. "Mode invisibility as a quantum nondemolition measurement of coherent light". In: *Phys. Rev. A* 90.3 (2014), p. 033847. DOI: 10.1103/PhysRevA.90.033847.

[105] P. Corona-Ugalde, M. Onuma-Kalu, and R. B. Mann. "Mode invisibility as a nondestructive probe of entangled qubit-cat states". In: *Phys. Rev. A* 96.3 (2017), p. 033845. DOI: 10.1103/PhysRevA.96.033845.

[106] D. S. Grebenkov and B.-T. Nguyen. "Geometrical Structure of Laplacian Eigenfunctions". In: *SIAM Review* 55.4 (2013), pp. 601–667. DOI: 10.1137/120880173.

[107] P. Robles and F. Claro. "Can there be massive photons? A pedagogical glance at the origin of mass". In: *Eur. J. Phys.* 33.5 (2012), pp. 1217–1226. DOI: 10.1088/0143-0807/33/5/1217.

[108] D. Hilbert and R. Courant. *Methoden der mathematischen Physik*. Vol. 1. Heidelberger Tachenbuecher Band 30. Springer, 1968.

[109] D. Hilbert and R. Courant. *Methoden der mathematischen Physik*. Vol. 2. Heidelberger Tachenbuecher Band 31. Springer, 1968.

[110] E. Tjoa and E. Martín-Martínez. "Zero mode suppression of superluminal signals in light-matter interactions". In: *Phys. Rev. D* 99.6 (2019), p. 065005. DOI: 10.1103/PhysRevD.99.065005.

[111] M. Kac. "Can One Hear the Shape of a Drum?" In: *Am. Math. Mon.* 73.4 (1966), pp. 1–23.

[112] D. Aasen, T. Bhamre, and A. Kempf. "Shape from Sound: Toward New Tools for Quantum Gravity". In: *Phys. Rev. Lett.* 110.12 (2013), p. 121301. DOI: 10.1103/PhysRevLett.110.121301.

[113] M. Panine and A. Kempf. "A convexity result in the spectral geometry of conformally equivalent metrics on surfaces". In: *Int. J. Geom. Methods Mod. Phys* 14.11 (2017), p. 1750157. DOI: 10.1142/S0219887817501572.

[114] H. Weyl. "Über die asymptotische Verteilung der Eigenwerte". In: *Nachrichten von der Gesellschaft der Wissenschaften zu Göttingen, Mathematisch-Physikalische Klasse* (1911), pp. 110–117.

[115] H. Weyl. "Das asymptotische Verteilungsgesetz der Eigenwerte linearer partieller Differentialgleichungen (mit einer Anwendung auf die Theorie der Hohlraumstrahlung)". In: *Math. Ann.* 71.4 (1912), pp. 441–479. DOI: 10.1007/BF01456804.

[116] B. J. McCartin. "Eigenstructure of the Equilateral Triangle, Part I: The Dirichlet Problem". In: *SIAM Review* 45.2 (2003), pp. 267–287.

[117] M. J. "Eigenstructure of the equilateral triangle, Part II: The Neumann problem". In: *Mathematical Problems in Engineering* 8 (2002). DOI: 10.1080/1024123021000053664.

[118] B. McCartin. "Eigenstructure of the equilateral triangle. Part III. The Robin problem". In: *International Journal of Mathematics and Mathematical Sciences* 2004 (2004). DOI: 10.1155/S0161171204306125.

[119] J. Hale. "Eigenvalues and Perturbed Domains". In: *10 Mathematical Essays on Approximation in Analysis and Topology*. Ed. by J. Ferrera, J. López-Gómez, and F. Ruiz del Portal. Amsterdam: Elsevier Science, 2005, pp. 95–123. DOI: 10.1016/B978-044451861-3/50003-3.

[120] V. Burenkov and E. Davies. "Spectral stability of the Neumann Laplacian". In: *J. Diff. Eq.* 186.2 (2002), pp. 485–508. DOI: 10.1016/S0022-0396(02)00033-5.

[121] R. Hempel, L. A. Seco, and B. Simon. "The essential spectrum of Neumann Laplacians on some bounded singular domains". In: *J. Funct. Anal.* 102.2 (1991), pp. 448–483. DOI: 10.1016/0022-1236(91)90130-W.

[122] W. Lamb, R. Schlicher, and M. Scully. "Matter-field interaction in atomic physics and quantum optics". In: *Phys. Rev. A* 36.6 (1987), pp. 2763–2772. DOI: 10.1103/PhysRevA.36.2763.

[123] M. Babiker. "Theory of momentum changes in atomic translation due to irradiation with resonant light". In: *J. Phys. B: At. Mol. Phys.* 17.24 (1984), p. 4877. DOI: 10.1088/0022-3700/17/24/021.

[124] R. G. Woolley. "Gauge invariant wave mechanics and the Power-Zienau-Woolley transformation". In: *J. Phys. A* 13.8 (1980), pp. 2795–2805. DOI: 10.1088/0305-4470/13/8/027.

[125] W. C. Röntgen. "Über die durch Bewegung eines im homogenen electrischen Felde befindlichen Dielectricums hervorgerufene electrodynamische Kraft". In: *Ann. Phys.* 271.10 (1888), pp. 264–270. DOI: 10.1002/andp.18882711003.

[126] L. G. Boussiakou, C. R. Bennett, and M. Babiker. "Quantum Theory of Spontaneous Emission by Real Moving Atoms". In: *Phys. Rev. Lett.* 89.12 (2002), p. 123001. DOI: 10.1103/PhysRevLett.89.123001.

[127] J. D. Cresser and S. M. Barnett. "The rate of spontaneous decay of a moving atom". In: *J. Phys. B: At. Mol. Opt. Phys.* 36.9 (2003), p. 1755. DOI: 10.1088/0953-4075/36/9/307.

[128] M. Sonnleitner and S. M. Barnett. "The Röntgen interaction and forces on dipoles in time-modulated optical fields". In: *Eur. Phys. J. D* 71.12 (2017), p. 336. DOI: 10.1140/epjd/e2017-80273-8.

[129] M. Sonnleitner and S. M. Barnett. "Mass-energy and anomalous friction in quantum optics". In: *Phys. Rev. A* 98.4 (2018), p. 042106. DOI: 10.1103/PhysRevA.98.042106.

[130] N. Stritzelberger and A. Kempf. "Coherent delocalization in the light-matter interaction". In: *Phys. Rev. D* 101.3 (2020), p. 036007. DOI: 10.1103/PhysRevD.101.036007.

[131] N. Stritzelberger et al. "Entanglement harvesting with coherently delocalized matter". In: *Phys. Rev. D* 103.1 (2021), p. 016007. DOI: 10.1103/PhysRevD.103.016007.

[132] P. Grochowski et al. "Quantum time dilation in atomic spectra". In: *ArXiv e-prints* (2020). arXiv: 2006.10084.

[133] C. Lämmerzahl. "A Hamilton operator for quantum optics in gravitational fields". In: *Phys. Lett. A* 203.1 (1995), pp. 12–17. DOI: 10.1016/0375-9601(95)00345-4.

[134] R. Maryam, H. Helm, and H. Breuer. "Entanglement between internal and external degrees of freedom of a driven trapped atom". In: *Phys. Scr.* T140 (2010), p. 014034. DOI: 10.1088/0031-8949/2010/t140/014034.

[135] A. Muthukrishnan and C. Stroud. "Entanglement of internal and external angular momenta of a single atom". In: *J. Opt. B: Quantum Semiclass. Opt.* 4.2 (2002), S73–S77. DOI: 10.1088/1464-4266/4/2/371.

[136] A. Retzker, J. I. Cirac, and B. Reznik. "Detecting Vacuum Entanglement in a Linear Ion Trap". In: *Phys. Rev. Lett.* 94.5 (2005), p. 050504. DOI: 10.1103/PhysRevLett.94.050504.

[137] S. Azzini et al. "Single-Particle Entanglement". In: *Adv. Quantum Technol.* 3.10 (2020), p. 2000014. DOI: 10.1002/qute.202000014.

[138] M. Nawaz, R. ul-Islam, and M. Ikram. "Remote state preparation through hyper-entangled atomic states". In: *J. Phys. B: At. Mol. Opt. Phys* 51.7 (2018), p. 075501. DOI: 10.1088/1361-6455/aaaf53.

[139] C. Luo et al. "Heisenberg-limited Sagnac interferometer with multiparticle states". In: *Phys. Rev. A* 95.2 (2017), p. 023608. DOI: 10.1103/PhysRevA.95.023608.

[140] M. Roghani, H. Helm, and H. Breuer. "Entanglement Dynamics of a Strongly Driven Trapped Atom". In: *Phys. Rev. Lett.* 106.4 (2011), p. 040502. DOI: 10.1103/PhysRevLett.106.040502.

[141] G. Breit. "Dirac's Equation and the Spin-Spin Interactions of Two Electrons". In: *Phys. Rev.* 39.4 (1932), pp. 616–624. DOI: 10.1103/PhysRev.39.616.

[142] H. Bethe and E. Salpeter. *Quantum Mechanics of One- and Two-electron Atoms*. Dover Publications, 2008.

[143] D. G. Currie, T. F. Jordan, and E. C. G. Sudarshan. "Relativistic Invariance and Hamiltonian Theories of Interacting Particles". In: *Rev. Mod. Phys.* 35.2 (1963), pp. 350–375. DOI: 10.1103/RevModPhys.35.350.

[144] E. Stefanovich. *Relativistic quantum dynamics*. Vol. 47. Walter de Gruyter GmbH & Co KG, 2018.

[145] E. H. Kerner. "Can the Position Variable be a Canonical Coordinate in a Relativistic Many-Particle Theory?" In: *J. Math. Phys.* 6.8 (1965), pp. 1218–1227. DOI: 10.1063/1.1704763.

[146] T. H. Boyer. "Illustrating some implications of the conservation laws in relativistic mechanics". In: *Am. J. Phys.* 77.6 (2009), pp. 562–569. DOI: 10.1119/1.3085744.

[147] E. Martín-Martínez, A. R. H. Smith, and D. R. Terno. "Spacetime structure and vacuum entanglement". In: *Phys. Rev. D* 93.4 (2016), p. 044001. DOI: 10.1103/PhysRevD.93.044001.

[148] D. L. Andrews et al. "Perspective: Quantum Hamiltonians for optical interactions". In: *J. Chem. Phys.* 148.4 (2018), p. 040901. DOI: 10.1063/1.5018399.

[149] A. Vukics, T. Grießer, and P. Domokos. "Elimination of the A-Square Problem from Cavity QED". In: *Phys. Rev. Lett.* 112.7 (2014), p. 073601. DOI: 10.1103/PhysRevLett.112.073601.

[150] F. Belinfante. "On the longitudinal and the transversal delta-function, with some applications". In: *Physica* 12.1 (1946), pp. 1–16. DOI: 10.1016/S0031-8914(46)80108-3.

[151] R. M. Wilcox. "Exponential Operators and Parameter Differentiation in Quantum Physics". In: *J. Math. Phys.* 8.4 (1967), pp. 962–982. DOI: 10.1063/1.1705306.

[152] F. E. Close and H. Osborn. "Relativistic Center-of-Mass Motion and the Electromagnetic Interaction of Systems of Charged Particles". In: *Phys. Rev. D* 2.10 (1970), pp. 2127–2140. DOI: 10.1103/PhysRevD.2.2127.

[153] R. Feynman. *Feynman lectures on physics. Volume 2: Mainly electromagnetism and matter*. 1964.

[154] *NIST Digital Library of Mathematical Functions*. http://dlmf.nist.gov/, Release 1.0.27 of 2020-06-15. F. W. J. Olver, A. B. Olde Daalhuis, D. W. Lozier, B. I. Schneider, R. F. Boisvert, C. W. Clark, B. R. Miller and B. V. Saunders, eds.

[155] S. Takagi. "Vacuum Noise and Stress Induced by Uniform Acceleration: Hawking-Unruh Effect in Rindler Manifold of Arbitrary Dimension". In: *Prog. Theor. Phys. Supp.* 88 (1986), pp. 1–142. DOI: 10.1143/PTP.88.1.

[156] S. Lin and B. Hu. "Backreaction and the Unruh effect: New insights from exact solutions of uniformly accelerated detectors". In: *Phys. Rev. D* 76.6 (2007), p. 064008. DOI: 10.1103/PhysRevD.76.064008.

[157] S. Lin, C. Chou, and B. Hu. "Disentanglement of two harmonic oscillators in relativistic motion". In: *Phys. Rev. D* 78.12 (2008), p. 125025. DOI: 10.1103/PhysRevD.78.125025.

[158] D. Ostapchuk et al. "Entanglement dynamics between inertial and non-uniformly accelerated detectors". In: *J. High Energy Phys.* 2012.7 (2012), p. 72. DOI: 10.1007/JHEP07(2012)072.

[159] A. Dragan and I. Fuentes. "Probing the spacetime structure of vacuum entanglement". In: *ArXiv e-prints* (2011). arXiv: 1105.1192.

[160] E. Brown et al. "Detectors for probing relativistic quantum physics beyond perturbation theory". In: *Phys. Rev. D* 87.8 (2013), p. 084062. DOI: 10.1103/PhysRevD.87.084062.

[161] V. Sudhir, N. Stritzelberger, and A. Kempf. "Unruh Effect of Detectors with Quantized Center-of-Mass". In: *ArXiv e-prints* (2021). arXiv: 2102.03367.

[162] W. Demtröder. *Atoms, Molecules and Photons*. Springer Berlin Heidelberg, 2010.

APPENDICES

Appendix A

The Effective Dipole Model and Atomic State Evolution

A.1 Deriving the Time-Evolved Density Matrix

In this section we will derive in detail the change of the reduced density matrix of the atom after interaction with the electromagnetic field. We will build on results of [24] and generalize the derivation to allow for initial atomic superposition states and present expressions for several switching functions. Starting from Eq. (2.36) and using the interaction Hamiltonian Eq. (3.1) we find

$$\begin{aligned}
&\mathrm{tr}_{\mathrm{F}}\left(\hat{\mathcal{U}}^{(2)}\hat{\rho}_0\right) \qquad (A.1)\\
&= \mathrm{tr}_{\mathrm{F}}\left(-\int_{\mathbb{R}}\mathrm{d}t\int_{-\infty}^{t}\mathrm{d}t'\chi(t)\chi(t')\int_{\mathbb{R}^3}\mathrm{d}\boldsymbol{x}\int_{\mathbb{R}^3}\mathrm{d}\boldsymbol{x}'\hat{d}^i(\boldsymbol{x},t)\hat{E}_i(\boldsymbol{x},t)\hat{d}^j(\boldsymbol{x}',t')\hat{E}_j(\boldsymbol{x}',t')\hat{\rho}_0\right)\\
&= -\int_{\mathbb{R}}\mathrm{d}t\int_{-\infty}^{t}\mathrm{d}t'\chi(t)\chi(t')\int_{\mathbb{R}^3}\mathrm{d}\boldsymbol{x}\int_{\mathbb{R}^3}\mathrm{d}\boldsymbol{x}'\hat{d}^i(\boldsymbol{x},t)\hat{d}^j(\boldsymbol{x}',t')\left|\Psi\right\rangle_{\mathrm{A}_i}\!\langle\Psi|\,{}_{\mathrm{F}}\langle 0|\,\hat{E}_i(\boldsymbol{x},t)\hat{E}_j(\boldsymbol{x}',t')\left|0\right\rangle_{\mathrm{F}},
\end{aligned}$$

where we employ Einstein sum convention and sum over double indices. Since the atomic state outer product $\left|\Psi\right\rangle_{\mathrm{A}}\!\langle\Psi|$ is on the right-hand side of the dipole operators, only terms with one raising and one lowering operator survive. Similarly,

$$\begin{aligned}
&\mathrm{tr}_{\mathrm{F}}\left(\hat{\mathcal{U}}^{(1)}\hat{\rho}_0\hat{\mathcal{U}}^{(1)\dagger}\right) \qquad (A.2)\\
&= \int_{\mathbb{R}}\mathrm{d}t\int_{\mathbb{R}}\mathrm{d}t'\chi(t)\chi(t')\int_{\mathbb{R}^3}\mathrm{d}\boldsymbol{x}\int_{\mathbb{R}^3}\mathrm{d}\boldsymbol{x}'\hat{d}^i(\boldsymbol{x},t)\left|\Psi\right\rangle_{\mathrm{A}_i}\!\langle\Psi|\,\hat{d}^j(\boldsymbol{x}',t')\,\mathrm{tr}_{\mathrm{F}}\Big(\hat{E}_i(\boldsymbol{x},t)\left|0\right\rangle_{\mathrm{F}}\!\langle 0|\,\hat{E}_j(\boldsymbol{x}',t')\Big),
\end{aligned}$$

where we used that $\hat{d}_i$ and $\hat{E}_i$ are Hermitian. This yields then

$$\begin{aligned}
&\mathrm{tr}_{\mathrm{F}}\left(\hat{\mathcal{U}}^{(2)}\hat{\rho}_0\right) \qquad (A.3)\\
=&-e^2\int_{\mathbb{R}}\mathrm{d}t\int_{-\infty}^{t}\mathrm{d}t'\chi(t)\chi(t')\int_{\mathbb{R}^3}\mathrm{d}\boldsymbol{x}\int_{\mathbb{R}^3}\mathrm{d}\boldsymbol{x}'\Big\{\left[\left(1-a^2\right)|e\rangle_{\mathrm{A}}\langle e|+a\sqrt{1-a^2}\,|e\rangle_{\mathrm{A}}\langle g|\right]e^{\mathrm{i}\Omega(t-t')}\\
&\times(F^i)^T(\boldsymbol{x})W_{ij}(\boldsymbol{x},\boldsymbol{x}';t,t')(F^j)^*(\boldsymbol{x}')+\left[a^2|g\rangle_{\mathrm{A}}\langle g|+a\sqrt{1-a^2}\,|g\rangle_{\mathrm{A}}\langle e|\right]e^{-\mathrm{i}\Omega(t-t')}\\
&\times(F^i)^{*^T}(\boldsymbol{x})W_{ij}(\boldsymbol{x},\boldsymbol{x}';t,t')F^j(\boldsymbol{x}')\Big\},\\
&\mathrm{tr}_{\mathrm{F}}\left(\hat{\mathcal{U}}^{(1)}\hat{\rho}_0\hat{\mathcal{U}}^{(1)\dagger}\right) \qquad (A.4)\\
=&e^2\int_{\mathbb{R}}\mathrm{d}t\int_{\mathbb{R}}\mathrm{d}t'\chi(t)\chi(t')\int_{\mathbb{R}^3}\mathrm{d}\boldsymbol{x}\int_{\mathbb{R}^3}\mathrm{d}\boldsymbol{x}'\Big\{a^2|e\rangle_{\mathrm{A}}\langle e|(F^i)^{*^T}(\boldsymbol{x}')W_{ij}(\boldsymbol{x}',\boldsymbol{x};t',t)(F^j)(\boldsymbol{x})e^{\mathrm{i}\Omega(t-t')}\\
&+\left(1-a^2\right)|g\rangle_{\mathrm{A}}\langle g|(F^i)^T(\boldsymbol{x}')W_{ij}(\boldsymbol{x}',\boldsymbol{x};t',t)(F^j)^*(\boldsymbol{x})e^{-\mathrm{i}\Omega(t-t')}\\
&+a\sqrt{1-a^2}\,|g\rangle_{\mathrm{A}}\langle e|(F^i)^{*^T}(\boldsymbol{x}')W_{ij}(\boldsymbol{x}',\boldsymbol{x};t',t)(F^j)^*(\boldsymbol{x})e^{-\mathrm{i}\Omega(t+t')}\\
&+a\sqrt{1-a^2}\,|e\rangle_{\mathrm{A}}\langle g|(F^i)^T(\boldsymbol{x}')W_{ij}(\boldsymbol{x}',\boldsymbol{x};t',t)F^j(\boldsymbol{x})e^{\mathrm{i}\Omega(t+t')}\Big\},
\end{aligned}$$

where we have defined the Wightman 2-tensor for the electric field, using (2.18),

$$\begin{aligned}
W_{ij}(t_2,t_1;\boldsymbol{x}_2,\boldsymbol{x}_1)&={}_{\mathrm{F}}\langle 0|\,\hat{E}_i(\boldsymbol{x}_2,t_2)\hat{E}_j(\boldsymbol{x}_1,t_1)\,|0\rangle_{\mathrm{F}}\\
&=\int_{\mathbb{R}^3}\frac{\mathrm{d}^3\boldsymbol{k}}{(2\pi)^3}\frac{|\boldsymbol{k}|}{2}e^{-\mathrm{i}|\boldsymbol{k}|(t_2-t_1)}e^{\mathrm{i}\boldsymbol{k}\cdot(\boldsymbol{x}_2-\boldsymbol{x}_1)}\left(\delta_{i,j}-\frac{k_ik_j}{|\boldsymbol{k}|^2}\right). \qquad (A.5)
\end{aligned}$$

To arrive at that expression the completeness relation of the polarization vectors $\boldsymbol{\epsilon}(\boldsymbol{k},s_i)$ was used [52, Ch. 3]:

$$\sum_{i=1}^{2}\boldsymbol{\epsilon}(\boldsymbol{k},s_i)\otimes\boldsymbol{\epsilon}(\boldsymbol{k},s_i)=\mathbb{1}-\frac{\boldsymbol{k}\otimes\boldsymbol{k}}{|\boldsymbol{k}|^2}. \qquad (A.6)$$

In the following we will drop the subscripts of the outer products belonging to the Hilbert space of atom A. We will separate the terms in the Wightman tensor according to the identity $\mathbb{1}$ and the dyadic product $\boldsymbol{k}\otimes\boldsymbol{k}$ (such that their sum corresponds to the complete expression), denoted by the corresponding subscripts. We wish to integrate over spherical coordinates, naturally suggested by the wave function $\Psi_{n\ell m}(\boldsymbol{x})=R_{n\ell}(|\boldsymbol{x}|)Y_{\ell m}(\hat{\boldsymbol{x}})$, where $Y_{\ell m}(\hat{\boldsymbol{x}})$ are the spherical harmonics with $\hat{\boldsymbol{x}}=(\theta_{\boldsymbol{x}},\phi_{\boldsymbol{x}})$ as the angular components of the unit radial vector, and $R_{n\ell}(|\boldsymbol{x}|)$ are the radial wave functions of a hydrogenoid atom [162,

Ch. 5]. The following two decompositions are helpful, using [154, Sec. 10.60(iii)]:

$$e^{\mathrm{i}\boldsymbol{x}\cdot\boldsymbol{y}} = \sum_{\ell=0}^{\infty}\sum_{m=-\ell}^{\ell} 4\pi \mathrm{i}^{\ell} j_\ell(|\boldsymbol{x}||\boldsymbol{y}|) Y_{\ell m}(\hat{\boldsymbol{x}}) Y^*_{\ell m}(\hat{\boldsymbol{y}}) = \sum_{\ell=0}^{\infty}\sum_{m=-\ell}^{\ell} 4\pi \mathrm{i}^{\ell} j_\ell(|\boldsymbol{x}||\boldsymbol{y}|) Y^*_{\ell m}(\hat{\boldsymbol{x}}) Y_{\ell m}(\hat{\boldsymbol{y}}), \tag{A.7}$$

$$\boldsymbol{x}\cdot\boldsymbol{y} = \frac{4\pi}{3}|\boldsymbol{x}||\boldsymbol{y}| \left[Y_{10}(\hat{\boldsymbol{x}})Y_{10}(\hat{\boldsymbol{y}}) - Y_{11}(\hat{\boldsymbol{x}})Y_{1-1}(\hat{\boldsymbol{y}}) - Y_{1-1}(\hat{\boldsymbol{x}})Y_{11}(\hat{\boldsymbol{y}})\right], \tag{A.8}$$

with the spherical Bessel functions $j_\ell(x)$. The first contribution to the time evolved density matrix then reads

$$\begin{aligned}
&\mathrm{tr}_{\mathrm{F}}\left(\hat{\mathcal{U}}^{(2)}\hat{\rho}_0\right)\Big|_{\mathbb{1}} \qquad\qquad (A.9)\\
&= -e^2 \int_0^\infty \frac{\mathrm{d}|\boldsymbol{k}|}{(2\pi)^3}\frac{|\boldsymbol{k}|^3}{2} \sum_{\ell=0}^{\infty}\sum_{m=-\ell}^{\ell} 4\pi\mathrm{i}^{\ell} \sum_{\ell'=0}^{\infty}\sum_{m'=-\ell'}^{\ell'} 4\pi\mathrm{i}^{\ell'}(-1)^{\ell'}\frac{4\pi}{3}\int_{\mathbb{R}}\mathrm{d}t\int_{-\infty}^{t}\mathrm{d}t'\chi(t)\chi(t')e^{-\mathrm{i}|\boldsymbol{k}|(t-t')}\\
&\quad\times\int_0^\infty \mathrm{d}|\boldsymbol{x}||\boldsymbol{x}|^3 R_{n_e\ell_e}(|\boldsymbol{x}|)R_{n_g\ell_g}(|\boldsymbol{x}|)j_\ell(|\boldsymbol{k}||\boldsymbol{x}|)\int_0^\infty \mathrm{d}|\boldsymbol{x}'||\boldsymbol{x}'|^3 R_{n_e\ell_e}(|\boldsymbol{x}'|)R_{n_g\ell_g}(|\boldsymbol{x}'|)j_{\ell'}(|\boldsymbol{k}||\boldsymbol{x}'|)\\
&\quad\times\int \mathrm{d}\Omega_k Y_{\ell m}(\hat{\boldsymbol{k}})Y_{\ell' m'}(\hat{\boldsymbol{k}})\int \mathrm{d}\Omega_x \int \mathrm{d}\Omega_{x'} Y^*_{\ell m}(\hat{\boldsymbol{x}})Y^*_{\ell' m'}(\hat{\boldsymbol{x}'})\\
&\qquad\times\left[Y_{10}(\hat{\boldsymbol{x}})Y_{10}(\hat{\boldsymbol{x}'}) - Y_{11}(\hat{\boldsymbol{x}})Y_{1-1}(\hat{\boldsymbol{x}'}) - Y_{1-1}(\hat{\boldsymbol{x}})Y_{11}(\hat{\boldsymbol{x}'})\right]\\
&\quad\times\Big\{\left[\left(1-a^2\right)|e\rangle\langle e| + a\sqrt{1-a^2}\,|e\rangle\langle g|\right]e^{\mathrm{i}\Omega(t-t')}Y^*_{\ell_e m_e}(\hat{\boldsymbol{x}})Y_{\ell_g m_g}(\hat{\boldsymbol{x}})Y_{\ell_e m_e}(\hat{\boldsymbol{x}'})Y^*_{\ell_g m_g}(\hat{\boldsymbol{x}'})\\
&\qquad+\left[a^2|g\rangle\langle g| + a\sqrt{1-a^2}\,|g\rangle\langle e|\right]e^{-\mathrm{i}\Omega(t-t')}Y_{\ell_e m_e}(\hat{\boldsymbol{x}})Y^*_{\ell_g m_g}(\hat{\boldsymbol{x}})Y^*_{\ell_e m_e}(\hat{\boldsymbol{x}'})Y_{\ell_g m_g}(\hat{\boldsymbol{x}'})\Big\},
\end{aligned}$$

where we have used the identity $Y_{\ell m}(-\hat{\boldsymbol{x}}) = (-1)^\ell Y_{\ell m}(\hat{\boldsymbol{x}})$ and that $R_{n\ell}(|\boldsymbol{x}|)$ is real. Also $\mathrm{d}\Omega = \mathrm{d}(\cos\Theta)\mathrm{d}\phi$ is the standard solid angle differential. The integral over $\mathrm{d}\Omega_k$ reads $\int \mathrm{d}\Omega_k Y_{\ell m}(\hat{\boldsymbol{k}})Y_{\ell' m'}(\hat{\boldsymbol{k}}) = (-1)^{m'}\delta_{\ell,\ell'}\delta_{m,-m'}$ by using $Y^*_{\ell m}(\hat{\boldsymbol{x}}) = (-1)^m Y_{\ell -m}(\hat{\boldsymbol{x}})$. This simplifies the integrals over the other two solid angles drastically such that we can use the following identity of spherical harmonics integrated over the unit sphere S^2 [154, Sec. 34.3(vii)]

$$\begin{aligned}
&\int \mathrm{d}\Omega\; Y^*_{\ell_1 m_1}(\hat{\boldsymbol{x}})Y^*_{\ell_3 m_3}(\hat{\boldsymbol{x}})Y_{\ell_2 m_2}(\hat{\boldsymbol{x}})Y_{\ell_4 m_4}(\hat{\boldsymbol{x}}) \qquad\qquad (A.10)\\
&= \sum_{\lambda=0}^{\infty}\sum_{\mu=-\lambda}^{\lambda}\frac{2\lambda+1}{4\pi}\sqrt{(2\ell_1+1)(2\ell_2+1)(2\ell_3+1)(2\ell_4+1)}\begin{pmatrix}\ell_1 & \ell_3 & \lambda\\ 0 & 0 & 0\end{pmatrix}\begin{pmatrix}\ell_2 & \ell_4 & \lambda\\ 0 & 0 & 0\end{pmatrix}\\
&\quad\times\begin{pmatrix}\ell_1 & \ell_3 & \lambda\\ -m_1 & -m_3 & -\mu\end{pmatrix}\begin{pmatrix}\ell_2 & \ell_4 & \lambda\\ m_2 & m_4 & \mu\end{pmatrix},
\end{aligned}$$

with $\begin{pmatrix} \ell_1 & \ell_2 & \ell_3 \\ m_1 & m_2 & m_3 \end{pmatrix}$ as the Wigner $3j$-symbols [154, Sec. 34.2]. With this formula, the sums over ℓ', m, m' and the integrals over the all solid angles can be executed. Let us concentrate first on the second term of the sum in the curly brackets of (A.9), coming from ${F_i^*}^T W_{ij} F_j$, which yields

$$
\begin{aligned}
&\sum_{\ell'=0}^{\infty} \sum_{m=-\ell}^{\ell} \sum_{m'=-\ell'}^{\ell'} \mathrm{i}^{\ell+\ell'} (-1)^{\ell'} j_{\ell'}(|\boldsymbol{k}||\boldsymbol{x}'|) \int \mathrm{d}\Omega_k Y_{\ell m}(\hat{\boldsymbol{k}}) Y_{\ell' m'}(\hat{\boldsymbol{k}}) \int \mathrm{d}\Omega_x Y_{\ell_e m_e}(\hat{\boldsymbol{x}}) Y^*_{\ell_g m_g}(\hat{\boldsymbol{x}}) Y^*_{\ell m}(\hat{\boldsymbol{x}}) \\
&\quad \times \int \mathrm{d}\Omega_{x'} Y^*_{\ell_e m_e}(\hat{\boldsymbol{x}}') Y_{\ell_g m_g}(\hat{\boldsymbol{x}}') Y^*_{\ell' m'}(\hat{\boldsymbol{x}}') \left[Y_{10}(\hat{\boldsymbol{x}}) Y_{10}(\hat{\boldsymbol{x}}') - Y_{11}(\hat{\boldsymbol{x}}) Y_{1-1}(\hat{\boldsymbol{x}}') - Y_{1-1}(\hat{\boldsymbol{x}}) Y_{11}(\hat{\boldsymbol{x}}') \right] \\
&= \frac{3(-1)^{m_g - m_e} \mathrm{i}^{2\ell} (-1)^{\ell}}{(4\pi)^2} (2\ell+1)(2\ell_e+1)(2\ell_g+1) \sum_{\lambda,\lambda'=0}^{\infty} (2\lambda+1)(2\lambda'+1) j_{\ell}(|\boldsymbol{k}||\boldsymbol{x}'|) \\
&\quad \times \begin{pmatrix} \ell & \ell_g & \lambda \\ 0 & 0 & 0 \end{pmatrix} \begin{pmatrix} \ell_e & 1 & \lambda \\ 0 & 0 & 0 \end{pmatrix} \begin{pmatrix} \ell & \ell_e & \lambda' \\ 0 & 0 & 0 \end{pmatrix} \begin{pmatrix} \ell_g & 1 & \lambda' \\ 0 & 0 & 0 \end{pmatrix} \Bigg[\begin{pmatrix} \ell & \ell_g & \lambda \\ m_g - m_e & -m_g & m_e \end{pmatrix} \\
&\qquad \times \begin{pmatrix} \ell_e & 1 & \lambda \\ m_e & 0 & -m_e \end{pmatrix} \begin{pmatrix} \ell & \ell_e & \lambda' \\ m_e - m_g & -m_e & m_g \end{pmatrix} \begin{pmatrix} \ell_g & 1 & \lambda' \\ m_g & 0 & -m_g \end{pmatrix} \\
&\qquad + \begin{pmatrix} \ell & \ell_g & \lambda \\ 1 + m_g - m_e & -m_g & m_e - 1 \end{pmatrix} \begin{pmatrix} \ell_e & 1 & \lambda \\ m_e & -1 & 1 - m_e \end{pmatrix} \begin{pmatrix} \ell_g & 1 & \lambda' \\ m_g & 1 & -1 - m_g \end{pmatrix} \\
&\qquad \times \begin{pmatrix} \ell & \ell_e & \lambda' \\ m_e - m_g - 1 & -m_e & 1 + m_g \end{pmatrix} + \begin{pmatrix} \ell_g & 1 & \lambda' \\ m_g & -1 & 1 - m_g \end{pmatrix} \begin{pmatrix} \ell_e & 1 & \lambda \\ m_e & 1 & -1 - m_e \end{pmatrix} \\
&\qquad \times \begin{pmatrix} \ell & \ell_e & \lambda' \\ 1 + m_e - m_g & -m_e & m_g - 1 \end{pmatrix} \begin{pmatrix} \ell & \ell_g & \lambda \\ m_g - m_e - 1 & -m_g & m_e + 1 \end{pmatrix} \Bigg],
\end{aligned}
\tag{A.11}
$$

where we used that $3j$-symbols vanish unless the sum of the lower entries is zero. The first term from (A.9) can be obtained from (A.11) by noting that effectively ℓ and ℓ', thus also m and m', are interchanged and hence $(-1)^{m_g - m_e} \to (-1)^{-m_g + m_e}$. Since this is equivalent, the first term can also be described by (A.11).

Therefore, in all generality (A.9) reads

$$\begin{aligned}
&\mathrm{tr}_{\mathrm{F}}\left(\hat{\mathcal{U}}^{(2)}\hat{\rho}_0\right)\Big|_{\mathbb{1}} \qquad\qquad (A.12)\\
&= -e^2\int_0^\infty \frac{\mathrm{d}|\boldsymbol{k}|}{(2\pi)^3}\frac{|\boldsymbol{k}|^3}{2}\sum_{\ell=0}^\infty \frac{(4\pi)^3}{3}(2\ell+1)(2\ell_e+1)(2\ell_g+1)\int_{\mathbb{R}}\mathrm{d}t\int_{-\infty}^t \mathrm{d}t'\chi(t)\chi(t')e^{-\mathrm{i}|\boldsymbol{k}|(t-t')}\\
&\quad\times\int_0^\infty \mathrm{d}|\boldsymbol{x}||\boldsymbol{x}|^3 R_{n_e\ell_e}(|\boldsymbol{x}|)R_{n_g\ell_g}(|\boldsymbol{x}|)j_\ell(|\boldsymbol{k}||\boldsymbol{x}|)\int_0^\infty \mathrm{d}|\boldsymbol{x}'||\boldsymbol{x}'|^3 R_{n_e\ell_e}(|\boldsymbol{x}'|)R_{n_g\ell_g}(|\boldsymbol{x}'|)j_\ell(|\boldsymbol{k}||\boldsymbol{x}'|)\\
&\quad\times\frac{3(-1)^{m_g-m_e}}{(4\pi)^2}\sum_{\lambda,\lambda'=0}^\infty(2\lambda+1)(2\lambda'+1)\begin{pmatrix}\ell & \ell_g & \lambda\\ 0&0&0\end{pmatrix}\begin{pmatrix}\ell_e & 1 & \lambda\\ 0&0&0\end{pmatrix}\begin{pmatrix}\ell & \ell_e & \lambda'\\ 0&0&0\end{pmatrix}\begin{pmatrix}\ell_g & 1 & \lambda'\\ 0&0&0\end{pmatrix}\\
&\quad\times\left[\begin{pmatrix}\ell & \ell_g & \lambda\\ m_g-m_e & -m_g & m_e\end{pmatrix}\begin{pmatrix}\ell_e & 1 & \lambda\\ m_e & 0 & -m_e\end{pmatrix}\begin{pmatrix}\ell & \ell_e & \lambda'\\ m_e-m_g & -m_e & m_g\end{pmatrix}\begin{pmatrix}\ell_g & 1 & \lambda'\\ m_g & 0 & -m_g\end{pmatrix}\right.\\
&\qquad+\begin{pmatrix}\ell & \ell_g & \lambda\\ 1+m_g-m_e & -m_g & m_e-1\end{pmatrix}\begin{pmatrix}\ell_e & 1 & \lambda\\ m_e & -1 & 1-m_e\end{pmatrix}\begin{pmatrix}\ell_g & 1 & \lambda'\\ m_g & 1 & -1-m_g\end{pmatrix}\\
&\qquad\times\begin{pmatrix}\ell & \ell_e & \lambda'\\ m_e-m_g-1 & -m_e & 1+m_g\end{pmatrix}+\begin{pmatrix}\ell & \ell_g & \lambda\\ m_g-m_e-1 & -m_g & m_e+1\end{pmatrix}\\
&\qquad\times\left.\begin{pmatrix}\ell_e & 1 & \lambda\\ m_e & 1 & -1-m_e\end{pmatrix}\begin{pmatrix}\ell & \ell_e & \lambda'\\ 1+m_e-m_g & -m_e & m_g-1\end{pmatrix}\begin{pmatrix}\ell_g & 1 & \lambda'\\ m_g & -1 & 1-m_g\end{pmatrix}\right]\\
&\quad\times\left\{\left[\left(1-a^2\right)|e\rangle\langle e|+a\sqrt{1-a^2}\,|e\rangle\langle g|\right]e^{\mathrm{i}\Omega(t-t')}+\left[a^2|g\rangle\langle g|+a\sqrt{1-a^2}\,|g\rangle\langle e|\right]e^{-\mathrm{i}\Omega(t-t')}\right\}.
\end{aligned}$$

Before specifying atomic transition or the switching function of the coupling to the electric field, we will derive the general expressions of the remaining terms, having derived terms containing $F_i^{*^T}W_{ij}F_j$ and $F_i^TW_{ij}F_j^*$ of the $\mathbb{1}$ part.

Secondly we look at the remaining $\mathbb{1}$ contribution:

$$\begin{aligned}
&\mathrm{tr}_{\mathrm{F}}\left(\hat{\mathcal{U}}^{(1)}\hat{\rho}_0\hat{\mathcal{U}}^{(1)\dagger}\right)\Big|_{\mathbb{1}} \qquad\qquad (A.13)\\
&= e^2\int_0^\infty\frac{\mathrm{d}|\boldsymbol{k}|}{(2\pi)^3}\frac{|\boldsymbol{k}|^3}{2}\sum_{\ell,\ell'=0}^\infty\sum_{m=-\ell}^{\ell}\sum_{m'=-\ell'}^{\ell'}(4\pi)^2\mathrm{i}^{\ell+\ell'}(-1)^{\ell'}\frac{4\pi}{3}\int_{\mathbb{R}}\mathrm{d}t\int_{\mathbb{R}}\mathrm{d}t'\chi(t)\chi(t')e^{-\mathrm{i}|\boldsymbol{k}|(t'-t)}\\
&\quad\times\int_0^\infty\mathrm{d}|\boldsymbol{x}||\boldsymbol{x}|^3R_{n_e\ell_e}(|\boldsymbol{x}|)R_{n_g\ell_g}(|\boldsymbol{x}|)j_\ell(|\boldsymbol{k}||\boldsymbol{x}|)\int_0^\infty\mathrm{d}|\boldsymbol{x}'||\boldsymbol{x}'|^3R_{n_e\ell_e}(|\boldsymbol{x}'|)R_{n_g\ell_g}(|\boldsymbol{x}'|)j_{\ell'}(|\boldsymbol{k}||\boldsymbol{x}'|)\\
&\quad\times\int\mathrm{d}\Omega_kY_{\ell m}(\hat{\boldsymbol{k}})Y_{\ell'm'}(\hat{\boldsymbol{k}})\int\mathrm{d}\Omega_x\int\mathrm{d}\Omega_{x'}Y^*_{\ell m}(\hat{\boldsymbol{x}})Y^*_{\ell'm'}(\hat{\boldsymbol{x}}')\left[Y_{10}(\hat{\boldsymbol{x}})Y_{10}(\hat{\boldsymbol{x}}')-Y_{11}(\hat{\boldsymbol{x}})Y_{1-1}(\hat{\boldsymbol{x}}')\right.
\end{aligned}$$

$$
\begin{aligned}
&-Y_{1-1}(\hat{\boldsymbol{x}})Y_{11}(\hat{\boldsymbol{x}}')\Big]\Big\{\big(1-a^2\big)|g\rangle\langle g|e^{-\mathrm{i}\Omega(t-t')}Y^*_{\ell_e m_e}(\hat{\boldsymbol{x}}')Y_{\ell_g m_g}(\hat{\boldsymbol{x}}')Y_{\ell_e m_e}(\hat{\boldsymbol{x}})Y^*_{\ell_g m_g}(\hat{\boldsymbol{x}})\\
&+a^2\,|e\rangle\langle e|\,e^{\mathrm{i}\Omega(t-t')}Y_{\ell_e m_e}(\hat{\boldsymbol{x}}')Y^*_{\ell_g m_g}(\hat{\boldsymbol{x}}')Y^*_{\ell_e m_e}(\hat{\boldsymbol{x}})Y_{\ell_g m_g}(\hat{\boldsymbol{x}})\\
&+a\sqrt{1-a^2}\,|g\rangle\langle e|\,e^{-\mathrm{i}\Omega(t+t')}Y_{\ell_e m_e}(\hat{\boldsymbol{x}}')Y^*_{\ell_g m_g}(\hat{\boldsymbol{x}}')Y_{\ell_e m_e}(\hat{\boldsymbol{x}})Y^*_{\ell_g m_g}(\hat{\boldsymbol{x}})\\
&+a\sqrt{1-a^2}\,|e\rangle\langle g|\,e^{\mathrm{i}\Omega(t+t')}Y^*_{\ell_e m_e}(\hat{\boldsymbol{x}}')Y_{\ell_g m_g}(\hat{\boldsymbol{x}}')Y^*_{\ell_e m_e}(\hat{\boldsymbol{x}})Y_{\ell_g m_g}(\hat{\boldsymbol{x}})\Big\}\,.
\end{aligned}
$$

From (A.11) we already know how to compute the first two terms in the curly brackets. The other two follow immediately by noting that they can be obtained from the known terms by including or removing the conjugate of one of the smearing functions. Either way, effectively $\ell_e \leftrightarrow \ell_g$ and $m_e \leftrightarrow m_g$ change in the corresponding term. As we recall from (A.11), we had the requirement that $m = -m'$ and hence all contributions disappear except when $m_e = m_g$ since the Wigner 3-j symbols vanish in case the sum of the lower components does not equal zero. Thus we find

$$
\begin{aligned}
&\mathrm{tr}_{\mathrm{F}}\left(\hat{\mathcal{U}}^{(1)}\hat{\rho}_0\hat{\mathcal{U}}^{(1)\dagger}\right)\Big|_{\mathbb{1}} \qquad\qquad (A.14)\\
&= e^2\int_0^\infty \frac{\mathrm{d}|\boldsymbol{k}|}{(2\pi)^3}\frac{|\boldsymbol{k}|^3}{2}\sum_{\ell=0}^\infty\frac{(4\pi)^3}{3}(2\ell+1)(2\ell_e+1)(2\ell_g+1)\int_{\mathbb{R}}\mathrm{d}t\int_{\mathbb{R}}\mathrm{d}t'\chi(t)\chi(t')e^{-\mathrm{i}|\boldsymbol{k}|(t'-t)}\\
&\quad\times\int_0^\infty \mathrm{d}|\boldsymbol{x}||\boldsymbol{x}|^3R_{n_e\ell_e}(|\boldsymbol{x}|)R_{n_g\ell_g}(|\boldsymbol{x}|)j_\ell(|\boldsymbol{k}||\boldsymbol{x}|)\int_0^\infty \mathrm{d}|\boldsymbol{x}'||\boldsymbol{x}'|^3R_{n_e\ell_e}(|\boldsymbol{x}'|)R_{n_g\ell_g}(|\boldsymbol{x}'|)j_\ell(|\boldsymbol{k}||\boldsymbol{x}'|)\\
&\quad\times\frac{3(-1)^{m_g-m_e}}{(4\pi)^2}\sum_{\lambda,\lambda'=0}^\infty(2\lambda+1)(2\lambda'+1)\Big\{\Big(\big(1-a^2\big)\,|g\rangle\langle g|\,e^{-\mathrm{i}\Omega(t-t')}+a^2\,|e\rangle\langle e|\,e^{\mathrm{i}\Omega(t-t')}\Big)\\
&\qquad\times\begin{pmatrix}\ell & \ell_g & \lambda\\ 0 & 0 & 0\end{pmatrix}\begin{pmatrix}\ell_e & 1 & \lambda\\ 0 & 0 & 0\end{pmatrix}\begin{pmatrix}\ell & \ell_e & \lambda'\\ 0 & 0 & 0\end{pmatrix}\begin{pmatrix}\ell_g & 1 & \lambda'\\ 0 & 0 & 0\end{pmatrix}\\
&\qquad\times\Bigg[\begin{pmatrix}\ell & \ell_g & \lambda\\ m_g-m_e & -m_g & m_e\end{pmatrix}\begin{pmatrix}\ell_e & 1 & \lambda\\ m_e & 0 & -m_e\end{pmatrix}\begin{pmatrix}\ell & \ell_e & \lambda'\\ m_e-m_g & -m_e & m_g\end{pmatrix}\begin{pmatrix}\ell_g & 1 & \lambda'\\ m_g & 0 & -m_g\end{pmatrix}\\
&\qquad\quad+\begin{pmatrix}\ell & \ell_g & \lambda\\ 1+m_g-m_e & -m_g & m_e-1\end{pmatrix}\begin{pmatrix}\ell_e & 1 & \lambda\\ m_e & -1 & 1-m_e\end{pmatrix}\begin{pmatrix}\ell_g & 1 & \lambda'\\ m_g & 1 & -1-m_g\end{pmatrix}\\
&\qquad\quad\times\begin{pmatrix}\ell & \ell_e & \lambda'\\ m_e-m_g-1 & -m_e & 1+m_g\end{pmatrix}+\begin{pmatrix}\ell_e & 1 & \lambda\\ m_e & 1 & -1-m_e\end{pmatrix}\begin{pmatrix}\ell_g & 1 & \lambda'\\ m_g & -1 & 1-m_g\end{pmatrix}\\
&\qquad\quad\times\begin{pmatrix}\ell & \ell_e & \lambda'\\ 1+m_e-m_g & -m_e & m_g-1\end{pmatrix}\begin{pmatrix}\ell & \ell_g & \lambda\\ m_g-m_e-1 & -m_g & m_e+1\end{pmatrix}\Bigg]
\end{aligned}
$$

$$
\begin{aligned}
&+\delta_{m_e,m_g} a\sqrt{1-a^2}\,|e\rangle\langle g|\,e^{\mathrm{i}\Omega(t+t')}
\begin{pmatrix}\ell & \ell_e & \lambda\\ 0 & 0 & 0\end{pmatrix}
\begin{pmatrix}\ell_g & 1 & \lambda\\ 0 & 0 & 0\end{pmatrix}
\begin{pmatrix}\ell & \ell_e & \lambda'\\ 0 & 0 & 0\end{pmatrix}
\begin{pmatrix}\ell_g & 1 & \lambda'\\ 0 & 0 & 0\end{pmatrix}\\
&\times\Bigg[\begin{pmatrix}\ell & \ell_e & \lambda\\ m_e-m_g & -m_e & m_g\end{pmatrix}
\begin{pmatrix}\ell_g & 1 & \lambda\\ m_g & 0 & -mg\end{pmatrix}
\begin{pmatrix}\ell & \ell_e & \lambda'\\ m_e-m_g & -m_e & m_g\end{pmatrix}
\begin{pmatrix}\ell_g & 1 & \lambda'\\ m_g & 0 & -m_g\end{pmatrix}\\
&\quad+\begin{pmatrix}\ell & \ell_e & \lambda\\ 1+m_e-m_g & -m_e & m_g-1\end{pmatrix}
\begin{pmatrix}\ell_g & 1 & \lambda\\ m_g & -1 & 1-mg\end{pmatrix}
\begin{pmatrix}\ell_g & 1 & \lambda'\\ m_g & 1 & -1-m_g\end{pmatrix}\\
&\quad\times\begin{pmatrix}\ell & \ell_e & \lambda'\\ m_e-m_g-1 & -m_e & 1+m_g\end{pmatrix}+\begin{pmatrix}\ell_g & 1 & \lambda'\\ m_g & -1 & 1-m_g\end{pmatrix}
\begin{pmatrix}\ell_g & 1 & \lambda\\ m_g & 1 & -1-mg\end{pmatrix}\\
&\quad\times\begin{pmatrix}\ell & \ell_e & \lambda\\ m_e-m_g-1 & -m_e & m_g+1\end{pmatrix}
\begin{pmatrix}\ell & \ell_e & \lambda'\\ 1+m_e-m_g & -m_e & m_g-1\end{pmatrix}\Bigg]\\
&+\delta_{m_e,m_g} a\sqrt{1-a^2}\,|g\rangle\langle e|\,e^{-\mathrm{i}\Omega(t+t')}
\begin{pmatrix}\ell & \ell_g & \lambda\\ 0 & 0 & 0\end{pmatrix}
\begin{pmatrix}\ell_e & 1 & \lambda\\ 0 & 0 & 0\end{pmatrix}
\begin{pmatrix}\ell & \ell_g & \lambda'\\ 0 & 0 & 0\end{pmatrix}
\begin{pmatrix}\ell_e & 1 & \lambda'\\ 0 & 0 & 0\end{pmatrix}\\
&\times\Bigg[\begin{pmatrix}\ell & \ell_g & \lambda\\ m_g-m_e & -m_g & m_e\end{pmatrix}
\begin{pmatrix}\ell_e & 1 & \lambda\\ m_e & 0 & -m_e\end{pmatrix}
\begin{pmatrix}\ell & \ell_g & \lambda'\\ m_g-m_e & -m_g & m_e\end{pmatrix}
\begin{pmatrix}\ell_e & 1 & \lambda'\\ m_e & 0 & -m_e\end{pmatrix}\\
&\quad+\begin{pmatrix}\ell & \ell_g & \lambda\\ 1+m_g-m_e & -m_g & m_e-1\end{pmatrix}
\begin{pmatrix}\ell_e & 1 & \lambda\\ m_e & -1 & 1-m_e\end{pmatrix}
\begin{pmatrix}\ell_e & 1 & \lambda'\\ m_e & 1 & -1-m_e\end{pmatrix}\\
&\quad\times\begin{pmatrix}\ell & \ell_g & \lambda'\\ m_g-m_e-1 & -m_g & 1+m_e\end{pmatrix}+\begin{pmatrix}\ell_e & 1 & \lambda'\\ m_e & -1 & 1-m_e\end{pmatrix}
\begin{pmatrix}\ell_e & 1 & \lambda\\ m_e & 1 & -1-m_e\end{pmatrix}\\
&\quad\times\begin{pmatrix}\ell & \ell_g & \lambda\\ m_g-m_e-1 & -m_g & m_e+1\end{pmatrix}
\begin{pmatrix}\ell & \ell_g & \lambda'\\ 1+m_g-m_e & -m_g & m_e-1\end{pmatrix}\Bigg]\Bigg\},
\end{aligned}
$$

where we explicitly used the Kronecker delta to indicate the dependence on m_e and m_g. One can derive the second from the first term in the curly brackets by exchanging $\ell_e \leftrightarrow \ell_g$ in terms associated to λ, and derive the third from the first term by exchanging $\ell_e \leftrightarrow \ell_g$ in terms associated to λ'.

Now we can determine the formulae for the dyadic part $\boldsymbol{k}\otimes\boldsymbol{k}$. We start from

$$\begin{aligned}
&\sum_{m=-\ell}^{\ell}\sum_{m'=-\ell'}^{\ell'}\int \mathrm{d}\Omega_x Y_{\ell_e m_e}(\hat{\boldsymbol{x}})Y^*_{\ell_g m_g}(\hat{\boldsymbol{x}})Y^*_{\ell m}(\hat{\boldsymbol{x}})\int \mathrm{d}\Omega_{x'} Y^*_{\ell_e m_e}(\hat{\boldsymbol{x}'})Y_{\ell_g m_g}(\hat{\boldsymbol{x}'})Y^*_{\ell' m'}(\hat{\boldsymbol{x}'})\\
&\times\int \mathrm{d}\Omega_k Y_{\ell m}(\hat{\boldsymbol{k}})Y_{\ell' m'}(\hat{\boldsymbol{k}})\left[Y_{10}(\hat{\boldsymbol{x}})Y_{10}(\hat{\boldsymbol{k}})-Y_{11}(\hat{\boldsymbol{x}})Y_{1-1}(\hat{\boldsymbol{k}})-Y_{1-1}(\hat{\boldsymbol{x}})Y_{11}(\hat{\boldsymbol{k}})\right]\\
&\times\left[Y_{10}(\hat{\boldsymbol{k}})Y_{10}(\hat{\boldsymbol{x}'})-Y_{11}(\hat{\boldsymbol{k}})Y_{1-1}(\hat{\boldsymbol{x}'})-Y_{1-1}(\hat{\boldsymbol{k}})Y_{11}(\hat{\boldsymbol{x}'})\right]\\
&=9(2\ell+1)(2\ell'+1)(2\ell_g+1)(2\ell_e+1)\sum_{\lambda',\lambda''=0}^{\infty}\frac{(2\lambda'+1)(2\lambda''+1)}{(4\pi)^3}\begin{pmatrix}\ell & \ell_g & \lambda'\\ 0 & 0 & 0\end{pmatrix}\begin{pmatrix}\ell_e & 1 & \lambda'\\ 0 & 0 & 0\end{pmatrix}\\
&\quad\times\begin{pmatrix}\ell' & \ell_e & \lambda''\\ 0 & 0 & 0\end{pmatrix}\begin{pmatrix}\ell_g & 1 & \lambda''\\ 0 & 0 & 0\end{pmatrix}(A+B),
\end{aligned}\tag{A.15}$$

with [24]

$$\begin{aligned}
A=&\sum_{\lambda=0}^{\infty}(2\lambda+1)\begin{pmatrix}1 & 1 & \lambda\\ 0 & 0 & 0\end{pmatrix}^2\begin{pmatrix}\ell & \ell' & \lambda\\ 0 & 0 & 0\end{pmatrix}\begin{pmatrix}\ell & \ell_g & \lambda'\\ m_g-m_e & -m_g & m_e\end{pmatrix}\begin{pmatrix}\ell_e & 1 & \lambda'\\ m_e & 0 & -m_e\end{pmatrix}\\
&\quad\times\begin{pmatrix}\ell & \ell' & \lambda\\ m_e-m_g & m_g-m_e & 0\end{pmatrix}\begin{pmatrix}\ell' & \ell_e & \lambda''\\ m_e-m_g & -m_e & m_g\end{pmatrix}\begin{pmatrix}\ell_g & 1 & \lambda''\\ m_g & 0 & -m_g\end{pmatrix}\\
&+\sum_{\lambda=0}^{\infty}(2\lambda+1)\begin{pmatrix}1 & 1 & \lambda\\ 0 & 0 & 0\end{pmatrix}\begin{pmatrix}1 & 1 & \lambda\\ 0 & 1 & -1\end{pmatrix}\begin{pmatrix}\ell & \ell' & \lambda\\ 0 & 0 & 0\end{pmatrix}\\
&\quad\times\left[\begin{pmatrix}\ell & \ell' & \lambda\\ m_e-m_g-1 & m_g-m_e & 1\end{pmatrix}\begin{pmatrix}\ell' & \ell_e & \lambda''\\ m_e-m_g & -m_e & m_g\end{pmatrix}\begin{pmatrix}\ell_g & 1 & \lambda''\\ m_g & 0 & -m_g\end{pmatrix}\right.\\
&\qquad\times\begin{pmatrix}\ell & \ell_g & \lambda'\\ m_g-m_e+1 & -m_g & m_e-1\end{pmatrix}\begin{pmatrix}\ell_e & 1 & \lambda'\\ m_e & -1 & 1-m_e\end{pmatrix}\\
&\qquad+\begin{pmatrix}\ell & \ell' & \lambda\\ m_e-m_g & m_g-m_e-1 & 1\end{pmatrix}\begin{pmatrix}\ell' & \ell_e & \lambda''\\ m_e-m_g+1 & -m_e & m_g-1\end{pmatrix}\\
&\qquad\left.\times\begin{pmatrix}\ell_g & 1 & \lambda''\\ m_g & -1 & 1-m_g\end{pmatrix}\begin{pmatrix}\ell & \ell_g & \lambda'\\ m_g-m_e & -m_g & m_e\end{pmatrix}\begin{pmatrix}\ell_e & 1 & \lambda'\\ m_e & 0 & -m_e\end{pmatrix}\right]\\
&+\sum_{\lambda=0}^{\infty}(2\lambda+1)\begin{pmatrix}1 & 1 & \lambda\\ 0 & 0 & 0\end{pmatrix}\begin{pmatrix}1 & 1 & \lambda\\ 0 & -1 & 1\end{pmatrix}\begin{pmatrix}\ell & \ell' & \lambda\\ 0 & 0 & 0\end{pmatrix}
\end{aligned}\tag{A.16}$$

$$
\begin{aligned}
&\times\Bigg[\begin{pmatrix} \ell & \ell' & \lambda \\ m_e-m_g+1 & m_g-m_e & -1 \end{pmatrix}\begin{pmatrix} \ell' & \ell_e & \lambda'' \\ m_e-m_g & -m_e & m_g \end{pmatrix}\begin{pmatrix} \ell_g & 1 & \lambda'' \\ m_g & 0 & -m_g \end{pmatrix}\\
&\quad\times\begin{pmatrix} \ell & \ell_g & \lambda' \\ m_g-m_e-1 & -m_g & m_e+1 \end{pmatrix}\begin{pmatrix} \ell_e & 1 & \lambda' \\ m_e & 1 & -1-m_e \end{pmatrix}\\
&\quad+\begin{pmatrix} \ell & \ell' & \lambda \\ m_e-m_g & m_g-m_e+1 & -1 \end{pmatrix}\begin{pmatrix} \ell' & \ell_e & \lambda'' \\ m_e-m_g-1 & -m_e & m_g+1 \end{pmatrix}\\
&\quad\times\begin{pmatrix} \ell_g & 1 & \lambda'' \\ m_g & 1 & -1-m_g \end{pmatrix}\begin{pmatrix} \ell & \ell_g & \lambda' \\ m_g-m_e & -m_g & m_e \end{pmatrix}\begin{pmatrix} \ell_e & 1 & \lambda' \\ m_e & 0 & -m_e \end{pmatrix}\Bigg]\\
&+\sum_{\lambda=0}^{\infty}(2\lambda+1)\begin{pmatrix} 1 & 1 & \lambda \\ 0 & 0 & 0 \end{pmatrix}\begin{pmatrix} 1 & 1 & \lambda \\ 1 & -1 & 0 \end{pmatrix}\begin{pmatrix} \ell & \ell' & \lambda \\ 0 & 0 & 0 \end{pmatrix}\\
&\quad\times\Bigg[\begin{pmatrix} \ell & \ell' & \lambda \\ m_e-m_g-1 & m_g-m_e+1 & 0 \end{pmatrix}\begin{pmatrix} \ell' & \ell_e & \lambda'' \\ m_e-m_g-1 & -m_e & m_g+1 \end{pmatrix}\\
&\quad\times\begin{pmatrix} \ell_g & 1 & \lambda'' \\ m_g & 1 & -1-m_g \end{pmatrix}\begin{pmatrix} \ell & \ell_g & \lambda' \\ m_g-m_e+1 & -m_g & m_e-1 \end{pmatrix}\begin{pmatrix} \ell_e & 1 & \lambda' \\ m_e & -1 & 1-m_e \end{pmatrix}\\
&\quad+\begin{pmatrix} \ell & \ell' & \lambda \\ m_e-m_g+1 & m_g-m_e-1 & 0 \end{pmatrix}\begin{pmatrix} \ell' & \ell_e & \lambda'' \\ m_e-m_g+1 & -m_e & m_g-1 \end{pmatrix}\\
&\quad\times\begin{pmatrix} \ell_g & 1 & \lambda'' \\ m_g & -1 & 1-m_g \end{pmatrix}\begin{pmatrix} \ell & \ell_g & \lambda' \\ m_g-m_e-1 & -m_g & m_e+1 \end{pmatrix}\begin{pmatrix} \ell_e & 1 & \lambda' \\ m_e & 1 & -1-m_e \end{pmatrix}\Bigg],
\end{aligned}
$$

$$
\begin{aligned}
B=&\sqrt{\frac{2}{3}}\begin{pmatrix} \ell & \ell' & 2 \\ 0 & 0 & 0 \end{pmatrix}\begin{pmatrix} \ell & \ell' & 2 \\ m_e-m_g-1 & m_g-m_e-1 & 2 \end{pmatrix}\begin{pmatrix} \ell' & \ell_e & \lambda'' \\ 1+m_e-m_g & -m_e & m_g-1 \end{pmatrix}\\
&\times\begin{pmatrix} \ell_g & 1 & \lambda'' \\ m_g & -1 & 1-m_g \end{pmatrix}\begin{pmatrix} \ell_e & 1 & \lambda' \\ m_e & -1 & 1-m_e \end{pmatrix}\begin{pmatrix} \ell & \ell_g & \lambda' \\ 1-m_e+m_g & -m_g & m_e-1 \end{pmatrix}\\
&+\sqrt{\frac{2}{3}}\begin{pmatrix} \ell & \ell' & 2 \\ 0 & 0 & 0 \end{pmatrix}\begin{pmatrix} \ell & \ell' & 2 \\ m_e-m_g+1 & m_g-m_e+1 & -2 \end{pmatrix}\begin{pmatrix} \ell' & \ell_e & \lambda'' \\ m_e-m_g-1 & -m_e & m_g+1 \end{pmatrix}\\
&\times\begin{pmatrix} \ell_g & 1 & \lambda'' \\ m_g & 1 & -1-m_g \end{pmatrix}\begin{pmatrix} \ell & \ell_g & \lambda' \\ m_g-m_e-1 & -m_g & m_e+1 \end{pmatrix}\begin{pmatrix} \ell_e & 1 & \lambda' \\ m_e & 1 & -1-m_e \end{pmatrix}.
\end{aligned}
\tag{A.17}
$$

This yields hence

$$
\begin{aligned}
&\mathrm{tr}_{\mathrm{F}}\left(\hat{\mathcal{U}}^{(2)}\hat{\rho}_0\right)\Big|_{\boldsymbol{k}\otimes\boldsymbol{k}} \\
&= e^2\int_0^\infty \frac{\mathrm{d}|\boldsymbol{k}|}{(2\pi)^3}\frac{|\boldsymbol{k}|^3}{2}\sum_{\ell,\ell'=0}^{\infty}\sum_{m=-\ell}^{\ell}\sum_{m'=-\ell'}^{\ell'}(4\pi)^2\mathrm{i}^{\ell+\ell'}(-1)^{\ell'}\left(\frac{4\pi}{3}\right)^2\int_{\mathbb{R}}\mathrm{d}t\int_{-\infty}^{t}\mathrm{d}t'\chi(t)\chi(t')e^{-\mathrm{i}|\boldsymbol{k}|(t-t')} \\
&\quad\times\int_0^\infty \mathrm{d}|\boldsymbol{x}||\boldsymbol{x}|^3 R_{n_e\ell_e}(|\boldsymbol{x}|)R_{n_g\ell_g}(|\boldsymbol{x}|)j_\ell(|\boldsymbol{k}||\boldsymbol{x}|)\int_0^\infty \mathrm{d}|\boldsymbol{x}'||\boldsymbol{x}'|^3 R_{n_e\ell_e}(|\boldsymbol{x}'|)R_{n_g\ell_g}(|\boldsymbol{x}'|)j_{\ell'}(|\boldsymbol{k}||\boldsymbol{x}'|) \\
&\quad\times\int \mathrm{d}\Omega_k Y_{\ell m}(\hat{\boldsymbol{k}})Y_{\ell' m'}(\hat{\boldsymbol{k}})\int\mathrm{d}\Omega_x\int\mathrm{d}\Omega_{x'}Y^*_{\ell m}(\hat{\boldsymbol{x}})Y^*_{\ell' m'}(\hat{\boldsymbol{x}'})\Big[Y_{10}(\hat{\boldsymbol{x}})Y_{10}(\hat{\boldsymbol{k}})-Y_{11}(\hat{\boldsymbol{x}})Y_{1-1}(\hat{\boldsymbol{k}}) \\
&\qquad -Y_{1-1}(\hat{\boldsymbol{x}})Y_{11}(\hat{\boldsymbol{k}})\Big]\Big[Y_{10}(\hat{\boldsymbol{k}})Y_{10}(\hat{\boldsymbol{x}'})-Y_{11}(\hat{\boldsymbol{k}})Y_{1-1}(\hat{\boldsymbol{x}'})-Y_{1-1}(\hat{\boldsymbol{k}})Y_{11}(\hat{\boldsymbol{x}'})\Big] \\
&\quad\times\Big\{\Big[\left(1-a^2\right)|e\rangle\langle e|+a\sqrt{1-a^2}\,|e\rangle\langle g|\Big]e^{\mathrm{i}\Omega(t-t')}Y^*_{\ell_e m_e}(\hat{\boldsymbol{x}})Y_{\ell_g m_g}(\hat{\boldsymbol{x}})Y_{\ell_e m_e}(\hat{\boldsymbol{x}'})Y^*_{\ell_g m_g}(\hat{\boldsymbol{x}'}) \\
&\qquad+\Big[a^2|g\rangle\langle g|+a\sqrt{1-a^2}\,|g\rangle\langle e|\Big]e^{-\mathrm{i}\Omega(t-t')}Y_{\ell_e m_e}(\hat{\boldsymbol{x}})Y^*_{\ell_g m_g}(\hat{\boldsymbol{x}})Y^*_{\ell_e m_e}(\hat{\boldsymbol{x}'})Y_{\ell_g m_g}(\hat{\boldsymbol{x}'})\Big\} \\
&= e^2\int_0^\infty \frac{\mathrm{d}|\boldsymbol{k}|}{(2\pi)^3}\frac{|\boldsymbol{k}|^3}{2}4\pi\int_{\mathbb{R}}\mathrm{d}t\int_{-\infty}^{t}\mathrm{d}t'\chi(t)\chi(t')e^{-\mathrm{i}|\boldsymbol{k}|(t-t')}\sum_{\ell,\ell'=0}^{\infty}\mathrm{i}^{\ell+\ell'}(2\ell+1)(2\ell'+1) \\
&\quad\times(2\ell_g+1)(2\ell_e+1)\int_0^\infty \mathrm{d}|\boldsymbol{x}||\boldsymbol{x}|^3 R_{n_e\ell_e}(|\boldsymbol{x}|)R_{n_g\ell_g}(|\boldsymbol{x}|)\int_0^\infty \mathrm{d}|\boldsymbol{x}'||\boldsymbol{x}'|^3 R_{n_e\ell_e}(|\boldsymbol{x}'|)R_{n_g\ell_g}(|\boldsymbol{x}'|) \\
&\quad\times\sum_{\lambda',\lambda''=0}^{\infty}(2\lambda'+1)(2\lambda''+1)\begin{pmatrix}\ell & \ell_g & \lambda'\\ 0 & 0 & 0\end{pmatrix}\begin{pmatrix}\ell_e & 1 & \lambda'\\ 0 & 0 & 0\end{pmatrix}\begin{pmatrix}\ell' & \ell_e & \lambda''\\ 0 & 0 & 0\end{pmatrix}\begin{pmatrix}\ell_g & 1 & \lambda''\\ 0 & 0 & 0\end{pmatrix}(A+B) \\
&\quad\times\Big\{(-1)^\ell j_\ell(|\boldsymbol{k}||\boldsymbol{x}'|)j_{\ell'}(|\boldsymbol{k}||\boldsymbol{x}|)\Big[\left(1-a^2\right)|e\rangle\langle e|+a\sqrt{1-a^2}\,|e\rangle\langle g|\Big]e^{\mathrm{i}\Omega(t-t')} \\
&\qquad+(-1)^{\ell'}j_\ell(|\boldsymbol{k}||\boldsymbol{x}|)j_{\ell'}(|\boldsymbol{k}||\boldsymbol{x}'|)\Big[a^2|g\rangle\langle g|+a\sqrt{1-a^2}\,|g\rangle\langle e|\Big]e^{-\mathrm{i}\Omega(t-t')}\Big\}, \qquad \text{(A.18)}
\end{aligned}
$$

where we redefined $\ell \leftrightarrow \ell'$ for the first term in the curly brackets to derive the last formula.

The last contribution we have to calculate is analogously

$$
\begin{aligned}
&\mathrm{tr}_{\mathrm{F}}\left(\hat{\mathcal{U}}^{(1)}\hat{\rho}_0\hat{\mathcal{U}}^{(1)\dagger}\right)\Big|_{\boldsymbol{k}\otimes\boldsymbol{k}}\\
&=-e^2\int_0^\infty\frac{\mathrm{d}|\boldsymbol{k}|}{(2\pi)^3}\frac{|\boldsymbol{k}|^3}{2}\sum_{\ell,\ell'=0}^{\infty}\sum_{m=-\ell}^{\ell}\sum_{m'=-\ell'}^{\ell'}(4\pi)^2\mathrm{i}^{\ell+\ell'}(-1)^{\ell'}\left(\frac{4\pi}{3}\right)^2\int_{\mathbb{R}}\mathrm{d}t\int_{\mathbb{R}}\mathrm{d}t'\chi(t)\chi(t')e^{-\mathrm{i}|\boldsymbol{k}|(t'-t)}\\
&\quad\times\int_0^\infty\mathrm{d}|\boldsymbol{x}||\boldsymbol{x}|^3R_{n_e\ell_e}(|\boldsymbol{x}|)R_{n_g\ell_g}(|\boldsymbol{x}|)j_\ell(|\boldsymbol{k}||\boldsymbol{x}|)\int_0^\infty\mathrm{d}|\boldsymbol{x}'||\boldsymbol{x}'|^3R_{n_e\ell_e}(|\boldsymbol{x}'|)R_{n_g\ell_g}(|\boldsymbol{x}'|)j_{\ell'}(|\boldsymbol{k}||\boldsymbol{x}'|)\\
&\quad\times\int\mathrm{d}\Omega_kY_{\ell m}(\hat{\boldsymbol{k}})Y_{\ell'm'}(\hat{\boldsymbol{k}})\int\mathrm{d}\Omega_x\int\mathrm{d}\Omega_{x'}Y^*_{\ell m}(\hat{\boldsymbol{x}})Y^*_{\ell'm'}(\hat{\boldsymbol{x}'})\Big[Y_{10}(\hat{\boldsymbol{x}})Y_{10}(\hat{\boldsymbol{k}})-Y_{11}(\hat{\boldsymbol{x}})Y_{1-1}(\hat{\boldsymbol{k}})\\
&\qquad-Y_{1-1}(\hat{\boldsymbol{x}})Y_{11}(\hat{\boldsymbol{k}})\Big]\Big[Y_{10}(\hat{\boldsymbol{k}})Y_{10}(\hat{\boldsymbol{x}'})-Y_{11}(\hat{\boldsymbol{k}})Y_{1-1}(\hat{\boldsymbol{x}'})-Y_{1-1}(\hat{\boldsymbol{k}})Y_{11}(\hat{\boldsymbol{x}'})\Big]\\
&\quad\times\Big\{\left(1-a^2\right)|g\rangle\langle g|\,e^{-\mathrm{i}\Omega(t-t')}Y^*_{\ell_e m_e}(\hat{\boldsymbol{x}'})Y_{\ell_g m_g}(\hat{\boldsymbol{x}'})Y_{\ell_e m_e}(\hat{\boldsymbol{x}})Y^*_{\ell_g m_g}(\hat{\boldsymbol{x}})\\
&\qquad+a^2|e\rangle\langle e|\,e^{\mathrm{i}\Omega(t-t')}Y_{\ell_e m_e}(\hat{\boldsymbol{x}'})Y^*_{\ell_g m_g}(\hat{\boldsymbol{x}'})Y^*_{\ell_e m_e}(\hat{\boldsymbol{x}})Y_{\ell_g m_g}(\hat{\boldsymbol{x}})\\
&\qquad+a\sqrt{1-a^2}\,|g\rangle\langle e|\,e^{-\mathrm{i}\Omega(t+t')}Y_{\ell_e m_e}(\hat{\boldsymbol{x}'})Y^*_{\ell_g m_g}(\hat{\boldsymbol{x}'})Y_{\ell_e m_e}(\hat{\boldsymbol{x}})Y^*_{\ell_g m_g}(\hat{\boldsymbol{x}})\\
&\qquad+a\sqrt{1-a^2}\,|e\rangle\langle g|\,e^{\mathrm{i}\Omega(t+t')}Y^*_{\ell_e m_e}(\hat{\boldsymbol{x}'})Y_{\ell_g m_g}(\hat{\boldsymbol{x}'})Y^*_{\ell_e m_e}(\hat{\boldsymbol{x}})Y_{\ell_g m_g}(\hat{\boldsymbol{x}})\Big\}\\
&=-e^2\int_0^\infty\frac{\mathrm{d}|\boldsymbol{k}|}{(2\pi)^3}\frac{|\boldsymbol{k}|^3}{2}4\pi\int_{\mathbb{R}}\mathrm{d}t\int_{\mathbb{R}}\mathrm{d}t'\chi(t)\chi(t')e^{-\mathrm{i}|\boldsymbol{k}|(t'-t)}\int_0^\infty\mathrm{d}|\boldsymbol{x}||\boldsymbol{x}|^3R_{n_e\ell_e}(|\boldsymbol{x}|)R_{n_g\ell_g}(|\boldsymbol{x}|)\\
&\quad\times\int_0^\infty\mathrm{d}|\boldsymbol{x}'||\boldsymbol{x}'|^3R_{n_e\ell_e}(|\boldsymbol{x}'|)R_{n_g\ell_g}(|\boldsymbol{x}'|)\sum_{\ell,\ell'=0}^{\infty}\mathrm{i}^{\ell+\ell'}(2\ell+1)(2\ell'+1)(2\ell_g+1)(2\ell_e+1)\\
&\quad\times\sum_{\lambda',\lambda''=0}^{\infty}(2\lambda'+1)(2\lambda''+1)\Bigg\{\begin{pmatrix}\ell&\ell_g&\lambda'\\0&0&0\end{pmatrix}\begin{pmatrix}\ell_e&1&\lambda'\\0&0&0\end{pmatrix}\begin{pmatrix}\ell'&\ell_e&\lambda''\\0&0&0\end{pmatrix}\begin{pmatrix}\ell_g&1&\lambda''\\0&0&0\end{pmatrix}(A+B)\\
&\qquad\times\Big[(-1)^\ell j_{\ell'}(|\boldsymbol{k}||\boldsymbol{x}'|)j_\ell(|\boldsymbol{k}||\boldsymbol{x}|)\left(1-a^2\right)|g\rangle\langle g|\,e^{-\mathrm{i}\Omega(t-t')}\\
&\qquad\quad+(-1)^{\ell'}j_\ell(|\boldsymbol{k}||\boldsymbol{x}'|)j_{\ell'}(|\boldsymbol{k}||\boldsymbol{x}|)a^2|e\rangle\langle e|\,e^{\mathrm{i}\Omega(t-t')}\Big]\\
&\qquad+\delta^{m_g}_{m_e}\begin{pmatrix}\ell&\ell_g&\lambda'\\0&0&0\end{pmatrix}\begin{pmatrix}\ell_e&1&\lambda'\\0&0&0\end{pmatrix}\begin{pmatrix}\ell'&\ell_g&\lambda''\\0&0&0\end{pmatrix}\begin{pmatrix}\ell_e&1&\lambda''\\0&0&0\end{pmatrix}\left(\tilde{A}+\tilde{B}\right)\\
&\qquad\quad\times(-1)^{\ell'}j_\ell(|\boldsymbol{k}||\boldsymbol{x}'|)j_{\ell'}(|\boldsymbol{k}||\boldsymbol{x}|)a\sqrt{1-a^2}\,|g\rangle\langle e|\,e^{-\mathrm{i}\Omega(t+t')}\\
&\qquad+\delta^{m_g}_{m_e}\begin{pmatrix}\ell&\ell_e&\lambda'\\0&0&0\end{pmatrix}\begin{pmatrix}\ell_g&1&\lambda'\\0&0&0\end{pmatrix}\begin{pmatrix}\ell'&\ell_e&\lambda''\\0&0&0\end{pmatrix}\begin{pmatrix}\ell_g&1&\lambda''\\0&0&0\end{pmatrix}\left(\tilde{\tilde{A}}+\tilde{\tilde{B}}\right)\\
&\qquad\quad\times(-1)^{\ell'}j_\ell(|\boldsymbol{k}||\boldsymbol{x}'|)j_{\ell'}(|\boldsymbol{k}||\boldsymbol{x}|)a\sqrt{1-a^2}\,|e\rangle\langle g|\,e^{\mathrm{i}\Omega(t+t')}\Bigg\},
\end{aligned}
\tag{A.19}
$$

with $\tilde{x}$ indicating $\ell_e \leftrightarrow \ell_g$ ($m_e \leftrightarrow m_g$) in $3j$-symbols involving λ'' (therefore also for the m-component of ℓ') and $\tilde{\tilde{x}}$ that $\ell_e \leftrightarrow \ell_g$ ($m_e \leftrightarrow m_g$) in $3j$-symbols involving λ' (also for the m-component of ℓ). For instance,

$$
\begin{aligned}
x &= \begin{pmatrix} \ell & \ell' & 2 \\ m_e - m_g - 1 & m_g - m_e - 1 & 2 \end{pmatrix} \begin{pmatrix} \ell_g & 1 & \lambda'' \\ m_g & -1 & 1 - m_g \end{pmatrix} \begin{pmatrix} \ell_e & 1 & \lambda' \\ m_e & -1 & 1 - m_e \end{pmatrix}, \\
\tilde{x} &= \begin{pmatrix} \ell & \ell' & 2 \\ m_e - m_g - 1 & m_e - m_g - 1 & 2 \end{pmatrix} \begin{pmatrix} \ell_e & 1 & \lambda'' \\ m_e & -1 & 1 - m_e \end{pmatrix} \begin{pmatrix} \ell_e & 1 & \lambda' \\ m_e & -1 & 1 - m_e \end{pmatrix}, \\
\tilde{\tilde{x}} &= \begin{pmatrix} \ell & \ell' & 2 \\ m_g - m_e - 1 & m_g - m_e - 1 & 2 \end{pmatrix} \begin{pmatrix} \ell_g & 1 & \lambda'' \\ m_g & -1 & 1 - m_g \end{pmatrix} \begin{pmatrix} \ell_g & 1 & \lambda' \\ m_g & -1 & 1 - m_g \end{pmatrix}.
\end{aligned}
$$

This implies that the coefficients contain terms of the form

$$
\begin{pmatrix} \ell & \ell' & \lambda \\ m_1 & m_2 & m_3 \end{pmatrix}, \; m_1 + m_2 + m_3 \neq 0. \tag{A.20}
$$

Therefore, unless $m_e = m_g$, the third and last term of the curly brackets vanish in (A.19). The Kronecker delta has been explicitly added to stress this fact.

Now all expressions are in generality and cannot be simplified more without specifying the atomic transition and the switching function.

A.2 Transition from Ground to First Excited State

In the following we will derive the time evolved density matrix by studying the $1s \to 2p_z$ transition ($\ell_g = 0$, $m_g = 0$, $\ell_e = 1$, $m_e = 1$). Then (A.9) can be simplified by using the properties of the Wigner $3j$-symbols. In particular the first $3j$-symbol forces $\ell = \lambda$, moreover we see that $\lambda' = 1$ and $\lambda = 0, 1, 2$. Thus it yields

$$
\begin{aligned}
&\mathrm{tr}_{\mathrm{F}} \left(\hat{\mathcal{U}}^{(2)} \hat{\rho}_0 \right) \Big|_{\mathbb{1}} \\
&= -e^2 \int_0^\infty \frac{\mathrm{d}|\boldsymbol{k}|}{(2\pi)^3} \frac{|\boldsymbol{k}|^3}{2} 4\pi \int_{\mathbb{R}} \mathrm{d}t \int_{-\infty}^t \mathrm{d}t' \chi(t)\chi(t') e^{-\mathrm{i}|\boldsymbol{k}|(t-t')} \int_0^\infty \mathrm{d}|\boldsymbol{x}||\boldsymbol{x}|^3 R_{2,1}(|\boldsymbol{x}|) R_{1,0}(|\boldsymbol{x}|) \\
&\quad \times \int_0^\infty \mathrm{d}|\boldsymbol{x}'||\boldsymbol{x}'|^3 R_{2,1}(|\boldsymbol{x}'|) R_{1,0}(|\boldsymbol{x}'|) \frac{1}{3} \left[j_0(|\boldsymbol{k}||\boldsymbol{x}|) j_0(|\boldsymbol{k}||\boldsymbol{x}'|) + 2 j_2(|\boldsymbol{k}||\boldsymbol{x}|) j_2(|\boldsymbol{k}||\boldsymbol{x}'|) \right] \\
&\quad \times \left\{ \left[\left(1 - a^2\right) |e\rangle\langle e| + a\sqrt{1 - a^2}\, |e\rangle\langle g| \right] e^{\mathrm{i}\Omega(t-t')} + \left[a^2 |g\rangle\langle g| + a\sqrt{1 - a^2}\, |g\rangle\langle e| \right] e^{-\mathrm{i}\Omega(t-t')} \right\}.
\end{aligned} \tag{A.21}
$$

We solve the integral over $|\boldsymbol{x}|$ and $|\boldsymbol{x}'|$ by using the following identity [24]

$$\int_0^\infty \mathrm{d}r\, r^3 R_{2,1}(r) R_{1,0}(r) j_\ell(|\boldsymbol{k}|r) = 8\sqrt{2\pi} 3^{-\ell-\frac{11}{2}} a_0^{\ell+1} |\boldsymbol{k}|^\ell \Gamma(\ell+5) \times {}_2\tilde{F}_1\left(\frac{\ell+5}{2}, \frac{\ell+6}{2}; \ell+\frac{3}{2}; -\frac{4}{9}a_0^2|\boldsymbol{k}|^2\right), \tag{A.22}$$

with ${}_2\tilde{F}_1\left(a,b;c;z\right) := {}_2F_1(a,b;c;z)/\Gamma(z)$ being the regularized hypergeometric function. Therefore we find

$$\begin{aligned}
&\mathrm{tr}_{\mathrm{F}}\left(\hat{\mathcal{U}}^{(2)}\hat{\rho}_0\right)\Big|_{\mathbb{1}} \qquad\qquad (A.23)\\
&= -e^2 a_0^2 \frac{663552}{\pi^2} \int_0^\infty \mathrm{d}|\boldsymbol{k}||\boldsymbol{k}|^3 \int_{\mathbb{R}} \mathrm{d}t \int_{-\infty}^t \mathrm{d}t' \chi(t)\chi(t') e^{-\mathrm{i}|\boldsymbol{k}|(t-t')} \frac{16a_0^4|\boldsymbol{k}|^4 - 8a_0^2|\boldsymbol{k}|^2 + 9}{\left(4a_0^2|\boldsymbol{k}|^2+9\right)^8}\\
&\times \left\{\left[\left(1-a^2\right)|e\rangle\langle e| + a\sqrt{1-a^2}\,|e\rangle\langle g|\right] e^{\mathrm{i}\Omega(t-t')} + \left[a^2|g\rangle\langle g| + a\sqrt{1-a^2}\,|g\rangle\langle e|\right] e^{-\mathrm{i}\Omega(t-t')}\right\}.
\end{aligned}$$

Before specifying the switching function $\chi(t)$ to integrate over the time integrals, we will simplify the other contributions to the time evolved density matrix. In particular we find analogously for (A.13)

$$\begin{aligned}
&\mathrm{tr}_{\mathrm{F}}\left(\hat{\mathcal{U}}^{(1)}\hat{\rho}_0\hat{\mathcal{U}}^{(1)\dagger}\right)\Big|_{\mathbb{1}} \qquad\qquad (A.24)\\
&= e^2 \int_0^\infty \frac{\mathrm{d}|\boldsymbol{k}|}{(2\pi)^3}\frac{|\boldsymbol{k}|^3}{2} 4\pi \int_{\mathbb{R}} \mathrm{d}t \int_{\mathbb{R}} \mathrm{d}t' \chi(t)\chi(t') e^{-\mathrm{i}|\boldsymbol{k}|(t'-t)} \int_0^\infty \mathrm{d}|\boldsymbol{x}||\boldsymbol{x}|^3 R_{2,1}(|\boldsymbol{x}|) R_{1,0}(|\boldsymbol{x}|)\\
&\quad\times \int_0^\infty \mathrm{d}|\boldsymbol{x}'||\boldsymbol{x}'|^3 R_{2,1}(|\boldsymbol{x}'|) R_{1,0}(|\boldsymbol{x}'|) \frac{1}{3}\left[j_0(|\boldsymbol{k}||\boldsymbol{x}|) j_0(|\boldsymbol{k}||\boldsymbol{x}'|) + 2j_2(|\boldsymbol{k}||\boldsymbol{x}|) j_2(|\boldsymbol{k}||\boldsymbol{x}'|)\right]\\
&\quad\times \Big\{\left(1-a^2\right)|g\rangle\langle g|\, e^{-\mathrm{i}\Omega(t-t')} + a^2|e\rangle\langle e|\, e^{\mathrm{i}\Omega(t-t')}\\
&\qquad + a\sqrt{1-a^2}\,|e\rangle\langle g|\, e^{\mathrm{i}\Omega(t+t')} + a\sqrt{1-a^2}\,|g\rangle\langle e|\, e^{-\mathrm{i}\Omega(t+t')}\Big\},
\end{aligned}$$

where we used for last term in the curly brackets that $\lambda = \lambda' = \ell$ and $\lambda = 0,1,2$. For the penultimate term in the curly brackets one finds $\lambda = \lambda' = 1$ and $\ell = 0,1,2$. By virtue of

(A.22) we arrive at

$$\begin{aligned}
&\mathrm{tr}_{\mathrm{F}}\left(\hat{\mathcal{U}}^{(1)}\hat{\rho}_0\hat{\mathcal{U}}^{(1)\dagger}\right)\Big|_{\mathbb{1}} \qquad (A.25)\\
&= e^2a_0^2\frac{663552}{\pi^2}\int_0^\infty \mathrm{d}|\boldsymbol{k}||\boldsymbol{k}|^3\int_{\mathbb{R}}\mathrm{d}t\int_{\mathbb{R}}\mathrm{d}t'\chi(t)\chi(t')e^{-\mathrm{i}|\boldsymbol{k}|(t'-t)}\frac{16a_0^4|\boldsymbol{k}|^4-8a_0^2|\boldsymbol{k}|^2+9}{\left(4a_0^2|\boldsymbol{k}|^2+9\right)^8}\\
&\quad\times\Big\{\left(1-a^2\right)|g\rangle\langle g|\,e^{-\mathrm{i}\Omega(t-t')}+a^2\,|e\rangle\langle e|\,e^{\mathrm{i}\Omega(t-t')}+a\sqrt{1-a^2}\,|e\rangle\langle g|\,e^{\mathrm{i}\Omega(t+t')}\\
&\qquad+a\sqrt{1-a^2}\,|g\rangle\langle e|\,e^{-\mathrm{i}\Omega(t+t')}\Big\}.
\end{aligned}$$

The same will be shown now for the dyadic contributions. Starting from (A.18) it yields

$$\begin{aligned}
&\mathrm{tr}_{\mathrm{F}}\left(\hat{\mathcal{U}}^{(2)}\hat{\rho}_0\right)\Big|_{\boldsymbol{k}\otimes\boldsymbol{k}} \qquad (A.26)\\
&= e^2\int_0^\infty\frac{\mathrm{d}|\boldsymbol{k}|}{(2\pi)^3}\frac{|\boldsymbol{k}|^3}{2}4\pi\int_{\mathbb{R}}\mathrm{d}t\int_{-\infty}^t\mathrm{d}t'\chi(t)\chi(t')e^{-\mathrm{i}|\boldsymbol{k}|(t-t')}\int_0^\infty\mathrm{d}|\boldsymbol{x}||\boldsymbol{x}|^3R_{2,1}(|\boldsymbol{x}|)R_{1,0}(|\boldsymbol{x}|)\\
&\quad\times\int_0^\infty\mathrm{d}|\boldsymbol{x}'||\boldsymbol{x}'|^3R_{2,1}(|\boldsymbol{x}'|)R_{1,0}(|\boldsymbol{x}'|)\frac{1}{9}\left[j_0(|\boldsymbol{k}||\boldsymbol{x}|)-2j_2(|\boldsymbol{k}||\boldsymbol{x}|)\right]\left[j_0(|\boldsymbol{k}||\boldsymbol{x}'|)-2j_2(|\boldsymbol{k}||\boldsymbol{x}'|)\right]\\
&\quad\times\left\{\left[\left(1-a^2\right)|e\rangle\langle e|+a\sqrt{1-a^2}\,|e\rangle\langle g|\right]e^{\mathrm{i}\Omega(t-t')}+\left[a^2\,|g\rangle\langle g|+a\sqrt{1-a^2}\,|g\rangle\langle e|\right]e^{-\mathrm{i}\Omega(t-t')}\right\},
\end{aligned}$$

by noting that $\lambda=\lambda'=1$ and ℓ, ℓ', $\lambda=0,1,2$. Solving again the spatial integrals we obtain the form

$$\begin{aligned}
&\mathrm{tr}_{\mathrm{F}}\left(\hat{\mathcal{U}}^{(2)}\hat{\rho}_0\right)\Big|_{\boldsymbol{k}\otimes\boldsymbol{k}} \qquad (A.27)\\
&= e^2a_0^2\frac{24576}{\pi^2}\int_0^\infty\mathrm{d}|\boldsymbol{k}||\boldsymbol{k}|^3\int_{\mathbb{R}}\mathrm{d}t\int_{-\infty}^t\mathrm{d}t'\chi(t)\chi(t')e^{-\mathrm{i}|\boldsymbol{k}|(t-t')}\frac{\left(9-20a_0^2|\boldsymbol{k}|^2\right)^2}{\left(4a_0^2|\boldsymbol{k}|^2+9\right)^8}\\
&\quad\times\left\{\left[\left(1-a^2\right)|e\rangle\langle e|+a\sqrt{1-a^2}\,|e\rangle\langle g|\right]e^{\mathrm{i}\Omega(t-t')}+\left[a^2\,|g\rangle\langle g|+a\sqrt{1-a^2}\,|g\rangle\langle e|\right]e^{-\mathrm{i}\Omega(t-t')}\right\}.
\end{aligned}$$

Finally, (A.19) gives

$$
\begin{aligned}
&\mathrm{tr}_{\mathrm{F}}\left(\hat{\mathcal{U}}^{(1)}\hat{\rho}_0\hat{\mathcal{U}}^{(1)\dagger}\right)\Big|_{\boldsymbol{k}\otimes\boldsymbol{k}} \\
&= -e^2\int_0^\infty \frac{\mathrm{d}|\boldsymbol{k}|}{(2\pi)^3}\frac{|\boldsymbol{k}|^3}{2}4\pi\int_{\mathbb{R}}\mathrm{d}t\int_{\mathbb{R}}\mathrm{d}t'\chi(t)\chi(t')e^{-\mathrm{i}|\boldsymbol{k}|(t'-t)} \\
&\quad\times\int_0^\infty \mathrm{d}|\boldsymbol{x}||\boldsymbol{x}|^3R_{2,1}(|\boldsymbol{x}|)R_{1,0}(|\boldsymbol{x}|)\int_0^\infty \mathrm{d}|\boldsymbol{x}'||\boldsymbol{x}'|^3R_{2,1}(|\boldsymbol{x}'|)R_{1,0}(|\boldsymbol{x}'|) \\
&\quad\times\frac{1}{9}\left[j_0(|\boldsymbol{k}||\boldsymbol{x}|)-2j_2(|\boldsymbol{k}||\boldsymbol{x}|)\right]\left[j_0(|\boldsymbol{k}||\boldsymbol{x}'|)-2j_2(|\boldsymbol{k}||\boldsymbol{x}'|)\right]\Big\{\left(1-a^2\right)|g\rangle\langle g|\,e^{-\mathrm{i}\Omega(t-t')} \\
&\qquad +a^2|e\rangle\langle e|\,e^{\mathrm{i}\Omega(t-t')}+a\sqrt{1-a^2}\,|g\rangle\langle e|\,e^{-\mathrm{i}\Omega(t+t')}+a\sqrt{1-a^2}\,|e\rangle\langle g|\,e^{\mathrm{i}\Omega(t+t')}\Big\} \\
&= -e^2a_0^2\frac{24576}{\pi^2}\int_0^\infty \mathrm{d}|\boldsymbol{k}||\boldsymbol{k}|^3\int_{\mathbb{R}}\mathrm{d}t\int_{\mathbb{R}}\mathrm{d}t'\chi(t)\chi(t')e^{-\mathrm{i}|\boldsymbol{k}|(t'-t)}\frac{\left(9-20a_0^2|\boldsymbol{k}|^2\right)^2}{\left(4a_0^2|\boldsymbol{k}|^2+9\right)^8} \\
&\quad\times\Big\{\left(1-a^2\right)|g\rangle\langle g|\,e^{-\mathrm{i}\Omega(t-t')}+a^2|e\rangle\langle e|\,e^{\mathrm{i}\Omega(t-t')}+a\sqrt{1-a^2}\,|g\rangle\langle e|\,e^{-\mathrm{i}\Omega(t+t')} \\
&\qquad +a\sqrt{1-a^2}\,|e\rangle\langle g|\,e^{\mathrm{i}\Omega(t+t')}\Big\}\,. \qquad\qquad (A.28)
\end{aligned}
$$

Now that we have found the analytic expressions evaluated except for the wave vector and time integrals, we can particularize to the desired switching functions and execute the remaining integrals.

A.3 Gaussian, Sudden, and Delta Switching

Here we present the results for three different switching functions: (i) $\chi^{\mathrm{G}}(t) = e^{-t^2/\sigma^2}$

$$\mathrm{tr}_{\mathrm{F}}\left(\hat{\mathcal{U}}^{(1)}\hat{\rho}_0\hat{\mathcal{U}}^{(1)\dagger}\right)\Big|_{\mathbb{1}} = \frac{663552}{\pi}(ea_0\sigma)^2\int_0^\infty \mathrm{d}|\boldsymbol{k}||\boldsymbol{k}|^3\frac{16a_0^4|\boldsymbol{k}|^4 - 8a_0^2|\boldsymbol{k}|^2+9}{(4a_0^2|\boldsymbol{k}|^2+9)^8} \times \begin{pmatrix} (1-a^2)e^{-\frac{1}{2}\sigma^2(|\boldsymbol{k}|-\Omega)^2} & a\sqrt{1-a^2}e^{-\frac{1}{2}\sigma^2(|\boldsymbol{k}|^2+\Omega^2)} \\ a\sqrt{1-a^2}e^{-\frac{1}{2}\sigma^2(|\boldsymbol{k}|^2+\Omega^2)} & a^2e^{-\frac{1}{2}\sigma^2(|\boldsymbol{k}|+\Omega)^2}\end{pmatrix}, \tag{A.29}$$

$$\mathrm{tr}_{\mathrm{F}}\left(\hat{\mathcal{U}}^{(1)}\hat{\rho}_0\hat{\mathcal{U}}^{(1)\dagger}\right)\Big|_{\boldsymbol{k}\otimes\boldsymbol{k}} = -\frac{24576}{\pi}(ea_0\sigma)^2\int_0^\infty \mathrm{d}|\boldsymbol{k}||\boldsymbol{k}|^3\frac{(9-20a_0^2|\boldsymbol{k}|^2)^2}{(4a_0^2|\boldsymbol{k}|^2+9)^8} \times \begin{pmatrix} (1-a^2)e^{-\frac{1}{2}\sigma^2(|\boldsymbol{k}|-\Omega)^2} & a\sqrt{1-a^2}e^{-\frac{1}{2}\sigma^2(|\boldsymbol{k}|^2+\Omega^2)} \\ a\sqrt{1-a^2}e^{-\frac{1}{2}\sigma^2(|\boldsymbol{k}|^2+\Omega^2)} & a^2e^{-\frac{1}{2}\sigma^2(|\boldsymbol{k}|+\Omega)^2}\end{pmatrix}, \tag{A.30}$$

$$\begin{aligned}\mathrm{tr}_{\mathrm{F}}\left(\hat{\mathcal{U}}^{(2)}\hat{\rho}_0\right)\Big|_{\mathbb{1}} =& -\frac{331776}{\pi}(ea_0\sigma)^2\int_0^\infty \mathrm{d}|\boldsymbol{k}||\boldsymbol{k}|^3\frac{16a_0^4|\boldsymbol{k}|^4 - 8a_0^2|\boldsymbol{k}|^2+9}{(4a_0^2|\boldsymbol{k}|^2+9)^8} \\ &\times\left[\mathrm{erfc}\left(\frac{\mathrm{i}\sigma(|\boldsymbol{k}|+\Omega)}{\sqrt{2}}\right)e^{-\frac{1}{2}\sigma^2(|\boldsymbol{k}|+\Omega)^2}\begin{pmatrix}a^2 & a\sqrt{1-a^2}\\ 0 & 0\end{pmatrix}\right. \\ &\left.+\mathrm{erfc}\left(\frac{\mathrm{i}\sigma(|\boldsymbol{k}|-\Omega)}{\sqrt{2}}\right)e^{-\frac{1}{2}\sigma^2(|\boldsymbol{k}|-\Omega)^2}\begin{pmatrix}0 & 0\\ a\sqrt{1-a^2} & 1-a^2\end{pmatrix}\right],\end{aligned} \tag{A.31}$$

$$\begin{aligned}\mathrm{tr}_{\mathrm{F}}\left(\hat{\mathcal{U}}^{(2)}\hat{\rho}_0\right)\Big|_{\boldsymbol{k}\otimes\boldsymbol{k}} =& \frac{12288}{\pi}(ea_0\sigma)^2\int_0^\infty \mathrm{d}|\boldsymbol{k}||\boldsymbol{k}|^3\frac{(9-20a_0^2|\boldsymbol{k}|^2)^2}{(4a_0^2|\boldsymbol{k}|^2+9)^8} \\ &\times\left[\mathrm{erfc}\left(\frac{\mathrm{i}\sigma(|\boldsymbol{k}|+\Omega)}{\sqrt{2}}\right)e^{-\frac{1}{2}\sigma^2(|\boldsymbol{k}|+\Omega)^2}\begin{pmatrix}a^2 & a\sqrt{1-a^2}\\ 0 & 0\end{pmatrix}\right. \\ &\left.+\mathrm{erfc}\left(\frac{\mathrm{i}\sigma(|\boldsymbol{k}|-\Omega)}{\sqrt{2}}\right)e^{-\frac{1}{2}\sigma^2(|\boldsymbol{k}|-\Omega)^2}\begin{pmatrix}0 & 0\\ a\sqrt{1-a^2} & 1-a^2\end{pmatrix}\right],\end{aligned} \tag{A.32}$$

where we have used the following for the nested time integrals:

$$\begin{aligned}
&\int_{-\infty}^{\infty}\mathrm{d}t\int_{-\infty}^{t}\mathrm{d}t' e^{\pm\mathrm{i}\Omega(t-t')}e^{-\frac{t^2}{\sigma^2}}e^{-\frac{t'^2}{\sigma^2}}e^{-\mathrm{i}|\boldsymbol{k}|(t-t')}\\
&=\sqrt{\pi}\frac{\sigma}{2}\int_{-\infty}^{\infty}\mathrm{d}t e^{-\frac{1}{4}(|\boldsymbol{k}|\mp\Omega)^2\sigma^2}e^{\mathrm{i}(\pm\Omega-|\boldsymbol{k}|)t}e^{-\frac{t^2}{\sigma^2}}\\
&=\frac{\pi\sigma^2}{2}e^{-\frac{1}{2}(\Omega^2+|\boldsymbol{k}|^2)\sigma^2}e^{\pm|\boldsymbol{k}|\Omega\sigma^2}I\left(\frac{\sigma}{2}(|\boldsymbol{k}|\mp\Omega),\sigma(|\boldsymbol{k}|\mp\Omega)\right)\\
&=\frac{\pi\sigma^2}{2}\mathrm{erfc}\left(\frac{\mathrm{i}\sigma(|\boldsymbol{k}|\mp\Omega)}{\sqrt{2}}\right)e^{\frac{1}{2}(-|\boldsymbol{k}|^2\sigma^2\pm|\boldsymbol{k}|\Omega\sigma^2-\Omega^2\sigma^2)}\\
&=\frac{\pi\sigma^2}{2}\mathrm{erfc}\left(\frac{\mathrm{i}\sigma(|\boldsymbol{k}|\mp\Omega)}{\sqrt{2}}\right)e^{\frac{1}{2}\sigma^2(|\boldsymbol{k}|\mp\Omega)^2},
\end{aligned}\tag{A.33}$$

with [46]

$$I(a,b)=\int_{-\infty}^{\infty}\mathrm{d}x e^{-a^2-\mathrm{i}bx-x^2}\mathrm{erf}(x-\mathrm{i}a)=-\mathrm{i}\sqrt{\pi}e^{-a^2-\frac{b^2}{4}}\mathrm{erf}\left(\frac{a+\frac{b}{2}}{\sqrt{2}}\right).\tag{A.34}$$

Then the whole change in the atomic state is

$$\begin{aligned}
\Delta\hat{\rho}^{\mathrm{G}}=&\frac{24576(a_0e\sigma)^2}{\pi}\int_0^{\infty}\mathrm{d}|\boldsymbol{k}|\frac{|\boldsymbol{k}|^3e^{-\frac{1}{2}\sigma^2(|\boldsymbol{k}|+\Omega)^2}}{\left(4a_0^2|\boldsymbol{k}|^2+9\right)^6}\left\{2\left[(1-a^2)e^{2|\boldsymbol{k}|\sigma^2\Omega}-a^2\right]\begin{pmatrix}1&0\\0&-1\end{pmatrix}\right.\\
&+\left(a\sqrt{1-a^2}\left[e^{2|\boldsymbol{k}|\sigma^2\Omega}\mathrm{erf}\left(\frac{\mathrm{i}\sigma(|\boldsymbol{k}|-\Omega)}{\sqrt{2}}\right)-\mathrm{erf}\left(\frac{\mathrm{i}\sigma(|\boldsymbol{k}|+\Omega)}{\sqrt{2}}\right)-\left(1-e^{|\boldsymbol{k}|\sigma^2\Omega}\right)^2\right]\right.\\
&\left.\left.\times\begin{pmatrix}0&0\\1&0\end{pmatrix}+\mathrm{H.c.}\right)\right\}
\end{aligned}\tag{A.35}$$

For the sudden top-hat switching (ii) $\chi^{\mathrm{s}}(t)=\Theta(t)\Theta(-t+\sigma)$, with the duration of

interaction σ,

$$\mathrm{tr}_{\mathrm{F}}\left(\hat{\mathcal{U}}^{(1)}\hat{\rho}_0\hat{\mathcal{U}}^{(1)\dagger}\right)\Big|_{\mathbb{1}} \tag{A.36}$$
$$= \frac{1327104}{\pi^2}(ea_0)^2\int_0^\infty \mathrm{d}|\boldsymbol{k}||\boldsymbol{k}|^3\frac{16a_0^4|\boldsymbol{k}|^4-8a_0^2|\boldsymbol{k}|^2+9}{(4a_0^2|\boldsymbol{k}|^2+9)^8}\left[\frac{1-\cos\left(\sigma(|\boldsymbol{k}|-\Omega)\right)}{(|\boldsymbol{k}|-\Omega)^2}\begin{pmatrix}1-a^2 & 0\\ 0 & 0\end{pmatrix}\right.$$
$$\left.+\frac{1-\cos\left(\sigma(|\boldsymbol{k}|+\Omega)\right)}{(|\boldsymbol{k}|+\Omega)^2}\begin{pmatrix}0 & 0\\ 0 & a^2\end{pmatrix}-a\sqrt{1-a^2}\frac{\cos\left(\sigma|\boldsymbol{k}|\right)-\cos\left(\sigma\Omega\right)}{|\boldsymbol{k}|^2+\Omega^2}\begin{pmatrix}0 & e^{-\mathrm{i}\Omega\sigma}\\ e^{\mathrm{i}\Omega\sigma} & 0\end{pmatrix}\right],$$

$$\mathrm{tr}_{\mathrm{F}}\left(\hat{\mathcal{U}}^{(1)}\hat{\rho}_0\hat{\mathcal{U}}^{(1)\dagger}\right)\Big|_{\boldsymbol{k}\otimes\boldsymbol{k}} \tag{A.37}$$
$$= -\frac{49152}{\pi^2}(ea_0)^2\int_0^\infty \mathrm{d}|\boldsymbol{k}||\boldsymbol{k}|^3\frac{(9-20a_0^2|\boldsymbol{k}|^2)^2}{(4a_0^2|\boldsymbol{k}|^2+9)^8}\left[\frac{1-\cos\left(\sigma(|\boldsymbol{k}|-\Omega)\right)}{(|\boldsymbol{k}|-\Omega)^2}\begin{pmatrix}1-a^2 & 0\\ 0 & 0\end{pmatrix}\right.$$
$$\left.+\frac{1-\cos\left(\sigma(|\boldsymbol{k}|+\Omega)\right)}{(|\boldsymbol{k}|+\Omega)^2}\begin{pmatrix}0 & 0\\ 0 & a^2\end{pmatrix}-a\sqrt{1-a^2}\frac{\cos\left(\sigma|\boldsymbol{k}|\right)-\cos\left(\sigma\Omega\right)}{|\boldsymbol{k}|^2+\Omega^2}\begin{pmatrix}0 & e^{-\mathrm{i}\Omega\sigma}\\ e^{\mathrm{i}\Omega\sigma} & 0\end{pmatrix}\right],$$

$$\mathrm{tr}_{\mathrm{F}}\left(\hat{\mathcal{U}}^{(2)}\hat{\rho}_0\right)\Big|_{\mathbb{1}} \tag{A.38}$$
$$= \frac{663552}{\pi^2}(ea_0)^2\int_0^\infty \mathrm{d}|\boldsymbol{k}||\boldsymbol{k}|^3\left[\frac{\mathrm{i}\sigma(|\boldsymbol{k}|+\Omega)+e^{-\mathrm{i}\sigma(|\boldsymbol{k}|+\Omega)}-1}{(|\boldsymbol{k}|+\Omega)^2}\begin{pmatrix}a^2 & a\sqrt{1-a^2}\\ 0 & 0\end{pmatrix}\right.$$
$$\left.+\frac{\mathrm{i}\sigma(|\boldsymbol{k}|-\Omega)+e^{-\mathrm{i}\sigma(|\boldsymbol{k}|-\Omega)}-1}{(|\boldsymbol{k}|-\Omega)^2}\begin{pmatrix}0 & 0\\ a\sqrt{1-a^2} & 1-a^2\end{pmatrix}\right]\frac{16a_0^4|\boldsymbol{k}|^4-8a_0^2|\boldsymbol{k}|^2+9}{(4a_0^2|\boldsymbol{k}|^2+9)^8},$$

$$\mathrm{tr}_{\mathrm{F}}\left(\hat{\mathcal{U}}^{(2)}\hat{\rho}_0\right)\Big|_{\boldsymbol{k}\otimes\boldsymbol{k}} \tag{A.39}$$
$$= -\frac{24576}{\pi^2}(ea_0)^2\int_0^\infty \mathrm{d}|\boldsymbol{k}||\boldsymbol{k}|^3\left[\frac{\mathrm{i}\sigma(|\boldsymbol{k}|+\Omega)+e^{-\mathrm{i}\sigma(|\boldsymbol{k}|+\Omega)}-1}{(|\boldsymbol{k}|+\Omega)^2}\begin{pmatrix}a^2 & a\sqrt{1-a^2}\\ 0 & 0\end{pmatrix}\right.$$
$$\left.+\frac{\mathrm{i}\sigma(|\boldsymbol{k}|-\Omega)+e^{-\mathrm{i}\sigma(|\boldsymbol{k}|-\Omega)}-1}{(|\boldsymbol{k}|-\Omega)^2}\begin{pmatrix}0 & 0\\ a\sqrt{1-a^2} & 1-a^2\end{pmatrix}\right]\frac{(9-20a_0^2|\boldsymbol{k}|^2)^2}{(4a_0^2|\boldsymbol{k}|^2+9)^8}.$$

Hence we find the total change of the atomic state to be

$$\begin{aligned}\Delta\hat{\rho}^{\mathrm{S}} =&\frac{49152(a_0 e)^2}{\pi^2}\int_0^\infty \frac{\mathrm{d}|\boldsymbol{k}||\boldsymbol{k}|^3}{\left(4a_0^2|\boldsymbol{k}|^2+9\right)^6\left(|\boldsymbol{k}|^2-\Omega^2\right)^2}\Bigg\{\Big[4|\boldsymbol{k}|\Omega+2a^2(|\boldsymbol{k}|-\Omega)^2\cos(\sigma(|\boldsymbol{k}|+\Omega))\\ &+2\left(1-2a^2\right)\left(|\boldsymbol{k}|^2+\Omega^2\right)+2(a^2-1)\cos(\sigma(|\boldsymbol{k}|-\Omega))(|\boldsymbol{k}|+\Omega)^2\Big]\begin{pmatrix}1&0\\0&-1\end{pmatrix}\\ &+\Bigg(\Big[e^{2\mathrm{i}\sigma\Omega}(|\boldsymbol{k}|^2-\Omega^2)+|\boldsymbol{k}|^2(2\mathrm{i}\sigma\Omega-1)+4\Omega e^{\mathrm{i}\sigma\Omega}(\Omega\cos(|\boldsymbol{k}|\sigma)-\mathrm{i}|\boldsymbol{k}|\sin(|\boldsymbol{k}|\sigma))\\ &-\Omega^2(3+2\mathrm{i}\sigma\Omega)\Big]a\sqrt{1-a^2}\begin{pmatrix}0&0\\1&0\end{pmatrix}+\mathrm{H.c.}\Bigg)\Bigg\}\end{aligned} \tag{A.40}$$

We can particularize to the gapless case ($\Omega = 0$), allowing then to perform the last remaining integral such that

$$\Delta\hat{\rho}^{\mathrm{S}}_{\Omega=0} =\frac{512e^2}{295245\pi^2}\left(1-2a^2\right)\left[24-\sqrt{\pi}G^{2,1}_{1,3}\left(\begin{matrix}0\\0,5,\frac{1}{2}\end{matrix}\,\middle|\,\frac{9\sigma^2}{16a_0^2}\right)\right]\begin{pmatrix}1&0\\0&-1\end{pmatrix}, \tag{A.41}$$

where $G^{m,n}_{p,q}\left(\begin{smallmatrix}a_1,\ldots,a_p\\b_1,\ldots,b_q\end{smallmatrix}\,\middle|\,z\right)$ is the Meijer G-function.

Finally for (iii) $\chi^{\text{D}}(t) = C\delta(t)$, where C is some constant with mass dimension $[C] = -1$,

$$\begin{aligned}
\text{tr}_{\text{F}}\left(\hat{\mathcal{U}}^{(1)}\hat{\rho}_0\hat{\mathcal{U}}^{(1)\dagger}\right)\Big|_{\mathbb{1}} =& \frac{663552C^2}{\pi^2}(ea_0)^2\int_0^\infty \text{d}|\boldsymbol{k}||\boldsymbol{k}|^3\frac{16a_0^4|\boldsymbol{k}|^4 - 8a_0^2|\boldsymbol{k}|^2 + 9}{(4a_0^2|\boldsymbol{k}|^2+9)^8} \\
&\times \begin{pmatrix} 1-a^2 & a\sqrt{1-a^2} \\ a\sqrt{1-a^2} & a^2 \end{pmatrix}, \qquad \text{(A.42)} \\
\text{tr}_{\text{F}}\left(\hat{\mathcal{U}}^{(1)}\hat{\rho}_0\hat{\mathcal{U}}^{(1)\dagger}\right)\Big|_{\boldsymbol{k}\otimes\boldsymbol{k}} =& -\frac{24576C^2}{\pi^2}(ea_0)^2\int_0^\infty \text{d}|\boldsymbol{k}||\boldsymbol{k}|^3\frac{(9-20a_0^2|\boldsymbol{k}|^2)^2}{(4a_0^2|\boldsymbol{k}|^2+9)^8} \\
&\times \begin{pmatrix} 1-a^2 & a\sqrt{1-a^2} \\ a\sqrt{1-a^2} & a^2 \end{pmatrix}, \qquad \text{(A.43)} \\
\text{tr}_{\text{F}}\left(\hat{\mathcal{U}}^{(2)}\hat{\rho}_0\right)\Big|_{\mathbb{1}} =& -\frac{331776C^2}{\pi^2}(ea_0)^2\int_0^\infty \text{d}|\boldsymbol{k}||\boldsymbol{k}|^3\frac{16a_0^4|\boldsymbol{k}|^4 - 8a_0^2|\boldsymbol{k}|^2 + 9}{(4a_0^2|\boldsymbol{k}|^2+9)^8} \\
&\times \begin{pmatrix} a^2 & a\sqrt{1-a^2} \\ a\sqrt{1-a^2} & 1-a^2 \end{pmatrix}, \qquad \text{(A.44)} \\
\text{tr}_{\text{F}}\left(\hat{\mathcal{U}}^{(2)}\hat{\rho}_0\right)\Big|_{\boldsymbol{k}\otimes\boldsymbol{k}} =& \frac{12288C^2}{\pi^2}(ea_0)^2\int_0^\infty \text{d}|\boldsymbol{k}||\boldsymbol{k}|^3\frac{(9-20a_0^2|\boldsymbol{k}|^2)^2}{(4a_0^2|\boldsymbol{k}|^2+9)^8} \\
&\times \begin{pmatrix} a^2 & a\sqrt{1-a^2} \\ a\sqrt{1-a^2} & 1-a^2 \end{pmatrix}. \qquad \text{(A.45)}
\end{aligned}$$

The nested time integrals over the two Dirac distributions are mathematically ambiguous (see [82]) and require us to understand them as some sort of limit of a sequence of functions. If the delta distribution is understood as the limit of a sequence of symmetric peaked functions of smaller and smaller width and constant area (e.g., the Dirac distribution is the short width limit —symmetrically taken— of a sudden top-hat or Gaussian function), as it is shown in the appendix of [82], one can show that

$$\int_{-\infty}^{\infty}\text{d}t\int_{-\infty}^{t}\text{d}t' e^{-\text{i}|\boldsymbol{k}|(t-t')}e^{\pm\text{i}\Omega(t-t')}\delta(t)\delta(t') = \frac{1}{2}. \qquad \text{(A.46)}$$

Our result can be integrated analytically and hence the change in the atomic state due to the delta switching is

$$\Delta\hat{\rho}^{\text{D}} = \frac{128C^2e^2}{10935\pi^2a_0^2}\left(1-2a^2\right)\begin{pmatrix} 1 & 0 \\ 0 & -1 \end{pmatrix}. \qquad \text{(A.47)}$$

In an equal superposition ($a = \frac{1}{\sqrt{2}}$) the atomic state does not get perturbed to second order in perturbation theory for the delta and gapless sudden switching. Thus the purity is preserved which yields $H_{\min} = 1$ bit. As can be easily checked, for all cases the perturbation is traceless and Hermitian.

Appendix B

The Unruh-DeWitt Model and Atoms in Optical Cavities

B.1 Solving for a Massless Scalar Field in a Cylindrical Cavity

First, we have to solve the massless Klein-Gordon equation for a cylindrical cavity with Dirichlet boundary conditions. We thus have a massless scalar field ϕ in a cavity of length L and radius R such that in cylindrical coordinates

$$\phi(t, r, \varphi, z) = 0 \quad \text{for} \quad z = 0,\ z = L,\ r = R. \tag{B.1}$$

The corresponding Klein-Gordon equation takes the form

$$\Box\phi = \frac{1}{r}\frac{\partial}{\partial r}\left(r\frac{\partial\phi}{\partial r}\right) + \frac{1}{r^2}\frac{\partial^2\phi}{\partial\varphi^2} + \frac{\partial^2\phi}{\partial z^2} - \frac{1}{c^2}\frac{\partial^2\phi}{\partial t^2} = 0, \tag{B.2}$$

and can be solved with the following separation ansatz: $\phi(t, r, \phi, z) = \mathcal{R}(r)\Psi(\varphi)Z(z)T(t)$. Hence (B.2) yields

$$\frac{1}{r\mathcal{R}}\frac{\partial}{\partial r}\left(r\frac{\partial\mathcal{R}}{\partial r}\right) + \frac{1}{r^2\Psi}\frac{\partial^2\Psi}{\partial\varphi^2} + \frac{1}{Z}\frac{\partial^2 Z}{\partial z^2} = \frac{1}{c^2 T}\frac{\partial^2 T}{\partial t^2}. \tag{B.3}$$

Since the right-hand side depends only on t and the left-hand side is independent of t, both sides must be equal to a separation constant $-\omega^2$. This gives

$$T(t) = e^{\pm i\omega t}, \tag{B.4}$$

where we omit here (to be computed later) the normalization constant. Therefore, (B.2) can be simplified and reads

$$\frac{1}{r\mathcal{R}}\frac{\partial}{\partial r}\left(r\frac{\partial\mathcal{R}}{\partial r}\right)+\frac{1}{r^2\Psi}\frac{\partial^2\Psi}{\partial\varphi^2}+\frac{1}{Z}\frac{\partial^2 Z}{\partial z^2}+\frac{\omega^2}{c^2}=0. \tag{B.5}$$

Following the same prescription for Z, we find using the separation constant α^2

$$\frac{1}{Z}\frac{\partial^2 Z}{\partial z^2}=-\frac{\omega^2}{c^2}+\alpha^2\Rightarrow Z(z)=\exp\Big(\pm\mathrm{i}\sqrt{\omega^2/c^2-\alpha^2}z\Big). \tag{B.6}$$

Employing the Dirichlet boundary conditions $Z(0)=Z(L)=0$, one arrives at

$$Z(z)=\sin\Big(\sqrt{\omega^2/c^2-\alpha^2}z\Big)=\sin\Big(\frac{n\pi}{L}z\Big), \tag{B.7}$$

where $\sqrt{\omega^2/c^2-\alpha^2}=\frac{n\pi}{L}$ and $n\in\mathbb{Z}^+$. Accordingly,

$$\frac{r}{\mathcal{R}}\frac{\partial}{\partial r}\left(r\frac{\partial\mathcal{R}}{\partial r}\right)+\alpha^2r^2=-\frac{1}{\Psi}\frac{\partial^2\Psi}{\partial\varphi^2}=m^2, \tag{B.8}$$

such that

$$\Psi(\varphi)=e^{\pm\mathrm{i}m\varphi}. \tag{B.9}$$

In order to have a single-valued solution, i.e. $\Psi(\varphi+2\pi)=\Psi(\varphi)$, $m\in\mathbb{Z}^+$. Finally, for the radial part

$$0=\frac{1}{r\mathcal{R}}\frac{\partial}{\partial r}\left(r\frac{\partial\mathcal{R}}{\partial r}\right)-\frac{m^2}{r^2}+\alpha^2\Rightarrow 0=\frac{\partial^2\mathcal{R}}{\partial r^2}+\frac{1}{r}\frac{\partial\mathcal{R}}{\partial r}+\left(\alpha^2-\frac{m^2}{r^2}\right)\mathcal{R}. \tag{B.10}$$

Substituting $\alpha r=x$ yields the Bessel differential equation which can be solved by the Bessel functions $J_m(\alpha r)$ and $Y_m(\alpha r)$ of the first and second kind, respectively. Requiring regularity at $r=0$ and the boundary condition $\mathcal{R}(R)=0$, we find

$$\mathcal{R}(r)=J_m\left(\frac{x_{m\ell}}{R}r\right), \tag{B.11}$$

where $\alpha=\frac{x_{m\ell}}{R}$, and $x_{m\ell}$ is the ℓ-th zero of the m-th Bessel function J_m. This gives

$$\omega=c\sqrt{\frac{x_{m\ell}^2}{R^2}+\frac{n^2\pi^2}{L^2}}. \tag{B.12}$$

Ultimately, and including a normalization factor $A_{m\ell n}$, the solution for the scalar field modes is

$$u_{m\ell n}(t,r,\varphi,z) = A_{m\ell n} e^{\mathrm{i}m\varphi} e^{-\mathrm{i}\omega t} \sin\!\left(\frac{n\pi}{L}z\right) J_m\left(\frac{x_{m\ell}}{R}r\right), \tag{B.13}$$

such that the quantized scalar field takes the form

$$\hat{\phi}(t,r,\varphi,z) = \sum_{\substack{m=0\\ n,\ell=1}}^{\infty} \left(u_{m\ell n}\hat{a}_{m\ell n} + u^*_{m\ell n}\hat{a}^\dagger_{m\ell n}\right), \tag{B.14}$$

where the creation and annihilation operators $\hat{a}^\dagger_{m\ell n}$ and $\hat{a}_{m\ell n}$ have with $[\hat{a}_{m\ell n}, \hat{a}^\dagger_{m'\ell' n'}] = \delta_{mm'}\delta_{\ell\ell'}\delta_{nn'}$ the usual commutation relations. The normalization factors can be found using the Klein-Gordon inner product:

$$\begin{aligned}
(u_{m\ell n}, u_{m'\ell' n'}) &= \mathrm{i}\int \mathrm{d}V \left(u^*_{m\ell n}\frac{\partial u_{m'\ell' n'}}{\partial(ct)} - u_{m'\ell' n'}\frac{\partial u^*_{m\ell n}}{\partial(ct)}\right) \\
&= \frac{2}{c}A^*_{m\ell n}A_{m'\ell' n'}\omega \int_0^s \mathrm{d}r r J_m\left(\frac{x_{m\ell}}{R}r\right) J_{m'}\left(\frac{x_{m'\ell'}}{R}r\right) \int_0^L \mathrm{d}z \sin\!\left(\frac{n\pi}{L}\right)\sin\!\left(\frac{n'\pi}{L}\right) \\
&\quad \times \int_0^{2\pi} \mathrm{d}\varphi e^{\mathrm{i}(m'-m)\varphi} \\
&= \frac{4\pi L R^2}{4c}|A_{m\ell n}|^2 \omega J_{m+1}(x_{m\ell})^2 \delta_{mm'}\delta_{\ell\ell'}\delta_{nn'}
\end{aligned} \tag{B.15}$$

where $\mathrm{d}V$ is a spacelike hypersurface, and we used the Sturm-Liouville orthogonality condition

$$\int_0^s \mathrm{d}r r J_m\left(\frac{x_{m\ell}}{R}r\right) J_m\left(\frac{x_{mj}}{R}r\right) = \frac{R^2}{2}\delta_{\ell j} J_{m+1}(x_{m\ell})^2. \tag{B.16}$$

Thus if we impose delta-normalization for the modes $(u_{m\ell n}, u_{m'\ell' n'}) = \delta_{mm'}\delta_{\ell\ell'}\delta_{nn'}$, then the normalization factor is obained as

$$A_{m\ell n} = \frac{\sqrt{c}}{R\sqrt{L\pi\omega}J_{m+1}(x_{m\ell})}. \tag{B.17}$$

B.2 Time-Evolved Field State

In this section we derive the state of the field after detector crossing. We recall from (2.37)

$$\hat{\rho}_{\text{F}} - |0\rangle_{\text{F}}\langle 0| = \text{tr}_{\text{D}}\left(\hat{\mathcal{U}}^{(1)}\hat{\rho}_0\hat{\mathcal{U}}^{(1)\dagger}\right) + \left(\text{tr}_{\text{D}}\left(\hat{\mathcal{U}}^{(2)}\hat{\rho}_0\right) + \text{H.c.}\right). \tag{B.18}$$

Note that we will drop the subscript F for the field states in the remainder of this appendix. Further, we will introduce the parameter α which is either 1 or 0 when the detector is initially in the ground or excited state, respectively. We find then

$$\begin{aligned}
\hat{\mathcal{U}}^{(1)}\hat{\rho}_0\hat{\mathcal{U}}^{(1)\dagger} &= c^2\lambda^2\int_0^T \mathrm{d}\tau\int_0^T \mathrm{d}\tau'\hat{\phi}(\boldsymbol{x}(\tau),t(\tau))\,|0\rangle\langle 0|\,\hat{\phi}(\boldsymbol{x}(\tau'),t(\tau')) \\
&\quad\times\hat{\mu}(\tau)(\delta_{\alpha 1}\,|g\rangle\langle g| + \delta_{\alpha 0}\,|e\rangle\langle e|)\hat{\mu}(\tau') \\
&= c^2\lambda^2\int_0^T \mathrm{d}\tau\int_0^T \mathrm{d}\tau'\Big(\delta_{\alpha 1}e^{\mathrm{i}\Omega(\tau-\tau')}\,|e\rangle\langle e| + \delta_{\alpha 0}e^{-\mathrm{i}\Omega(\tau-\tau')}\,|g\rangle\langle g|\Big) \\
&\quad\times\sum_{\substack{m=0\\m'=0}}^{\infty}\sum_{\substack{n,\ell=1\\n',\ell'=1}}^{\infty} u^*_{m\ell n}(\tau)u_{m'\ell'n'}(\tau')\,|(m\ell n)\rangle\langle(m'\ell'n')|\,.
\end{aligned} \tag{B.19}$$

Thus after tracing over the detector's degrees of freedom

$$\text{tr}_{\text{D}}\left(\hat{\mathcal{U}}^{(1)}\hat{\rho}_0\hat{\mathcal{U}}^{(1)\dagger}\right) = c^2\lambda^2\int_0^T\mathrm{d}\tau\int_0^T\mathrm{d}\tau' e^{\pm\mathrm{i}\Omega(\tau-\tau')}\sum_{\substack{m=0\\m'=0}}^{\infty}\sum_{\substack{n,\ell=1\\n',\ell'=1}}^{\infty} u^*_{m\ell n}(\tau)u_{m'\ell'n'}(\tau')\,|(m\ell n)\rangle\langle(m'\ell'n')|\,, \tag{B.20}$$

where here, and in the following, the top sign of either $\pm$ or $\mp$ is associated with the initial ground state of the detector, and the bottom sign with its excited state. For the remaining correction term:

$$\begin{aligned}
\hat{\mathcal{U}}^{(2)}\hat{\rho}_0 &= -c^2\lambda^2\int_0^T\mathrm{d}\tau\int_0^\tau\mathrm{d}\tau'\hat{\phi}(\boldsymbol{x}(\tau),t(\tau))\hat{\phi}(\boldsymbol{x}(\tau'),t(\tau'))\,|0\rangle\langle 0|\,\mu(\tau)\mu(\tau')(\delta_{\alpha 1}\,|g\rangle\langle g| + \delta_{\alpha 0}\,|e\rangle\langle e|) \\
&= -c^2\lambda^2\int_0^T\mathrm{d}\tau\int_0^\tau\mathrm{d}\tau'(\delta_{\alpha 1}e^{-\mathrm{i}\Omega(\tau-\tau')}\,|g\rangle\langle g| + \delta_{\alpha 0}e^{\mathrm{i}\Omega(\tau-\tau')}\,|e\rangle\langle e|) \\
&\quad\times\sum_{\substack{m=0\\m'=0}}^{\infty}\sum_{\substack{n,\ell=1\\n',\ell'=1}}^{\infty}\big[u^*_{m\ell n}(\tau)u^*_{m'\ell'n'}(\tau')\,|(m\ell n),(m'\ell'n')\rangle\langle 0| \\
&\qquad\qquad +\delta_{mm'}\delta_{\ell\ell'}\delta_{nn'}u_{m\ell n}(\tau)u^*_{m\ell n}(\tau')\,|0\rangle\langle 0|\big]\,.
\end{aligned} \tag{B.21}$$

Then after tracing out it yields

$$\mathrm{tr}_{\mathrm{D}}\left(\hat{\mathcal{U}}^{(2)}\hat{\rho}_0\right) = -c^2\lambda^2\int_0^T \mathrm{d}\tau \int_0^\tau \mathrm{d}\tau' e^{\mp \mathrm{i}\Omega(\tau-\tau')} \sum_{\substack{m=0\\ m'=0}}^{\infty}\sum_{\substack{n,\ell=1\\ n',\ell'=1}}^{\infty}\Big[u^*_{m\ell n}(\tau)u^*_{m'\ell' n'}(\tau')\,|(m\ell n),(m'\ell' n')\rangle\langle 0| + \delta_{mm'}\delta_{\ell\ell'}\delta_{nn'}u_{m\ell n}(\tau)u^*_{m\ell n}(\tau')\,|0\rangle\langle 0|\Big]. \tag{B.22}$$

B.2.1 Particularizing to Longitudinal Motion

We consider the case that the detector crosses the cavity longitudinally such that the field modes are as in (4.8). To study the number of excitations and corresponding energy deposited in each field mode after a single run we only need to be concerned with the diagonal elements $|(m\ell n)\rangle\langle(m\ell n)|$. To that end, (B.20) can be separated in diagonal and off-diagonal terms, where the former takes the form

$$\mathrm{tr}_{\mathrm{D}}\left(\hat{\mathcal{U}}^{(1)}\hat{\rho}_0\hat{\mathcal{U}}^{(1)\dagger}\right)\Big|_{\mathrm{diag}} = c^2\lambda^2\sum_{n,\ell=1}^{\infty}|A_{0\ell n}|^2\,|(0\ell n)\rangle\langle(0\ell n)| \times\left|\int_0^T \mathrm{d}\tau e^{\pm\mathrm{i}\Omega\tau}e^{\mathrm{i}\frac{\omega c}{a}\sinh(a\tau/c)}\sin\left(\frac{n\pi c^2}{aL}\left(\cosh(a\tau/c)-1\right)\right)\right|^2. \tag{B.23}$$

Therefore the number expectation value in modes n, ℓ reads

$$N_{\ell,n} = c^2\lambda^2|A_{0\ell n}|^2\left|\int_0^T \mathrm{d}\tau e^{\pm\mathrm{i}\Omega\tau}e^{\mathrm{i}\frac{\omega c}{a}\sinh(a\tau/c)}\sin\left(\frac{n\pi c^2}{aL}\left(\cosh(a\tau/c)-1\right)\right)\right|^2, \tag{B.24}$$

where $\ell, n \geq 1$. It is not necessary to study the contribution coming from $\mathrm{tr}_{\mathrm{D}}\left(\hat{\mathcal{U}}^{(2)}\hat{\rho}_0\right)$ as the only diagonal term is $|0\rangle\langle 0|$, which can be found by making use of the vanishing trace of the corrections to density operators in perturbation theory at every order respectively.

The probability $\mathcal{P}^+$ of finding the detector that was initially in its ground state excited after crossing the cavity is, to leading order, given by

$$\begin{aligned}\mathcal{P}^+ &= \sum_{n,\ell=1}^{\infty}|\,\langle(0,n,m),e|\,\hat{\mathcal{U}}^{(1)}\,|0,e\rangle\,|^2 = \langle e|\,\mathrm{tr}_{\mathrm{F}}\left(\hat{\mathcal{U}}^{(1)}\hat{\rho}_0\hat{\mathcal{U}}^{(1)\dagger}\right)|e\rangle \\ &= c^2\lambda^2\sum_{n,\ell=1}^{\infty}\left|\int_0^T \mathrm{d}\tau e^{\mathrm{i}\Omega\tau}u^*_{0ln}(\tau)\right|^2 = \sum_{n,\ell=1}^{\infty}N_{\ell n}.\end{aligned} \tag{B.25}$$

Similarly, we find the probability $\mathcal{P}^-$ of an initially excited detector to be in its ground state after leaving the cavity to be

$$\begin{aligned}\mathcal{P}^- &= \sum_{n,\ell=1}^{\infty} |\langle (0,n,m),g|\hat{\mathcal{U}}^{(1)}|0,g\rangle|^2 = \langle g|\,\mathrm{tr}_{\mathrm{F}}\left(\hat{\mathcal{U}}^{(1)}\hat{\rho}_0\hat{\mathcal{U}}^{(1)\dagger}\right)|g\rangle \\ &= c^2\lambda^2\sum_{n,\ell=1}^{\infty}\left|\int_0^T \mathrm{d}\tau e^{-\mathrm{i}\Omega\tau}u^*_{0\ell n}(\tau)\right|^2 = \sum_{n,\ell=1}^{\infty} N_{\ell n}. \end{aligned} \tag{B.26}$$

Therefore, for each corresponding initial detector setting, the total number of excitations in the field equals either of the detector probabilities. Hence, the resonant mode contribution to the total excitations in the field equals the ratio of the resonant mode contribution to the total vacuum excitation or spontaneous emission probability, depending on the initial detector state (suppressing the superscripts):

$$\frac{N_{\mathrm{res}}}{\sum_{n,\ell=1}^{\infty} N_{\ell n}} = \frac{\mathcal{P}_{\mathrm{res}}}{\mathcal{P}}. \tag{B.27}$$

B.3 Parameter Space

In this appendix we look at different dimensionless parameters, in contrast to the previously used measure for relativistic behavior aL/c^2, and investigate the influence on the expected number of excitations in the field after the detector's crossing. In particular, the following parameters will be studied: $a/(\Omega c)$, $\Omega L/c$, Ω/ω_0, and L/ρ. The results are collected in Figures B.1, B.2, and B.3. It is recognizable that, as the 'lack of resonance' intuition dictates, if the detector's energy gap is small compared to the energy of any field mode, the excitations are centered around $(\ell, n) = (1, 1)$ (the closest-to-zero energy mode), spread over many modes, and there is not much qualitative difference between excited and ground state.

When the gap is comparable with a cavity mode energy we observe the same phenomenology as in Fig. 4.2: The excited detector releases energy in the modes close to resonance and changing the detector's gap will change the location of the resonance, and the Doppler shift for it. Conversely, given a detector gap resonant with a field mode, a detector flying into the cavity in its ground state does not effect any narrowly localized field excitations.

If we analyze the dependence on the cavity width, R/L, taking the opposite limit to Sec. 4.4, i.e. $R \gg L$, we see (Fig. B.1) that excitations are mainly localized at modes of

constant n corresponding to resonance with Ω distributed in a very spread manner among a variety of ℓ modes if the detector is initially excited. Conversely, a initially ground-state detector excites the field in a big spread of modes, the same as what we saw before. It may be emphasized that, as expected, the number expectations values are larger for an excited detector as compared to one in the ground state, usually by several orders of magnitude. Moreover, increasing the acceleration increases the number expectation values for both detector settings.

In the following, we will study once more the ratio of the resonant contribution to the transition probabilities. This will yield additional insight into the validity of the single-mode approximation. We choose as resonant modes those which are within 2% of the detector's gap. In case no mode fulfills the criterion, we choose the one closest in energy. On the other hand, in certain regimes there will be more modes added as resonant than is actually justified from the energy distribution point of view. However, this will only strengthen our argument. In Table B.1 we present the ratio for when several of the dimensionless parameters, i.e. $a/(\Omega c)$, $\Omega L/c$, Ω/ω_0 and L/ρ, are either very small or very large. It can be seen that, for an initially accelerated detector, with non-relativistic trajectories the single-mode approximation may be sufficient, depending on the specific parameters. However, as soon as the acceleration is increased the approximation fails inevitably. If the detector is initially in the ground state, the single-mode approximation will not even for non-relativistic trajectories reproduce the exact results.

Large Radial Extension $R \gg L$

Detector initially in excited state | Detector initially in ground state

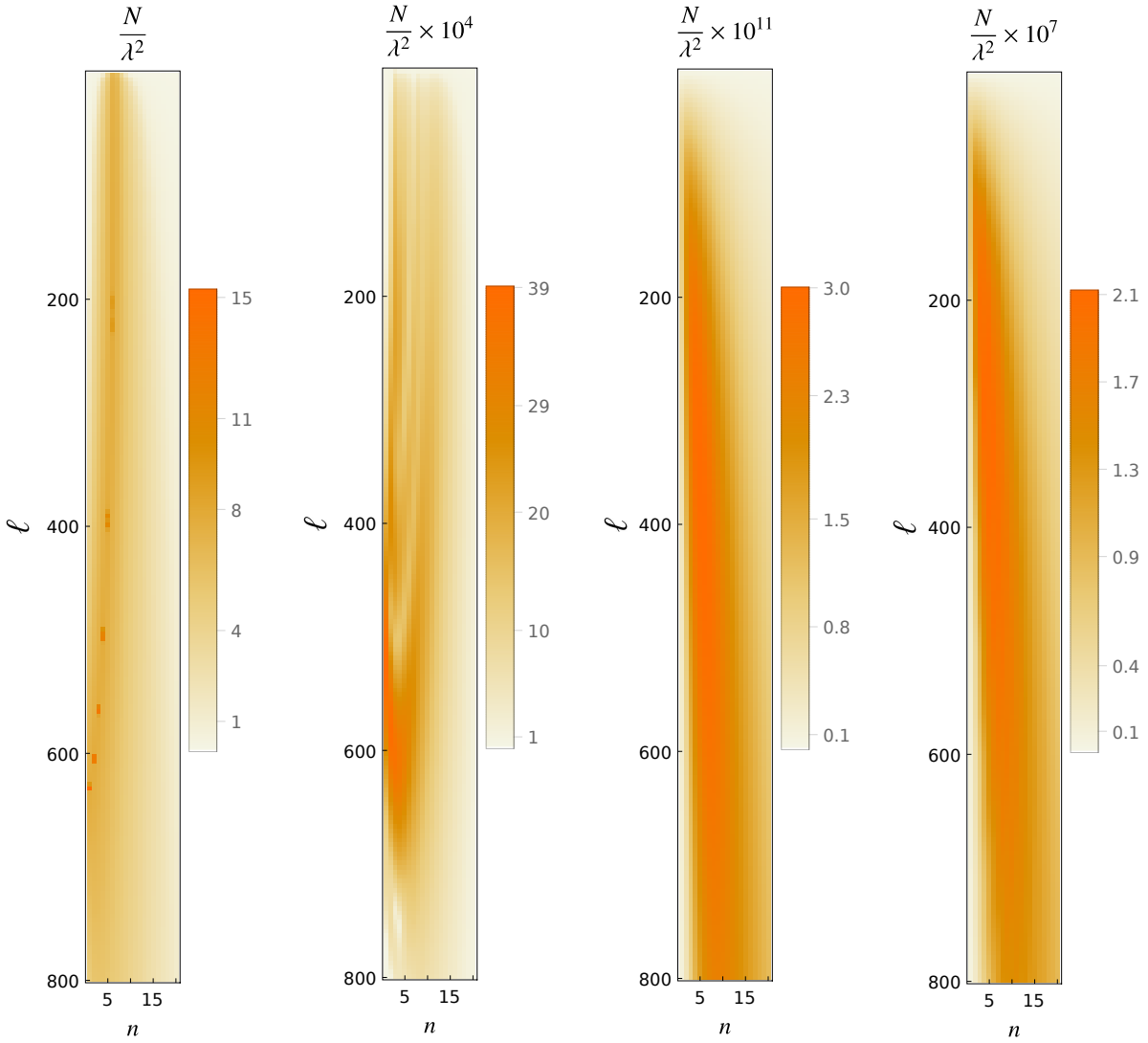

(a) $aL/c^2 = 0.00005$ (b) $aL/c^2 = 0.5$ (c) $aL/c^2 = 0.00005$ (d) $aL/c^2 = 0.5$

Figure B.1: Number expectation value N as a function of mode numbers n and ℓ for an exemplary $R/L \gg 1$ setting. The parameters are $R/L = 100$, $\Omega L = 20$ such that $\{(\ell, n)|(\ell, n) = (212-214, 6), (394-395, 5), (495-496, 4), (562, 3), (604-605, 2), (629, 1)\}$ are most resonant with the detector's energy gap (assuming at most a 0.1%-difference in energy from the detector's gap).

Limits	$\Omega = 0$	$L \ll R, c/\Omega$	$R \ll L, c/\Omega$	$L \gg R, c/\Omega$
Resonant modes	off-resonant	off-resonant	off-resonant	146 modes
aL/c^2	5×10^{-5}	5×10^{-11}	5×10^{-5}	5×10^{-2}
$a/(\Omega c)$	∞	2.5×10^{-6}	2.5×10^{-6}	5×10^{-6}
$\Omega L/c$	0	2×10^{-5}	20	10^4
Ω/ω_0	0	4.16	8.3×10^{-3}	2.08
R/L	0.5	5×10^5	10^{-3}	5×10^{-4}
$\mathcal{P}^-_{\rm res}/\mathcal{P}^- \leq$	6.5×10^{-2}	3.1×10^{-5}	2.9×10^{-9}	7×10^{-2}
$\mathcal{P}^+_{\rm res}/\mathcal{P}^+ \leq$	6.9×10^{-2}	3.1×10^{-5}	2.8×10^{-9}	5.4×10^{-3}

Limits	$L \approx R \approx c/\Omega$			$R \gg L, c/\Omega$	
Resonant modes	10 modes	10 modes	10 modes	680 modes	680 modes
aL/c^2	5×10^{-5}	5×10^{-4}	5×10^{-3}	5×10^{-5}	5×10^{-4}
$a/(\Omega c)$	10^{-6}	10^{-5}	10^{-4}	5×10^{-6}	5×10^{-5}
$\Omega L/c$	50	50	50	10	10
Ω/ω_0	10.4	10.4	10.4	4158.3	4158.3
R/L	0.5	0.5	0.5	10^3	10^3
$\mathcal{P}^-_{\rm res}/\mathcal{P}^- \leq$	0.9999	0.978	0.53	0.999	0.88
$\mathcal{P}^+_{\rm res}/\mathcal{P}^+ \leq$	6.5×10^{-5}	6.5×10^{-5}	6.5×10^{-5}	1.7×10^{-2}	1.7×10^{-2}

Table B.1: Estimating an upper bound to the ratio of the resonant contribution to the full transition probabilities. We have chosen those modes for the resonant contribution which differ in energy from Ω by at most 2%. In case there is no mode resonant with the detector's energy gap (first 3 cases), we have chosen $(\ell, n) = (1, 1)$ as closest in energy to the detector's gap. As the cut-offs for the sums over n and ℓ we have 10^4 and 200, respectively. Note however that for the 8th and 9th case we used 10^4 and 4000 as cut-offs for the sums over n and ℓ, respectively.

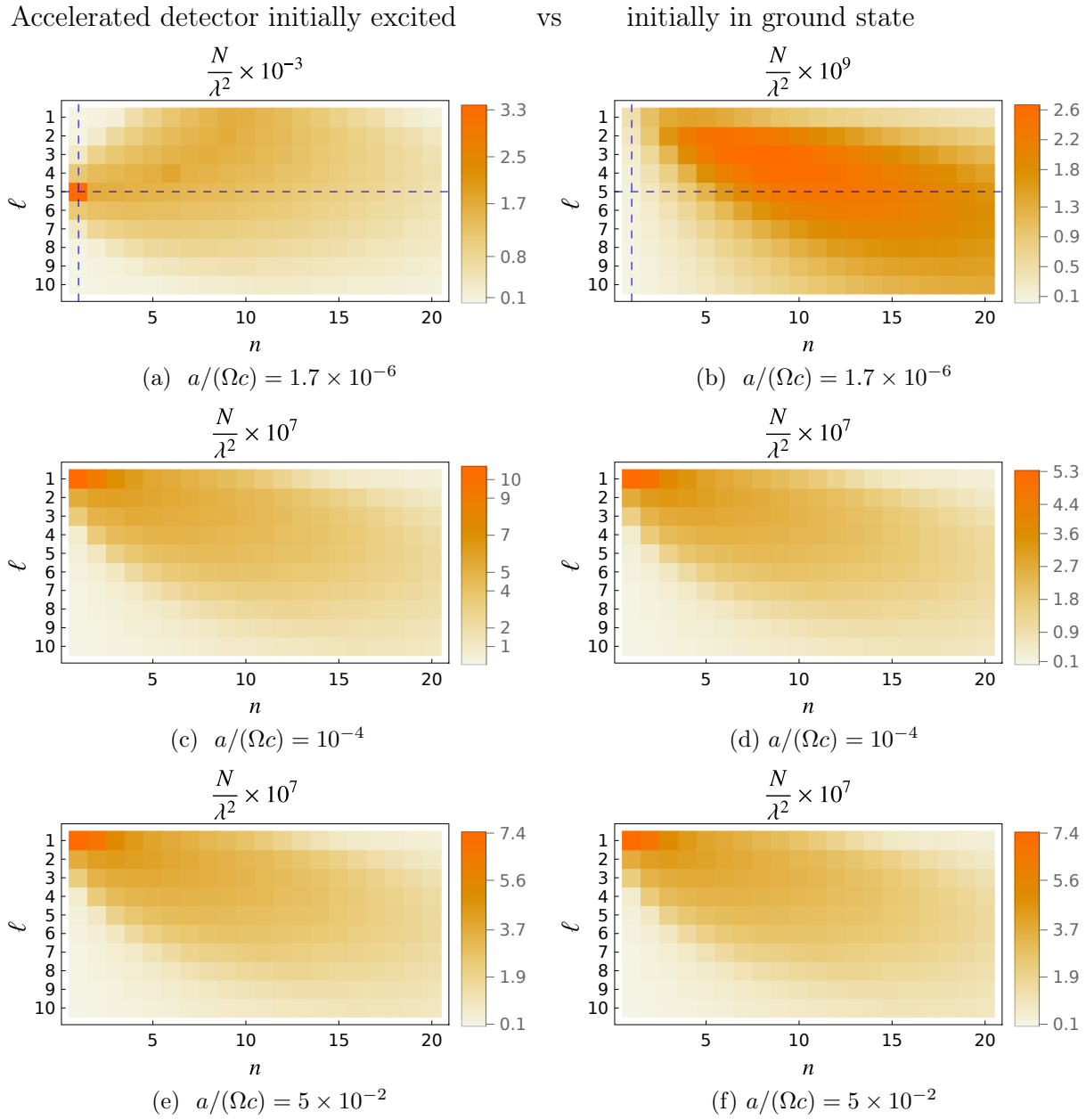

(a) $a/(\Omega c) = 1.7 \times 10^{-6}$ (b) $a/(\Omega c) = 1.7 \times 10^{-6}$

(c) $a/(\Omega c) = 10^{-4}$ (d) $a/(\Omega c) = 10^{-4}$

(e) $a/(\Omega c) = 5 \times 10^{-2}$ (f) $a/(\Omega c) = 5 \times 10^{-2}$

Figure B.2: Number expectation value N as a function of mode numbers n and ℓ for different values of $a/(\Omega c)$. Parameters are $R/L = 0.5$, $aL/c^2 = 0.00005$ such that the detector's gap is (a, b) most resonant with $(\ell, n) = (5, 1)$ (intersection of dashed line); (c, d, e, f) off-resonant with any field mode.

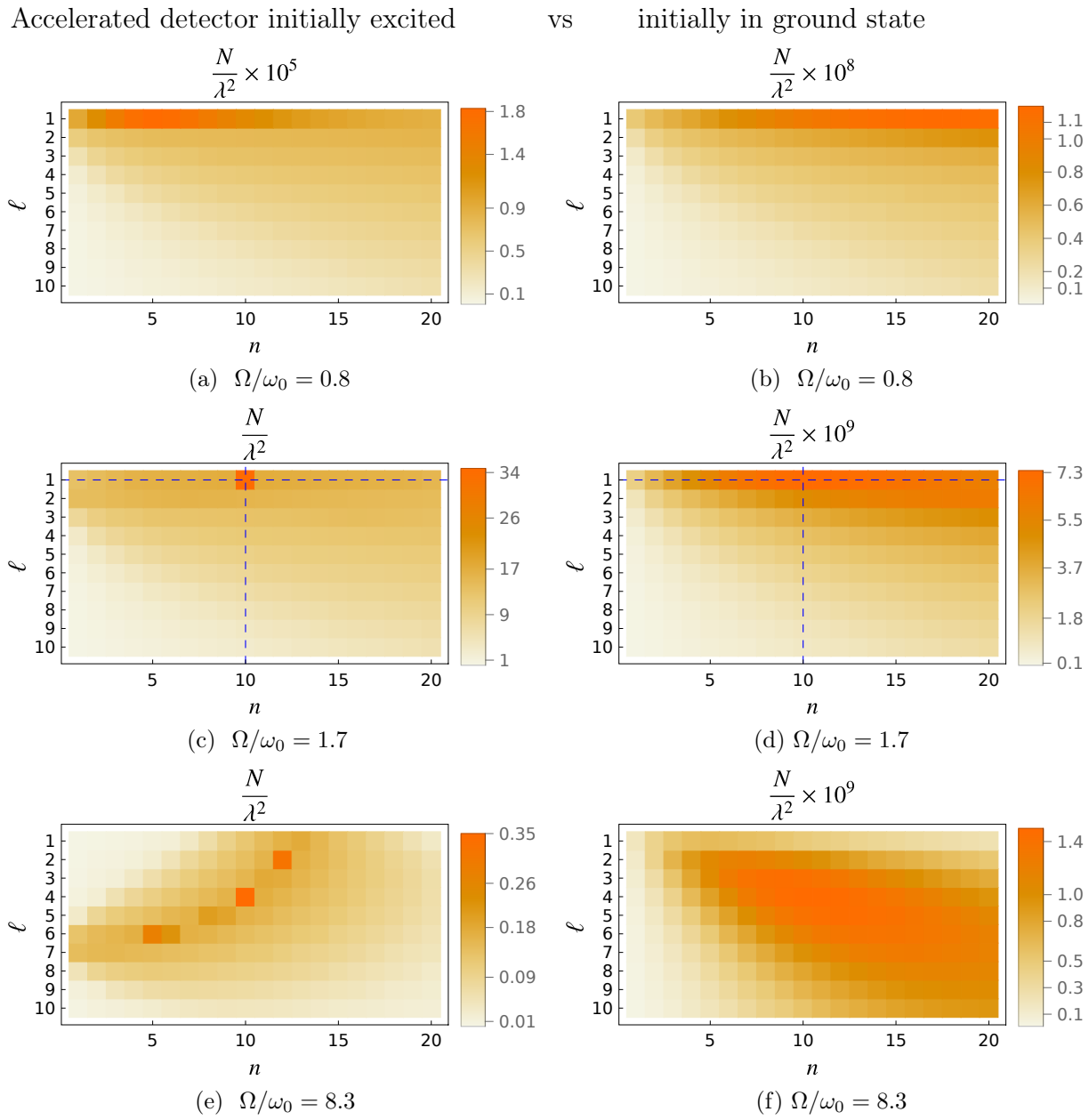

(a) $\Omega/\omega_0 = 0.8$ (b) $\Omega/\omega_0 = 0.8$

(c) $\Omega/\omega_0 = 1.7$ (d) $\Omega/\omega_0 = 1.7$

(e) $\Omega/\omega_0 = 8.3$ (f) $\Omega/\omega_0 = 8.3$

Figure B.3: Number expectation value N as a function of mode numbers n and ℓ for different values of Ω/ω_0, where $\omega_0 = cx_{01}/R$. Parameters are $aL/c^2 = 0.00005$, $\Omega L/c = 40$. The detector's gap Ω is (a, b) off-resonant with any mode; (c, d) most resonant with $(\ell, n) = (1, 10)$ (intersection of dashed lines); (e, f) most resonant with $\{(\ell, n)|(\ell, n) = (2, 12), (4, 10), (6, 5)\}$ (recognizable by the three peaks in (e)).

Appendix C

The Multipolar Coupling Hamiltonian

C.1 Comparing the Power-Zienau-Woolley and Dirac-Heisenberg Transformation

In this section we prove that the Dirac-Heisenberg transformation from Eq. (6.11) is identical to the PZW transformation of Eq. (6.12) to all orders. To do so, we expand the field around the position of the COM coordinate $\boldsymbol{R}$ and perform the integral over parameter λ:

$$
\begin{aligned}
\hat{\Lambda}^{\mathrm{PZW}} &= \sum_{i=e,p} \frac{e_i}{|e|} (\hat{\boldsymbol{r}}^i - \hat{\boldsymbol{R}}) \cdot \int_0^1 \mathrm{d}\lambda\, \hat{\boldsymbol{A}} \left(t, \hat{\boldsymbol{R}} + \lambda (\hat{\boldsymbol{r}}^i - \hat{\boldsymbol{R}}) \right) \\
&= \int_{\mathbb{R}^3} \mathrm{d}^3\boldsymbol{R} \int_{\mathbb{R}^3} \mathrm{d}^3\boldsymbol{r}\, |\boldsymbol{R}\rangle\langle\boldsymbol{R}| \otimes |\boldsymbol{r}\rangle\langle\boldsymbol{r}|\, \boldsymbol{r} \cdot \int_0^1 \mathrm{d}\lambda \sum_{i=e,p} \frac{m_i}{M} \hat{\boldsymbol{A}} \left(t, \boldsymbol{R} + \mathrm{sgn}(e_i) \lambda \frac{m_i}{M} \boldsymbol{r} \right) \\
&= \int_{\mathbb{R}^3} \mathrm{d}^3\boldsymbol{R} \int_{\mathbb{R}^3} \mathrm{d}^3\boldsymbol{r}\, |\boldsymbol{R}\rangle\langle\boldsymbol{R}| \otimes |\boldsymbol{r}\rangle\langle\boldsymbol{r}| \int_0^1 \mathrm{d}\lambda \sum_{n=0}^{\infty} \frac{\lambda^n}{n!} \boldsymbol{r}^n \cdot \boldsymbol{\nabla}_{\boldsymbol{R}}^n (\boldsymbol{r} \cdot \hat{\boldsymbol{A}}(t, \boldsymbol{R})) \\
&\quad \times \left[\left(\frac{m_p}{M} \right)^{n+1} + (-1)^n \left(\frac{m_e}{M} \right)^{n+1} \right] \\
&= \int_{\mathbb{R}^3} \mathrm{d}^3\boldsymbol{R} \int_{\mathbb{R}^3} \mathrm{d}^3\boldsymbol{r}\, |\boldsymbol{R}\rangle\langle\boldsymbol{R}| \otimes |\boldsymbol{r}\rangle\langle\boldsymbol{r}| \sum_{n=0}^{\infty} \frac{\boldsymbol{r}^n \cdot \boldsymbol{\nabla}_{\boldsymbol{R}}^n (\boldsymbol{r} \cdot \hat{\boldsymbol{A}}(t, \boldsymbol{R}))}{(n+1)!} \\
&\quad \times \left[\left(\frac{m_p}{M} \right)^{n+1} + (-1)^n \left(\frac{m_e}{M} \right)^{n+1} \right], \qquad \text{(C.1)}
\end{aligned}
$$

where for the second line we used

$$\hat{\boldsymbol{r}}_e = \hat{\boldsymbol{R}} + \frac{m_p}{M}\hat{\boldsymbol{r}}, \quad \hat{\boldsymbol{r}}_p = \hat{\boldsymbol{R}} - \frac{m_e}{M}\hat{\boldsymbol{r}}. \tag{C.2}$$

From Eq. (6.11) we get

$$\begin{aligned}\hat{\Lambda} &= \int_{\mathbb{R}^3} \mathrm{d}^3\boldsymbol{R} \int_{\mathbb{R}^3} \mathrm{d}^3\boldsymbol{r}\, |\boldsymbol{R}\rangle\langle\boldsymbol{R}| \otimes |\boldsymbol{r}\rangle\langle\boldsymbol{r}| \int_0^1 \mathrm{d}\lambda \sum_{n=0}^{\infty} \frac{1}{n!} \boldsymbol{r}^n \cdot \boldsymbol{\nabla}^n_{\boldsymbol{R}}(\boldsymbol{r}\cdot\hat{\boldsymbol{A}}(t,\boldsymbol{R})) \left(\lambda - \frac{m_e}{M}\right)^n \\ &= \int_{\mathbb{R}^3} \mathrm{d}^3\boldsymbol{R} \int_{\mathbb{R}^3} \mathrm{d}^3\boldsymbol{r}\, |\boldsymbol{R}\rangle\langle\boldsymbol{R}| \otimes |\boldsymbol{r}\rangle\langle\boldsymbol{r}| \sum_{n=0}^{\infty} \frac{\boldsymbol{r}^n \cdot \boldsymbol{\nabla}^n_{\boldsymbol{R}}(\boldsymbol{r}\cdot\hat{\boldsymbol{A}}(t,\boldsymbol{R}))}{(n+1)!} \left[\left(\frac{m_p}{M}\right)^{n+1} + (-1)^n \left(\frac{m_e}{M}\right)^{n+1}\right].\end{aligned} \tag{C.3}$$

We can see that truncating after the first two terms yields $\hat{\Lambda}^{(1)}$, i.e. Eq. (6.10). We can conclude that the PZW transformation of (C.1) and the Dirac-Heisenberg transformation of (C.3) are identical to all orders, and that, therefore, we will obtain the multipolar Hamiltonian after canonical transformation.

C.2 Commutator Computations

Through derivatives acting on

$$\left[\hat{A}^i(t,\boldsymbol{x}), \hat{A}^j(t,\boldsymbol{x}')\right] = \int_{\mathbb{R}^3} \frac{\mathrm{d}^3k}{(2\pi)^3} \frac{\hbar}{2\epsilon_0 c|\boldsymbol{k}|} (\delta^{ij} - e^i_{\boldsymbol{k}} e^j_{\boldsymbol{k}}) \left(e^{\mathrm{i}\boldsymbol{k}\cdot(\boldsymbol{x}-\boldsymbol{x}')} - e^{-\mathrm{i}\boldsymbol{k}\cdot(\boldsymbol{x}-\boldsymbol{x}')}\right), \tag{C.4}$$

we find the commutators

$$\left[\hat{A}^i(t,\boldsymbol{x}),\partial_l\hat{A}^j(t,\boldsymbol{x}')\right]=\int_{\mathbb{R}^3}\frac{\mathrm{d}^3k}{(2\pi)^3}\frac{-\mathrm{i}\hbar}{2\epsilon_0 c|\boldsymbol{k}|}k_l(\delta^{ij}-e^i_{\boldsymbol{k}}e^j_{\boldsymbol{k}})\left(e^{\mathrm{i}\boldsymbol{k}\cdot(\boldsymbol{x}-\boldsymbol{x}')}+e^{-\mathrm{i}\boldsymbol{k}\cdot(\boldsymbol{x}-\boldsymbol{x}')}\right), \tag{C.5}$$

$$\left[\partial_l\hat{A}^i(t,\boldsymbol{x}),\partial_m\hat{A}^j(t,\boldsymbol{x}')\right]=\int_{\mathbb{R}^3}\frac{\mathrm{d}^3k}{(2\pi)^3}\frac{\hbar}{2\epsilon_0 c|\boldsymbol{k}|}k_mk_l(\delta^{ij}-e^i_{\boldsymbol{k}}e^j_{\boldsymbol{k}})\left(e^{\mathrm{i}\boldsymbol{k}\cdot(\boldsymbol{x}-\boldsymbol{x}')}-e^{-\mathrm{i}\boldsymbol{k}\cdot(\boldsymbol{x}-\boldsymbol{x}')}\right), \tag{C.6}$$

$$\left[\hat{A}^i(t,\boldsymbol{x}),\partial_t\partial_l\hat{A}^j(t,\boldsymbol{x}')\right]=\int_{\mathbb{R}^3}\frac{\mathrm{d}^3k}{(2\pi)^3}\frac{\hbar}{2\epsilon_0}k_l(\delta^{ij}-e^i_{\boldsymbol{k}}e^j_{\boldsymbol{k}})\left(e^{\mathrm{i}\boldsymbol{k}\cdot(\boldsymbol{x}-\boldsymbol{x}')}-e^{-\mathrm{i}\boldsymbol{k}\cdot(\boldsymbol{x}-\boldsymbol{x}')}\right), \tag{C.7}$$

$$\left[\partial_l\hat{A}^i(t,\boldsymbol{x}),\partial_t\hat{A}^j(t,\boldsymbol{x}')\right]=\int_{\mathbb{R}^3}\frac{\mathrm{d}^3k}{(2\pi)^3}\frac{\hbar}{2\epsilon_0}(-k_l)(\delta^{ij}-e^i_{\boldsymbol{k}}e^j_{\boldsymbol{k}})\left(e^{\mathrm{i}\boldsymbol{k}\cdot(\boldsymbol{x}-\boldsymbol{x}')}-e^{-\mathrm{i}\boldsymbol{k}\cdot(\boldsymbol{x}-\boldsymbol{x}')}\right), \tag{C.8}$$

$$\begin{aligned}\left[\hat{A}^i(t,\boldsymbol{x}),\partial_t\hat{A}^j(t,\boldsymbol{x}')\right]&=\int_{\mathbb{R}^3}\frac{\mathrm{d}^3k}{(2\pi)^3}\frac{\mathrm{i}\hbar}{2\epsilon_0}(\delta^{ij}-e^i_{\boldsymbol{k}}e^j_{\boldsymbol{k}})\left(e^{\mathrm{i}\boldsymbol{k}\cdot(\boldsymbol{x}-\boldsymbol{x}')}+e^{-\mathrm{i}\boldsymbol{k}\cdot(\boldsymbol{x}-\boldsymbol{x}')}\right)\\&=\frac{\mathrm{i}\hbar}{\epsilon_0}\delta^{ij,(\mathrm{tr})}(\boldsymbol{x}-\boldsymbol{x}'),\end{aligned} \tag{C.9}$$

$$\begin{aligned}\left[\partial_l\hat{A}^i(t,\boldsymbol{x}),\partial_t\partial_m\hat{A}^j(t,\boldsymbol{x}')\right]&=\int_{\mathbb{R}^3}\frac{\mathrm{d}^3k}{(2\pi)^3}\frac{\mathrm{i}\hbar}{2\epsilon_0}k_lk_m(\delta^{ij}-e^i_{\boldsymbol{k}}e^j_{\boldsymbol{k}})\left(e^{\mathrm{i}\boldsymbol{k}\cdot(\boldsymbol{x}-\boldsymbol{x}')}+e^{-\mathrm{i}\boldsymbol{k}\cdot(\boldsymbol{x}-\boldsymbol{x}')}\right)\\&=\frac{\mathrm{i}\hbar}{\epsilon_0}\frac{\partial^2\delta^{ij,(\mathrm{tr})}(\boldsymbol{x}-\boldsymbol{x}')}{\partial x^l\partial x'^m},\end{aligned} \tag{C.10}$$

note that $\partial_t\hat{A}^j=-\hat{E}^j$, and $\delta^{ij,(\mathrm{tr})}(\boldsymbol{x})=\frac{1}{(2\pi)^3}\int_{\mathbb{R}^3}\mathrm{d}^3\boldsymbol{k}(\delta^{ij}-e^j_{\boldsymbol{k}}e^j_{\boldsymbol{k}})e^{\mathrm{i}\boldsymbol{k}\cdot\boldsymbol{x}}$ is the transverse delta function [150]. We see that in the coincidence limit $\boldsymbol{x}=\boldsymbol{x}'$, Eq. (C.4) – (C.8) vanish. Eq. (C.5) vanishes due to parity: there is always an odd number of powers of k_i being integrated over the whole momentum space. The other commutators are zero due to the cancellations of the plane waves. As all spatial commutators (without any time derivative being involved) vanish, this implies that the vector potential is left invariant under the unitary operator generated by Eq. (6.10). As we work in the dipole approximation, no higher derivatives will be needed to compute $\hat{\tilde{H}}^{(1)}$ in Eq. (6.16).

C.3 Relations Between the Electromagnetic Wightman Tensors

The Wightman tensors in integral form are derived by using $\langle 0|\hat{a}_{\boldsymbol{k},s}\hat{a}^\dagger_{\boldsymbol{k}',s'}|0\rangle = \delta_{s,s'}\delta(\boldsymbol{k}-\boldsymbol{k}')$, and the completeness relations of the polarization vectors [52, Ch. 3]

$$\sum_{s=1}^{2}\epsilon^i_{\boldsymbol{k},s}\epsilon^j_{\boldsymbol{k},s} = \delta^{ij} - e^j_{\boldsymbol{k}}e^j_{\boldsymbol{k}} = \mathcal{F}(\delta^{ij,(\mathrm{tr})}), \tag{C.11}$$

where $\mathcal{F}$ represents the Fourier transform from $\boldsymbol{x}$ to $\boldsymbol{k}$. It turns out that knowing two Wightman tensors suffices to characterize all remaining Wightman tensors of the electromagnetic field strength tensor. Starting with the purely electric field case, we get

$$\begin{aligned} W^{ij}_E[t,t';\boldsymbol{x},\boldsymbol{x}'] &= \langle 0|\,\hat{E}^i(t,\boldsymbol{x})\hat{E}^j(t',\boldsymbol{x}')\,|0\rangle \\ &= \sum_{s,s'=1}^{2}\frac{\hbar c}{2(2\pi)^3\epsilon_0}\int_{\mathbb{R}^3}\mathrm{d}^3\boldsymbol{k}\int_{\mathbb{R}^3}\mathrm{d}^3\boldsymbol{k}'\sqrt{|\boldsymbol{k}||\boldsymbol{k}'|}\epsilon^i_{\boldsymbol{k},s}\epsilon^j_{\boldsymbol{k},s'}\,\langle 0|\hat{a}_{\boldsymbol{k},s}\hat{a}^\dagger_{\boldsymbol{k}',s'}|0\rangle \\ &\quad\times e^{-\mathrm{i}c(|\boldsymbol{k}|t-|\boldsymbol{k}'|t')}e^{\mathrm{i}(\boldsymbol{k}\cdot\boldsymbol{x}-\boldsymbol{k}'\cdot\boldsymbol{x}')} \\ &= \frac{\hbar c}{2\epsilon_0}\int_{\mathbb{R}^3}\frac{\mathrm{d}^3\boldsymbol{k}}{(2\pi)^3}|\boldsymbol{k}|e^{-\mathrm{i}c|\boldsymbol{k}|(t-t')}e^{\mathrm{i}\boldsymbol{k}\cdot(\boldsymbol{x}-\boldsymbol{x}')}\left(\delta^{ij}-e^i_{\boldsymbol{k}}e^j_{\boldsymbol{k}}\right). \end{aligned} \tag{C.12}$$

For the purely magnetic Wightman function we make use of (assuming a right-handed orthonormal basis)

$$\boldsymbol{e}_{\boldsymbol{k}}\times\boldsymbol{\epsilon}_{\boldsymbol{k},s} = \begin{cases}\boldsymbol{\epsilon}_{\boldsymbol{k},2}, & s=1\\ -\boldsymbol{\epsilon}_{\boldsymbol{k},1}, & s=2\end{cases} \quad\Rightarrow\quad \sum_{s=1}^{2}(\boldsymbol{e}_{\boldsymbol{k}}\times\boldsymbol{\epsilon}_{\boldsymbol{k},s})^i(\boldsymbol{e}_{\boldsymbol{k}}\times\boldsymbol{\epsilon}_{\boldsymbol{k},s})^j = \sum_{s=1}^{2}\epsilon^i_{\boldsymbol{k},s}\epsilon^j_{\boldsymbol{k},s}. \tag{C.13}$$

It follows then simply

$$W^{ij}_B[t,t';\boldsymbol{x},\boldsymbol{x}'] = \langle 0|\,\hat{B}^i(t,\boldsymbol{x})\hat{B}^j(t',\boldsymbol{x}')\,|0\rangle = \frac{W^{ij}_E[t,t';\boldsymbol{x},\boldsymbol{x}']}{c^2}. \tag{C.14}$$

For the remaining Wightman functions we need

$$\sum_{s=1}^{2}(\boldsymbol{e}_{\boldsymbol{k}}\times\boldsymbol{\epsilon}_{\boldsymbol{k},s})^i\epsilon^j_{\boldsymbol{k},s} = \epsilon^i_{\boldsymbol{k},2}\epsilon^j_{\boldsymbol{k},1} - \epsilon^i_{\boldsymbol{k},1}\epsilon^j_{\boldsymbol{k},2} = -\epsilon^{ijk}(e_{\boldsymbol{k}})_k. \tag{C.15}$$

Hence, we find

$$W^{ij}_{BE}[t,t';\boldsymbol{x},\boldsymbol{x}'] = \langle 0|\, \hat{B}^i(t,\boldsymbol{x})\hat{E}^j(t',\boldsymbol{x}')\,|0\rangle = -\frac{\hbar}{2\epsilon_0}\int_{\mathbb{R}^3}\frac{\mathrm{d}^3\boldsymbol{k}}{(2\pi)^3}|\boldsymbol{k}|e^{-\mathrm{i}c|\boldsymbol{k}|(t-t')}e^{\mathrm{i}\boldsymbol{k}\cdot(\boldsymbol{x}-\boldsymbol{x}')}\epsilon^{ijk}(e_{\boldsymbol{k}})_k$$
$$= W^{ji}_{EB}[t,t';\boldsymbol{x},\boldsymbol{x}']. \tag{C.16}$$